05-4506832 pustaka.upsi.edu.my Perpustakaan Tuanku Bainun Kampus Sultan Abdul Jalil Shah PustakaTBainun ptbupsi

QUANTITATIVE OPTICAL MANIPULATION OF A SINGLE 4-CYANO-4'-PENTYLBIPHENYL MICRODROPLET IN WATER FOR ACTUATING AND SENSING APPLICATIONS

05-4506832 pustaka.upsi.edu.my Perpustakaan Tuanku Bainun Kampus Sultan Abdul Jalil Shah PustakaTBainun ptbupsi

MUHAMAD SAFUAN BIN MAT YENG @ MAT ZIN

SULTAN IDRIS EDUCATION UNIVERSITY

2024

05-4506832 pustaka.upsi.edu.my Perpustakaan Tuanku Bainun Kampus Sultan Abdul Jalil Shah PustakaTBainun ptbupsi

05-4506832 pustaka.upsi.edu.my Perpustakaan Tuanku Bainun Kampus Sultan Abdul Jalil Shah PustakaTBainun ptbupsi

QUANTITATIVE OPTICAL MANIPULATION OF A SINGLE 4-CYANO-4'-PENTYLBIPHENYL MICRODROPLET IN WATER FOR ACTUATING AND SENSING APPLICATIONS

MUHAMAD SAFUAN BIN MAT YENG @ MAT ZIN

05-4506832 pustaka.upsi.edu.my Perpustakaan Tuanku Bainun Kampus Sultan Abdul Jalil Shah PustakaTBainun ptbupsi

THESIS PRESENTED TO QUALIFY FOR A DOCTOR OF PHILOSOPHY

FACULTY OF SCIENCE AND MATHEMATICS
SULTAN IDRIS EDUCATION UNIVERSITY

2024

05-4506832 pustaka.upsi.edu.my Perpustakaan Tuanku Bainun Kampus Sultan Abdul Jalil Shah PustakaTBainun ptbupsi

UNIVERSITI PENDIDIKAN SULTAN IDRIS
SULTAN IDRIS EDUCATION UNIVERSITY

Please tick (√)
Project Paper
Masters by Research
Master by Mixed Mode
PhD

/

INSTITUTE OF GRADUATE STUDIES

DECLARATION OF ORIGINAL WORK

This declaration is made on the .....6.....day of....FEB.....20.24...

i. Student's Declaration:

I, MUHAMAD SAFUAN BIN MAT YENG @ MAT ZIN, P20201000025, FSM (PLEASE INDICATE STUDENT'S NAME, MATRIC NO. AND FACULTY) hereby declare that the work entitled QUANTITATIVE OPTICAL MANIPULATION OF A SINGLE 4-CYANO-4'-PENTYLBIPHENYL MICRODROPLET IN WATER FOR ACTUATING AND SENSING APPLICATIONS is my original work. I have not copied from any other students' work or from any other sources except where due reference or acknowledgement is made explicitly in the text, nor has any part been written for me by another person.

Signature of the student

ii. Supervisor's Declaration:

I ASSOC. PROF. DR. Ts. SHAHRUL KADRI BIN AYOP (SUPERVISOR'S NAME) hereby certifies that the work entitled QUANTITATIVE OPTICAL MANIPULATION OF A SINGLE 4-CYANO-4'-PENTYLBIPHENYL MICRODROPLET IN WATER FOR ACTUATING AND SENSING APPLICATIONS (TITLE) was prepared by the above named student, and was submitted to the Institute of Graduate Studies as a [redacted]/full fulfillment for the conferment of DOCTOR OF PHILOSOPHY (PHYSICS) (PLEASE INDICATE THE DEGREE), and the aforementioned work, to the best of my knowledge, is the said student's work.

6/2/2024
Date

Signature of the Supervisor

Prof. Madya Ts. Dr. SHAHRUL KADRI BIN AYOP

UNIVERSITI PENDIDIKAN SULTAN IDRIS
SULTAN IDRIS EDUCATION UNIVERSITY

INSTITUT PENGAJIAN SISWAZAH /
INSTITUTE OF GRADUATE STUDIES

BORANG PENGESAHAN PENYERAHAN TESIS/~~DISERTASI/LAPORAN KERTAS PROJEK~~
DECLARATION OF THESIS/~~DISSERTATION/PROJECT PAPER FORM~~

Tajuk / *Title*: QUANTITATIVE OPTICAL MANIPULATION OF A SINGLE 4-CYANO-4'-PENTYLBIPHENYL MICRODROPLET IN WATER FOR ACTUATING AND SENSING APPLICATIONS

No. Matrik /*Matric's No.*: P20201000025

Saya / *I* : MUHAMAD SAFUAN BIN MAT YENG @ MAT ZIN

(Nama pelajar / *Student's Name*)

mengaku membenarkan Tesis/~~Disertasi/Laporan Kertas Projek~~ (Kedoktoran/~~Sarjana~~)* ini disimpan di Universiti Pendidikan Sultan Idris (Perpustakaan Tuanku Bainun) dengan syarat-syarat kegunaan seperti berikut:-
acknowledged that Universiti Pendidikan Sultan Idris (Tuanku Bainun Library) reserves the right as follows:-

1. Tesis/~~Disertasi/Laporan Kertas Projek~~ ini adalah hak milik UPSI.
   The thesis is the property of Universiti Pendidikan Sultan Idris
2. Perpustakaan Tuanku Bainun dibenarkan membuat salinan untuk tujuan rujukan dan penyelidikan.
   Tuanku Bainun Library has the right to make copies for the purpose of reference and research.
3. Perpustakaan dibenarkan membuat salinan Tesis/Disertasi ini sebagai bahan pertukaran antara Institusi Pengajian Tinggi.
   The Library has the right to make copies of the thesis for academic exchange.
4. Sila tandakan (√) bagi pilihan kategori di bawah */ Please tick (√) for category below:-*

☐	**SULIT/*CONFIDENTIAL***	Mengandungi maklumat yang berdarjah keselamatan atau kepentingan Malaysia seperti yang termaktub dalam Akta Rahsia Rasmi 1972. / *Contains confidential information under the Official Secret Act 1972*
☐	**TERHAD/*RESTRICTED***	Mengandungi maklumat terhad yang telah ditentukan oleh organisasi/badan di mana penyelidikan ini dijalankan. / *Contains restircted information as specified by the organization where research was done.*
☑	**TIDAK TERHAD / *OPEN ACCESS***	

(Tandatangan Pelajar/ Signature)

Tarikh: 8 FEBRUARY 2024

(Tandatangan Penyelia / *Signature of Supervisor*)
& (Nama & Cop Rasmi / *Name & Official Stamp*)

Prof. Madya Ts. Dr. SHAHRUL KADRI BIN AYOP
Universiti Pendidikan Sultan Idris
bit.ly/kadrimy

Catatan: Jika Tesis/Disertasi ini **SULIT @ TERHAD**, sila lampirkan surat daripada pihak berkuasa/organisasi berkenaan dengan menyatakan sekali sebab dan tempoh laporan ini perlu dikelaskan sebagai **SULIT** dan **TERHAD**.

Notes: If the thesis is CONFIDENTAL or RESTRICTED, please attach with the letter from the organization with period and reasons for confidentiality or restriction.

05-4506832 pustaka.upsi.edu.my Perpustakaan Tuanku Bainun Kampus Sultan Abdul Jalil Shah PustakaTBainun ptbupsi

ACKNOWLEDGEMENT

Alhamdulillah, first and foremost, I would like to thank Allah SWT for everything. Without his blessing, I might not have been able to complete this work. My most excellent commitment and appreciation is to my supervisors, Assoc. Prof. Dr. Ts. Shahrul Kadri bin Ayop and Dr. Izan Roshawaty binti Mustapa, thank you for your guidance and brilliant insights in my journey toward completing this thesis. Your excellent care and motivating support have helped me on this challenging but healing journey. Many thanks to the Faculty of Science and Mathematics staff, who are directly or indirectly involved in this research. Without their help, this thesis would not have been possible in its current form. I also thank the Ministry of Higher Education Malaysia (MOHE) especially MyBrainSc Scholarship for funding my PhD studies. I would also like to thank the Photo-Physics System Laboratory, Research Institute for Electronic Science (RIES) at Hokkaido University, especially Prof. Dr. Keiji Sasaki, Dr. An-Chieh Cheng and Dr. Christophe Pin for supervising and guiding my research work for 3 months research attachment. Thank you to all my friends, Siti Azizah, Nur Izzati, Nur Farah Nadia, Wong Yeong Yi, Anis Nabila and Faiz Farhan, for all the beautiful and fun memories. Finally, I want to thank my family, who have always been supportive and kind.

05-4506832 pustaka.upsi.edu.my Perpustakaan Tuanku Bainun Kampus Sultan Abdul Jalil Shah PustakaTBainun ptbupsi

05-4506832 pustaka.upsi.edu.my Perpustakaan Tuanku Bainun Kampus Sultan Abdul Jalil Shah PustakaTBainun ptbupsi

ABSTRACT

The study aims to formulate the production of 4-cyano-4'-pentylbiphenyl **(**5CB) microdroplets within a suitable range to be optically trapped, to optically trap a single 5CB microdroplet in water within a suitable size range, to optically micro-control the microdroplet using a circularly polarized laser, and to quantitatively determine factors affecting the optical manipulation of the microdroplet. 0.5 µL 5CB was mixed with the deionized water and sonicated to produce bipolar and radial 5CB microdroplet suspensions. The 5CB microdroplet was observed under optical microscopy and its size distribution was measured using ImageJ, while its stability was measured using UV-Vis spectroscopy. A linearly polarized laser beam of 976 nm wavelength was used to optically trap a single 5CB microdroplet in water at a specific laser power density. A circularly polarized laser beam was used to optically trap a single 5CB microdroplet to study its orientation control, rotatability control, and simultaneous translation micro-control. A single 5CB microdroplet was trapped and introduced to the cetyltrimethylammonium bromide (CTAB) solution to study its visual internal configuration change and optical signal. The finding shows that the size distribution of 5CB microdroplet suspension decreased with time. However, it was stable and sustained in 1-hour monitoring. The 5CB microdroplet could be linearly translated and rotated, enabling the simultaneous translation-micro-control. The corner frequency (f_c) and angular speed (ω) showed an increasing trend with optical power density (P) increment. Exposing CTAB solution to the trapped 5CB microdroplet changed its internal configuration from bipolar to radial, optical signal and displacement variance (σ^2). In conclusion, the trapped 5CB microdroplet could be micro-controlled as a microactuator while f_c, ω, and σ^2 measurements were characteristics of microdroplet-based sensors. This study implies that the optical trapping of a single 5CB microdroplet in water has potential for prospective actuating and sensing applications.

05-4506832 pustaka.upsi.edu.my Perpustakaan Tuanku Bainun Kampus Sultan Abdul Jalil Shah PustakaTBainun ptbupsi

05-4506832 pustaka.upsi.edu.my Perpustakaan Tuanku Bainun Kampus Sultan Abdul Jalil Shah PustakaTBainun ptbupsi

PEMANIPULASIAN OPTIK KUANTITATIF BAGI SATU MIKROTITISAN 4-SAIANO-4'-PENTILBIFENIL TUNGGAL DALAM AIR UNTUK APLIKASI PENGGERAKAN DAN PENDERIAAN

ABSTRAK

Kajian ini bertujuan untuk merumuskan penghasilan mikrotitisan 4-saiano-4'-pentilbifenil (5CB) dalam julat yang sesuai untuk diperangkap secara optik, untuk memerangkap secara optik satu mikrotitisan 5CB tunggal di dalam air dalam julat saiz yang sesuai, untuk memikrokawal mikrotitisan tersebut menggunakan alur laser berkutub bulat, dan untuk menentukan secara kuantitatif faktor-faktor yang mempengaruhi pemanipulasian optik mikrotitisan tersebut. 0.5 µL 5CB telah dicampur dengan air ternyahion dan disonikasi dalam tempoh masa yang khusus untuk menghasilkan ampaian mikrotitisan 5CB dwikutub dan jejarian di dalam air. Mikrotitisan 5CB telah diperhatikan melalui mikroskopi optik dan taburan saiznya diukur menggunakan ImageJ manakala kestabilannya diukur menggunakan spektroskopi UV-Vis. Satu alur laser berkutub linear yang mempunyai panjang gelombang 976 nm digunakan untuk merangkap secara optik satu mikrotitisan 5CB tunggal pada ketumpatan kuasa laser tertentu. Alur laser berkutub bulat pula telah digunakan untuk merangkap secara optik satu mikrotitisan 5CB tunggal bagi mengkaji kawalan orientasi, kawalan kebolehputaran, dan translasi mikrokawalan serentak mikrotitisan tersebut. Satu mikrotitisan 5CB tunggal juga diperangkap dan didedahkan kepada larutan setiltrimetilammonium bromida (CTAB) untuk mengkaji perubahan konfigurasi dalaman secara visual dan signal optik mikrotitisan tersebut. Dapatan menunjukkan bahawa taburan saiz ampaian mikrotitisan 5CB berkurang dengan masa. Akan tetapi, mikrotitisan tersebut stabil dan kekal dalam pemantauan selama 1 jam. Mikrotitisan 5CB tersebut juga boleh diperangkap secara linear dan diputar, membolehkan translasi-mikrokawalan serentak. Frekuensi penjuru (f_c) dan kelajuan sudut (ω) menunjukkan trend yang meningkat dengan peningkatan ketumpatan kuasa laser P. Pendedahan larutan CTAB terhadap mikrotitisan 5CB yang diperangkap telah menukarkan konfigurasi dalaman daripada dwikutub kepada jejarian, isyarat optik dan sesaran varians (σ^2) mikrotitisan tersebut. Kesimpulannya, mikrotitisan 5CB tunggal yang diperangkap boleh dimikrokawal sebagai mikropenggerak manakal pengukuran f_c, ω, dan σ^2 pula merupakan ciri-ciri penderia berasaskan mikrotitisan. Kajian ini menunjukkan bahawa perangkap optik satu mikrotitisan 5CB tunggal dalam air berpotensi untuk prospektif aplikasi penggerakan dan penderiaan.

05-4506832 pustaka.upsi.edu.my Perpustakaan Tuanku Bainun Kampus Sultan Abdul Jalil Shah PustakaTBainun ptbupsi

05-4506832 pustaka.upsi.edu.my Perpustakaan Tuanku Bainun Kampus Sultan Abdul Jalil Shah PustakaTBainun ptbupsi

TABLE OF CONTENT

		Page
DECLARATION OF ORIGINAL WORK		ii
DECLARATION OF THESIS		iii
ACKNOWLEDGEMENT		iv
ABSTRACT		v
ABSTRAK		vi
TABLE OF CONTENT		vii
LIST OF TABLES		xii
LIST OF FIGURES		xiii
LIST OF SYMBOLS		xxvii
LIST OF CONSTANTS		xxviii
LIST OF ABREVIATIONS		xxix
APPENDIX LIST		xxx
CHAPTER 1	**INTRODUCTION**	1
	1.1 Research Background	1
	1.2 Problem Statement	6
	1.3 Research Objective	9
	1.4 Significance of Research	10
	1.5 Limitation of Research	11
	1.6 Thesis Outline	13
	1.7 Summary	14

05-4506832 pustaka.upsi.edu.my Perpustakaan Tuanku Bainun Kampus Sultan Abdul Jalil Shah PustakaTBainun ptbupsi

05-4506832 pustaka.upsi.edu.my Perpustakaan Tuanku Bainun Kampus Sultan Abdul Jalil Shah PustakaTBainun ptbupsi

CHAPTER 2	**LITERATURE REVIEW**	15
	2.1 Introduction	15
	2.2 Principle of Optical Tweezers	16
	2.3 Optical Trapping Regimes	17
	2.3.1 Rayleigh Regime	18
	2.3.2 Mie Regime	19
	2.4 Optical Stiffness Calibration of Optical Trapping	22
	2.5 Optical Stiffness Calibration	28
	2.5.1 Equipartition Theorem (ET)	29
	2.5.2 Boltzmann Statistics (BS) Theorem	30
	2.5.3 Power Spectrum Density (PSD) Theorem	32
	2.5.4 Comparison between Boltzmann Statistics (BS), Equipartition Theorem (ET), and Power Spectrum Density (PSD)	34
	2.6 Optical Torque	36
	2.7 Cross-Polarization in Optical Tweezers	38
	2.8 Optical Trapping of Solid Dielectric Particle	40
	2.9 Optical Trapping of Soft Liquid Microdroplet	43
	2.10 Liquid Crystal Introduction	47
	2.11 Classification of Liquid Crystal	49
	2.12 Effective Refractive Index (n_{eff}) of the Nematic LC	53
	2.13 Nematic Liquid Crystal Internal Configuration	55
	2.13.1 Flat Surface	56
	2.13.2 Spherical Geometry	57
	2.14 4-Cyano-4'-Pentylbiphenyl (5CB)	60

05-4506832 pustaka.upsi.edu.my Perpustakaan Tuanku Bainun Kampus Sultan Abdul Jalil Shah PustakaTBainun ptbupsi

05-4506832 pustaka.upsi.edu.my Perpustakaan Tuanku Bainun Kampus Sultan Abdul Jalil Shah PustakaTBainun ptbupsi

2.15 Technique for Microdroplet Production 61

2.16 Nematic Liquid Crystal Microdroplet Production 63

2.17 Distribution Size by Mechanical Technique 66

2.18 Microdroplet Internal Configuration Modification 71

2.19 Nematic Liquid Crystal Microdroplet Study Stability 75

2.20 Nematic Liquid Crystal Microdroplet Optical Trap 77

2.21 Nematic Liquid Crystal Microactuator 95

2.22 Nematic Liquid Crystal Sensor 99

2.22.1 Microdroplet-Based Sensor 102

2.22.2 Whispering Gallery Mode (WGM) Sensing 107

2.23 Summary 115

CHAPTER 3 METHODOLOGY 125

3.1 Introduction 125

3.2 Research Flow Chart 126

3.3 Optical Tweezers System [Phase 1] 129

3.3.1 Trapping Module 131

3.3.2 Observation Module 138

3.3.3 Detection Module 143

3.3.4 Optical Tweezers Performance Test 148

3.4 Preparation of 5CB Microdroplet Solution [Phase 2] 150

3.4.1 Bipolar 5CB Microdroplet Solution Preparation 151

3.4.2 Radial 5CB Microdroplet Solution Preparation 155

3.4.3 5CB Microdroplet Observation by Optical Microscopy 159

3.4.4 ImageJ Optical Microscope Calibration 161

05-4506832 pustaka.upsi.edu.my Perpustakaan Tuanku Bainun Kampus Sultan Abdul Jalil Shah PustakaTBainun ptbupsi

05-4506832 pustaka.upsi.edu.my Perpustakaan Tuanku Bainun Kampus Sultan Abdul Jalil Shah PustakaTBainun ptbupsi

3.4.5 ImageJ Distribution Size (r) Measurement 165

3.4.6 5CB Microdroplet Stability Measurement 173

3.5 The 5CB Microdroplet Micro-Control [Phase 3] 174

3.5.1 Microdroplet Internal Configuration Control 175

3.5.2 5CB Microdroplet Rotational Control 178

3.5.3 Translation and Polarization Control 180

3.5.4 Trajectory Analysis of 5CB Microdroplet 183

3.6 Corner Frequency (f_c) and Angular Speed (ω) Measurement [Phase 4] 188

3.6.1 Corner Frequency (f_c) Flowchart Analysis 188

3.6.2 5CB Microdroplet Radius (r) Measurement 191

3.6.3 Corner Frequency (f_c) Analysis 195

3.6.4 Angular Speed (ω) Measurement 201

3.6.5 5CB Microdroplet Angular Speed (ω) Analysis 203

3.7 Microdroplet Trapping in CTAB Solution [Phase 5] 204

3.7.1 5CB Microdroplet Trapping in CTAB Solution 206

3.7.2 Displacement Variance (σ^2) Analysis 209

3.8 Summary 212

CHAPTER 4 RESULTS AND DISCUSSION 213

4.1 Introduction 213

4.2 The Production of 5CB Microdroplet Suspension 214

4.2.1 Effect of Sonication Time on the Size of 5CB Microdroplet 214

4.2.2 5CB Microdroplet Suspension Stability in Water 223

4.3 Linearly Polarized Laser 5CB Microdroplet Trapping 229

05-4506832 pustaka.upsi.edu.my Perpustakaan Tuanku Bainun Kampus Sultan Abdul Jalil Shah PustakaTBainun ptbupsi

05-4506832 pustaka.upsi.edu.my Perpustakaan Tuanku Bainun Kampus Sultan Abdul Jalil Shah PustakaTBainun ptbupsi

	4.4	5CB Microdroplet Orientation Control	233
	4.5	Rotatability of 5CB Microdroplet	240
	4.6	5CB Microdroplet Translational and Micro-control	242
	4.7	Corner Frequency (f_c) Analysis	249
	4.8	Angular Speed (ω) Analysis	262
	4.9	Trapped 5CB Microdroplet Sensing Mechanism	279
		4.9.1 5CB Microdroplet CTAB Sensing	281
	4.10	Summary	287
CHAPTER 5	**CONCLUSIONS AND RECOMMENDATION**		290
	5.1	Introduction	290
	5.2	Conclusion	291
	5.3	The Research Novelties	293
	5.4	Implications	295
	5.5	Recommendations	297
	5.6	Summary	299
REFERENCES			301
APPENDICES			314

05-4506832 pustaka.upsi.edu.my Perpustakaan Tuanku Bainun Kampus Sultan Abdul Jalil Shah PustakaTBainun ptbupsi

05-4506832 pustaka.upsi.edu.my Perpustakaan Tuanku Bainun Kampus Sultan Abdul Jalil Shah PustakaTBainun ptbupsi

LIST OF TABLES

Table No.		Page
2.1	Comparison between Boltzmann Statistics (BS), Equipartition Theorem (ET), and Power Spectrum Density (PSD) calibration.	35
2.2	Advantages and disadvantages of previous research.	116
3.1	Module and Component of OTKB.	131
3.2	List of used laser current, power, and power density.	137
3.3	Measurement of length in unit pixels by ImageJ.	142
3.4	Measurement of length in unit pixels by ImageJ.	164
4.1	The comparison of 5CB microdroplet size produced from sonication.	221
4.2	Comparison of $\frac{f_c}{r}$ at P = 6.1 to 6.3 MW/cm^2 for chloroform, toluene, 1,2-dicholorobenzene and 5CB microdroplets.	259
4.3	Comparison of density, refractive index, and solubility of Chloroform, Toluene, 1,2-dichlorobenzene, and 5CB.	261
4.4	Comparison of $\frac{\omega}{r}$ for bipolar 5CB reported by Murazawa and this study.	275
4.5	Comparison of $\frac{\omega}{r}$ for radial 5CB reported by Murazawa and this study.	276
4.6	Displacement variance (σ^2) at a particular time.	286

05-4506832 pustaka.upsi.edu.my Perpustakaan Tuanku Bainun Kampus Sultan Abdul Jalil Shah PustakaTBainun ptbupsi

05-4506832 pustaka.upsi.edu.my Perpustakaan Tuanku Bainun Kampus Sultan Abdul Jalil Shah PustakaTBainun ptbupsi

LIST OF FIGURES

Figure No.		Page
1.1	(Left) Laser trapping principle. (Right) Schematic representations for the trapping and assembly of nanoparticles, polymers, and molecular clusters. [Adapted from (Sugiyama et al., 2012).	3
1.2	5CB chemical structure. Adapted from (Yeng, Ayop, & Sasaki, 2022).	4
1.3	Liquid crystal internal configuration in a nematic liquid crystal microdroplet (a) bipolar and (b) radial. Observation under cross-polarization view [Adapted from ((Brasselet & Juodkazis, 2009)].	5
2.1	Forces exerting on a colloid microparticle near a focused beam. Adapted from (Konyshev & Byvalov, 2021).	16
2.2	The origin of the gradient force acting on a spherical particle near a non-focused (left) and focused (right) laser beam. Adapted from (Konyshev & Byvalov, 2021).	20
2.3	The F_r is acting on the trapped particle due to slight displacement from the laser trap center.	23
2.4	Linear graph of the trap stiffness versus beam powers (Aziz et al., 2016).	24
2.5	Trap stiffness as a function of laser power at the specimen plane, using the passive stiffness calibration method based on the power spectral density (Mohammad et al., 2014).	25
2.6	The optical stiffness graph against the chloroform microdroplet's size. Adapted from (Yusuf & Ayop, 2020).	27
2.7	Illustration of stuck bead sediment at the glass wall.	31
2.8	Microscopy images (top: brightfield, bottom: cross-polarized view correspond to the identical exact particles) of native corn starch granules (a and e), SMC60 particles (b and f), SMC65 particles (c and g), and SMC70 particles (d and h) in water (Wulff et al., 2020).	39

05-4506832 pustaka.upsi.edu.my Perpustakaan Tuanku Bainun Kampus Sultan Abdul Jalil Shah PustakaTBainun ptbupsi

05-4506832 pustaka.upsi.edu.my Perpustakaan Tuanku Bainun Kampus Sultan Abdul Jalil Shah PustakaTBainun ptbupsi

2.9	The developed system's optical trapping and manipulation of the 6 µm and 10 µm (Patel et al., 2021).	41
2.10	The graph of the x-axis position histogram for polystyrene microbead trapped in water for (a) p_1 and p_2.	42
2.11	The optimal microdroplet number for optical trapping (Yusof et al., 2020).	44
2.12	f_c for various microdroplet sizes at a 6.3 MW/cm^2 laser power density. The eye guides are drawn to indicate the trend of the f_c (Yusof et al., 2020).	45
2.13	The image of aerosol droplet optically trapped (a) 6.7 µm and (b) 2.0 µm (Taylor et al., 2005).	46
2.14	The molecular features of calamatic and discotic liquid crystals (Shen & Dierking, 2019).	49
2.15	Illustrates the thermotropic liquid crystal molecules arrangement the in the nematic, cholesteric, and sematic phases (Khoo, 2009).	50
2.16	The transition of the liquid crystal phase started from crystal to isotropic due to the heating process (Dierking & Al-zangana, 2017).	51
2.17	Schematic representation of the phase diagram of an amphiphilic surfactant in an isotropic solvent that forms lyotropic phases. (Dierking & Al-zangana, 2017).	52
2.18	Index ellipsoid for the case of uniaxial materials. (a) A plane perpendicular to the wave vector defines the plane of the electric field components experienced (n_o) and (n_{eff}). (b) The effective refractive index n_{eff} can be calculated with a geometric construction in the plane of incidence. Adapted from (Scharf, 2007).	53
2.19	The schematic diagram of the zenithal (θ) and azimuthal (φ) definition director angles to characterize the preferred orientation of a liquid crystal, set by alignment (easy axis) on a flat surface. Adapted from (Esteves et al., 2020).	56
2.20	(a) Planar alignment and (b) homeotropic director configuration of the liquid crystal molecules on the flat surface. $\vec{N}$ is a vector orthogonal to the plane surface and $\vec{n}$ is the director of the liquid crystal molecules. Adapted from (Esteves et al., 2020).	57
2.21	a) The illustration of bipolar configuration because of planar anchoring, (b) radial configuration because of homeotropic anchoring in droplet form. Adapted from (Esteves et al., 2020).	58

05-4506832 pustaka.upsi.edu.my Perpustakaan Tuanku Bainun Kampus Sultan Abdul Jalil Shah PustakaTBainun ptbupsi

05-4506832 pustaka.upsi.edu.my Perpustakaan Tuanku Bainun Kampus Sultan Abdul Jalil Shah PustakaTBainun ptbupsi

2.22	The snapshot of the polarized light microscopy images of nematic droplets (a) radial and (c) bipolar. The snapshot of bright field microscopy of (b) radial and (d) bipolar. The scale bar corresponds to 10 μm. Adapted from (Esteves et al., 2020).	59
2.23	5CB molecular structure (Khoo, 2009).	60
2.24	Method of making liquid crystal droplets. A: Vortex LC in water. B: Emulsifying liquid crystals using a homogenizer. C: Ultrasonic treatment of liquid crystals in water. D: Emulsifying liquid crystal in glycerol. E: Encapsulation of liquid crystals in polymeric microcapsules. F: Production of liquid crystal droplets using microfluidics. Adapted from (Wang et al., 2017).	62
2.25	An individual NLC microdroplet with a diameter of about 40 μm overhung out of one end of the microtube (Yan et al., 2017).	65
2.26	Micrographs of the stearic acid-doped 5CB microdroplets with different diameters (Duan et al., 2019).	65
2.27	Polarization optical microscopy images of 5CB droplets with different stirring times (a) 6 s; (b) 60 s; (c) 120 s; (d) 180 s; (e) 240 s; (f) relationship of the average diameter of droplets formed with stirring time. Scale bar: 500 μm. Adapted from (Niu et al., 2016).	67
2.28	The resulting mean droplet diameter (MDD) and polydispersity index (span) from different ultrasonic times of nanoemulsions. Adapted from (Asadinezhad et al., 2019).	69
2.29	The average droplet size is a function of exposure time on ultrasounds. Adapted from (Adamow et al., 2017).	70
2.30	The particle size of the gelation emulsion was treated with different sonication times. Adapted from (Li et al., 2023).	71
2.31	Concentration-diameter phase diagram of the 5CB liquid crystal droplets as a function of droplet diameter and SDS concentration. (a) All configurations, (b) bipolar, (c) monopolar and (d) radial are collectively represented (Shechter, Atzin, Moza, et al., 2020).	74
2.32	(a) Probability of a 5CB droplet having the internal radial alignment versus the concentration of cationic surfactant, 5CB internal configuration (b) radial and (c) bipolar (Murazawa, S. Juodkazis, 2005).	75
2.33	Visual image of bare E7 emulsion immediately after preparation (a), after storage 15 minutes and (c) 30 minutes respectively. Adapted from (Aery et al., 2023).	76

05-4506832 pustaka.upsi.edu.my Perpustakaan Tuanku Bainun Kampus Sultan Abdul Jalil Shah PustakaTBainun ptbupsi

05-4506832 pustaka.upsi.edu.my Perpustakaan Tuanku Bainun Kampus Sultan Abdul Jalil Shah PustakaTBainun ptbupsi

2.34	Variation of the diameter of 5CB microdroplets with time dispersed in PDMS. (Inset) Polarized optical microscope image of microdroplet with defects. Adapted from (Sofi & Dhara, 2019).	77
2.35	The schematic representation of polarization control of the incident trapping beam, the liquid crystal droplet was aligned according to the plane of polarization of the incident beam as shown in (a) to (e) (scale bar: 10 µm). Adapted from (Juodkazis et al., 1999).	79
2.36	(a)-(e) shows the spinning of the rotation of the liquid crystal droplet by circularly polarized light. Scale bar: 10 µm. Adapted from (Juodkazis et al., 1999).	80
2.37	Spinning radial 5CB droplet at 310 mW dragged floating droplet into orbiting motion. Scale bar, 10 µm. Adapted from (Murazawa, Juodkazis, & Misawa, 2005).	81
2.38	(a) Graph of rotation frequency, ω, of bipolar CB5 droplets against laser-power for diameters 3.2 µm (1), 2.5 µm (2), and 1.9 µm (3). (b) Graph of the rotation frequency of radial-5CB droplets against power for diameters 7.8 µm (1), 6.7 µm (2), 5.4 µm (3), and 4.8 µm (4). The lines act as guides for the eye. Adapted from (Murazawa, Juodkazis, & Misawa, 2005).	82
2.39	Sequences of the time evolution of POM images of an individual bipolar nematic 5CB droplet optically trapped by a linearly polarized trapping beam at (a) 130 mW (or 54 MW/cm^2) and (b) 850 mW (or 360 MW/cm^2). Adapted from (Usman et al., 2013).	84
2.40	Sequences of the time evolution of POM images of an individual bipolar nematic 5CB droplet optically trapped by a circularly (left-handed) polarized laser beam (a) at laser power 460 mW or 190 MW/cm^2, (b) an orbit of a tiny droplet around the rotating optically trapped droplet (the time is in seconds after the droplet starts to rotate), and (c) at laser power 940 mW or 390 MW/cm^2. (Usman et al., 2013).	85
2.41	The trapping location of the radial nematic liquid crystal (green rods) droplet shifted away from the droplet center under a linearly polarized light-trapping laser (red beam) (Phanphak et al., 2014).	88
2.42	A radial nematic liquid crystal droplet of 11.5 µm in diameter under the linearly polarized light optical trap of the following power: (a) without laser, (b) 28 mW, (c) 130 mW, (d) 246 mW. Adapted from (Phanphak et al., 2014).	89

05-4506832 pustaka.upsi.edu.my Perpustakaan Tuanku Bainun Kampus Sultan Abdul Jalil Shah PustakaTBainun ptbupsi

05-4506832 pustaka.upsi.edu.my Perpustakaan Tuanku Bainun Kampus Sultan Abdul Jalil Shah PustakaTBainun ptbupsi

2.43	A radial nematic liquid crystal microdroplet of 16.8 μm in diameter under 28 mW elliptical polarize optical light trap of the following elliptical angle: (a) without laser, (b) $\chi = 18^{\circ}$, (c) $\chi = 30^{\circ}$ and (d) $\chi = 45^{\circ}$. Adapted from (Phanphak et al., 2014).	90
2.44	An NLC droplet was found rotating clockwise under a linearly polarized laser trap at laser power 298 mW. The laser polarization direction was set at an angle $\beta = 135^{\circ}$ to the horizontal. Adapted from (Kiang-Ia et al., 2021).	93
2.45	The same 19-μm NLC droplet in Figure 2.44 rotated in the reverse direction under the same linearly polarized laser trap at a higher laser power of 635 mW. Adapted from (Kiang-Ia et al., 2021).	93
2.46	The graph of threshold laser power against droplet size clockwise and counterclockwise rotation. Adapted from (Kiang-Ia et al., 2021).	94
2.47	Optical micrograph of a micro-gear (r = 4 μm, h = 14 μm) rotating first to the left and then to the right under the control of the phase plate. Adapted with permission (Ito et al., 2012).	96
2.48	Experimental diagram of metalens-based optical tweezers. Adapted under the terms of the Creative Commons Attribution license (T-thienprasert, Limtrakul, Zentgraf, & Chattham, 2019).	97
2.49	Trapped bipolar and radial nematic liquid crystal microdroplet at P = 30 mW by circularly polarized light. Adapted under the terms of the Creative Commons Attribution (T-thienprasert, Limtrakul, Zentgraf, & Chattham, 2019).	98
2.50	Schematic diagram of the sensor using liquid crystal (Popov et al., 2017).	101
2.51	Liquid crystal droplet-based sensor for CA detection at varied concentrations. (a): 0 M; (b): 5 μM; (c): 25 μM; and (d): 50 μM. Scale bar: 200 μm. Adapted from (Niu et al., 2016).	104
2.52	The images of AIgG-anchored LC microdroplets incubated in PBS) with varied IgG concentrations at fixed liquid crystal microdroplets density (9×10^3 microdroplets per mL) anchored with 5 $mgmL^{-1}$ of AIgG under polarized optical microscopy at 30 minutes contact time and room temperature. IgG concentration: (a) 10 ng ml^{-1}, (b) 20 ng ml^{-1}, and (c) 50 ng ml^{-1}. Adapted from (Lee et al., 2015).	105

05-4506832 pustaka.upsi.edu.my Perpustakaan Tuanku Bainun Kampus Sultan Abdul Jalil Shah PustakaTBainun ptbupsi

05-4506832 pustaka.upsi.edu.my Perpustakaan Tuanku Bainun Kampus Sultan Abdul Jalil Shah PustakaTBainun ptbupsi

2.53	Experiment setup to monitor trapped 5CB light emission. Adapted from (Humar & Muševič, 2011).	108
2.54	5CB droplet structure (Figure 2.54 (a)), 5CB bright field microscopy images (Figure 2.54 (b)), and 5CB crossed polarization view images (Figure 2.54 (c)), the light emission concentration dependence of 5CB microdroplets in water (Figure 2.54 (d)-(e)). Adapted from (Humar & Muševič, 2011).	110
2.55	Illustration of the experimental setup for sensing. Adapted from (Duan et al., 2019).	112
2.56	(a) The series stearic acid-dope 5CB microdroplet of polarized optical microscope (POM) images exposed to 200 pM copper (II) chloride in PBS solution at a specific time, (b) corresponding lasing spectra of POM images. Black dots represent the position of the WGM selected to monitor the spectral shifting of the droplet lasing emission. Scale bar: 20 μm. Adapted from (Duan et al., 2019).	113
3.1	The research flowchart.	128
3.2	The actual (OTKB/M) system.	129
3.3	OTKB/M schematic diagram for optical trapping.	132
3.4	The snapshot of piezostage with labeled components.	133
3.5	The actual image of the butterfly laser diode used as the trapping laser source.	134
3.6	The image of a compact laser diode driver for controlling laser diode power.	134
3.7	The image of the laser power meter used in current-to-power calibration.	135
3.8	The plot of laser power (P) versus laser current (I) for calibrating the trapping laser in front of the objective lens.	136
3.9	A 100× magnification, 1.25 NA, 0.23 mm WD oil immersion objective.	138
3.10	Test cell under observation.	139
3.11	The live image of the CCD camera is displayed on the PC.	140
3.12	The front panel of the uploaded image of the calibration slide micro ruler in the ImageJ software.	141

05-4506832 pustaka.upsi.edu.my Perpustakaan Tuanku Bainun Kampus Sultan Abdul Jalil Shah PustakaTBainun ptbupsi

05-4506832 pustaka.upsi.edu.my Perpustakaan Tuanku Bainun Kampus Sultan Abdul Jalil Shah PustakaTBainun ptbupsi

3.13	The snapshot of the ImageJ front panel shows the straight-line measurement to determine the distance between two consecutive scales in pixels.	141
3.14	A QPD (PDQ80A, Thorlabs) is used for position sensing in OTKB/M.	144
3.15	The laser alignment procedure displays the position of the laser spot on the QPD via the APT user program.	144
3.16	The QPD diagram with four quadrant labels labeled a, b, c, and d.	145
3.17	Voltage waveform display on the Yokogawa DL6054 digital oscilloscope.	147
3.18	The graph of corner frequency (f_c) against laser optical power density (P) for optically trapped polystyrene microbeads in water.	149
3.19	The graph of optical stiffness (k_T) against laser optical power density (P) for optically trapped polystyrene microbeads in water.	149
3.20	The schematic diagram of the 5CB internal configuration (a) bipolar and (b) radial.	150
3.21	The snapshot of purchased 4-cyano-4'-pentylbiphenyl (5CB) in a glass bottle.	152
3.22	The schematic diagram of bipolar 5CB microdroplet suspension solution production.	152
3.23	The snapshot of the sonication process of liquid 5CB and deionized water mixture to produce a 5CB microdroplet suspension solution.	153
3.24	The snapshot of the mixture of the liquid 5CB and deionized water (a) before and (b) after the sonication process. The cloudy solution was formed after sonication, indicating the formation of the 5CB microdroplet suspension.	154
3.25	The image of the cell chamber (a) the 5CB microdroplet suspension was dropped on the glass slide, (b) the cover glass was assembled to the glass slide with two strips of double-sided tape, and (c) the schematic diagram of the cell chamber.	155
3.26	The effect of the CTAB solution volume on the formation of the radial 5CB microdroplet suspension.	156

05-4506832 pustaka.upsi.edu.my Perpustakaan Tuanku Bainun Kampus Sultan Abdul Jalil Shah PustakaTBainun ptbupsi

05-4506832 pustaka.upsi.edu.my Perpustakaan Tuanku Bainun Kampus Sultan Abdul Jalil Shah PustakaTBainun ptbupsi

3.27	The schematic diagram summarizes the production of the radial 5CB microdroplet suspension solution.	158
3.28	The actual image of the Inverted Metallurgical Microscope GX51 for observing and viewing purposes.	159
3.29	The schematic diagram of the Inverted Metallurgical Microscope GX51.	160
3.30	The actual particles (5CB microdroplet images) are seen at the specific focal plane.	161
3.31	Front Panel of ImageJ software.	161
3.32	(a) The image of the calibration slide ruler was observed under an inverted optical microscope (20× objective lens), (b) the front panel of an uploaded image of the calibration slide ruler in ImageJ software.	162
3.33	The snapshot of the straight-line measurement function is labeled with a dashed circle.	162
3.34	The zoomed Figure 3.32 (b) to demonstrates the Measurement of the distance between two scales of calibration ruler by a straight-line measurement. The obtained length was 40.608 pixels.	163
3.35	The snapshot of the (a) uncalibrated 5CB microdroplet image under an optical microscope and (b) front panel of uploaded 5CB microdroplets images by ImageJ software.	165
3.36	(a) Front panel for analysis and set scale function, (b) set scale front panel for calibration.	166
3.37	(a) Front panel for 8-bit image conversion and (b) image of 5CB microdroplets after 8-bit conversion.	167
3.38	The snapshot of the ImageJ front panel (a) front panel to impose bandpass filter, (b) FFT bandpass filter setting, and (c) the resulting image of the FFT bandpass filter imposed on the 5CB microdroplet image.	168
3.39	The snapshot of the (a) front panel for the Threshold option and (b) front panel for the “Threshold” setting.	169
3.40	(a) ImageJ automatic threshold highlighting the visible 5CB microdroplet with the red color, (b) the image of 5CB microdroplet after threshold measurement made by ImageJ.	170
3.41	(a) ImageJ front panel view for Analyze Particle option, Figure 3.41 (b) The front panel of Analyze Particles popup.	171

05-4506832 pustaka.upsi.edu.my Perpustakaan Tuanku Bainun Kampus Sultan Abdul Jalil Shah PustakaTBainun ptbupsi

05-4506832 pustaka.upsi.edu.my Perpustakaan Tuanku Bainun Kampus Sultan Abdul Jalil Shah PustakaTBainun ptbupsi

3.42	(a) Outlines the measured 5CB microdroplet area, and (b) the tabulated number and area of each measured 5CB microdroplet.	172
3.43	Schematic diagram of the 5CB microdroplet suspension (1.8 mL) for stability inspection by UV-Vis spectroscopy.	174
3.44	The actual image of the half-wave plate and (b) the position of the half-wave plate inserted in the optical path of the optical tweezers setup.	176
3.45	The schematic diagram shows the half-wave plate was oriented to angle θ, to the incoming perpendicular direction linearly polarized laser beam produced a horizontal linearly polarized laser beam to angle 2θ. Adapted from Standa Photonics.	177
3.46	The actual image of the quarter wave-plate and (b) the position of the quarter-wave plate inserted in the optical path of the optical tweezers setup.	178
3.47	The schematic diagram shows the quarter wave-plate was oriented to angle $\theta = 45^{o}$, to the incoming perpendicular direction linearly polarized laser beam produced a left-handed circularly polarized laser beam. Adapted from Standa Photonics.	179
3.48	The snapshot of the APT's User Software interface to control the translation of the piezostage.	180
3.49	The schematic diagram of the translation of the trapped particle by the piezostage control.	181
3.50	The front panel of the APT's User translates the piezostage 5 μm to the right.	182
3.51	The schematic diagram of the translation and micro-control of the trapped 5CB microdroplet under a circularly polarized laser beam. The trapped 5CB microdroplet was rotated when the laser beam trapped it.	183
3.52	The screenshot of the Tracker Software to import the recorded video of the trapped 5CB microdroplet.	184
3.53	The snapshot of the calibrated recorded video of the trapped 5CB microdroplet by the Tracker Software.	185
3.54	The snapshot of the Tracker Software interface demonstrated the tracking procedure on the respected interest particle.	186
3.55	The snapshot of the Tracker Software's main front panel and the Autotracker function's front panel.	186

05-4506832 pustaka.upsi.edu.my Perpustakaan Tuanku Bainun Kampus Sultan Abdul Jalil Shah PustakaTBainun ptbupsi

05-4506832 pustaka.upsi.edu.my Perpustakaan Tuanku Bainun Kampus Sultan Abdul Jalil Shah PustakaTBainun ptbupsi

3.56	The snapshot of the Tracker Software, on the right side, shows the result of the tracked particle presented in the form of graph position in the *x*-direction and *y*-direction against time.	187
3.57	The snapshot of the trajectory data from the translation of the trapped particle.	188
3.58	The flowchart for measuring 5CB microdroplet radius (r) and corner frequency (f_c) using the ImageJ program and OSCal program.	190
3.59	The snapshot of the ImageJ Software front panel showed the uploaded and calibrated image of the trapped 5CB microdroplet.	191
3.60	The snapshot of the converted trapped 5CB microdroplet RGB image in Figure 3.59 to 8-bit.	192
3.61	(a) The snapshot of the Threshold front panel and (b) the corresponding display of the threshold measured on the trapped 5CB microdroplet image.	193
3.62	The snapshot of the image of the trapped 5CB microdroplet measured according to the set threshold in Figure 3.76 and (b) The snapshot of the Analyze Particles front panel to measure the area of the trapped 5CB microdroplet.	194
3.63	(a) The snapshot of the front panel shows the measured area of the trapped 5CB microdroplet image by ImageJ software. Figure 3.63 (b) The snapshot front panel shows the result of the area measured of the trapped 5CB microdroplet image by ImageJ Software.	194
3.64	Process of deleting headers inside Columns A1 to C15 of the signal data in Excel.	196
3.65	The interface of OSCal without any voltage signal data.	197
3.66	Selecting the directory of the data stored in the USB drive.	197
3.67	Data selection to upload into OSCal software.	198
3.68	The QPD voltage signal is displayed in the OSCal interface.	199
3.69	OSCal interface for Y-Power Spectrum of 3.0 μm 5CB microdroplet.	200
3.70	The result of the power spectrum fitted with Lorentzian fitting.	201
3.71	The flowchart for the rotatability of trapped 5CB microdroplet analysis.	202

05-4506832 pustaka.upsi.edu.my Perpustakaan Tuanku Bainun Kampus Sultan Abdul Jalil Shah PustakaTBainun ptbupsi

05-4506832 pustaka.upsi.edu.my Perpustakaan Tuanku Bainun Kampus Sultan Abdul Jalil Shah PustakaTBainun ptbupsi

3.72	The graph is plotted from the QPD signal to determine the average time for a complete 2π rotation.	203
3.73	The flow chart of the optical trapping of a single 5CB microdroplet in CTAB solution.	205
3.74	The schematic diagram of the cell chamber (a) top view and (b) side view. The actual image of the cell chamber is shown in (c).	206
3.75	Schematic diagram of adding CTAB solution to the sample chamber edge.	208
3.76	The graph of voltage against time represents the trajectory of the trapped single 5CB microdroplet in water.	211
4.1	The snapshots of bipolar 5CB microdroplet suspension under optical microscopy sonicated at (a) t = 1 minute, (b) t = 2 minutes, (c) t = 3 minutes, and (d) t = 10 minutes for V_{H2O} = 1 mL. The inset shows the internal configuration of the bipolar 5CB microdroplet.	216
4.2	The snapshots of bipolar 5CB microdroplet suspension under optical microscopy sonicated at (a) t = 1 minute, (b) t = 2 minutes, (c) t = 3 minutes, and (d) t = 10 minutes for V_{H2O} = 1 mL. The inset shows the internal configuration of the radial 5CB microdroplet.	217
4.3	The average radius r, of 5CB microdroplets versus sonication time for (a) bipolar and (b) radial.	218
4.4	The absorption spectrum of 5CB for a 1-hour monitoring period.	225
4.5	The graph of peak versus time is in Figure 4.4 for (a) bipolar and (b) radial 5CB microdroplet suspension in water.	227
4.6	The graph of peak versus time in Figure 4.5 absorbance against time (a) bipolar 5CB and water, (b) radial 5CB, water, and CTAB.	228
4.7	Image sequence of the 0.7 μm bipolar 5CB microdroplet capturing into optical tweezers trap (red dash circle) at 0.2 MW/cm^2. The red arrows indicate the polarization direction of the trapping laser.	230
4.8	Image sequence of the 1.0 μm radial 5CB microdroplet capturing into optical tweezers trap (red dash circle) at 0.2 MW/cm^2. The red arrows indicate the polarization direction of the trapping laser.	231

05-4506832 pustaka.upsi.edu.my Perpustakaan Tuanku Bainun Kampus Sultan Abdul Jalil Shah PustakaTBainun ptbupsi

05-4506832 pustaka.upsi.edu.my Perpustakaan Tuanku Bainun Kampus Sultan Abdul Jalil Shah PustakaTBainun ptbupsi

4.9	The snapshot of 2.0 μm bipolar 5CB microdroplet trap at 0.2 MW/cm^2 at varied polarization direction, θ. The red arrows indicate the polarization direction of the trapping laser.	234
4.10	The snapshot of 2.0 μm bipolar 5CB microdroplet trap at 0.2 MW/cm^2 at varied polarization direction, θ under cross-polarized view. The red arrows indicate the polarization direction of the trapping laser.	234
4.11	The schematic diagram of 5CB molecules orientation inside the microdroplet to the polarization direction of linearly polarized light. The red arrows indicate the polarization direction of the trapping laser.	235
4.12	The snapshot of 3.3 μm radial 5CB microdroplet trap at 0.2 MW/cm^2 at varied polarization direction, θ. The red arrows indicate the polarization direction of the trapping laser.	237
4.13	The snapshot of 3.3 μm radial 5CB microdroplet trap at 0.2 MW/cm^2 at varied polarization direction, θ under cross-polarized view. The red arrows indicate the polarization direction of the trapping laser.	238
4.14	The schematic diagram of 5CB molecules orientation inside the microdroplet to the polarization direction of linearly polarized light. The red arrows indicate the polarization direction of the trapping laser.	238
4.15	The snapshot of a rotated bipolar 5CB microdroplet of 2.1 μm diameter in water by a circularly polarized laser beam.	240
4.16	(a) Schematic diagram of bipolar 5CB microdroplet rotates in an optical trap and (b) QPD signal of the rotated 5CB microdroplet.	240
4.17	The snapshot of rotated radial 5CB microdroplet of 2.9 μm diameter in water by a circularly polarized laser beam.	241
4.18	(a) The schematic diagram of a radial 5CB microdroplet rotates about a circle (b), which is the typical QPD signal of the rotating 5CB microdroplet.	241
4.19	The translation and micro-control of a single 1.8 μm bipolar 5CB microdroplet by a linearly polarized laser beam at 0.2 MW/cm^2. A: The 5CB microdroplet was trapped in the optical trap at t_1= 1 s. B: The 5CB microdroplet translation 5 μm to the right at t_2 = 10 s. C: The 5CB microdroplet retrapped at t_3 = 15 s. D: The 5CB microdroplet translation 5 μm to the left at t_4 = 25 s. E: The 5CB microdroplet retrapped at t_5 = 27 s.	243

05-4506832 pustaka.upsi.edu.my Perpustakaan Tuanku Bainun Kampus Sultan Abdul Jalil Shah PustakaTBainun ptbupsi

05-4506832 pustaka.upsi.edu.my Perpustakaan Tuanku Bainun Kampus Sultan Abdul Jalil Shah PustakaTBainun ptbupsi

4.20	The translation and micro-control of a single 1.8 μm bipolar 5CB microdroplet by a circularly polarized laser beam at 0.2 MW/cm^2. A: The 5CB microdroplet was trapped and rotated in the optical trap at t_1 = 1 s. B: The 5CB microdroplet translation 5 μm to the right at t_2 = 10 s. C: The 5CB microdroplet retrapped and rotated at t_3 = 13 s. D: The 5CB microdroplet translation 5 μm to the left at t_4 = 25 s. E: The 5CB microdroplet retrapped and rotated at t_5 = 28 s.	243
4.21	(a) The *x*-axis trajectory of the trapped bipolar 5CB microdroplet is in Figure 4.19 and (b) in Figure 4.20.	245
4.22	The translation and micro-control of a single 3.3 μm radial 5CB microdroplet by a linearly polarized laser beam at 0.2 MW/cm2. A: The 5CB microdroplet was trapped in the optical trap at t_1 = 1 s. B: The 5CB microdroplet translation 5 μm to the right at t_2 = 10 s. C: The 5CB microdroplet retrapped at t_3 = 11 s. D: The 5CB microdroplet translation 5 μm to the left at t_4 = 25 s. E: The 5CB microdroplet retrapped at t_5 = 28 s.	246
4.23	The translation and micro-control of a single 3.3 μm radial 5CB microdroplet by a circularly polarized laser beam at 0.2 MW/cm^2. A: The 5CB microdroplet was trapped and rotated in the optical trap at t_1 = 1 s. B: The 5CB microdroplet translation 5 μm to the right at t_2 = 10 s. C: The 5CB microdroplet retrapped and rotated at t_3 = 13 s. D: The 5CB microdroplet translation 5 μm to the left at t_4= 25 s. E: The 5CB microdroplet retrapped and rotated at t_5 = 32 s.	246
4.24	(a) The *x*-axis trajectory of the trapped radial 5CB microdroplet is in Figure 4.22 and (b) in Figure 4.23.	248
4.25	Graph of corner frequency (f_c) versus optical power density (P) for (a) bipolar and (b) radial.	251
4.26	Graph of corner frequency per microdroplet radius ($\frac{f_c}{r}$) versus optical power density (P) for (a) bipolar and (b) radial.	252
4.27	Graph of corner frequency per microdroplet radius ($\frac{f_c}{r}$) against microdroplet radius at varied optical power density.	255
4.28	The ray optics diagram of laser focus of w_0 beam waist trapped two spheres of diameter d_1 and d_2 (Malagnino et al., 2002).	256
4.29	Graph of angular speed (ω) versus optical power density (P) of clockwise rotation for (a) bipolar 5CB and (b) radial 5CB microdroplets.	265

05-4506832 pustaka.upsi.edu.my Perpustakaan Tuanku Bainun Kampus Sultan Abdul Jalil Shah PustakaTBainun ptbupsi

05-4506832 pustaka.upsi.edu.my Perpustakaan Tuanku Bainun Kampus Sultan Abdul Jalil Shah PustakaTBainun ptbupsi

4.30	Graph of angular speed per microdroplet radius ($\frac{\omega}{r}$) versus optical power density (P) of clockwise rotation for (a) bipolar 5CB and (b) radial 5CB microdroplets.	268
4.31	Graph of angular speed (ω) versus optical power density (P) of counterclockwise rotation for (a) bipolar 5CB and (b) radial 5CB microdroplets.	270
4.32	Graph of angular speed per microdroplet radius ($\frac{\omega}{r}$) versus optical power density (P) of clockwise rotation for (a) bipolar 5CB and (b) radial 5CB microdroplets.	273
4.33	The schematic mechanism of the interaction between the 5CB microdroplet with the CTAB molecules and the effect on the internal configuration inside the microdroplet.	279
4.34	The transition sequence changed of the bipolar 5CB microdroplet to the radial internal configuration of 1.4 μm trapped at 0.2 MW/cm^2 linearly polarized laser beam.	283
4.35	Graph of displacement variance (σ^2) versus time of 1.4 μm bipolar 5CB microdroplet trapped by a linearly polarized laser beam at 0.2 MW/cm^2.	285

05-4506832 pustaka.upsi.edu.my Perpustakaan Tuanku Bainun Kampus Sultan Abdul Jalil Shah PustakaTBainun ptbupsi
05-4506832 pustaka.upsi.edu.my Perpustakaan Tuanku Bainun Kampus Sultan Abdul Jalil Shah PustakaTBainun ptbupsi

05-4506832 pustaka.upsi.edu.my Perpustakaan Tuanku Bainun Kampus Sultan Abdul Jalil Shah PustakaTBainun ptbupsi

LIST OF SYMBOLS

SYMBOLS	MEANING	UNITS
r	Radius	m
k_B	Boltzmann constant	J/K
T	Temperature	K
F_g	Gradient force	N
F_s	Scattering force	N
D	Diameter	m
λ	Wavelength	nm
n	Refractive index	---
F_r	Restoring force	N
σ^2	Displacement variance	V^2
k	Optical stiffness	pN/μm
f_c	Corner frequency	Hz
ω	Angular speed	Hz
Γ	Optical torque	Nm
P	Optical power density	MW/cm^2

05-4506832 pustaka.upsi.edu.my Perpustakaan Tuanku Bainun Kampus Sultan Abdul Jalil Shah PustakaTBainun ptbupsi

05-4506832 pustaka.upsi.edu.my Perpustakaan Tuanku Bainun Kampus Sultan Abdul Jalil Shah PustakaTBainun ptbupsi

LIST OF CONSTANT

SYMBOLS	MEANING	UNITS
π	Pi constant	
k_B	Boltzmann constant	J/K

05-4506832 pustaka.upsi.edu.my Perpustakaan Tuanku Bainun Kampus Sultan Abdul Jalil Shah PustakaTBainun ptbupsi
05-4506832 pustaka.upsi.edu.my Perpustakaan Tuanku Bainun Kampus Sultan Abdul Jalil Shah PustakaTBainun ptbupsi

05-4506832 pustaka.upsi.edu.my Perpustakaan Tuanku Bainun Kampus Sultan Abdul Jalil Shah PustakaTBainun ptbupsi

LIST OF ABBREVIATIONS

ASCII	American Standard Code for Information Interchange
CCD	Charged Couple Device
NA	Numerical Aperture
PSD	Power Spectrum Density
QPD	Quadrant-Photodiode
WD	Working distance
ET	Equipartition Theorem
BS	Boltzmann Statistics
NLCM	Nematic Liquid Crystal Microdroplet
PDMS	Polydimethylsiloxane
LC	Liquid Crystal
SDS	Sodium Dodecyl Sulfate
CTAB	Centrimonium Bromide

05-4506832 pustaka.upsi.edu.my Perpustakaan Tuanku Bainun Kampus Sultan Abdul Jalil Shah PustakaTBainun ptbupsi

05-4506832 pustaka.upsi.edu.my Perpustakaan Tuanku Bainun Kampus Sultan Abdul Jalil Shah PustakaTBainun ptbupsi

APPENDIX LIST

A	Knowledge Dissemination
B	System Specification
C	Corner Frequency per Microdroplet Radius Comparison
D	Angular Speed per Microdroplet Radius Comparison

05-4506832 pustaka.upsi.edu.my Perpustakaan Tuanku Bainun Kampus Sultan Abdul Jalil Shah PustakaTBainun ptbupsi
05-4506832 pustaka.upsi.edu.my Perpustakaan Tuanku Bainun Kampus Sultan Abdul Jalil Shah PustakaTBainun ptbupsi

05-4506832 pustaka.upsi.edu.my Perpustakaan Tuanku Bainun Kampus Sultan Abdul Jalil Shah PustakaTBainun ptbupsi

CHAPTER 1

INTRODUCTION

05-4506832 pustaka.upsi.edu.my Perpustakaan Tuanku Bainun Kampus Sultan Abdul Jalil Shah PustakaTBainun ptbupsi

1.1 Research Background

The light radiation pressure exerts a force when it comes into contacts with a particle. The force that arises from the light radiation pressure is called optical force. The optical force was applied in an instrument called optical tweezers. Arthur Ashkin, the pioneer of optical trapping, was awarded the 2018 Nobel Prize in Physics for his invention of optical tweezers for biological applications (Goswami, 2018). Optical tweezers use a strong, focused laser beam to confine the particle by benefiting optical force. Optical

05-4506832 pustaka.upsi.edu.my Perpustakaan Tuanku Bainun Kampus Sultan Abdul Jalil Shah PustakaTBainun ptbupsi

05-4506832 pustaka.upsi.edu.my Perpustakaan Tuanku Bainun Kampus Sultan Abdul Jalil Shah PustakaTBainun ptbupsi

forces mainly contributed to the pulling gradient force and pushing scattering force in optical trapping.

It is possible to manipulate small objects in the range of micrometers or smaller using light by optical tweezers (Malmqvist & Hertz, 1992; Pai, Zandrini, Mart, & Bragheri, 2018). The intense focus laser beam creates an optical trap where it provides non-contact micro-manipulation of a non-destructive technique of the trap particle. Subsequently, optical trapping provides minimization of the sample flaw, especially when handling soft and fragile particles like biological material. Optical trapping not only provides manipulation of the trap particle but also provides several applications. In the context of optical trapping applications, it is possible to conduct physical measurements such as viscosity, stiffness, and elasticity for example, DNA, with the help of polystyrene or silica probing (Buosciolo et al., 2004; Müllenbroich et al., 2013). The study of the microparticle trajectory by the optical trapping is useful for microrheological measurement (Aziz et al., 2015). These are the several applications performed by the optical trapping.

Optical trapping is also used in the chemistry field. This process is called laser trapping. Laser trapping application involves the system domain from quantum-scale atom trapping to the micro-scale system (David et al., 2013; Neves et al., 2015). Laser trapping shows a novel potential for light-matter interaction in molecular systems by triggering nucleation-induced crystallization growth and supramolecular assemblies (Sugiyama et al., 2012; Supian et al., 2010). Figure 1.1 (left) illustrates the laser trapping principle, while Figure 1.1 (right) illustrates the trapping assembly of

05-4506832 pustaka.upsi.edu.my Perpustakaan Tuanku Bainun Kampus Sultan Abdul Jalil Shah PustakaTBainun ptbupsi

05-4506832 pustaka.upsi.edu.my Perpustakaan Tuanku Bainun Kampus Sultan Abdul Jalil Shah PustakaTBainun ptbupsi

nanoparticles, polymers, and molecular clusters. The red parabolic line represents the optical potential energy in the sample.

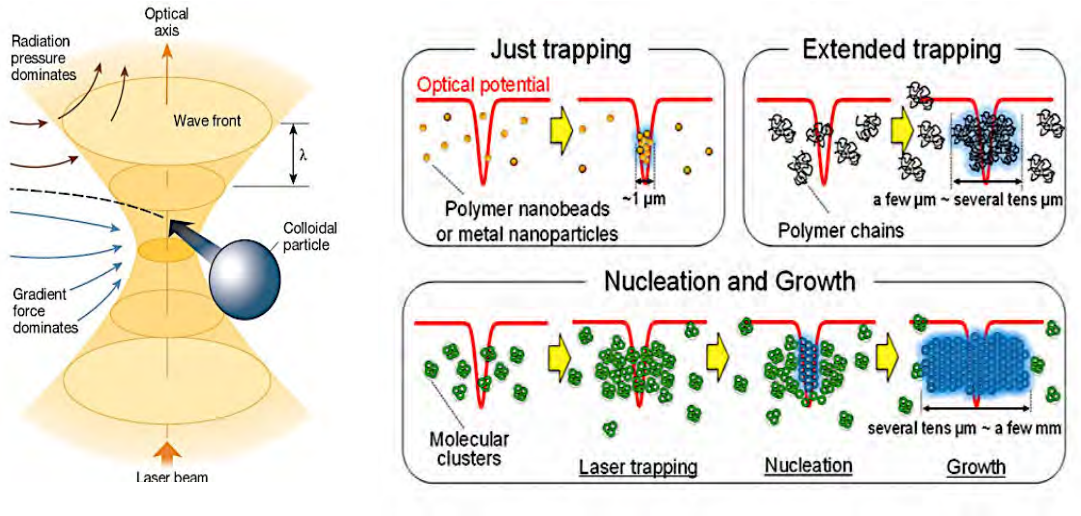


Figure 1.1. (Left) Laser trapping principle. (Right) Schematic representations for the trapping and assembly of nanoparticles, polymers, and molecular clusters. [Adapted from (Sugiyama et al., 2012).

05-4506832 pustaka.upsi.edu.my Perpustakaan Tuanku Bainun Kampus Sultan Abdul Jalil Shah PustakaTBainun ptbupsi

The application of laser trapping can be classified into Just trapping, Extended trapping, and Nucleation and Growth. The "Just trapping" refers to the laser trapping of polymers that occurs within the laser spot size in the range of ~ 1 μm. The "Extended trapping" of polymer chains can occur within a few to several tens microns beyond laser spot size due to the nature of the polymer, for example, due to intermolecular interactions. Lastly, in the context of nucleation and growth, nucleation is induced, resulting in a large crystal scale from several ten microns to a few millimeters. The extension of optical trapping beyond just trapping capability has opened a new direction in molecular control using light.

05-4506832 pustaka.upsi.edu.my Perpustakaan Tuanku Bainun Kampus Sultan Abdul Jalil Shah PustakaTBainun ptbupsi

05-4506832 pustaka.upsi.edu.my Perpustakaan Tuanku Bainun Kampus Sultan Abdul Jalil Shah PustakaTBainun ptbupsi

Recently, the optical trapping has shifted from trapping solid matter to soft matter, such as liquid crystals. Liquid crystal has unique properties where it co-exists in between solid and liquid states, anisotropic, birefringent, and sensitive to electric and magnetic fields (Brasselet & Juodkazis, 2009; Phanphak et al., 2014). Optical trapping of the liquid crystal can be performed in the form of a liquid film or a microdroplet (Brasselet, 2008; Brasselet et al., 2003). Interestingly, liquid crystal obtains multiple domain configurations, such as nematic, smectic, and cholesteric, which are sensitive to the light polarization state (Brasselet & Juodkazis, 2009). 4'-Pentyl-4-cyanobiphenyl (5CB) is one of the most attractive nematic liquid crystals (NLC) as it exhibits liquid crystal properties of nematic phase domain at room temperature (18–35 °C) (Hanemann et al., 1995). Therefore, 5CB is a suitable model compound to study the physical behavior of simple nematics. Figure 1.2 shows the chemical structure of 5CB.

05-4506832 Perpustakaan Tuanku Bainun Kampus Sultan Abdul Jalil Shah PustakaTBainun ptbupsi

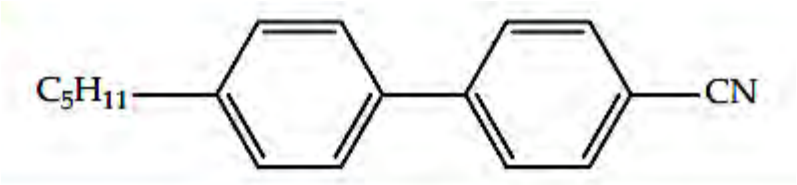


Figure 1.2. 5CB chemical structure. Adapted from (Yeng, Ayop, & Sasaki, 2022).

The dispersion of liquid crystals with an immiscible solvent such as water creates liquid crystal droplets. For example, 5CB produces a nematic liquid crystal droplet in water. In droplet form, the nematic liquid crystal has a unique internal configuration. Internal configuration refers to the domain alignment within the nematic liquid crystal droplet. The internal configuration can be controlled by surface modification with a surfactant. Tailored polarization of light can manipulate a single

05-4506832 pustaka.upsi.edu.my Perpustakaan Tuanku Bainun Kampus Sultan Abdul Jalil Shah PustakaTBainun ptbupsi

05-4506832 pustaka.upsi.edu.my Perpustakaan Tuanku Bainun Kampus Sultan Abdul Jalil Shah PustakaTBainun ptbupsi

nematic liquid crystal microdroplet (Usman et al., 2011). Figure 1.3 shows an example of the internal configuration of a nematic liquid crystal microdroplet.

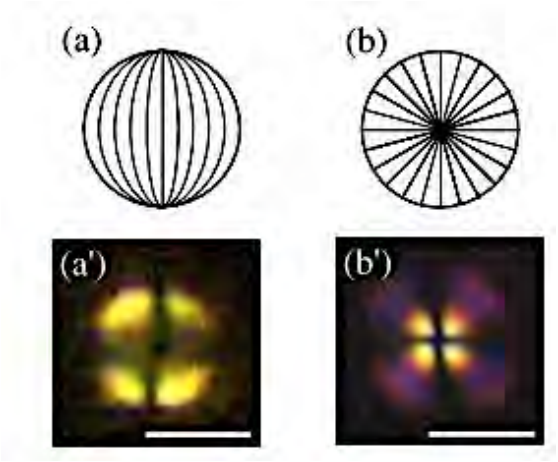


Figure 1.3. Liquid crystal internal configuration in a nematic liquid crystal microdroplet (a) bipolar and (b) radial. Observation under cross-polarization view [Adapted from ((Brasselet & Juodkazis, 2009)].

05-4506832 pustaka.upsi.edu.my Perpustakaan Tuanku Bainun Kampus Sultan Abdul Jalil Shah PustakaTBainun ptbupsi

Optical trapping of nematic liquid crystal microdroplets is possible when the refractive index of the droplet is larger than the surrounding refractive index. Instead of using solid silica and polymer particles, an optically engineered liquid crystal microdroplet is flexibly shaped, allowing rotational control when exposed to the light polarization during optical trapping (Pai et al., 2018). This proposed study will help to design microfluidic devices that integrate liquid crystals as optically controlled microactuators in water filtration devices, lab-on-chips, liquid crystal-based sensors, or new technologies.

As sensitive sensors, liquid crystal droplets are indispensable in environmental and biomedical science (Niu et al., 2016). This is because liquid crystal droplets are a potential optical, biological sensor due to high birefringence and high sensitivity of

05-4506832 pustaka.upsi.edu.my Perpustakaan Tuanku Bainun Kampus Sultan Abdul Jalil Shah PustakaTBainun ptbupsi

05-4506832 pustaka.upsi.edu.my Perpustakaan Tuanku Bainun Kampus Sultan Abdul Jalil Shah PustakaTBainun ptbupsi

liquid alignment of liquid crystal molecules to minute variation on the surface. Molecular events occurring at an interface between liquid crystal and water can be amplified and converted into electrical signals by the change in orientation of liquid crystal molecules, which are visible to the naked eye under a polarizing microscope (Niu et al., 2016). The liquid crystal-based sensor can detect proteins, nucleic acids, acetylcholine, glucose, enzymes, cholic acid, antibodies, and other molecules during sensing application.

1.2 Problem Statement

Optical tweezers are commonly used to trap and manipulate particles in a liquid. For example, most microscopic biological particles must be trapped within the liquid. Recent studies showed that microparticles in liquids can form two-dimensional structures by laser guidance (Kudo et al., 2016; Shih et al., 2021; Wu et al., 2018). However, it was experimentally successful with gold nanoparticles and polystyrene beads, even if the theoretical explanation of the observed phenomena is not yet mature. One hypothesis states that the lattice-like arrangement is due to light propagation through the dielectric properties of the trapped particles. Liquid crystals can have both solid-like and liquid-like properties. The magnetic, electrical, and optical methods can control the internal configuration inside the liquid crystal droplet. The physical properties of liquid crystals depend highly on the alignment of liquid crystal molecules in a closed cell. The study of optical trapping utilizing light propagation catalyzes new pathways in the assembly, manipulation, and crystallization

05-4506832 pustaka.upsi.edu.my Perpustakaan Tuanku Bainun Kampus Sultan Abdul Jalil Shah PustakaTBainun ptbupsi

05-4506832 pustaka.upsi.edu.my Perpustakaan Tuanku Bainun Kampus Sultan Abdul Jalil Shah PustakaTBainun ptbupsi

of microparticles, nanoparticles, supramolecules, and soft matter, as anticipated in this study.

The previous researcher reports that the general formulation of nematic liquid crystal microdroplet production thus leads to a reproducibility problem (Choi et al., 2015; Juodkazis et al., 1999; Lee et al., 2015; Murazawa, S. Juodkazis, 2005; Suga et al., 2018; Z. Wang et al., 2020). There are no specific formulations, recipes, or technical reports to prepare nematic liquid crystal microdroplets. The reported nematic liquid crystal microdroplet was relatively large (>10 μm) (Duan et al., 2019; Kiang-Ia et al., 2021; Shechter et al., 2020). The nematic liquid crystal microdroplet must be a small, miniaturized version of the liquid crystal-based probe. The bigger liquid crystal microdroplet is inert with a small optical force in optical trapping application. The smaller probe can increase surface volume sensitivity for sensing applications.

Furthermore, although previous researchers reported optical trapping of a single nematic liquid crystal microdroplet, they only reported qualitative observation of nematic liquid crystal microdroplet trapping by studying the behavior of the trapped liquid crystal microdroplet under light polarization (Phanphak et al., 2014; Shechter et al., 2020; Usman et al., 2013). No study quantifies the change in the internal configuration of the nematic liquid crystal microdroplets in terms of optical signal but instead just observing the changes visually (Murazawa, Juodkazis, Matsuo, et al., 2005; Shechter et al., 2020). The study of the optical stiffness of nematic liquid crystal microdroplets based on the optical which is relevant for evaluating the strength of the optical trap, is also not reported. Hence, there is a lack of information on the trend of

05-4506832 pustaka.upsi.edu.my Perpustakaan Tuanku Bainun Kampus Sultan Abdul Jalil Shah PustakaTBainun ptbupsi

05-4506832 pustaka.upsi.edu.my Perpustakaan Tuanku Bainun Kampus Sultan Abdul Jalil Shah PustakaTBainun ptbupsi

optical stiffness with exposure to different optical power densities and microdroplet sizes for soft matter optical trapping.

In addition, the optical manipulation of the liquid crystal microdroplet has been reported on the dynamic behavior when the laser polarization state used is varied (Saito & Kimura, 2022). However, there is no combination of simultaneous translational and polarization control of liquid crystal microdroplet has been reported. This combination is expected to enrich liquid crystal microdroplets for actuating application. In the context of rotational study, the laser power used is larger, and the size of the microdroplet is bigger, as reported by previous researchers. This becomes an issue when the use of strong laser power tends to destroy the liquid crystal nematic phase, and bigger microdroplets are challenging to actuate in tiny areas of actuation. Hence, there is a requirement to reduce laser power and microdroplet size for actuating application using liquid crystal microdroplet trapping.

The conventional liquid crystal-based sensor observes the transition liquid crystal configuration without converting the changes into a quantitative signal, possibly causing the false judgment when the liquid crystal microdroplet is smaller (Lee et al., 2015; Niu et al., 2016). The existing liquid crystal-based sensor requires many large liquid crystal droplet sizes for detection because the detection is based on the internal configurational change of bigger microdroplets (Lee et al., 2015; Niu et al., 2016). The current liquid crystal-based sensor applied a lasing technique to increase the detection sensitivity by using only a single microdroplet. However, the microdroplet used for detection is stuck on the glass slide or hung at the end of the micro syringe which causes deformation in shape because of poor control, immobilize and bigger droplet size,

05-4506832 pustaka.upsi.edu.my Perpustakaan Tuanku Bainun Kampus Sultan Abdul Jalil Shah PustakaTBainun ptbupsi

05-4506832 pustaka.upsi.edu.my Perpustakaan Tuanku Bainun Kampus Sultan Abdul Jalil Shah PustakaTBainun ptbupsi

leading to a reduction in sensitivity (Duan et al., 2019; Duan, Hao, et al., 2020; Duan, Li, et al., 2020). Determining the properties of liquid crystal-based probes is essential for future use in microactuators and microsensors in liquids.

This study uses a nematic liquid crystal microdroplet solution. The challenge of this study is to produce a nematic solution with a homogeneous size with a specific internal configuration in the 5CB microdroplet and quantifying the optical manipulation of 5CB microdroplet due to the nature of soft matter. The molecular alignment that determines the internal configuration is possible by inducing surface modification of the microdroplets. Furthermore, this study develops the optical manipulation of a single microdroplet for a liquid-crystal-based actuator and a liquid-crystal-based sensor involving optical signal transition in a liquid-crystal configuration with a quadrant photodiode (QPD).

05-4506832 pustaka.upsi.edu.my Perpustakaan Tuanku Bainun Kampus Sultan Abdul Jalil Shah PustakaTBainun ptbupsi

1.3 Research Objective

This study aims to optically trap and manipulate 4-Cyano-4'-pentylbiphenyl (5CB) microdroplets in water. The objectives of the study are:

1. To formulate the production of 5CB microdroplets within a suitable range to be optically trapped.
2. To optically trap a single 5CB microdroplet in water within a suitable size range using 976 nm laser.
3. To optically micro-control a single 5CB microdroplet in water using a circularly polarized laser.

05-4506832 pustaka.upsi.edu.my Perpustakaan Tuanku Bainun Kampus Sultan Abdul Jalil Shah PustakaTBainun ptbupsi

05-4506832 pustaka.upsi.edu.my Perpustakaan Tuanku Bainun Kampus Sultan Abdul Jalil Shah PustakaTBainun ptbupsi

4. To quantitatively determine factors that affect the optical manipulation of the 5CB microdroplet for actuating and sensing applications.

1.4 Significance of Research

This research examines the optical trapping array of nematic liquid crystal microdroplets. This research studies and observes the interaction of light with 5CB microdroplets. It explains the physical interaction between 5CB micro-droplets for non-contact micro-actuators in liquid crystal-based sensor applications.

In addition, the importance of this research lies in the polarization control of light using 5CB microdroplets. This study hypothesizes that light polarization affects the capture of 5CB microdroplets as they are prone to a light polarization state. Varying the laser polarization state used leads directly to a change in the intrinsic configuration of the 5CB microdroplet. The cross-polarization view and electrical signal from QPD observe and detect intrinsic configurational changes within the 5CB microdroplet.

Because liquid crystal is inherently birefringent, this study assumes that the optical strength of 5CB microdroplet capture varies with the polarization state of the capture laser at the same optical density. In addition, due to internal light loss and light loss at the interface, it is expected that the optical strength is not constant for all 5CB microdroplet sizes in the tuned range.

05-4506832 pustaka.upsi.edu.my Perpustakaan Tuanku Bainun Kampus Sultan Abdul Jalil Shah PustakaTBainun ptbupsi

05-4506832 pustaka.upsi.edu.my Perpustakaan Tuanku Bainun Kampus Sultan Abdul Jalil Shah PustakaTBainun ptbupsi

The optical signal change of the internal configuration of the 5CB microdroplet is characterized in the context of corner frequency and optical stiffness measurements. This finding is crucial for application in microactuators and sensor applications. Determining optical stiffness is useful for precisely controlling liquid crystal-based probe applications because optical stiffness shows the trend of the optical trapping with respect to varied parameters such as laser power and microdroplet size. Hence, the researcher can predict the suitable laser power and probe size for prospective application. In addition, optical stiffness measurement results are expected to vary for the internal configuration of bipolar and radial 5CB microdroplets. This finding helps to precisely characterize the transient change of liquid crystal-based sensors especially during the transitional change from bipolar to the radial internal configuration of liquid crystal microdroplets, to determine the significant difference to be applied for quantitative sensing mechanism, instead of observing them visually, in the microsensor application.

1.5 Limitation of Research

This study focuses on 5CB microdroplet trapping. The phase selected for trapping is nematic. The single droplet in the nematic phase is optically captured. 5CB is used as the primary liquid crystal to produce a 5CB microdroplet. As already mentioned, 5CB exists as a liquid crystal at room temperature; Thus, it instantly creates 5CB micro-droplets in the water. Deionized water is chosen as the primary liquid for optical capture. Other liquid crystals could exist as a pure solids or liquids at room

05-4506832 pustaka.upsi.edu.my Perpustakaan Tuanku Bainun Kampus Sultan Abdul Jalil Shah PustakaTBainun ptbupsi

05-4506832 pustaka.upsi.edu.my Perpustakaan Tuanku Bainun Kampus Sultan Abdul Jalil Shah PustakaTBainun ptbupsi

temperature, which is unsuitable for producing microdroplets. Therefore, the 5CB is dispersed and homogenized in deionized water at room temperature.

The laser tweezers optically trap a single 5CB microdroplet in water with a radius of 0.6 µm to 3.7 µm. The 5CB micro-droplet radius of less than 0.5 µm is challenging to see clearly under the CCD camera due to the resolution limitation of the optical tweezers. In addition, capturing more than one droplet at a time can be problematic as it disrupts the 5CB optical signal. Subsequently, the internal configuration of the 5CB microdroplets is focused on the bipolar and radial configurations.

The optical trapping process of this experiment depends on the optical tweezers OTKB(/M). Furthermore, the setup of the optical trap of this experiment depends on the oil immersion objective lens (NA 1.25, 100×) and the optical resolution ≈ of 500 nm. Optical resolution is the limitation of the instrument used to perform optical capture. The laser power ranges from 0.2 MW/cm^2 to 7.3 MW/cm^2. The lower laser power is essential for capturing 5CB microdroplets sensitive to temperature changes. Too much laser power severely destroys the nematic phase of the 5CB microdroplet.

05-4506832 pustaka.upsi.edu.my Perpustakaan Tuanku Bainun Kampus Sultan Abdul Jalil Shah PustakaTBainun ptbupsi

05-4506832 pustaka.upsi.edu.my Perpustakaan Tuanku Bainun Kampus Sultan Abdul Jalil Shah PustakaTBainun ptbupsi

1.6 Thesis Outline

This thesis essentially consists of 5 chapters. Chapter 1 provides the background to the study and the direction and goal of the research. The central part of this chapter is the problem and the research goal.

Chapter 2 deals with the principle of optical trapping. The theory for calibrating the optical stiffness of the optical tweezers is presented. The previous reports on the optical trapping of solid particles and liquid microdroplets are presented. The introduction of liquid crystals, and the optical capture of liquid crystals are also discussed. In addition, the use of liquid crystal microdroplets in actuator and sensor applications is also described.

05-4506832 pustaka.upsi.edu.my Perpustakaan Tuanku Bainun Kampus Sultan Abdul Jalil Shah PustakaTBainun ptbupsi

Chapter 3 describes the methodology of the research. The first part of the methodology is the setup and alignment of optical tweezers. The second part involves the preparation of the 5CB microdroplet suspensions in water. The fourth part is the optical trapping of the 5CB microdroplet in water using a linearly and circularly polarized laser beam. The methodology's last part analyzes the distribution size and stability of the 5CB microdroplet suspension, the simultaneous translation and micro control, the corner frequency, the angular velocity, and the displacement variance of the captured single 5CB microdroplet.

In Chapter 4, the results of the conducted experiment are discussed. The 5CB treatment generates the ultrasonic microdroplet and is observed under the optical microscope. The distribution size and the stability of the 5CB microdroplet are

05-4506832 pustaka.upsi.edu.my Perpustakaan Tuanku Bainun Kampus Sultan Abdul Jalil Shah PustakaTBainun ptbupsi

05-4506832 pustaka.upsi.edu.my Perpustakaan Tuanku Bainun Kampus Sultan Abdul Jalil Shah PustakaTBainun ptbupsi

presented. In addition, the effect of the linearly and circularly polarized laser beam on the trapped 5CB microdroplet is observed. The corner frequency and angular velocity of the trapped 5CB microdroplet are discussed. In addition, the transitional change in the internal configuration of 5CB is quantitatively calculated and presented.

Chapter 5 discusses the conclusion of the research findings on the research findings. Finally, recommendations are given to improve and expand the research for further studies.

1.7 Summary

05-4506832 pustaka.upsi.edu.my Perpustakaan Tuanku Bainun Kampus Sultan Abdul Jalil Shah PustakaTBainun ptbupsi

This chapter presents the background of the study, the problem, the research goals, the importance of the research, and its limitations.

05-4506832 pustaka.upsi.edu.my Perpustakaan Tuanku Bainun Kampus Sultan Abdul Jalil Shah PustakaTBainun ptbupsi

05-4506832 pustaka.upsi.edu.my Perpustakaan Tuanku Bainun Kampus Sultan Abdul Jalil Shah PustakaTBainun

CHAPTER 2

LITERATURE REVIEW

05-4506832 pustaka.upsi.edu.my Perpustakaan Tuanku Bainun Kampus Sultan Abdul Jalil Shah PustakaTBainun ptbupsi

2.1 Introduction

This chapter will discuss the theory of optical trapping to study the origin of the optical force and how it interacts with matter. The theory of calibrating optical tweezers and previous optical trapping on solid particles and liquid microdroplets will be discussed. In addition, the theory of liquid crystal and its history will also be discussed. The previously described liquid crystals in microdroplets will be extensively discussed. Finally, the use of liquid crystals in microactuators and biosensors will also discuss be discussed in this chapter.

05-4506832 pustaka.upsi.edu.my Perpustakaan Tuanku Bainun Kampus Sultan Abdul Jalil Shah PustakaTBainun ptbupsi

05-4506832 pustaka.upsi.edu.my Perpustakaan Tuanku Bainun Kampus Sultan Abdul Jalil Shah PustakaTBainun ptbupsi

2.2 Principle of Optical Tweezers

Optical tweezers are potent instruments to trap and manipulate particles using light. Arthur Ashkin showed the motion of manipulated micron dielectric particles in water by radiation pressure in the 1970s (Ashkin, 1997; Ribeiro et al., 2017). Optical tweezers can hold and manipulate dielectric particles within Femto-newton to pico-newton force. The process of manipulating a particle using a tightly focused laser beam is called optical trapping. Controlling microparticle movement using light develops an understanding of microparticles in physical and life science (Ribeiro et al., 2017; Zhang et al., 2016). The principle of the optical trapping is shown in Figure 2.1.

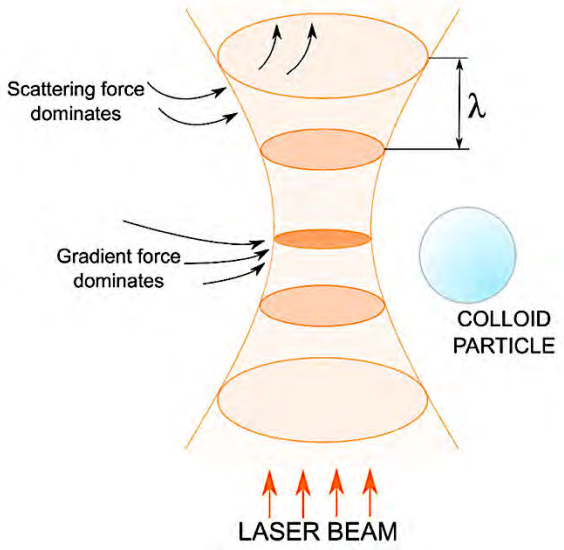


Figure 2.1. Forces exerting on a colloid microparticle near a focused beam. Adapted from (Konyshev & Byvalov, 2021).

Optical tweezers can trap a particle due to the optical force. Optical tweezers form optical traps using an intensely focused laser beam to manipulate dielectric colloid microparticles by exerting two types of forces, which are scattering (F_s) and gradient (F_g) as shown in Figure 2.1 (Konyshev & Byvalov, 2021). The scattering force results

05-4506832 pustaka.upsi.edu.my Perpustakaan Tuanku Bainun Kampus Sultan Abdul Jalil Shah PustakaTBainun ptbupsi

05-4506832 pustaka.upsi.edu.my Perpustakaan Tuanku Bainun Kampus Sultan Abdul Jalil Shah PustakaTBainun ptbupsi

from the striking of photons on the particle along its direction of propagation. The intensity gradient of light produces gradient force. For example, a Gaussian laser beam has an intense beam in the middle of the laser spot, which indicates a strong gradient force. The refraction and reflection of light resulted in the generation of gradient and scattering forces. The change in light momentum occurs when the colloid microsphere refracts the incident light. As a result, an equal and opposite momentum change occurs inside the microsphere due to the conservation of momentum. In a condition where the particle's refractive index is more significant than the surrounding medium refractive index, the direction of gradient forces in the direction of the intensity gradient. It pushes the microsphere toward the area of higher light intensity.

Meanwhile, the effect of light absorption and reflection by the trapped microsphere resulted in scattering force in the direction of light propagation. The light must be focused to produce a stable optical trap. Hence, the net forces always lead the trapped particle toward the focused beam. When the particle displaces from the beam's focus, the imbalance of the net forces will always pull the particle back to equilibrium.

2.3 Optical Trapping Regimes

Optical trapping behavior is classified into two typical regimes: Mie and Rayleigh (Dienerowitz et al., 2010). The vital parameter, such as relative trapped particle size (let it be the sphere with the radius (r) and the laser beam's wavelength (λ), is used to distinguish between Mie and Rayleigh regimes (Konyshev & Byvalov, 2021).

05-4506832 pustaka.upsi.edu.my Perpustakaan Tuanku Bainun Kampus Sultan Abdul Jalil Shah PustakaTBainun ptbupsi

05-4506832 pustaka.upsi.edu.my Perpustakaan Tuanku Bainun Kampus Sultan Abdul Jalil Shah PustakaTBainun ptbupsi

2.3.1 Rayleigh Regime

In the context of the Rayleigh regime ($r << \lambda$), the size of the trapped particle (r) is smaller compared to the wavelength (λ) of the laser beam (Polimeno et al., 2018). Due to this fact, the ray optics approach is not applicable to describe the trapping behavior in the Rayleigh regime because of particle geometrical limitations. Nonetheless, the Rayleigh regime needs electromagnetic theory to explain the force's interaction on the trapped particle. In the Rayleigh regime, the trapped particle is considered a point dipole (Neuman & Block, 2004). The laser polarization state causes the particle to induce a dipole moment in the Rayleigh regime. The equation represents the scattering force (F_S) in Rayleigh regime

$$F_s = \frac{I_0 \sigma n_m}{c} \tag{2.1}$$

05-4506832 pustaka.upsi.edu.my Perpustakaan Tuanku Bainun Kampus Sultan Abdul Jalil Shah PustakaTBainun ptbupsi

$$\sigma = \frac{128\pi^5 r^6}{3\lambda^4}\left(\frac{m^2-1}{m^2+1}\right)^2 \tag{2.2}$$

where I_0 is the light intensity, σ is the scattering cross-section for photons, c is the speed of light in vacuum, n_m is the refractive index of the medium, and m is the ratio of the refractive index of the particle (n_p) to the refractive index of the medium ($\frac{n_p}{n_m}$) and λ is the wavelength of the light. The magnitude of the gradient force averaged over time is mediated by the interaction of a dipole with the electromagnetic field and depends on the refractive index of particles and polarizability (α). The equation represents the gradient force (F_g) in Rayleigh regime

05-4506832 pustaka.upsi.edu.my Perpustakaan Tuanku Bainun Kampus Sultan Abdul Jalil Shah PustakaTBainun ptbupsi

05-4506832 pustaka.upsi.edu.my Perpustakaan Tuanku Bainun Kampus Sultan Abdul Jalil Shah PustakaTBainun ptbupsi

$$F_g = \frac{2\pi\alpha}{cn_m^2}\nabla I_0 \tag{2.3}$$

$$\alpha = n_m^2 r^3 \left(\frac{m^2-1}{m^2+2}\right) \tag{2.4}$$

From equations 2.1 and 2.3, the light intensity and trapped particle size contributed to the F_g and F_s.

The trapped particle polarization resulted in force interaction in the Rayleigh regime. Hence, Rayleigh's regime shows more complexity to explain than the Mie regime.

05-4506832 pustaka.upsi.edu.my Perpustakaan Tuanku Bainun Kampus Sultan Abdul Jalil Shah PustakaTBainun ptbupsi

2.3.2 Mie Regime

In the Mie regime condition, ($r >> \lambda$), the trapped particle size (r) is larger than the wavelength (λ) of the laser beam, optical pressure can be understood within the framework of ray optics or geometrical optics (Tsuji et al., 2022). Mie regime describes the optical force as uncomplicated, straightforward, and intuitive (Mas et al., 2011). Mie regime describes the component of the optical forces using ray optics. The geometrical optics approach pictures the forces involved in the optical trapping process more efficiently and simply. In the geometrical optics approach, the refraction of light contributes to the gradient force (F_g) while the reflection contributes to the scattering force (F_s).

05-4506832 pustaka.upsi.edu.my Perpustakaan Tuanku Bainun Kampus Sultan Abdul Jalil Shah PustakaTBainun ptbupsi

05-4506832 pustaka.upsi.edu.my Perpustakaan Tuanku Bainun Kampus Sultan Abdul Jalil Shah PustakaTBainun ptbupsi

Figure 2.2 (left) shows the gradient force acting on a spherical particle near a non-focused laser beam. Ray *b* is more intense than Ray *a*. In the context of ray *a*, the refraction of ray *a* and *a'* cause the change in momentum (dp_a) in positive *x*-direction. This resulted in the weak force ($-dp_a$) in the negative *x*-direction. Meanwhile, the intense ray *b* also undergoes momentum change (dp_b) in the negative *x*-direction due to the refraction. Meanwhile, this creates a strong force ($-dp_b$) in the positive *x*-direction. The net force of ($-dp_a$ and $-dp_b$) is toward the positive *x*-direction of intense light region and contributes to the pulling gradient force (F_{grad}). The scattering force (F_s) pushes the spherical particle along the direction of laser propagation, as shown in Figure 2.2 (left).

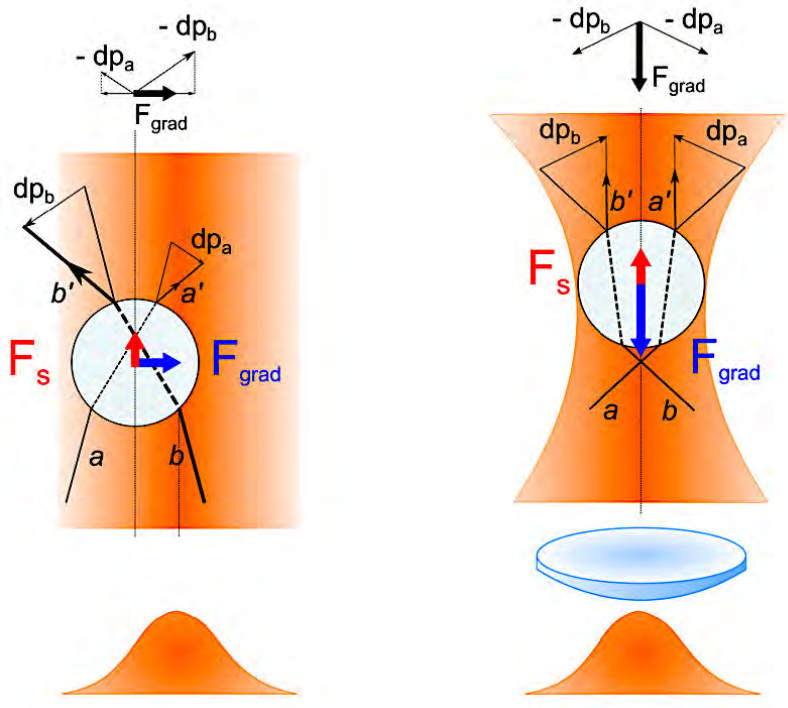


Figure 2.2. The origin of the gradient force acting on a spherical particle near a non-focused (left) and focused (right) laser beam. Adapted from (Konyshev & Byvalov, 2021).

Meanwhile Figure 2.2 (right) shows the origin of the gradient force acting on a spherical particle of a focused laser beam. Rays *a* and *b* have the same intensity, and

05-4506832 pustaka.upsi.edu.my Perpustakaan Tuanku Bainun Kampus Sultan Abdul Jalil Shah PustakaTBainun ptbupsi

05-4506832 pustaka.upsi.edu.my Perpustakaan Tuanku Bainun Kampus Sultan Abdul Jalil Shah PustakaTBainun ptbupsi

the spherical particle is slightly displaced away from the center of laser focus along the positive *y*-direction. The refraction of *a* and *a'* cause the light momentum change (dp_a) in the negative *x*-direction. Hence, this also creates the reaction force ($-dp_a$) in the positive *x*-direction. Meanwhile, the refraction of rays *b* and *b'* cause the light momentum change (dp_b) in positive *x*-direction and create reaction force ($-dp_b$) in the negative *x*-direction. This resultant reaction force of ($-dp_a$ and $-dp_b$) creates a gradient force that pulls the spherical sphere back to the laser focus in the direction of negative *y*-direction, as shown in Figure 2.2 (right).

In the Mie regime, ray optics approximation explains optical, scattering, and gradient forces. These optical forces, including the scattering component, can be calculated directly from ray optics for a uniform dielectric sphere. Optical forces depend on several parameters. For example, maximum trapping force depends on controlling parameters like laser power (P), a refractive index of the medium (n_m) and particle refractive index (n_p), the numerical aperture of the objective lens (NA), the wavelength of laser power (λ) and others (Rui et al., 2021). Calculation of gradient and scattering force in the Mie regime can be done based on Equations 2.5 and 2.6:

$$F_s = \frac{n_m P}{c} x[1 + R\cos(2\theta_i) - T^2 \frac{\cos(2\theta_i - 2\theta_r) + R\cos(2\theta_i)}{1 + R^2 + 2R\cos(2\theta_r)}] \tag{2.5}$$

$$F_g = \frac{n_m P}{c} x[1 + R\sin(2\theta_i) - T^2 \frac{\cos(2\theta_i - 2\theta_r) + R\sin(2\theta_i)}{1 + R^2 + 2R\cos(2\theta_r)}] \tag{2.6}$$

T and R represent Fresnel transmission and reflection coefficients, while θ_i and θ_r represent incident and reflection angles, and c is the speed of light (Mas et al., 2011;

05-4506832 pustaka.upsi.edu.my Perpustakaan Tuanku Bainun Kampus Sultan Abdul Jalil Shah PustakaTBainun ptbupsi

05-4506832 pustaka.upsi.edu.my Perpustakaan Tuanku Bainun Kampus Sultan Abdul Jalil Shah PustakaTBainun ptbupsi

Wright et al., 1994). Equations 2.5 and 2.6 show that the laser power (P) and relative refractive index (n) contribute to the gradient and scattering forces. The refractive index of particle, n_p also influence the trapping force despite not appearing in the equation. The effective refractive index of the particle, n, is defined by Ashkin as the ratio between n_p and n_m ($n = \frac{n_p}{n_m}$). The increasing of n_p, significantly increased n. For n in the range of $1.1 < n < 1.6$, the theoretical calculation indicates the magnitude of F_g is greater than or almost equivalent to F_s. Also, in the case in which n increases to values greater than 1.6, the theoretical calculation of the magnitude of F_g is smaller than F_s (Ashkin, 1992). Optical tweezer calibration is compulsory before conducting a force-related measurement. Different optical tweezers will have different optical stiffness.

05-4506832 pustaka.upsi.edu.my Perpustakaan Tuanku Bainun Kampus Sultan Abdul Jalil Shah PustakaTBainun ptbupsi

2.4 Optical Stiffness Calibration of Optical Trapping

Optical stiffness is the measurement of how strong an optical trap is. The behavior of the trapped particle is illustrated in Figure 2.3. Ideally, when a particle gets trapped in an optical trap, it behaves like a Hookean spring with a certain radial displacement (r) from a laser focus and optical stiffness (k_T) is illustrated as ab imaginary spring. F_g and F_s would interact together to produce restoring force (F_r). In stable trapping, the trapped particle vibrates forward and backward in the optical trap region. As the optical trap behaves as a linear spring, the relation of radial optical stiffness, restoring force, and radial displacement are

$$F_r = -k_T r \tag{2.7}$$

05-4506832 pustaka.upsi.edu.my Perpustakaan Tuanku Bainun Kampus Sultan Abdul Jalil Shah PustakaTBainun ptbupsi

05-4506832 pustaka.upsi.edu.my Perpustakaan Tuanku Bainun Kampus Sultan Abdul Jalil Shah PustakaTBainun ptbupsi

where k_r is radial optical stiffness (Nieminen et al., 2014). From the equation, optical stiffness is the proportionality constant of restoring force and radial displacement of the trapped particle.

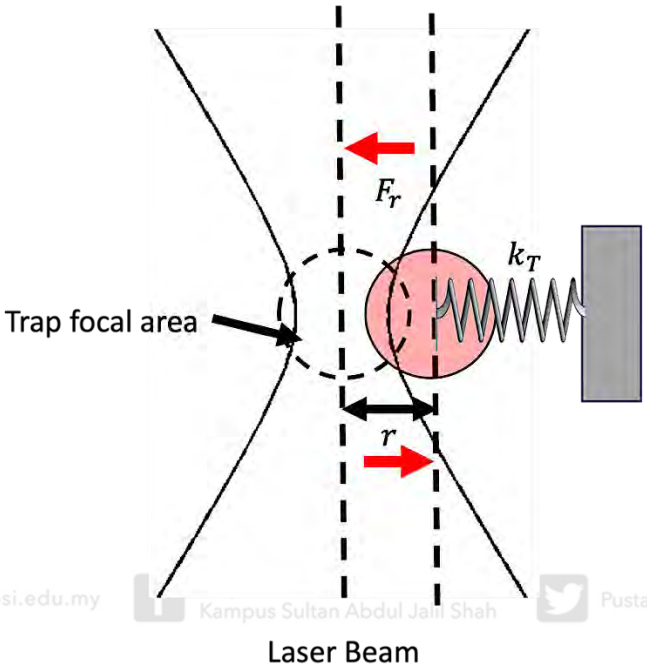


Figure 2.3. The F_r is acting on the trapped particle due to slight displacement from the laser trap center.

The optical stiffness depends on setting parameters like laser power and wavelength, particle size and type, the numerical aperture of the objective lens, and the refractive index of the medium and particle. The higher k_T values represent the increase of particle confinement in the optical trap and vice versa.

The previous researcher reported the trend of the optical stiffness concerning the laser power and size of the parameter. For example, the typical optical stiffness for a 3 μm polystyrene bead trapped by a 975 nm wavelength trapping laser beam in water

05-4506832 pustaka.upsi.edu.my Perpustakaan Tuanku Bainun Kampus Sultan Abdul Jalil Shah PustakaTBainun ptbupsi

05-4506832 pustaka.upsi.edu.my Perpustakaan Tuanku Bainun Kampus Sultan Abdul Jalil Shah PustakaTBainun ptbupsi

at varied laser power was reported (Aziz et al., 2016). Figure 2.4 shows the graph of the trap stiffness of the 3 μm polystyrene bead in water at different laser power. The trap stiffness was calculated using the Equipartition Theorem (ET). As a result, the trap stiffness increased as laser power increased for both the *x*-direction and *y*-direction in the range of laser power used from 47 to 122 mW as illustrated in Figure 2.4. In another study, the use of laser power from 0.2 to 0.5 mW showed an increasing trend of stiffness of polystyrene active colloid (PSAC) trapping (Paul et al., 2022). There is no information on the trap stiffness reported beyond 122 mW of laser power. It is expected that the trap stiffness will increase with the increasing laser power applied as the stiffness is proportionate to the laser power. In the range of 47 – 85 mW, the optical trap is more confined in the *x*-direction and at 122 mW the optical trap is more confined in the *y*-direction. The possible reason that causes this effect is the unsymmetry of the laser spot due to geometric aberrations hence contributing to the unbalance of the optical force on the trapped particle.

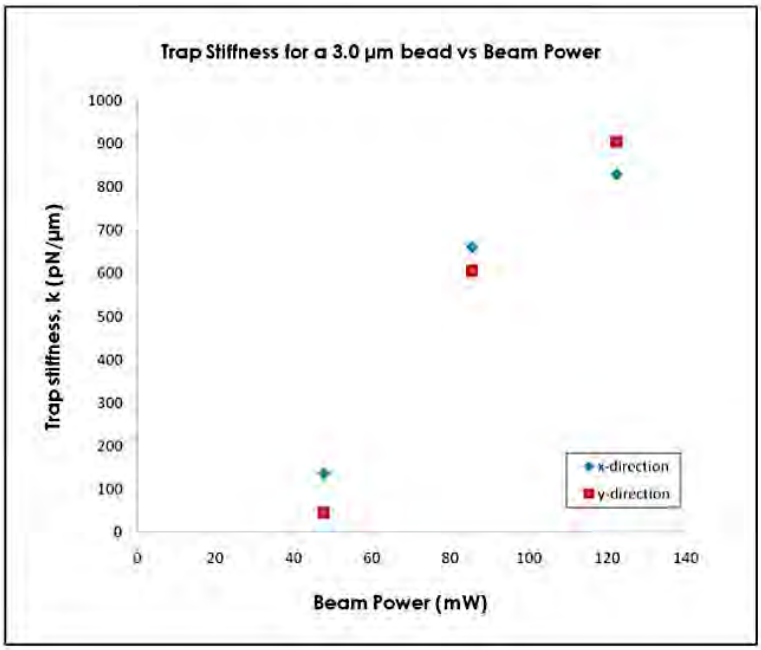


Figure 2.4. Linear graph of the trap stiffness versus beam powers (Aziz et al., 2016).

05-4506832 pustaka.upsi.edu.my Perpustakaan Tuanku Bainun Kampus Sultan Abdul Jalil Shah PustakaTBainun ptbupsi

05-4506832 pustaka.upsi.edu.my Perpustakaan Tuanku Bainun Kampus Sultan Abdul Jalil Shah PustakaTBainun ptbupsi

Furthermore, the optical stiffness of 4.2 μm and 8.0 μm of sulfate-modified fluorescent polystyrene beads were also studied (Mohammad et al., 2014). The optical trapping of the polystyrene beads of different sizes was performed using a 1064 nm trapping laser beam at different laser powers. Their reported optical stiffness was determined using Power Spectrum Density (PSD), and the result was summarized in Figure 2.5.

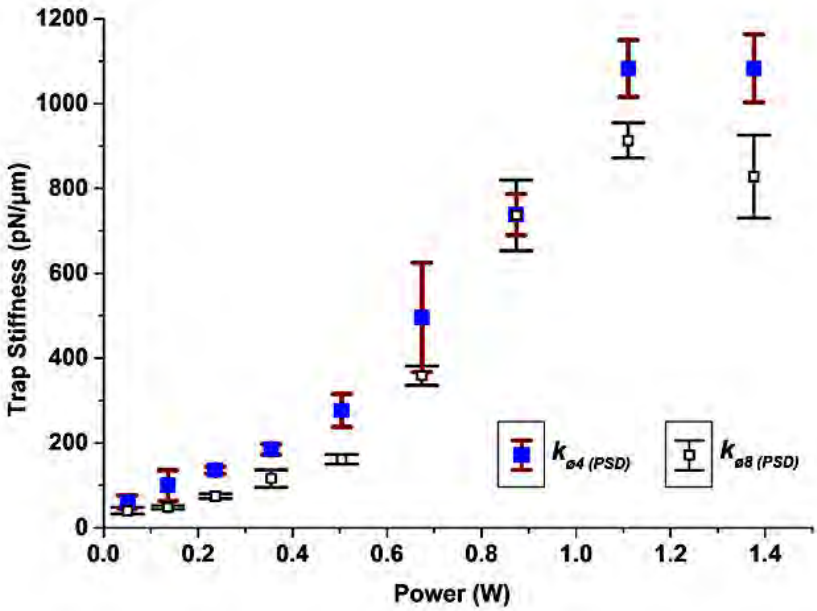


Figure 2.5. Trap stiffness as a function of laser power at the specimen plane, using the passive stiffness calibration method based on the power spectral density (Mohammad et al., 2014).

The small polystyrene bead of 4.2 μm diameter obtained larger optical trap stiffness than the 8.0 μm size from 50 to 500 mW laser power used, as shown in Figure 2.5. The correlation between the trap stiffness and laser powers is linear up to the trapping laser power of 504 mW, as shown in Figure 2.5. However, at higher trapping powers, the uncertainty in the estimated stiffness values by the PSD calibration method increases, with reduced sensitivity of the stiffness estimates to power increments and deviation from a linear trend. The possible reason for the deviation of the linear trend

05-4506832 pustaka.upsi.edu.my Perpustakaan Tuanku Bainun Kampus Sultan Abdul Jalil Shah PustakaTBainun ptbupsi

05-4506832 pustaka.upsi.edu.my Perpustakaan Tuanku Bainun Kampus Sultan Abdul Jalil Shah PustakaTBainun ptbupsi

is due to the laser heating effect when the laser power is used beyond 500 mW. The solvent absorbs heat at higher laser power and significantly changes the solvent viscosity (Català et al., 2017; Peterman et al., 2003). Since PSD considers viscosity as one of the vital parameters to calibrate stiffness, the increased solvent temperature due to laser power (>500 mW) affects the stiffness, and this no longer follows PSD that requires solvent viscosity to be fixed (Català et al., 2017; Peterman et al., 2003).

In addition, the optical stiffness becomes more complex when the trapped particle has soft and liquid physical properties. The effect of the laser power and size on the optical stiffness was also investigated (Yusuf & Ayop, 2020). In his research, the chloroform microdroplet in water was trapped by a 915 nm trapping laser beam at different laser power densities, which were 6.3 MW/cm^2, 7.4 MW/cm^{2,} and 8.4 MW/cm^2. The graph of optical stiffness against the size of the chloroform microdroplet at varied laser power used is illustrated in Figure 2.6.

05-4506832 pustaka.upsi.edu.my Perpustakaan Tuanku Bainun Kampus Sultan Abdul Jalil Shah PustakaTBainun ptbupsi

05-4506832 pustaka.upsi.edu.my Perpustakaan Tuanku Bainun Kampus Sultan Abdul Jalil Shah PustakaTBainun ptbupsi

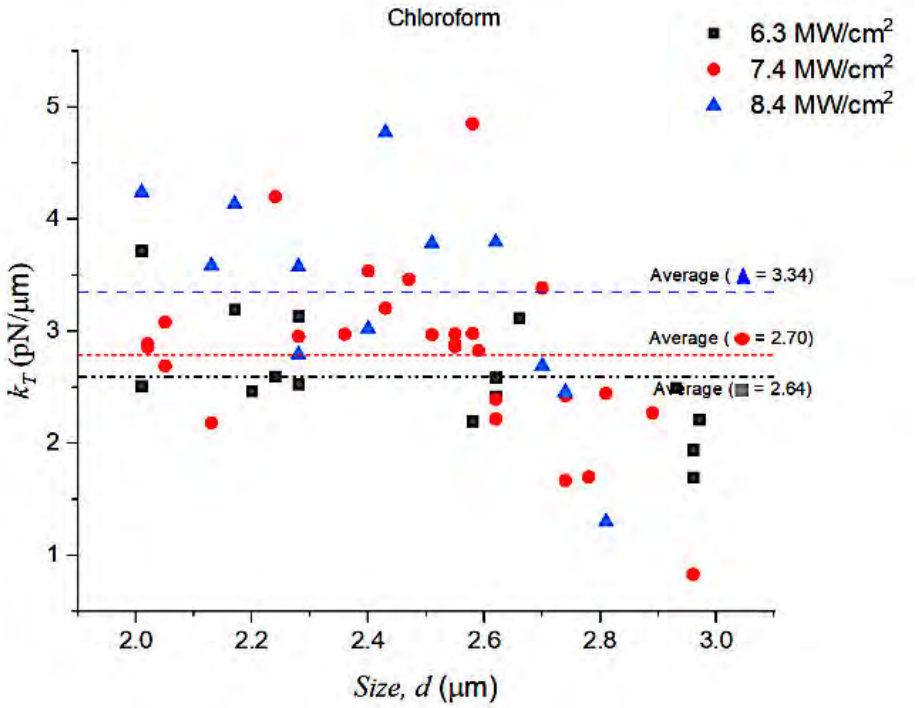


Figure 2.6. The optical stiffness graph against the chloroform microdroplet's size. Adapted from (Yusuf & Ayop, 2020).

Based on Figure 2.6, the different sizes of the direct relationship between the trap stiffness and the chloroform microdroplet size were difficult to deduce. k_T showed the variation with the *d* of the microdroplet. One of the possible reasons for the scattered plot of data was the shape of the microdroplets (Yusof et al., 2020). Since the particle was liquid, the shape was not perfectly spherical. This would result in the variation of measured k_T. However, the laser power density affects the trap stiffness by taking the average trap stiffness at the respective laser power density. For example, 8.4 MW/cm^2 laser power has the highest average trap stiffness (3.34 pN/μm), as the trap stiffness is proportionate to the laser power used. Meanwhile, 6.3 MW/cm^2 laser power showed the most negligible value of the average optical stiffness of 2.64 pN/μm. The limitation of this study is that the laser power density used was in the range of 6.3 to 8.4 MW/cm^2.

05-4506832 pustaka.upsi.edu.my Perpustakaan Tuanku Bainun Kampus Sultan Abdul Jalil Shah PustakaTBainun ptbupsi

05-4506832 pustaka.upsi.edu.my Perpustakaan Tuanku Bainun Kampus Sultan Abdul Jalil Shah PustakaTBainun ptbupsi

The trend of optical stiffness when the laser power is used less than 6.3 MW/cm^2 has not been studied.

The optical stiffness of the solid particles has been well-reported compared to the soft liquid particles. Besides, the existing equation was developed for a perfect spherical shape and specific solid particles. Determining the optical stiffness of a liquid microdroplet remains challenging. The possible reason is the complexity and the softness of soft liquid particles to maintain uniform shape during optical trapping specifically microdroplets (Yusof et al., 2020; Yusuf & Ayop, 2020). This is because any slight force applied to the soft matter will significantly cause the deformation. This small deformation might be invisible or visible under an optical microscope, but the sensitive optical tweezers detect this deformation and translate it into stiffness measurement. The trends of optical stiffness with laser power and size for microdroplets is unclear and lacking due to complexity (Yusof et al., 2020; Yusuf & Ayop, 2020). Hence, this factor affects the measurement of the optical stiffness parameter for soft liquid particles such as droplets.

2.5 Optical Stiffness Calibration

Every optical tweezer system is unique. Each optical tweezer setup has the sensitivity and stiffness of its optical trap (Aziz et al., 2016). A particle will always fluctuate in Brownian motion. When it gets trapped, its motion approximates the harmonic oscillator.

05-4506832 pustaka.upsi.edu.my Perpustakaan Tuanku Bainun Kampus Sultan Abdul Jalil Shah PustakaTBainun ptbupsi

05-4506832 pustaka.upsi.edu.my Perpustakaan Tuanku Bainun Kampus Sultan Abdul Jalil Shah PustakaTBainun ptbupsi

The methods for quantification of the optical stiffness are numerous. Some of the established methods are the equipartition theorem, Boltzmann statistics and the power spectrum method (Baek et al., 2007; Wang et al., 2011).

2.5.1 Equipartition Theorem (ET)

ET states that the local temperature determines the particle's kinetic energy (Eom et al., 2014). The equipartition theorem uses the spatial distribution of the trapped particle data in an available unit of length. This theorem assumes the trapped particle behaves like a harmonic oscillator confined in potential, so average thermal energy can be calculated. The average thermal energy is

05-4506832 pustaka.upsi.edu.my Perpustakaan Tuanku Bainun Kampus Sultan Abdul Jalil Shah PustakaTBainun ptbupsi

$$E = \frac{1}{2}k_B T \tag{2.8}$$

The average square displacement in known unit length is expressed as

$$(\sigma)^2 = < \left(x - x_{avg}\right)^2 > \tag{2.9}$$

Based on the theorem, the potential energy of the trapped particle and the average thermal energy can be expressed as an equation

$$\frac{1}{2}k_B T = \frac{1}{2}k_T(\sigma)^2 \tag{2.10}$$

05-4506832 pustaka.upsi.edu.my Perpustakaan Tuanku Bainun Kampus Sultan Abdul Jalil Shah PustakaTBainun ptbupsi

05-4506832 pustaka.upsi.edu.my Perpustakaan Tuanku Bainun Kampus Sultan Abdul Jalil Shah PustakaTBainun ptbupsi

Therefore, we can determine the optical stiffness of the trapped particle by analyzing the data on the spatial distribution of the trapped particle along known direction and length.

$$k_T = \frac{k_B T}{(\sigma)^2} \tag{2.11}$$

where k_B is Boltzmann constant, T is temperature, k_T is optical stiffness, x is the displacement along the x-direction, x_{avg} is the average of x-displacement and $(\sigma)^2$ is the average time square of bead position along the lateral x-direction direction.

2.5.2 Boltzmann Statistics (BS) Theorem

05-4506832 pustaka.upsi.edu.my Perpustakaan Tuanku Bainun Kampus Sultan Abdul Jalil Shah PustakaTBainun ptbupsi

Meanwhile, BS calculates optical stiffness based on the Brownian motion in an optical trap's potential well. BS is way more complicated. k_T is determined from the quadratic fit of optical trapping potential energy. The displacement histogram was plotted using the spatial distribution data of trapped particles. Normalization is performed on the histogram by integration under the graph area. The probability distribution, $\rho(x)$ related to the spatial distribution of optical trap trajectory is

$$\rho(x) = Ce^{\frac{-U(x)}{k_B T}} \tag{2.12}$$

where C is constant resulted from the normalized of histogram $\rho(x)$ to provide a good estimation of spatial probability density ρ'

05-4506832 pustaka.upsi.edu.my Perpustakaan Tuanku Bainun Kampus Sultan Abdul Jalil Shah PustakaTBainun ptbupsi

05-4506832 pustaka.upsi.edu.my Perpustakaan Tuanku Bainun Kampus Sultan Abdul Jalil Shah PustakaTBainun ptbupsi

$$\rho'(x) = \rho(x)C \tag{2.13}$$

The possible explanation of this method is due to the lower energy level of the trap potential, $U(x)$, particle in Brownian motion is positioned more frequently in it. The trap potential energy can be expressed as

$$U(x) = -\ln(\rho'(x)) \tag{2.14}$$

A quadratic fitting $ax^2 + b$ near the trap's center is performed on $U(x) = -\ln(p(x))$ to get a coefficient a. Since $ax^2 \approx \frac{1}{2}k_T x^2$, the approximation of optical stiffness is determined from

$$k_T = 2ak_B T \tag{2.15}$$

05-4506832 pustaka.upsi.edu.my Perpustakaan Tuanku Bainun Kampus Sultan Abdul Jalil Shah PustakaTBainun ptbupsi

Position data for ET and BS need video recording analysis or QPD (Neuman & Block, 2004). However, the data must be calibrated in a unit of length, mainly when the signal is acquired using QPD (Wang et al., 2011) The stuck bead method (SBM) is vital to determining a signal-to-displacement calibration (Yeng et al., 2017). Figure 2.7 shows the illustration of bead sediment on the glass wall.

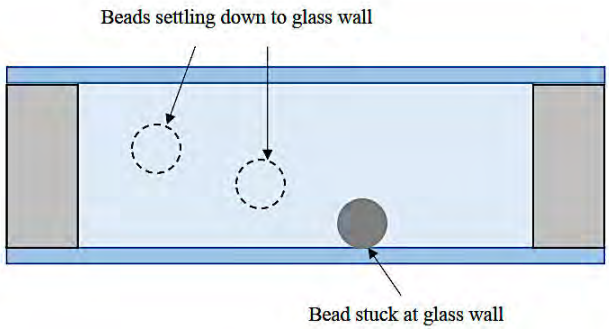


Figure 2.7. Illustration of stuck bead sediment at the glass wall.

05-4506832 pustaka.upsi.edu.my Perpustakaan Tuanku Bainun Kampus Sultan Abdul Jalil Shah PustakaTBainun ptbupsi

05-4506832 pustaka.upsi.edu.my Perpustakaan Tuanku Bainun Kampus Sultan Abdul Jalil Shah PustakaTBainun ptbupsi

In SBM, the particle sticks to a glass wall. This condition is unsuitable for the droplet as it might alter or change its uniform sphere shape. The liquid droplet will remain spherical if no external force is acting on it.

2.5.3 Power Spectrum Density (PSD) Theorem

The PSD method can determine the optical stiffness calibration of an optical trap. This PSD method uses the power spectrum of the movement of an optically trapped particle to determine the optical stiffness. This study uses the PSD method to calculate the optical stiffness of the trapped single 5CB microdroplet in water. Compared to other methods, the advantage of using PSD is that it does not require prior signal-to-length calibration, even though it is algorithmically more challenging to perform. Einstein-Ornstein-Uhlenbeck interprets the power spectrum of the trapped particle's Brownian motion, which predicts a Lorentzian spectrum (Berg-Sørensen & Flyvbjerg, 2004). Displacement against the time signal is a standard signal obtained from the oscillating system. However, a complex system such as OT might produce a mixed and ambiguous signal. PSD analysis can help to eliminate distortion and disruption of signal.

A QPD can provide the power spectrum required for PSD analysis in optical trapping. This voltage signal from QPD will be Fourier transform using signal analysis software. Over damp Langevin equation of one dimension is required to calculate the power spectrum of a trapped particle (Berg-Sørensen & Flyvbjerg, 2004)

05-4506832 pustaka.upsi.edu.my Perpustakaan Tuanku Bainun Kampus Sultan Abdul Jalil Shah PustakaTBainun ptbupsi

05-4506832 pustaka.upsi.edu.my Perpustakaan Tuanku Bainun Kampus Sultan Abdul Jalil Shah PustakaTBainun ptbupsi

$$\frac{dx(t)}{dt} + 2\pi f_c x(t) = \sqrt{2D} W_x t \tag{2.16}$$

where $x(t)$ is the position of the particle relative to the trap center, D is the diffusion coefficient, $W_x t$ is the white noise, and f_c is corner frequency. Optical stiffness k_T is related to the f_c by equation

$$f_c = \frac{k_T}{2\pi\gamma_0} \tag{2.17}$$

where $\gamma_o = 6\pi nr$, n is a medium viscosity, and r is particle radius. f_c definition is the frequency where the particle in the optical trap no longer experiences the trap's effect (Hegner et al., 2003). Equation 2.16 after the Fourier transform changed to

$$2\pi(f_c - if)\check{X}(f) = \sqrt{2D}\widetilde{W_x}(f) \tag{2.18}$$

05-4506832 pustaka.upsi.edu.my Perpustakaan Tuanku Bainun Kampus Sultan Abdul Jalil Shah PustakaTBainun ptbupsi

where $\check{X}(f)$ and $\widetilde{W_x}(f)$ is the Fourier transform of $x(t)$ and $W_x(t)$, respectively. Square modulus is applied to Equation 2.18 to produce PSD of particle motion, as stated in Equation 2.16.

$$P_x(f) = \left|\check{X}(f)\right|^2 = \frac{D/(2\pi)^2}{f_c^2 + f^2} \tag{2.19}$$

Parameter f_c determines the optical stiffness k_T. The practical way to calibrate an optical trap is by fitting the power spectrum obtained from the Fourier transform of the trapped particle voltage signal (Berg-Sørensen & Flyvbjerg, 2004; Garratt &

05-4506832 pustaka.upsi.edu.my Perpustakaan Tuanku Bainun Kampus Sultan Abdul Jalil Shah PustakaTBainun ptbupsi

05-4506832 pustaka.upsi.edu.my Perpustakaan Tuanku Bainun Kampus Sultan Abdul Jalil Shah PustakaTBainun ptbupsi

Bachega, 2013; Neuman & Block, 2004). Previous researchers used f_c to differentiate healthy and infected red blood cells from malaria, interpret cluster sizes, and observe local heating at laser spots (Yusof et al., 2020).

2.5.4 Comparison between Boltzmann Statistics (BS), Equipartition Theorem (ET), and Power Spectrum Density (PSD)

The calibration of the optical force of the trapped particle can be measured using Boltzmann Statistics (BS), Equipartition Theorem (ET), Power Spectrum Density (PSD), and other calibration methods. The summarization of the comparison between BS, ET, and PSD methods is shown in Table 2.1.

05-4506832 pustaka.upsi.edu.my Perpustakaan Tuanku Bainun Kampus Sultan Abdul Jalil Shah PustakaTBainun ptbupsi
05-4506832 pustaka.upsi.edu.my Perpustakaan Tuanku Bainun Kampus Sultan Abdul Jalil Shah PustakaTBainun ptbupsi

05-4506832 pustaka.upsi.edu.my Perpustakaan Tuanku Bainun Kampus Sultan Abdul Jalil Shah PustakaTBainun ptbupsi

Table 2.1

Comparison between Boltzmann Statistics (BS), Equipartition Theorem (ET), and Power Spectrum Density (PSD) calibration.

Method	Equipartition Theorem (ET)	Boltzmann Statistics (BS)	Power Spectrum Density (PSD)
Requirement for spatial distribution data	Yes	Yes	Yes
Requirement for signal data in defined unit length	Yes	Yes	No
Requirement for voltage to displacement calibration	Yes	Yes	No
k_T expression	$k_T = \frac{k_B T}{(\sigma)^2}$	$k_T = 2ak_B T$	$k_T = 2\pi\gamma_o f_c$

The method used to calibrate the optical trap depends on what type of particle to be trapped. For example, measuring the optical force on rugged and solid particles such as polystyrene beads and silica beads can be calibrated using ET and BS methods. This is because polystyrene and silica beads can undergo an intermediate step, the stuck bead method, to obtain position signal data in a defined unit of length. This step is possible because their shape remains spherical and rigid when the polystyrene or silica beads stick to the glass.

05-4506832 pustaka.upsi.edu.my Perpustakaan Tuanku Bainun Kampus Sultan Abdul Jalil Shah PustakaTBainun ptbupsi

05-4506832 pustaka.upsi.edu.my Perpustakaan Tuanku Bainun Kampus Sultan Abdul Jalil Shah PustakaTBainun ptbupsi

In soft and liquid particles such as liquid microdroplets or biomaterials such as cells or DNA, measuring the optical force requires the PSD method. For example, since the liquid microdroplet is considered fragile and soft, it can deform easily and instantaneously alter its spherical shape. Hence, the PSD method is the most suitable method to calibrate optical force on soft matter and does not require position signal data in a defined unit of length.

2.6 Optical Torque

In general, light carries momentum. This momentum can be transferred to the particle during optical capture. The polarization of the light state has a significant impact on the momentum that is transmitted during the optical capture process. The linearly polarized light carries a linear momentum that causes the particle to be attracted to the higher-intensity light gradient. If the polarization is changed from linearly polarized to circularly polarized, angular momentum can be transferred to the trapped particle, causing the trapped particle to rotate. However, not every material can be rotated by circularly polarized light. Birefringent material is the typical material that reacts and rotates under circularly polarized light. An example of birefringent material is liquid crystal.

In optical trapping, the essential components that convert linearly polarized light to circularly polarized light are quarter-wave plates. The circularly polarized light carries angular momentum transferred to the birefringence material during optical trapping. The angular momentum of the circularly polarized light transferred to the

05-4506832 pustaka.upsi.edu.my Perpustakaan Tuanku Bainun Kampus Sultan Abdul Jalil Shah PustakaTBainun ptbupsi

05-4506832 pustaka.upsi.edu.my Perpustakaan Tuanku Bainun Kampus Sultan Abdul Jalil Shah PustakaTBainun ptbupsi

birefringence material produced an optical torque. This optical torque causes the trapped birefringence material to be rotated. The resulting light passing from the birefringence material during the rotation of the birefringence material is linearly polarized.

The optical torque resulting from the trapped 5CB microdroplet-induced rotation can be related by balancing optical torque with the viscous torque from the solution. When a droplet exhibits stationary rotation with frequency ω, the optical torque Γ received from the laser beam is balanced by the viscous torque from the solution as

$$\Gamma = D\omega \tag{2.20}$$

05-4506832 pustaka.upsi.edu.my Perpustakaan Tuanku Bainun Kampus Sultan Abdul Jalil Shah PustakaTBainun ptbupsi

where Γ is optical torque, D is the rotational drag coefficient (Stoke's coefficient) $D = 8\pi\eta r^3$ where η is liquid viscosity, r is microdroplet radius, and ω is angular speed (Murazawa, Juodkazis, & Misawa 2005).The final expression of Equation 2.20 becomes

$$\Gamma = 8\pi\eta r^3\omega \tag{2.21}$$

The optical torque increased with the increasing optical power density used. The angular speed of the rotating microdroplet is inversely proportional to the radius of the rotating trapped microdroplet.

05-4506832 pustaka.upsi.edu.my Perpustakaan Tuanku Bainun Kampus Sultan Abdul Jalil Shah PustakaTBainun ptbupsi

05-4506832 pustaka.upsi.edu.my Perpustakaan Tuanku Bainun Kampus Sultan Abdul Jalil Shah PustakaTBainun ptbupsi

The ellipticity angle φ, of the laser beam, affects the optical torque. The linearly polarized laser beam corresponds to φ = 0, and the circularly polarized beam corresponds to φ = π/4. The nematic liquid crystal droplet starts rotating, and *v* increases with increasing $|\varphi|$ if the polarization of the trapping beam approaches circular polarization above a particular critical value $|\varphi_c|$. The waveplate effect explains this behavior. The equation represents the relationship between optical torque Γ at φ

$$\Gamma = \frac{P}{\varpi}[(1 - \cos\Delta)\sin 2\varphi - \sin\Delta\cos 2\varphi \sin 2\theta] \tag{2.22}$$

where *P* represents the laser power, ϖ; trapping beam frequency, Δ is the retardance represent by formula $\Delta = \frac{2\pi\Delta nd}{\lambda}$ (Δn: birefringence, and λ: the trapping beam wavelength), Furthermore, θ the angle between the polarization ellipse's central axis and the object's optical axis (Saito & Kimura, 2022). The expression $(1 - \cos\Delta)$ from Equation 2.16 relates the spin angular momentum that rotates the object in the same direction as the rotation for the elliptical polarization. The terms $(\sin\Delta\cos 2\varphi \sin 2\theta)$ describe the effect of alignment along the central axis of the elliptical polarization, except if the incident beam is circularly polarized.

2.7 Cross-Polarization in Optical Tweezers

The cross-polarization view comprises two polarizers that are perpendicular to each other. The material that exhibits birefringence traits is visible under the cross-polarization view. Some researchers reported the use of a cross-polarization view to

05-4506832 pustaka.upsi.edu.my Perpustakaan Tuanku Bainun Kampus Sultan Abdul Jalil Shah PustakaTBainun ptbupsi

05-4506832 pustaka.upsi.edu.my Perpustakaan Tuanku Bainun Kampus Sultan Abdul Jalil Shah PustakaTBainun ptbupsi

inspect birefringence material. The cross-polarization view was used to characterize internal cavity modulation of corn starch microcapsule (SMC) in water at T = 60 °C (SMC60), T = 65 °C, (SMC65) and T = 70 °C (SMC70) (Wulff et al., 2020). Figure 2.8 shows the microscopy image (top: brightfield, down: cross-polarized view) of native corn starch granules and corn starch microcapsules (SMCs) at different temperatures in water.

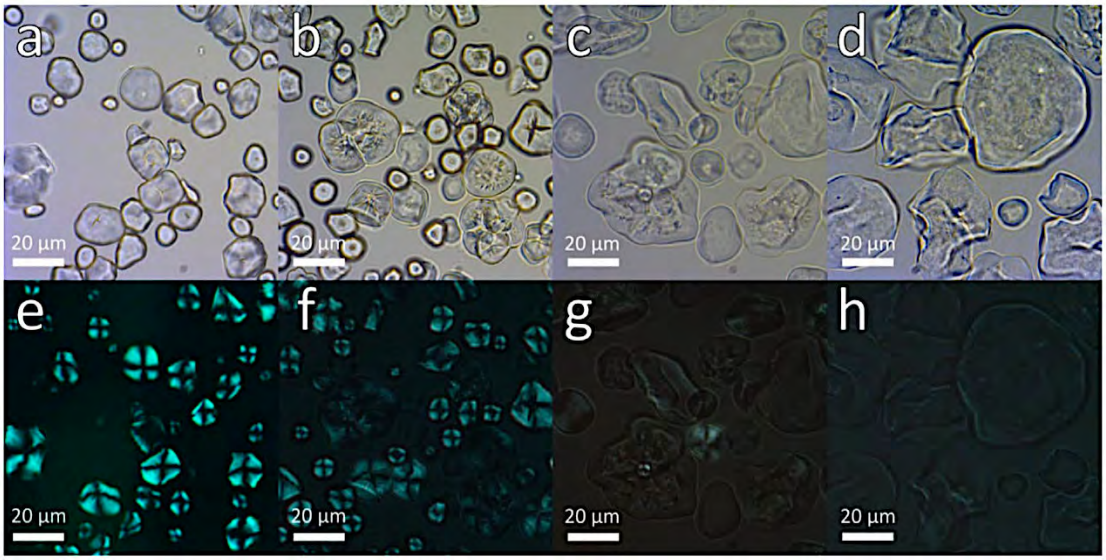


Figure 2.8. Microscopy images (top: brightfield, bottom: cross-polarized view correspond to the identical exact particles) of native corn starch granules (a and e), SMC60 particles (b and f), SMC65 particles (c and g), and SMC70 particles (d and h) in water (Wulff et al., 2020).

The brightfield microscopy images show the swelling process from (a) to (d) as the size of the particles increases when heated at higher temperatures when the particle is thoroughly wet and in water. The cross-polarization view monitors the crystallinity of the corn starch granules from (e) to (h). The cross-polarization view blocks light, and the corn starch granule allows light to scatter due to birefringence properties, resulting in the visibility under the cross-polarized view. The birefringence of starch granules

05-4506832 pustaka.upsi.edu.my Perpustakaan Tuanku Bainun Kampus Sultan Abdul Jalil Shah PustakaTBainun ptbupsi

05-4506832 pustaka.upsi.edu.my Perpustakaan Tuanku Bainun Kampus Sultan Abdul Jalil Shah PustakaTBainun ptbupsi

diminishes from (e) to (h) as shown in Figure 2.8. The “Maltese cross” structure shows the radial configuration representing high order inside the corn starch granules. However, this birefringence loss is due to melting of crystallites due to heating. In another experiment, the cross-polarization view was also used to differentiate flour based on the difference in morphology of the “Maltese cross” of the starch of different flours (Fernández-Canto et al., 2023).

2.8 Optical Trapping of Solid Dielectric Particle

Optical tweezers create a trap spot that attracts and captures dielectric particles. In a state where the spherical dielectric particles move freely in a liquid medium (water), the trapped particles are confined within the trapping spot. In contrast, the free particle keeps moving. Once the particle has been optically trapped, it can be moved in x, y, and z directions by controlling the position of a linearly polarized laser beam. In addition, converting the linearly polarized laser beam into a circularly polarized laser beam can rotate the trapped particle.

Several researchers reported the observation of optical force by optical tweezers on the trapped particle. One of the research presents optical tweezers with integrated digital holographic microscopy (Patel et al., 2021). Figure 2.9 illustrates the developed system's optical trapping and manipulation of the 6 μm.

05-4506832 pustaka.upsi.edu.my Perpustakaan Tuanku Bainun Kampus Sultan Abdul Jalil Shah PustakaTBainun ptbupsi

05-4506832 pustaka.upsi.edu.my Perpustakaan Tuanku Bainun Kampus Sultan Abdul Jalil Shah PustakaTBainun ptbupsi

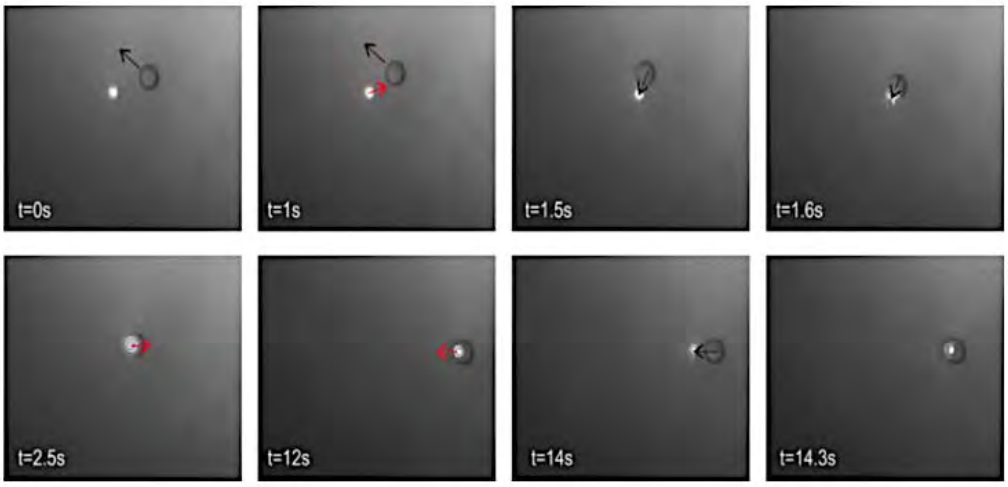


Figure 2.9. the developed system's optical trapping and manipulation of the 6 µm and 10 µm (Patel et al., 2021).

The red and black arrows indicate the trapping and polystyrene beams' movements. The trapping beam is immobile at t = 0 s, while the polystyrene beam is moved freely in the solution medium. At t = 1 s, the trapping beam moves towards the free polystyrene bead. The polystyrene bead is attracted to the trapping beam at t = 1.5 s and t = 1.6 s. The polystyrene bead is in the middle of the trapping beam. As observation time increases, at t = 2.5 s, the trapped polystyrene bead is confined at the center of the trapping beam, and it follows the movement of the trapping beam in the right direction. As the trapping beam moves to the left, the polystyrene bead remains confined and follows the trapping beam movement at t = 12 and 14 s. As the trapping beam movement was immobile, the trapped polystyrene bead remained at the center of the trapping beam at t = 14.3 s. Experimental studies show that the optical trapping system can immobilize and manipulate microparticles such as polystyrene beads.

05-4506832 pustaka.upsi.edu.my Perpustakaan Tuanku Bainun Kampus Sultan Abdul Jalil Shah PustakaTBainun ptbupsi

05-4506832 pustaka.upsi.edu.my Perpustakaan Tuanku Bainun Kampus Sultan Abdul Jalil Shah PustakaTBainun ptbupsi

In another experiment, the effect of laser power and size on the optical trapping of polystyrene beads in water was studied (Hamid et al., 2016). The study aimed to measure the spatial distribution of the optically trapped microbeads by using different lasers powers and different microbead sizes. In their experiment, two laser powers were chosen to trap a single polystyrene microbead (1 to 3 μm). The laser power used was p_1 = 85 mW and p_2 = 122 mW.

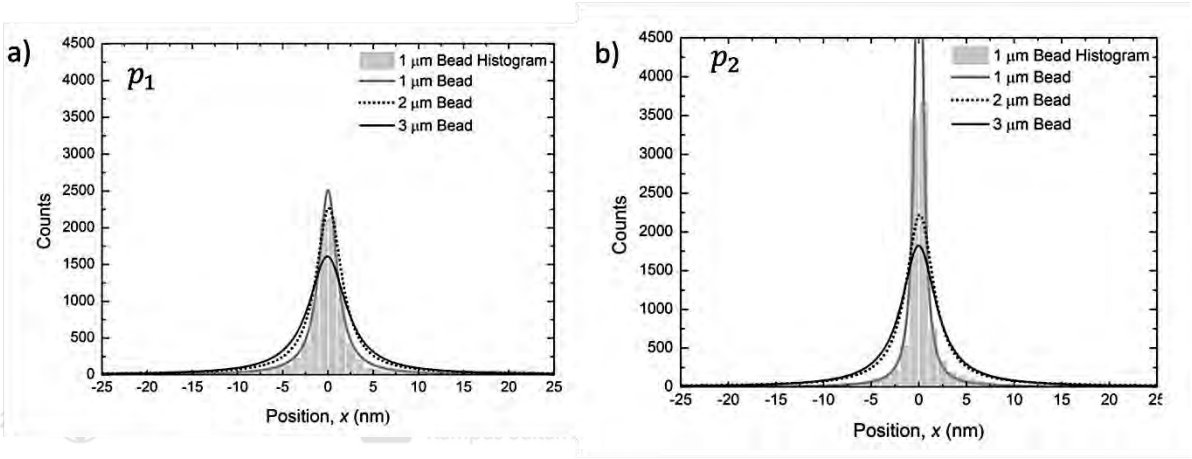


Figure 2.10. The graph of the *x*-axis position histogram for polystyrene microbead trapped in water for (a) p_1 and p_2 , (Hamid et al., 2016).

Figure 2.10 shows the graph of the *x*-axis position histogram for polystyrene microbeads trapped in (a) p_1 and (b) p_2. There were three sizes of the polystyrene microbead 1 μm, 2 μm and 3 μm were trapped in water at p_1 and p_2. The histogram peak was higher in Figure 2.10 (b) compared to the histogram peak in Figure 2.10 (a). This indicated that the optical trapping force was stronger for the higher laser power used, which was p_2. The intense laser power pushed the trapped polystyrene bead closer to the center of the laser trap and caused the mean position to become smaller, as shown in Figure 2.10 (b). This highlights that the mean of the microbead position was closer to the initial position (zero) when the laser power was higher. Based on Figure 2.10 (a)

05-4506832 pustaka.upsi.edu.my Perpustakaan Tuanku Bainun Kampus Sultan Abdul Jalil Shah PustakaTBainun ptbupsi

05-4506832 pustaka.upsi.edu.my Perpustakaan Tuanku Bainun Kampus Sultan Abdul Jalil Shah PustakaTBainun ptbupsi

and (b), the histogram peak was higher for 1 μm polystyrene microbead and lowest for 3 μm polystyrene bead for both p_1 and p_2. They also measure the effective lateral radius r_{eff} based on the histogram of the microbead position. The result highlights that the effective lateral radius r_{eff} increase with the polystyrene microbead sizes at the fixed laser power used. In addition, the effective lateral radius r_{eff} decreased with the increasing laser power compared to the same polystyrene microbead size. This proved that laser power significantly affects the strength of the optical force. The strength of the optical force reduces with an increase in the polystyrene microbead. However, this study only focuses on the trapping of polystyrene beads of range 1-3 μm and 85-122 mW laser power. The behavior of the trapping is within this constraint.

05-4506832 pustaka.upsi.edu.my Perpustakaan Tuanku Bainun Kampus Sultan Abdul Jalil Shah PustakaTBainun ptbupsi

2.9 Optical Trapping of Soft Liquid Microdroplet

Optical tweezers are capable of optically trapping a single liquid microdroplet. Typically, the insoluble liquid forms a microdroplet in a dispersion medium (for example, water) due to the insolubility factor and surface tension. The liquid microdroplet can be optically trapped with optical tweezers if there is a refractive index mismatch between the trapped liquid microdroplet and the surrounding medium. To be precise, the refractive index of the liquid microdroplet must be greater than the refractive index of the surrounding medium (Yusof et al., 2020). It is, therefore, essential to ensure that the gradient force generated by optical tweezers is greater than the scattering force. Thus, the liquid microdroplet can be trapped. Optical trapping of the liquid microdroplet is challenging due to the liquid nature of the microdroplet. For example, the shape of the liquid microdroplet can change, deform, or damage when a

05-4506832 pustaka.upsi.edu.my Perpustakaan Tuanku Bainun Kampus Sultan Abdul Jalil Shah PustakaTBainun ptbupsi

05-4506832 pustaka.upsi.edu.my Perpustakaan Tuanku Bainun Kampus Sultan Abdul Jalil Shah PustakaTBainun ptbupsi

solid optical force is applied. This condition could affect the optical signal of the trapped liquid microdroplet.

The former researcher studied the optical manipulation of a liquid microdroplet. First, the quantitative optical trapping of organic solvents microdroplet optical trapping was studied (Yusof et al., 2020). Organic solvents: ethanol, chloroform, and ethyl acetate, exhibit low melting and boiling points, and optical trapping in a water medium offers technical flexibility (Yusof et al., 2020). This experiment uses an infrared laser beam with a wavelength of 915 nm as the primary trapping laser source. The laser power densities used in this study for optical trapping are 6.3 MW/cm^2. Figure 2.11 shows the optimal microdroplet count for optical trapping. Figure 2.12 shows the f_c of various microdroplet sizes at a 6.3 MW/cm^2 laser power density for 1,2-dichlorobenzene, toluene, and chloroform.

05-4506832 pustaka.upsi.edu.my Perpustakaan Tuanku Bainun Kampus Sultan Abdul Jalil Shah PustakaTBainun ptbupsi

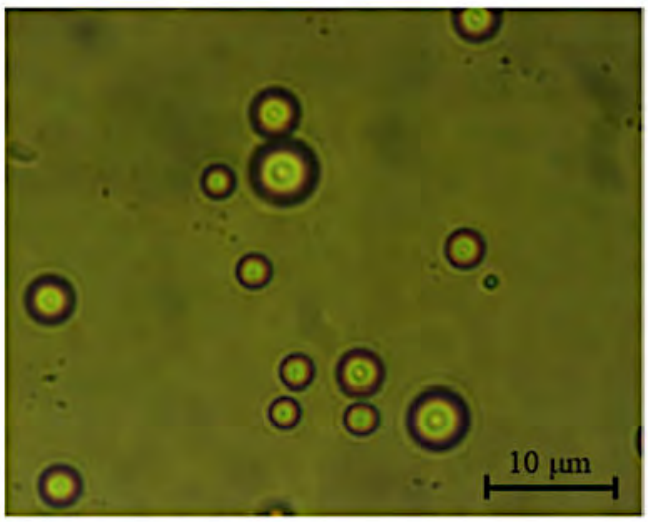


Figure 2.11. The optimal microdroplet number for optical trapping (Yusof et al., 2020).

05-4506832 pustaka.upsi.edu.my Perpustakaan Tuanku Bainun Kampus Sultan Abdul Jalil Shah PustakaTBainun ptbupsi

05-4506832 pustaka.upsi.edu.my Perpustakaan Tuanku Bainun Kampus Sultan Abdul Jalil Shah PustakaTBainun ptbupsi

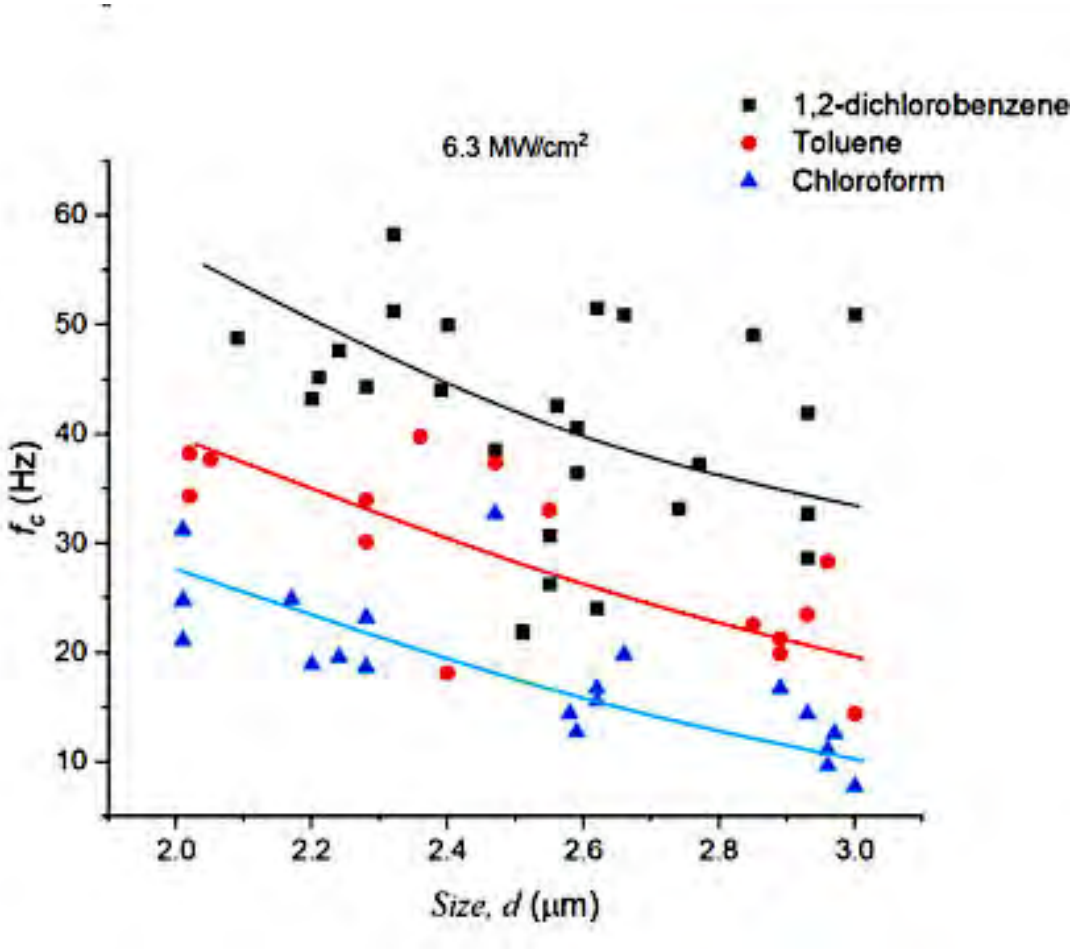


Figure 2.12. f_c for various microdroplet sizes at a 6.3 MW/cm^2 laser power density. The eye guides are drawn to indicate the trend of the f_c (Yusof et al., 2020).

Their study highlights that organic solvent microdroplet optical trapping was possible (Yusof et al., 2020; Yusuf & Ayop, 2020). Figure 2.12 shows that f_c plot is scattered for microdroplet size from 2 to 3 μm. The eye guides are drawn to show the exponential decrease of f_c trend when microdroplet size decreases despite with the scattered plot. Hence, the size of the particle affects f_c at fixed k_T. However, this study focuses on the f_c trend specifically for microdroplet sizes ranging from 2 to 3 μm and at a fixed laser power of 6.3 MW/cm^2. There is no information on the f_c trend for microdroplet size less than 2 μm and at lower laser power used. In addition, this study recommends using the correct physical properties of trapped particles with their

05-4506832 pustaka.upsi.edu.my Perpustakaan Tuanku Bainun Kampus Sultan Abdul Jalil Shah PustakaTBainun ptbupsi

05-4506832 pustaka.upsi.edu.my Perpustakaan Tuanku Bainun Kampus Sultan Abdul Jalil Shah PustakaTBainun ptbupsi

environment, such as density, water solubility, and refractive index for organic solvent microdroplet optical trapping. Despite that, the finding also highlights that optical control strength varies with the size and density of the organic solvent microdroplet. This finding shows that trapping a single organic solvent with optical tweezers is possible.

In addition, it was reported that the airborne hydrocarbon droplets fabricated from oil mist can be optical trapped (Taylor et al., 2005). This optical technique creates a trapped environment using higher trap strength to confine single droplets from a mist at the focal point. The droplet image was recorded by a CCD camera mounted for inverted microscopy. Figure 2.13 shows the image of the trapped aerosol droplet.

05-45068

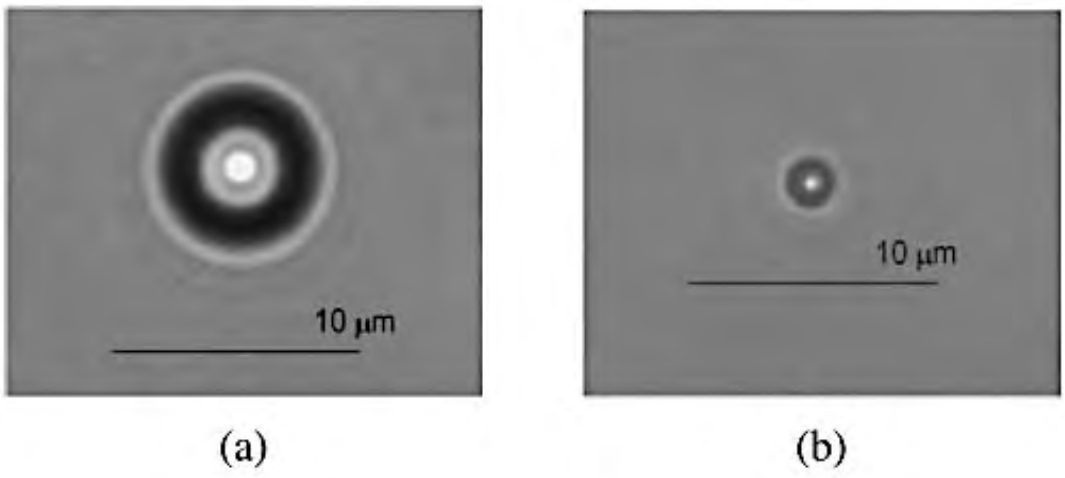


Figure 2.13. The image of aerosol droplet optically trapped (a) 6.7 µm and (b) 2.0 µm (Taylor et al., 2005).

Figure 2.13 shows how the optical tweezers successfully capture airborne droplets with a diameter of 6.7 µm and 2.0 µm. The trapped droplets in the air can be used to study droplet interaction (Taylor et al., 2005). This study manages to capture and control the size of air droplets by adjusting the depth of the laser focus in the sample

05-4506832 pustaka.upsi.edu.my Perpustakaan Tuanku Bainun Kampus Sultan Abdul Jalil Shah PustakaTBainun ptbupsi

05-4506832 pustaka.upsi.edu.my Perpustakaan Tuanku Bainun Kampus Sultan Abdul Jalil Shah PustakaTBainun ptbupsi

chamber or by manipulating and merging multiple droplets. Although the study presented manipulation and control of the captured airborne droplet, physical measurement of the magnitude of the optical force required to capture a single airborne droplet was not performed.

Optical trapping of a liquid microdroplet, such as an organic solvent, an aerosol droplet, or an oleic acid droplet, is possible using optical tweezers (Aas et al., 2013; Miura et al., 2020; Parmentier et al., 2021; Wei et al., 2019; Yusof et al., 2020; Yusuf & Ayop, 2020). The stable trapping of microdroplets has been well reported, but the measurement of optical stiffness has not been performed. Due to this fact, the information on the optical stiffness of the microdroplet is still missing. Only limited information has been reported on the optical stiffness of the microdroplet, for example, the organic solvent (Yusof et al., 2020; Yusuf & Ayop, 2020). This finding underscores that the f_c and k_T show the variation with laser power and microdroplet size. This leads to difficulties in deriving the relationship between f_c and k_T with microdroplet size. Compared to soft particle trapping with solid particle trapping, solid particle trapping shows the precise relationship between f_c and k_T (Aziz et al., 2016; Hamid et al., 2016; Sarshar et al., 2014).

2.10 Liquid Crystal Introduction

Liquid crystal material is unique because it simultaneously exhibits liquid and crystal properties (Prakash et al., 2020; Zeng, 2017). Liquid crystals flow like a liquid, while their molecules are aligned crystal-like (Iwabata et al., 2013). A liquid is isotropic, and

05-4506832 pustaka.upsi.edu.my Perpustakaan Tuanku Bainun Kampus Sultan Abdul Jalil Shah PustakaTBainun ptbupsi

05-4506832 pustaka.upsi.edu.my Perpustakaan Tuanku Bainun Kampus Sultan Abdul Jalil Shah PustakaTBainun ptbupsi

its molecules lack positional and translational order. In contrast, a crystal is a phase in which the molecules are characterized by positional and translational order. The molecule in a liquid crystal phase has partial positional and translational order.

Liquid crystal is an anisotropic liquid. Anisotropic liquids have properties intermediate between liquid and solid crystals (Smalyukh et al., 2006). Liquid crystals are anisotropic liquids because they flow like liquids. They are composed of anisotropic molecules and exhibit long-ranging orientational order and varying degrees of positional order (Smalyukh et al., 2006). Anisotropic liquid crystal has features that make it easy to manipulate, such as rich elastic complexity, self-assembly in various supramolecular structures, and fast response functions to electric and magnetic fields (Lee et al., 2013).

05-4506832 pustaka.upsi.edu.my Perpustakaan Tuanku Bainun Kampus Sultan Abdul Jalil Shah PustakaTBainun ptbupsi

For this reason, they have anisotropic physical properties such as refractive index, dielectric constant, elastic behavior, or viscosity, to name just a few (Dierking & Al-zangana, 2017). For example, the anisotropic liquid crystal has a unique double index of refraction. They have birefringence, where light enters the sample and is split into two parts. Both rays are oppositely polarized, travel at different speeds, and show color effects when observed under polarizing filters (Prakash et al., 2020).

Due to the anisotropic properties of liquid crystals, liquid crystal molecules can be controlled and manipulated by a specific technique. For example, LC molecules can be aligned and manipulated using electric and magnetic fields (Mertelj & Lisjak, 2017; Upadhyay et al., 2015). Furthermore, electric field (pyroelectric) (Merola et al., 2013) and light (optical trapping) (Gleeson et al., 2006; Lee et al., 2013) are specific methods

05-4506832 pustaka.upsi.edu.my Perpustakaan Tuanku Bainun Kampus Sultan Abdul Jalil Shah PustakaTBainun ptbupsi

05-4506832 pustaka.upsi.edu.my Perpustakaan Tuanku Bainun Kampus Sultan Abdul Jalil Shah PustakaTBainun ptbupsi

used to manipulate the internal configuration of birefringent nematic liquid crystal nematic director and shape. Furthermore, due to their orientational elasticity, LC can self-assemble and thus preserve topological defect structures, giving them the potential for further use in modern display technologies (Prakash et al., 2020).

2.11 Classification of Liquid Crystal

The liquid crystal can be classified according to its molecular characteristics. The standard molecular feature of liquid crystals is calamatic (rod shape) or discotic (disc shape). The liquid crystal of calamatic molecular structure has a rod-shaped molecule. Meanwhile, the discotic liquid crystal has disc-shaped molecular features. The representation of the calamatic and discotic liquid crystal is shown in Figure 2.14.

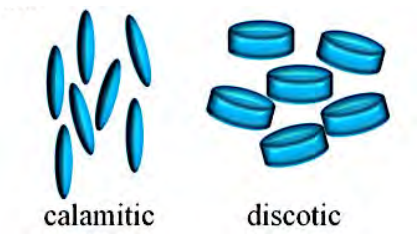


Figure 2.14. The molecular features of calamatic and discotic liquid crystals (Shen & Dierking, 2019).

The liquid crystal can be classified into thermotropic, lyotropic, and amphotropic. Thermotropic liquid crystals have rod-like organic molecules, demonstrating that phase transition to liquid crystal depends on temperature. Thermotropic liquid crystal material obtains liquid crystal characteristics at specific temperature ranges. Figure 2.15 shows the thermotropic liquid crystal characterized as

05-4506832 pustaka.upsi.edu.my Perpustakaan Tuanku Bainun Kampus Sultan Abdul Jalil Shah PustakaTBainun ptbupsi

05-4506832 pustaka.upsi.edu.my Perpustakaan Tuanku Bainun Kampus Sultan Abdul Jalil Shah PustakaTBainun ptbupsi

nematic, sematic, and cholesteric according to the arrangement of molecules (Khoo, 2009; Kulkarni et al., 2021; Palffy-muhoray, 2007).

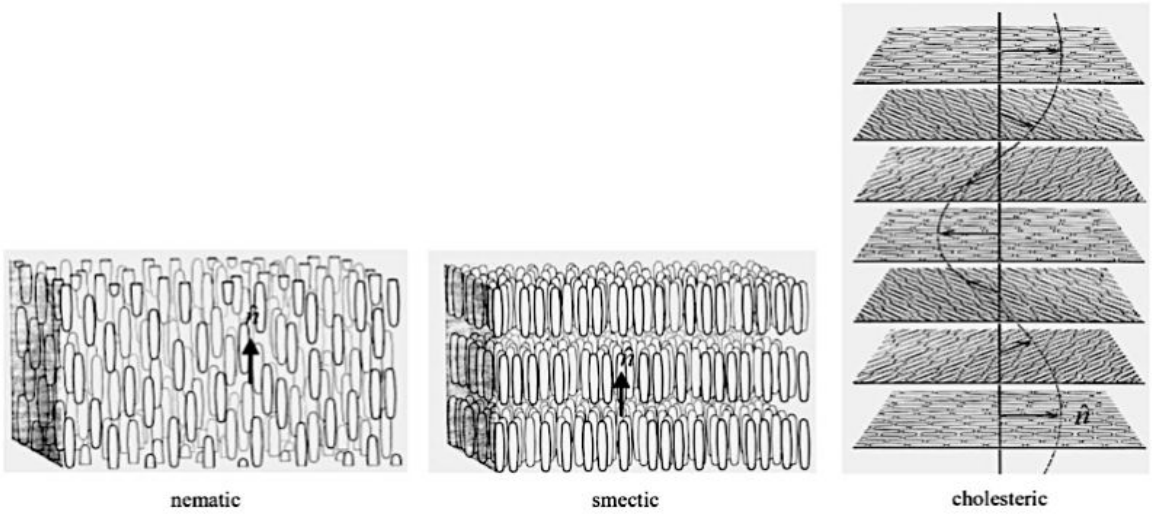


Figure 2.15. Illustrates the thermotropic liquid crystal molecules arrangement the in the nematic, cholesteric, and sematic phases (Khoo, 2009).

A nematic phase is a common phase of thermotropic liquid crystals. The molecules in the nematic phase lack order of position and are self-assembled in a parallel, distant direction to each other, according to director n (Mirantsev et al., 2016; Taylor et al., 2006; Wo et al., 2015). In addition, the direction molecules alignment of the nematic liquid crystal is unique. The optical industry applied nematic liquid crystals because of simple reorientation and uniaxial alignment. (Zeng, 2017). The axis of nematic crystals is susceptible to external field perturbation, resulting in exceptional light-scattering capability (Khoo, 2009). The nematic phase is recorded with a cross-polarization microscope for optical characterization. The smectic phase of the thermotropic liquid crystal takes place at a lower temperature. Its structure consists of perpendicular distinguishable layers to the orientation of long-distance axes. The smectic phase has a layer of structures n . In addition, n is oriented perpendicular to the layer as in smectic-A or at an oblique angle as in smectic-C. A unique structure

05-4506832 pustaka.upsi.edu.my Perpustakaan Tuanku Bainun Kampus Sultan Abdul Jalil Shah PustakaTBainun ptbupsi

05-4506832 pustaka.upsi.edu.my Perpustakaan Tuanku Bainun Kampus Sultan Abdul Jalil Shah PustakaTBainun ptbupsi

layer with appropriate molecule arrangement for every layer characterized the smectic liquid crystal. In addition, orientation order of some degree in smectic liquid.

Next, the thermotropic liquid crystal in the cholesteric phase exhibits a helical (chiral) structure where the absent of positional order with the present organized layer (Khoo, 2009). The director, *n,* spiral around an axis with a pitch in the cholesteric phase. The solid, smectic, nematic, and isotropic phases are ordered based on temperature dependency.

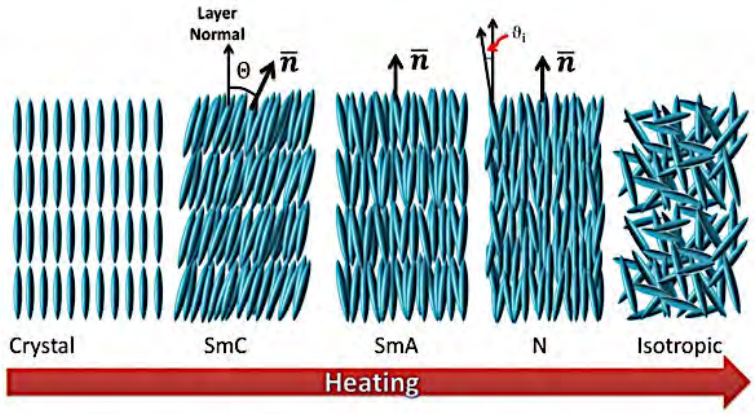


Figure 2.16. The transition of the liquid crystal phase started from crystal to isotropic due to the heating process (Dierking & Al-zangana, 2017).

Figure 2.16 shows the transition change of the liquid crystal phase started from crystal to isotropic due to heating. Upon heating the crystalline state, smectic phases such as smectic C and smectic A are preserved in a partial positional order and the orientational order of a long molecular existence of often rod-like molecules with continuous heating. However, the constant heating of smectic phases caused the loss of positional order, transitioning to the nematic phase of only possess orientation order. In the end, reaching the clearing point causes the loss of all liquid crystalline order, resulting in an isotropic liquid (Dierking & Al-zangana, 2017).

05-4506832 pustaka.upsi.edu.my Perpustakaan Tuanku Bainun Kampus Sultan Abdul Jalil Shah PustakaTBainun ptbupsi

05-4506832 pustaka.upsi.edu.my Perpustakaan Tuanku Bainun Kampus Sultan Abdul Jalil Shah PustakaTBainun ptbupsi

Lyotropic is another type of liquid crystal. The self-assembly of liquid crystals forms lyotropic bilayers, micelles, and vesicles according to specific solvent concentrations (Dierking & Al-zangana, 2017). The detergent (sodium decyl sulfate-decanol water) (Liu et al., 2011), soap, and inorganic liquid crystals vanadium pentoxide (V_2O_5) is the example of lyotropic liquid crystals in which either anisotropic or surfactant molecules isotropically (Dierking & Al-zangana, 2017). Figure 2.17 illustrates the lyotropic phases' dependency on amphiphilic molecule concentration in water or solvents. The amphiphile molecules disperse in the solvent in a condition below the critical micelle concentration (CMC). However, at higher concentrations, the amphiphilic molecules form micelles of various shapes, such as spherical, disc, or rod-shaped, based on the molecule's shape. The micelles at concentrated solvent aggregate into structural order and form an inverse-type hexagonal, cubic, or lamellar phase. The phase diagram of the experiment is complex and primarily dependent on temperature and concentration.

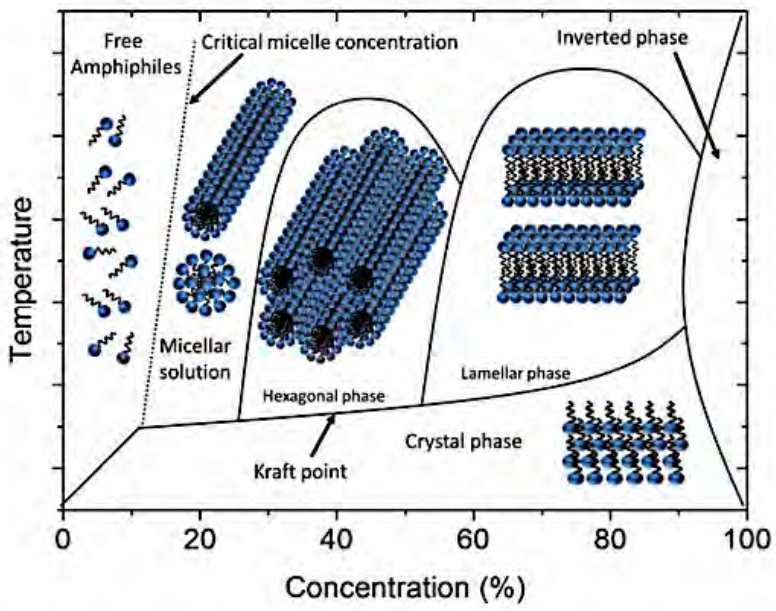


Figure 2.17. Schematic representation of the phase diagram of an amphiphilic surfactant in an isotropic solvent that forms lyotropic phases. (Dierking & Al-zangana, 2017).

05-4506832 pustaka.upsi.edu.my Perpustakaan Tuanku Bainun Kampus Sultan Abdul Jalil Shah PustakaTBainun ptbupsi

05-4506832 pustaka.upsi.edu.my Perpustakaan Tuanku Bainun Kampus Sultan Abdul Jalil Shah PustakaTBainun ptbupsi

2.12 Effective Refractive Index (n_{eff}) of the Nematic LC

Liquid crystal molecules have birefringent properties. A single liquid crystal molecule is modeled as an ellipsoid, as shown in Figure 2.18. Liquid crystal typically has two indices of refraction. In general, for a given direction of propagation, the refractive index can take two values corresponding to the fast and slow polarization of the beam. In uniaxial crystals, one polarization is necessary perpendicular to the optic axis and called ordinary polarization; the other, the extraordinary polarization, is orthogonal to the ordinary polarization and the wave vector. Depending on the relative magnitudes of the ordinary refractive index (n_o) and the extraordinary refractive index (n_e), a uniaxial crystal is known to be positively uniaxial ($n_e > n_o$) or negatively uniaxial ($n_e < n_o$). As the crystal orientation changes, the ordinary index of refraction remains constant, and the extraordinary refractive index varies. In this case, the index ellipsoid is rotating, as shown in Figure 2.18.

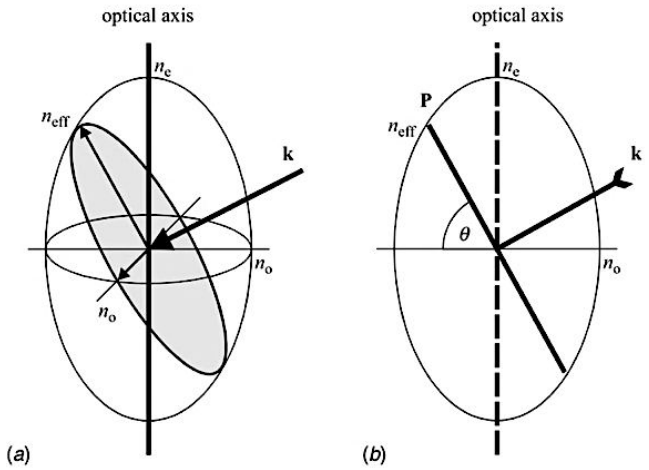


Figure 2.18. Index ellipsoid for the case of uniaxial materials. (a) A plane perpendicular to the wave vector defines the plane of the electric field components experienced (n_o) and (n_{eff}) (b) The effective refractive index n_{eff} can be calculated with a geometric construction in the plane of incidence. Adapted from (Scharf, 2007).

05-4506832 pustaka.upsi.edu.my Perpustakaan Tuanku Bainun Kampus Sultan Abdul Jalil Shah PustakaTBainun ptbupsi

05-4506832 pustaka.upsi.edu.my Perpustakaan Tuanku Bainun Kampus Sultan Abdul Jalil Shah PustakaTBainun ptbupsi

The ordinary direction of oscillation lies in the circular section of the indicatrix (i.e., perpendicular to the optical axis) with a refractive index (n_o). Light moving along the optical axis experiences exactly this refractive index, the ordinary refractive index. The extraordinary direction of oscillation lies in the plane of the wavefront and perpendicular to the ordinary direction of oscillation and has a refractive index (n_{eff}). The value of n_{eff} is determined from the ordinary index of refraction and the principal extraordinary index of refraction (n_e) as follows. Consider a cross-section of the indicatrix as shown in Figure 2.18 (b), which includes the optical axis and the extraordinary direction of oscillation. The equation for this ellipse is

$$\frac{X^2}{n_0^2} + \frac{Y^2}{n_e^2} = 1 \tag{2.23}$$

05-4506832 pustaka.upsi.edu.my Perpustakaan Tuanku Bainun Kampus Sultan Abdul Jalil Shah PustakaTBainun ptbupsi

For point P, it can be seen that $X = n_{eff} \cos\theta$ and $Y = n_{eff} \sin\theta$. Therefore

$$\frac{\left(n_{eff} \cos\theta\right)^2}{n_0^2} + \frac{\left(n_{eff} \sin\theta\right)^2}{n_e^2} = 1 \tag{2.24}$$

which directly to the equation of n_{eff},

$$n_{eff} = \frac{n_e n_0}{\sqrt{n_e^2(\cos\theta)^2 + n_o^2(\sin\theta)^2}} \tag{2.25}$$

which fulfills the definition of the effective refractive index.

05-4506832 pustaka.upsi.edu.my Perpustakaan Tuanku Bainun Kampus Sultan Abdul Jalil Shah PustakaTBainun ptbupsi

05-4506832 pustaka.upsi.edu.my Perpustakaan Tuanku Bainun Kampus Sultan Abdul Jalil Shah PustakaTBainun ptbupsi

It is so interesting that liquid crystal molecules have a n_{eff} value that changes depending on the director orientation of the liquid crystal molecules on a flat surface or the curve interface. Since optical force depends on the refractive index of the trapped material, changing in the n_{eff} of liquid crystal molecules is expected to affect the optical force.

2.13 Nematic Liquid Crystal Internal Configuration

"Nematic" refers to the liquid crystal molecule arrangement in the typical thermotropic liquid crystal. In this state, the molecules exhibit orientation order of the molecular long axis without positional order of center of mass. As a result, the liquid crystal molecules align with the average direction of the molecules represented by the director ($\vec{n}$). The control of director orientation at the surface or interface is the basis for all liquid crystal applications. The careful selection of surface or interface is essential to enforce specific orientation, which propagates over macroscopic distances within the material and the LC confinement in a specific geometry. The easy axis determines the preferred orientation of the director near an interface. Figure 2.19 defines zenith (θ) and azimuth (φ) angles counting from the *z* and *x* axes.

05-4506832 pustaka.upsi.edu.my Perpustakaan Tuanku Bainun Kampus Sultan Abdul Jalil Shah PustakaTBainun ptbupsi

05-4506832 pustaka.upsi.edu.my Perpustakaan Tuanku Bainun Kampus Sultan Abdul Jalil Shah PustakaTBainun ptbupsi

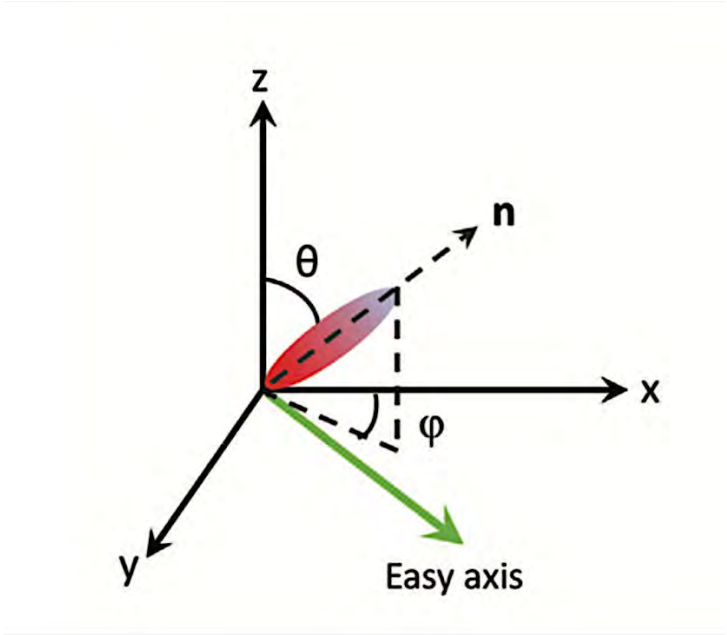


Figure 2.19. The schematic diagram of the zenithal (θ) and azimuthal (φ) definition director angles to characterize the preferred orientation of a liquid crystal, set by alignment (easy axis) on a flat surface. Adapted from (Esteves et al., 2020).

05-4506832 pustaka.upsi.edu.my Perpustakaan Tuanku Bainun Kampus Sultan Abdul Jalil Shah PustakaTBainun ptbupsi

2.13.1 Flat Surface

The first type of interface forms between a liquid crystal and a flat surface, for example, a solid (Esteves et al., 2020). In electro-optical application, the liquid crystal is sandwiched between two treated glass substrates to produce preferential alignment, and this template has been widely studied. The intermolecular interaction between the liquid crystal and interface results from various techniques such as mechanical rubbing of organic polymer-coated substrates, photoalignment (exposure to polarize light of photoreactive alignment chemicals), oblique evaporation (usually SiO), and particularly in the case of liquid crystal-assisted gas sensor formats, chemical functionalization of the surface. Figures 2.20 (a) and (b) show the typical director configuration of the liquid crystal molecules on a flat surface.

05-4506832 pustaka.upsi.edu.my Perpustakaan Tuanku Bainun Kampus Sultan Abdul Jalil Shah PustakaTBainun ptbupsi

05-4506832 pustaka.upsi.edu.my Perpustakaan Tuanku Bainun Kampus Sultan Abdul Jalil Shah PustakaTBainun ptbupsi

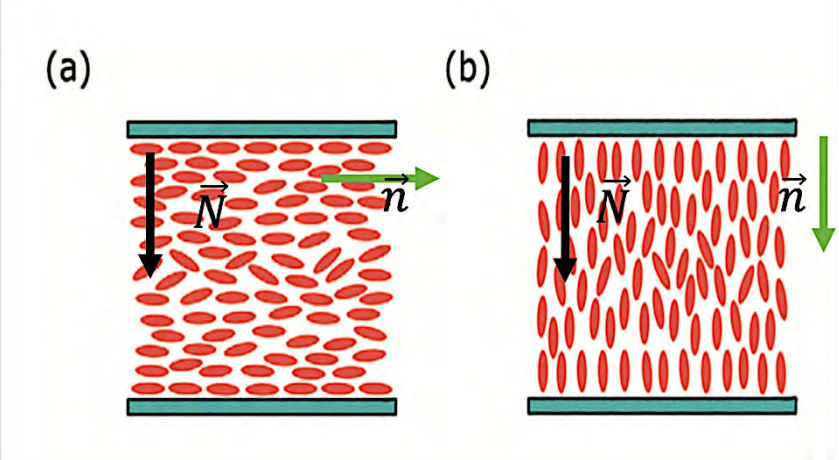


Figure 2.20. (a) Planar alignment and (b) homeotropic director configuration of the liquid crystal molecules on the flat surface. $\vec{N}$ is a vector orthogonal to the plane surface and $\vec{n}$ is the director of the liquid crystal molecules. Adapted from (Esteves et al., 2020).

Figure 2.20 (a) shows the planar alignment since the liquid crystal molecules that are close to the surface are aligned parallel to the surface ($\theta = 90°$) while Figure 2.20 (b) shows the homeotropic alignment since the aligned liquid crystal molecules perpendicular to the flat surface ($\theta = 0°$). Changes in the director configuration of the liquid crystal molecules also change the effective index of refraction of the liquid crystal system for the planar surface.

2.13.2 Spherical Geometry

The second interface type is created by the confinement of liquid crystals in spherical geometries, typically distributed within a second immiscible medium (Esteves et al., 2020). The typical director configuration of the liquid crystal molecules due to the spherical interfaces is shown in Figure 2.21.

05-4506832 pustaka.upsi.edu.my Perpustakaan Tuanku Bainun Kampus Sultan Abdul Jalil Shah PustakaTBainun ptbupsi

05-4506832 pustaka.upsi.edu.my Perpustakaan Tuanku Bainun Kampus Sultan Abdul Jalil Shah PustakaTBainun ptbupsi

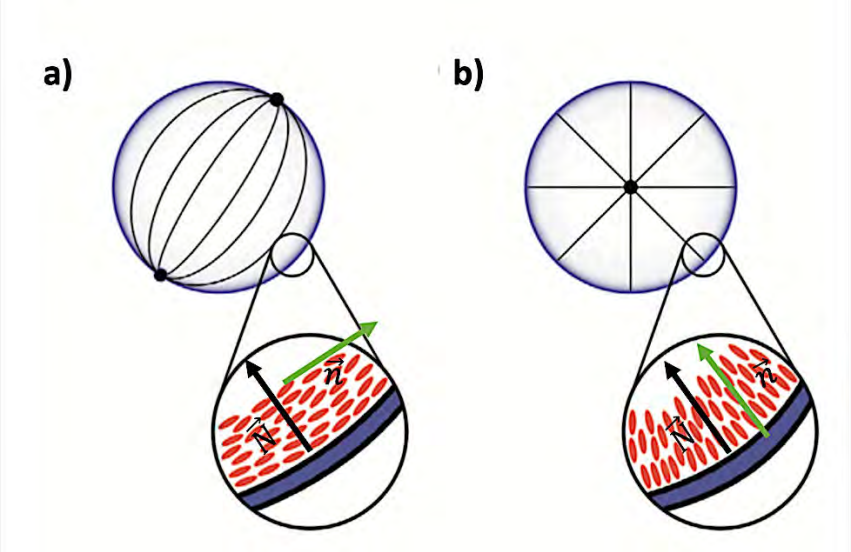


Figure 2.21. (a) The illustration of bipolar configuration because of planar anchoring, (b) radial configuration because of homeotropic anchoring in droplet form. Adapted from (Esteves et al., 2020).

The director alignment inside the liquid crystal droplet depends on the interfacial and elastic balancing contributions to the free energy and droplet size. However, the system's geometry cannot withstand continuous loading of the liquid crystal (such as a combination of spreading, bending, and twisting) as dictated by the anchoring conditions. Hence, the topological defects form and stabilize (or destabilize) the configuration of the director. A starting point for determining the director profile within a drop would be the anchoring conditions. Nematic droplets have a simple topology where planar anchoring conditions result in the two-point defect at diametrically opposite positions on the droplet's surface (boojums), called bipolar configuration.

In contrast, the director field adopts a radial configuration for homeotropic anchoring. Figure 2.22 (a) and (b) illustrate that the radial configuration has a central point defect in the droplet's core called a hedgehog. Figure 2.22 (b) and (d) shows the

05-4506832 pustaka.upsi.edu.my Perpustakaan Tuanku Bainun Kampus Sultan Abdul Jalil Shah PustakaTBainun ptbupsi

05-4506832 pustaka.upsi.edu.my Perpustakaan Tuanku Bainun Kampus Sultan Abdul Jalil Shah PustakaTBainun ptbupsi

homeotropic and planar anchoring of nematic droplets observed under bright field microscopy. The bright-field microscopy can be used to visualize the hedgehog of the core defect of the radial director. The position of the sample with the crossed polarizers determines the bipolar and radial optical texture, as shown in Figure 2.22 (a) and (c). Bright-field microscopy can be used to identify surface defects or boojums, as shown in Figure 2.22 (b) and (d).

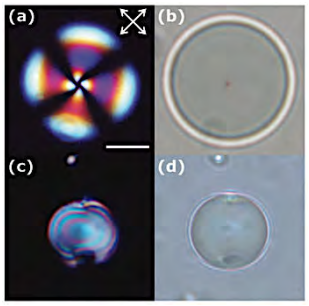


Figure 2.22. The snapshot of the polarized light microscopy images of nematic droplets (a) radial and (c) bipolar. The snapshot of bright field microscopy of (b) radial and (d) bipolar. The scale bar corresponds to 10 µm. Adapted from (Esteves et al., 2020).

05-4506832 pustaka.upsi.edu.my Perpustakaan Tuanku Bainun Kampus Sultan Abdul Jalil Shah PustakaTBainun ptbupsi

Various stable or metastable spherical geometry with various director configurations have been reported. The intermediate spherical geometry is formed between radial and bipolar configurations. The transition of radial to bipolar nematic configuration is possible by adjusting the anchoring conditions. The change in the director field was observed significantly from a bipolar nematic droplet during the change of surface anchoring. The formation of a defect ring is observable in a plane perpendicular to the boojum axis when boojums disappear. The shrinking of the ring to a point defect located at one of the droplet poles. Then the homeotropic was observed when the point defect moved into the core.

05-4506832 pustaka.upsi.edu.my Perpustakaan Tuanku Bainun Kampus Sultan Abdul Jalil Shah PustakaTBainun ptbupsi

05-4506832 pustaka.upsi.edu.my Perpustakaan Tuanku Bainun Kampus Sultan Abdul Jalil Shah PustakaTBainun ptbupsi

2.14 4-Cyano-4'-Pentylbiphenyl (5CB)

One commonly used thermotropic liquid crystal is 4-Cyano-4'-pentylbiphenyl (5CB) ($C_{18}H_{19}N$). 5CB is used to study liquid crystal material because it exists in the nematic phase at room temperature. It can be used as a suitable model compound to study simple nematic physical behavior (Hanemann et al., 1995). At room temperature, 5CB is a nematic liquid crystal (Sengupta, Herminghaus, & Bahr, 2014). The high temperature ($T \approx 34^{\circ}C$) causes 5CB nematic phase to change to isotropic phase (Sengupta et al., 2014). Conversely, the low temperature ($T \approx 22.4^{\circ}C$) causes the 5CB nematic phase to cool down to the crystal phase (Sengupta et al., 2014).

The thermotropic nematic liquid crystal molecules consist of a core and a side chain (Iwabata et al. 2013). The core part (rigid body) of the 5CB molecules provides anisotropic properties and shape, and the side chain (flexible part) is responsible for molecule flow and mobility. Figure 2.23 shows the 5CB molecular structure.

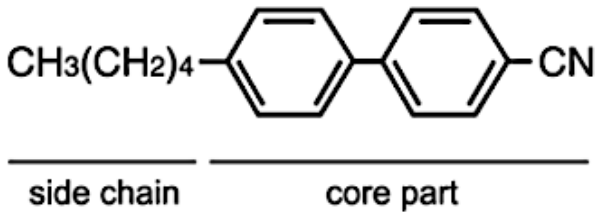


Figure 2.23. 5CB molecular structure (Khoo, 2009).

Figure 2.23 shows the 5CB molecular structure, which comprises a side chain with two or more aromatic rings connected by linking groups and connected to an end

05-4506832 pustaka.upsi.edu.my Perpustakaan Tuanku Bainun Kampus Sultan Abdul Jalil Shah PustakaTBainun ptbupsi

05-4506832 pustaka.upsi.edu.my Perpustakaan Tuanku Bainun Kampus Sultan Abdul Jalil Shah PustakaTBainun ptbupsi

group at the other end. The liquid crystals' properties, for instance, dielectric constants, elastic constants, viscosities, absorption spectra, phase transition temperatures, conductivity, and photosensitivity, depend on these molecular components (Khoo, 2009).

Related to the physical properties, the 5CB water solubility is 0.07 mg/L (Peddireddy et al., 2012). 5CB has two refractive indices called ordinary and extraordinary refractive indices of 1.54 and 1.74 (Usman et al., 2013). The density of 5CB is 1.008 g/mL. The nematic phase is recorded with a cross-polarized microscope for optical characterization. The 5CB uniqueness is due to birefringent properties with directed indices of refraction. Due to birefringence properties, the light imposed the linear and angular momentum on the 5CB microdroplet, resulting in droplet confinement and rotation.

05-4506832 pustaka.upsi.edu.my Perpustakaan Tuanku Bainun Kampus Sultan Abdul Jalil Shah PustakaTBainun ptbupsi

Next, the internal configuration inside the 5CB can be controlled or affected by employing a surfactant unique to the study. The dispersion of 5CB creates microdroplets in water that can be employed as microactuators and sensor probes. Interestingly, thermotropic liquid crystal, especially 5CB, is temperature-dependent or temperature-sensitive.

2.15 Technique for Microdroplet Production

Liquid crystal, an incredibly thermotropic liquid crystal, disperses in water due to the surface tension and forms microdroplets. The liquid crystal hydrophobicity property in

05-4506832 pustaka.upsi.edu.my Perpustakaan Tuanku Bainun Kampus Sultan Abdul Jalil Shah PustakaTBainun ptbupsi

05-4506832 pustaka.upsi.edu.my Perpustakaan Tuanku Bainun Kampus Sultan Abdul Jalil Shah PustakaTBainun ptbupsi

the immiscible medium causes the formation of spherical droplets (Josue, 2012; Murazawa, Juodkazis, Matsuo, et al., 2005; Niu et al., 2016). 5CB shows that liquid crystals disperse in water and form tiny spherical microdroplets.

The preparation technique of the liquid crystal microdroplet can be from vortexing, sonication, homogenization, and hand stirring and begin with the addition of liquid crystal to an immiscible liquid, as shown in Figure 2.24 (A-D) (Concellón, 2023; Wang et al., 2017). Typically, the mixture of 6 to 10 µL of liquid crystal with 2 ml of a uniform aqueous/glycerol phase produces an emulsion of diluted liquid crystal droplets with minimum coalescence initial to polymerization (Tadros, 2013).

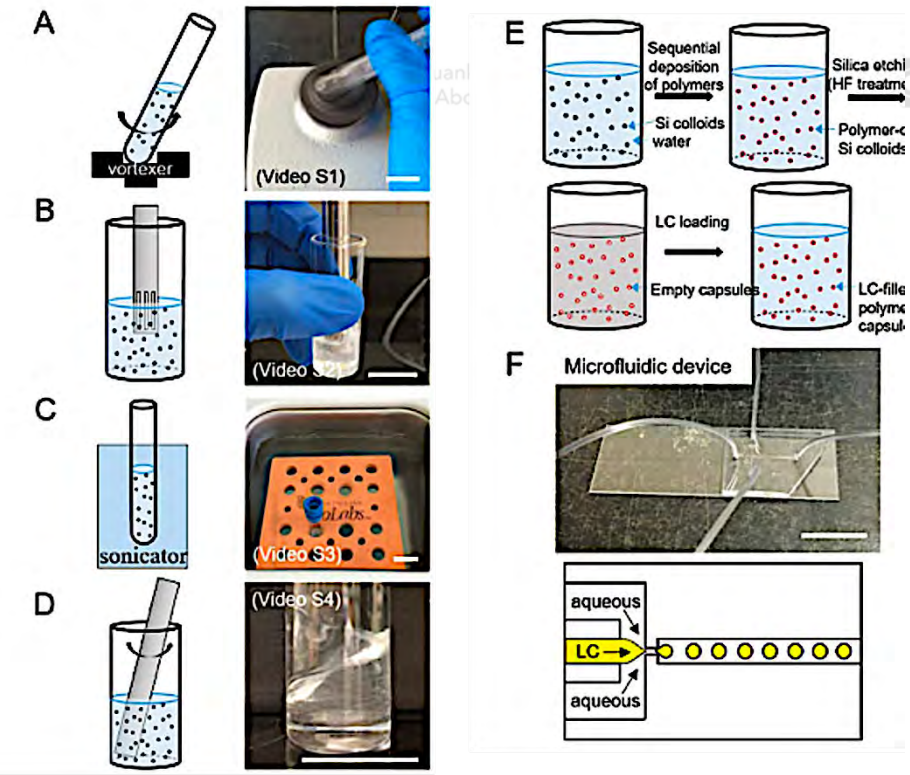


Figure 2.24. Method of making liquid crystal droplets. A: Vortex LC in water. B: Emulsifying liquid crystals using a homogenizer. C: Ultrasonic treatment of liquid crystals in water. D: Emulsifying liquid crystal in glycerol. E: Encapsulation of liquid crystals in polymeric microcapsules. F: Production of liquid crystal droplets using microfluidics. Adapted from (Wang et al., 2017).

05-4506832 pustaka.upsi.edu.my Perpustakaan Tuanku Bainun Kampus Sultan Abdul Jalil Shah PustakaTBainun ptbupsi

05-4506832 pustaka.upsi.edu.my Perpustakaan Tuanku Bainun Kampus Sultan Abdul Jalil Shah PustakaTBainun ptbupsi

Wang et al. (2017), reports the study on the relative merits of liquid crystal droplet preparation methods for polymerization. They demonstrated a few techniques to prepare liquid crystal microdroplets as polymerization templates. The method illustrated in Figure 2.24 (A), quickly produces polydisperse-size liquid crystal droplets. The vortex mixer generates a relatively large liquid crystal droplet, inefficient for the viscous continuous phase like glycerol. Meanwhile, the liquid crystal droplet in a diameter range of 1-50 μm uses homogenizers (Figure 2.24 (B)), while manual shearing generates 10 μm or larger droplets. In addition, a small sample size as low as ~ 100 μL is suitable for the ultrasonic generator technique. The liquid crystal droplet of ~ 100 nm to 10 μm is produced using an ultrasonic generator. Methods 2.24 (A-D) resulted in a polydisperse liquid crystal droplet.

There is also a method that produces monodisperse liquid crystal droplets. The encapsulation of the liquid crystal droplets in polymer capsules generates ~ 0.7 μm to 10 μm, as shown in Figure 2.24 (E). In addition, the use of microfluidic also generates monodisperse liquid crystal droplets. For instance, Figure 2.24 (F) illustrates the microfluidic system constructed from PDMS generating droplet diameter of 10 – 100 μm. The disadvantage of using the microfluidic system is the complexity of avoiding channel clogging and keeping channel walls hydrophilic.

2.16 Nematic Liquid Crystal Microdroplet Production

The production of liquid crystal microdroplets has been reported in previous studies (Juodkazis et al. 1999; Shechter et al. 2020; Usman et al. 2013). Nevertheless, most

05-4506832 pustaka.upsi.edu.my Perpustakaan Tuanku Bainun Kampus Sultan Abdul Jalil Shah PustakaTBainun ptbupsi

05-4506832 pustaka.upsi.edu.my Perpustakaan Tuanku Bainun Kampus Sultan Abdul Jalil Shah PustakaTBainun ptbupsi

studies provided general information about the formulation of liquid crystal microdroplets rather than the specific approach used. Therefore, the generated microdroplets can differ, leading to reproducibility problems. Most previous researchers created a uniform liquid crystal microdroplet by either shaking or stirring the liquid crystal mixture and deionized water. However, it was reported that liquid crystal microdroplet size decreased with increasing stirring time (Niu et al., 2016).

Furthermore, some researchers dispersed the micron size droplet using micropipette injection in the medium. It was reported that 1-2 μL of liquid crystal was injected into ~ 1000 μL of polymer and produced well-separated microdroplets with defined structures dispersed in polymer (PDMS) (Sofi & Dhara, 2019). It also reported the fabrication of liquid crystal emulsion (E7-in water-emulsion) using high-pressure homogenization at 8000 rpm for 1 minute using Ultra turrax homogenizer (Aery et al., 2023). In another study, a polydisperse emulsion of liquid crystal droplet generation is prepared by mechanically agitating in order to stabilize the individual liquid crystal droplet forms (Oster et al., 2022).

The microdroplet size is poorly controlled using shaking or stirring techniques, and the final product is usually inhomogeneous (Concellón, 2023). To avoid these problems, some researchers used special techniques, such as a glass capillary microtube connected to a pump-controlled microchannel to create and manipulate liquid crystal microdroplets of the desired size (Duan et al., 2019; Wang et al., 2016; Yan et al., 2017). For example, Yan et al. (2017), reported the preparation of nematic liquid crystal microdroplets using an 8 μm diameter glass capillary microtube filled with NLC

05-4506832 pustaka.upsi.edu.my Perpustakaan Tuanku Bainun Kampus Sultan Abdul Jalil Shah PustakaTBainun ptbupsi

05-4506832 pustaka.upsi.edu.my Perpustakaan Tuanku Bainun Kampus Sultan Abdul Jalil Shah PustakaTBainun ptbupsi

solution. As shown in Figure 2.25, the single NLC microdroplet with a diameter of 40 µm was overhung at the end of the microtube (Yan et al., 2017).

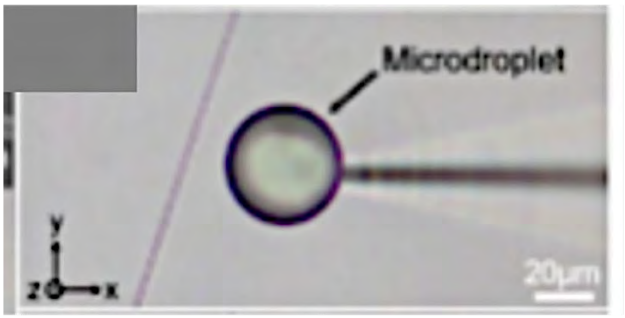


Figure 2.25. An individual NLC microdroplet with a diameter of about 40 µm overhung out of one end of the microtube (Yan et al., 2017).

Likewise, Duan et al. (2019), reported the production of microdroplets using a microtube connected to a syringe pump to disperse the 5CB solution. Again, different sizes of 5CB microdroplets were generated by controlling the injection speed and pump operation time. For example, the microtube produced microdroplets with a diameter of 30 µm to 80 µm, as shown in Figure 2.26.

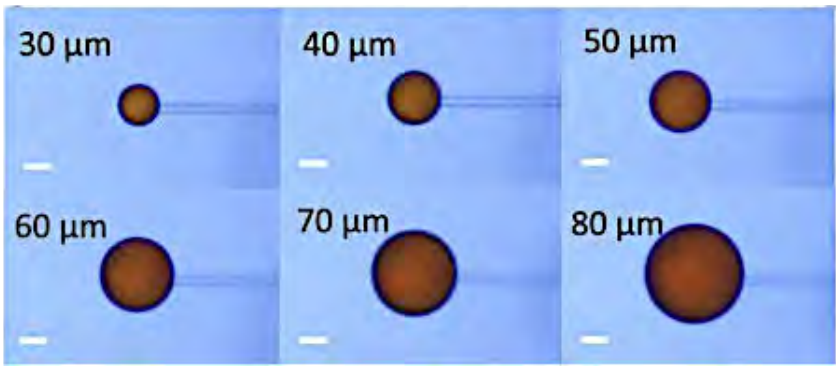


Figure 2.26. Micrographs of the stearic acid-doped 5CB microdroplets with different diameters (Duan et al., 2019).

This microtubing technique has dramatically improved the control of liquid crystal microdroplet production at a specific size. However, the droplet size is larger

05-4506832 pustaka.upsi.edu.my Perpustakaan Tuanku Bainun Kampus Sultan Abdul Jalil Shah PustakaTBainun ptbupsi

05-4506832 pustaka.upsi.edu.my Perpustakaan Tuanku Bainun Kampus Sultan Abdul Jalil Shah PustakaTBainun ptbupsi

(Duan et al., 2019). The introduction of the microfluidic technique in generating monodisperse liquid crystal microdroplets is helpful for size control; however, obtaining smaller-sized microdroplets remain challenging (Deng et al., 2021). The application of microfluidic in liquid crystal microdroplet involves the production of monodisperse Potato Protein Microgel (PoPM), PoPM-stabilized liquid crystal emulsion production of ~15 μm size (Aery et al., 2023). Therefore, trapping relatively large microdroplets in optical trapping measurements is difficult. In addition, the larger droplet size associated with liquid crystal optical trapping requires more laser power and could damage the internal configuration of liquid crystal. Hence, reducing the microdroplet size is crucial in optical trapping applications.

05-4506832 pustaka.upsi.edu.my Perpustakaan Tuanku Bainun PustakaTBainun ptbupsi

2.17 Distribution Size by Using Mechanical Technique

The study of microdroplet distribution size investigation is essential to selecting appropriate sizes of microdroplets formed for specific target applications. Each microdroplet production technique produces a range of microdroplet sizes. The size of the microdroplet distribution indicates the overall size of the microdroplets formed in a sample.

The production of 4-cyano-4-pentylbiphenyl microdroplets dispersed in Sodium Dodecyl Sulfate (SDS) and Phosphate Buffer Saline (PBS) solution was reported (Niu et al., 2016). According to Oscar's report, droplets in a critical state should fragment from a large to a small size (Sotolongo-Costa et al., 1996). In the formation of liquid crystal droplets, the size of the liquid crystal droplets depends on the stirring

05-4506832 pustaka.upsi.edu.my Perpustakaan Tuanku Bainun Kampus Sultan Abdul Jalil Shah PustakaTBainun ptbupsi

05-4506832 pustaka.upsi.edu.my Perpustakaan Tuanku Bainun Kampus Sultan Abdul Jalil Shah PustakaTBainun ptbupsi

time when mixing. Figure 2.27 (a)–(e) shows polarization optical microscopy images of 5CB droplets with a different stirring time of 6 s, 60 s, 120 s, 180 s, and 240 s, where the stirring speed is 600 rpm, and the volume ratio of LC and SDS is 1:15. Figure 2.27 (f) shows the different diameters obtained under different stirring time.

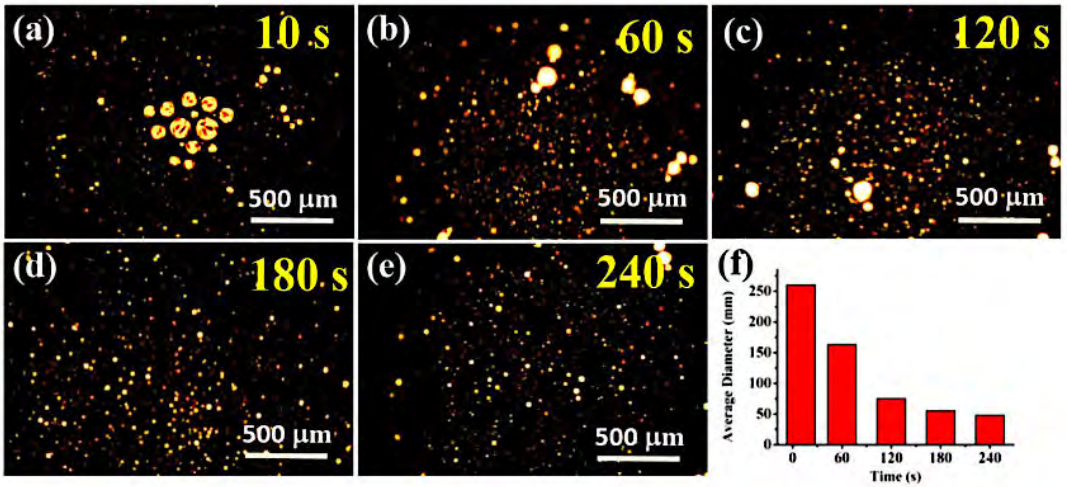


Figure 2.27. Polarization optical microscopy images of 5CB droplets with different stirring times (a) 6 s; (b) 60 s; (c) 120 s; (d) 180 s; (e) 240 s; (f) relationship of the average diameter of droplets formed with stirring time. Scale bar: 500 µm. Adapted from (Niu et al., 2016).

Based on the observation of the formed 5CB microdroplet, the stirring time impacts the size of the 5CB microdroplet. As the stirring time increased, the size of the 5CB microdroplets formed decreased. The average size of the 5CB microdroplet generated by the stirring method ranges from 60 µm to 250 µm, as shown in Figure 2.27 (f). Although the stirring technique can reduce the size of the 5CB microdroplets by increasing the stirring time, the stirring method produced a significantly large 5CB microdroplet size. In addition, the 5CB microdroplet was generated in the PBS solution and not in the water. In optical microdroplet trapping, the stirring technique is unsuitable for the trapping application because the larger 5CB microdroplet is inert with the weak trapping force of optical tweezers.

05-4506832 pustaka.upsi.edu.my Perpustakaan Tuanku Bainun Kampus Sultan Abdul Jalil Shah PustakaTBainun ptbupsi

05-4506832 pustaka.upsi.edu.my Perpustakaan Tuanku Bainun Kampus Sultan Abdul Jalil Shah PustakaTBainun ptbupsi

Apart from that, the effect of ultrasound time on particle size is studied (Asadinezhad et al., 2019). The nanoemulsions (orange oil, sunflower oil, and surfactant) are prepared by a combination of low-energy (spontaneous emulsification) and high-energy (ultrasonic emulsification) methods. In short, Asadinezhad et al. (2019), used emulsification and ultrasonic methods together to create a nanoemulsion. The combination of techniques produced a nanoemulsion in the 70 nm to 130 nm range based on the graph of mean droplet diameter versus ultrasound time shown in Figure 2.28. Examining the trend in mean droplet diameter versus ultrasound time in Figure 2.28 is fascinating. The mean droplet diameter decreases from 0 minutes to 10 minutes of ultrasound application. This indicates the breaking and splitting of particles due to the ultrasonic energy. The previous studies typically showed a decreasing trend in mean particle size with ultrasound time, but not as reported by Asadinezhad. They found that the mean droplet diameter increased when the sonication time exceeded 10 minutes. The possible explanation is that the smaller droplets merge and grow into the larger droplets. This study trend is helpful in predicting the distribution size of nanoelmusions of oil-based material. However, it is but not comparable to the liquid crystal-based material due to differences in their physical properties.

05-4506832 pustaka.upsi.edu.my Perpustakaan Tuanku Bainun Kampus Sultan Abdul Jalil Shah PustakaTBainun ptbupsi

05-4506832 pustaka.upsi.edu.my Perpustakaan Tuanku Bainun Kampus Sultan Abdul Jalil Shah PustakaTBainun ptbupsi

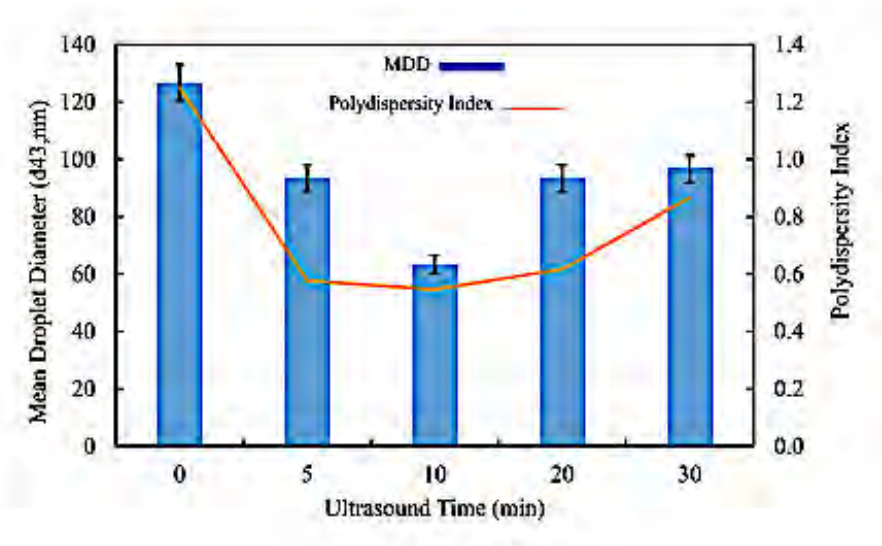


Figure 2.28. The resulting mean droplet diameter (MDD) and polydispersity index (span) from different ultrasonic times of nanoemulsions. Adapted from (Asadinezhad et al., 2019).

In another experiment, Adamow et al. (2017), reported an investigation to prepare different emulsions of liquid crystal and polyvinyl alcohol (PVA) with a different size distribution of liquid crystal domains depending on the time of exposure to ultrasonic waves during homogenization (Adamow et al., 2017). In short, Adamow et al. (2017), successfully introduced a technique to generate different emulsions of liquid crystal and PVA with different size distributions of liquid crystal domains depending on the exposure time of ultrasonic waves during homogenization. The 10-, 15-, 20- and 30-minute ultrasound exposure resulted in 34.17, 8.53, 8.13, and 4.79 µm of liquid crystal microdroplet diameter. Their result shows that the average diameter of the microdroplets decreases significantly with exposure time, as shown in Figure 2.29. The range of liquid crystal microdroplets generated was between 4.79 µm and 34.17 µm. Although the distribution size was measured throughout the study, the liquid crystal microdroplets generated were larger. The liquid crystal microdroplet generation process involves PVA, water, and dye mixtures of different physical quantities. Too

05-4506832 pustaka.upsi.edu.my Perpustakaan Tuanku Bainun Kampus Sultan Abdul Jalil Shah PustakaTBainun ptbupsi

05-4506832 pustaka.upsi.edu.my Perpustakaan Tuanku Bainun Kampus Sultan Abdul Jalil Shah PustakaTBainun ptbupsi

many mixtures mixed could be the reason the microdroplets formed are larger. It would be helpful to find the distribution size of pure liquid crystal in water without chemicals or dye to obtain the primary size of the liquid crystal microdroplet sizes. The limitation of this study is the unclear trend of average microdroplet diameter from 0 to 10 minutes of exposure time. Hence, it is challenging to estimate the average microdroplet diameter at a shorter sonication time.

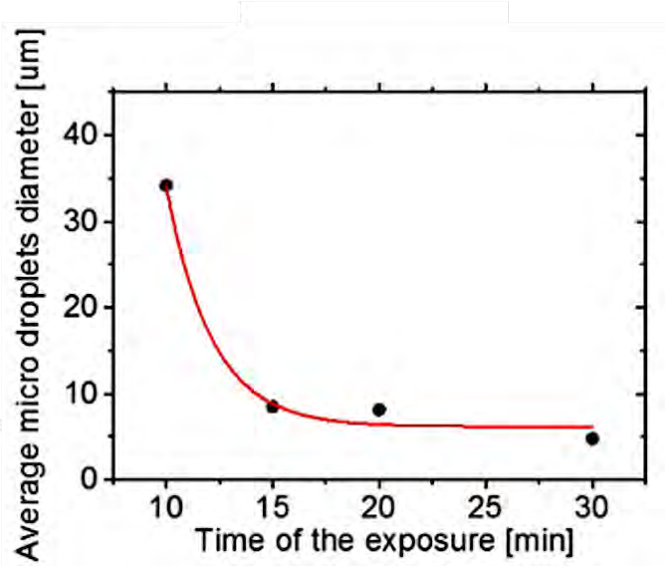


Figure 2.29. The average droplet size is a function of exposure time on ultrasounds. Adapted from (Adamow et al., 2017).

In addition, the effect of the ultrasonic time on the gelation emulsification was investigated (Li et al., 2023). The different sonication times of 0, 3, 6, 9, 12 and 15 minutes of 20 kHz and 400 W were applied to the gelation emulsification process. Figure 2.30 shows the graph of particle size of gelatin emulsion treated with different sonication times. The particle size of the gelation emulsion before ultrasonication was 10.57 μm. The particle size of the gelation emulsion decreases as small as 5.92 μm at 12 minutes and increases to 6.15 μm at 15 minutes. The possible explanation for the increase in the particle size of the gelatin emulsion is the aggregation of droplets into

05-4506832 pustaka.upsi.edu.my Perpustakaan Tuanku Bainun Kampus Sultan Abdul Jalil Shah PustakaTBainun ptbupsi

05-4506832 pustaka.upsi.edu.my Perpustakaan Tuanku Bainun Kampus Sultan Abdul Jalil Shah PustakaTBainun ptbupsi

larger droplets due to mechanical vibration turbulence of the dispersed phase into the continuous phase (Li et al., 2023). The limitation of this study is that the estimation of particle size trend beyond 15 minutes is unclear. The particle size trend might be useful for gelatin-based material but not suitable to be compared with liquid-crystal-based due to the difference in physical characteristics.

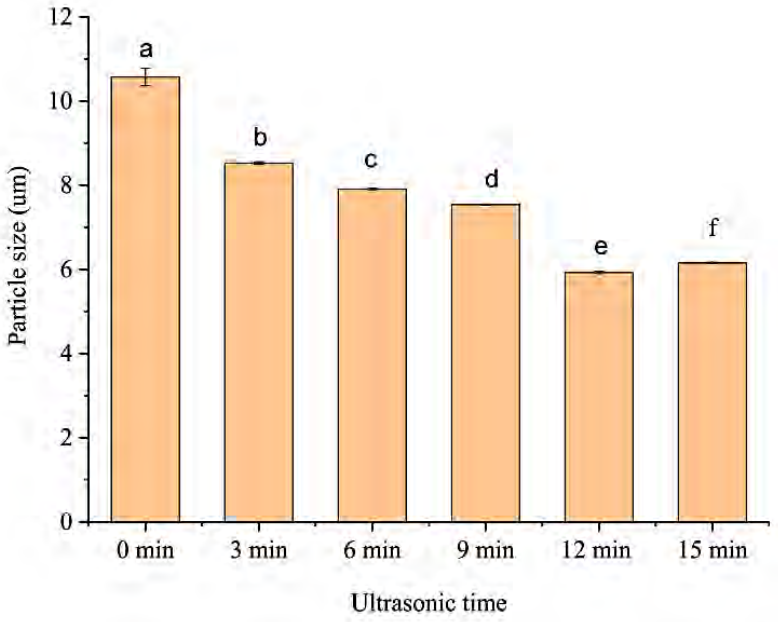


Figure 2.30. The particle size of the gelation emulsion was treated with different sonication times. Adapted from (Li et al., 2023).

2.18 Microdroplet Internal Configuration Modification

The liquid crystal can generally be prepared in thin film or microdroplets (Loussert et al., 2013; Sen et al., 2013; Škarabot et al., 2014). Several studies have highlighted that liquid crystals form a spherical droplet in immiscible liquid due to their hydrophobicity (Josue H., 2012; Murazawa, Juodkazis, Matsuo, et al., 2005; Niu et al., 2016). Besides

05-4506832 pustaka.upsi.edu.my Perpustakaan Tuanku Bainun Kampus Sultan Abdul Jalil Shah PustakaTBainun ptbupsi

05-4506832 pustaka.upsi.edu.my Perpustakaan Tuanku Bainun Kampus Sultan Abdul Jalil Shah PustakaTBainun ptbupsi

discussing the technique to control the size of the liquid crystal microdroplet generated in water, it is also interesting to control and modify the internal configuration inside the liquid crystal microdroplet. The liquid crystal microdroplet can take on various internal configurations. The stable internal configuration of the liquid crystal microdroplet is bipolar and radial. The intermediate internal configuration phase is monopolar, preradial, and others.

The study focuses on stable liquid crystal microdroplets with bipolar and radial internal configurations. The liquid crystal molecules inside the microdroplet are rearranged into a preferred configuration depending on surface modification or chemical interaction at the microdroplet interface. The fabrication of the liquid crystal microdroplet is simple but not straightforward. Liquid crystal samples, suspending media such as water, and surfactants are required to produce liquid crystal microdroplets with a specific internal configuration. Conversely, liquid crystal microdroplets with a bipolar internal configuration can be generated by mixing deionized water and liquid crystal.

One of the most common stable internal configurations of liquid crystal is the bipolar. A bipolar internal configuration of the liquid crystal results when the liquid crystal is dispersed in deionized water. No surfactant is required to prepare the liquid crystal having a bipolar internal configuration. The fabrication of the liquid crystal microdroplet with bipolar internal configuration is a straightforward and fast process. The bipolar internal configuration of the liquid crystal microdroplet can be examined under a cross-polarization view.

05-4506832 pustaka.upsi.edu.my Perpustakaan Tuanku Bainun Kampus Sultan Abdul Jalil Shah PustakaTBainun ptbupsi

05-4506832 pustaka.upsi.edu.my Perpustakaan Tuanku Bainun Kampus Sultan Abdul Jalil Shah PustakaTBainun ptbupsi

The other stable state of the internal configuration of the liquid crystal microdroplet is radial. The deionized water and additional surface modification by an additional surfactant are required to generate radially configured liquid crystal microdroplets. The function of the surfactant is to disperse the liquid crystal microdroplet and radially induce the internal configuration within the liquid crystal microdroplet. The surfactant is often used to fix the internal configuration inside the liquid crystal microdroplet. Various types of surfaces are available to anchor and generate radial liquid crystal microdroplets. Examples of surfactants that generally produce a stable liquid crystal droplet formulation are the neutral (ethoxylate derivative of sorbitan monolaurate, Tween 20), anionic (sodium dodecyl sulfate, SDS), and cationic (hexadecyltrimethylammonium bromide, CTAB) surfactants (Murazawa, Juodkazis, & Misawa, 2005). The controlled surfactant concentration must create a perfect internal radial configuration to achieve the internal configuration of liquid crystal microdroplets. The surfactant concentration can vary for different surfactants that produce radial liquid crystal microdroplets. Researchers have reported different surfactant concentrations used to achieve the internal configuration of liquid crystal microdroplets internal configuration (Murazawa, Juodkazis, & Misawa, 2005; Shechter et al., 2020). Figure 2.31 illustrates the dependence of the SDS concentration on the LC microdroplet configuration.

05-4506832 pustaka.upsi.edu.my Perpustakaan Tuanku Bainun Kampus Sultan Abdul Jalil Shah PustakaTBainun ptbupsi

05-4506832 pustaka.upsi.edu.my Perpustakaan Tuanku Bainun Kampus Sultan Abdul Jalil Shah PustakaTBainun ptbupsi

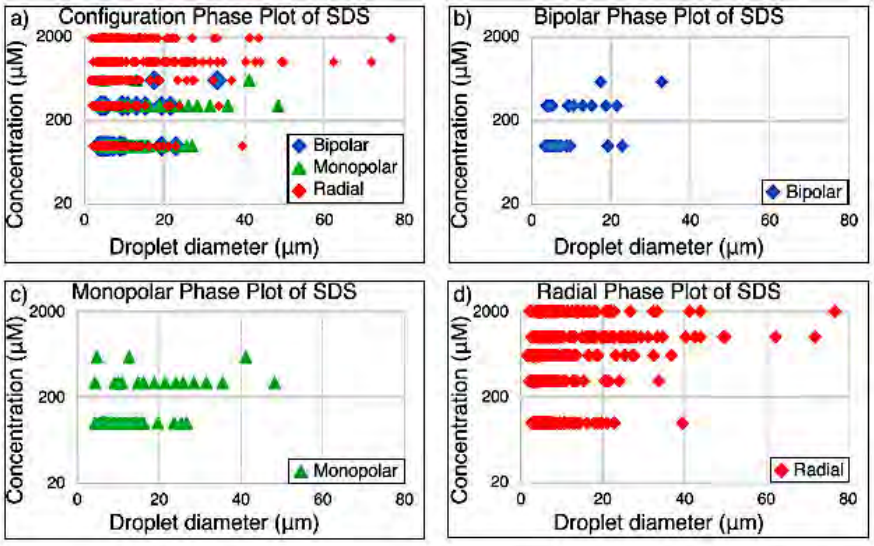


Figure 2.31. Concentration-diameter phase diagram of the 5CB liquid crystal droplets as a function of droplet diameter and SDS concentration. (a) All configurations, (b) bipolar, (c) monopolar and (d) radial are collectively represented (Shechter et al., 2020).

As shown in Figure 2.31, the liquid crystal microdroplet's specific orientation or internal configuration is triggered when the SDS concentration changes. For example, at an SDS concentration of 600 μM, all microdroplets were radial, while at an SDS concentration of 200 μM, bipolar and monopolar microdroplets were observed. The effect of surfactant on the internal configuration formation inside liquid crystal microdroplet was also extended to a surfactant and amphiphilic molecules such as PEG-P10 surfactant to reverse the configurational change process (Oster et al., 2022).

Figure 2.32 depicts the probability of bipolar and radial droplet production based on the CTAB concentration used. The internal configuration inside the LC microdroplet was bipolar for CTAB concentration below 4 μM. In the region between 4 μM to 10 μM CTAB concentration, the small and big LC microdroplets demonstrated bipolar and radial internal configuration, respectively. Meanwhile, the LC microdroplet yielded a radial configuration as the CTAB concentration increased beyond 10 μM.

05-4506832 pustaka.upsi.edu.my Perpustakaan Tuanku Bainun Kampus Sultan Abdul Jalil Shah PustakaTBainun ptbupsi

05-4506832 pustaka.upsi.edu.my Perpustakaan Tuanku Bainun Kampus Sultan Abdul Jalil Shah PustakaTBainun ptbupsi

These findings revealed the need to control the surfactant concentration to produce microdroplets with a specific internal configuration. It was reported that the critical micelle concentration (CMC) of CTAB is 13 μM (Murazawa, Juodkazis, Matsuo, et al., 2005). Hence, the surfactant concentration used must be higher than the CMC value to trigger the bipolar 5CB to change to radial 5CB.

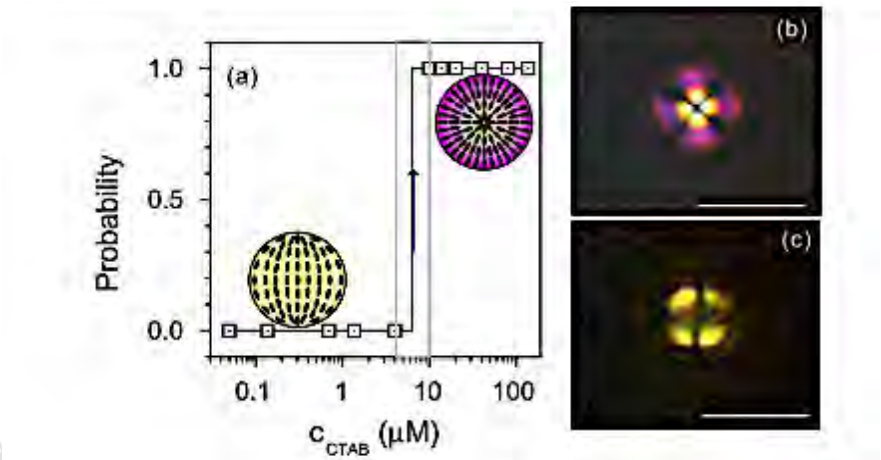


Figure 2.32. (a) Probability of a 5CB droplet having the internal radial alignment versus the concentration of cationic surfactant, 5CB internal configuration (b) radial and (c) bipolar (Murazawa & Juodkazis, 2005).

2.19 Nematic Liquid Crystal Microdroplet Study Stability

The stability of the microdroplet study is critical to ensure that the microdroplet keeps its shape, spreads evenly, does not sink to the bottom, and coagulates with others, thus maintaining the number of microdroplets throughout the experiment. In the meantime, it is also essential to estimate how long the microdroplet can be sustained in the suspension of the study sample suspension. The stability of the microdroplet can be

05-4506832 pustaka.upsi.edu.my Perpustakaan Tuanku Bainun Kampus Sultan Abdul Jalil Shah PustakaTBainun ptbupsi

05-4506832 pustaka.upsi.edu.my Perpustakaan Tuanku Bainun Kampus Sultan Abdul Jalil Shah PustakaTBainun ptbupsi

observed visually under the imaging microscope (Aery et al., 2023; Sofi & Dhara, 2019).

According to Aery et al., (2023), bare (E7, a type of liquid crystal) E7 emulsion in water generated from high-pressure homogenization was unstable with low shelf life where liquid-crystal droplets lasted for 15 minutes. It separated from the emulsion, as shown in Figure 2.33. However, this stability measurement is limited to observation and is not quantitative.

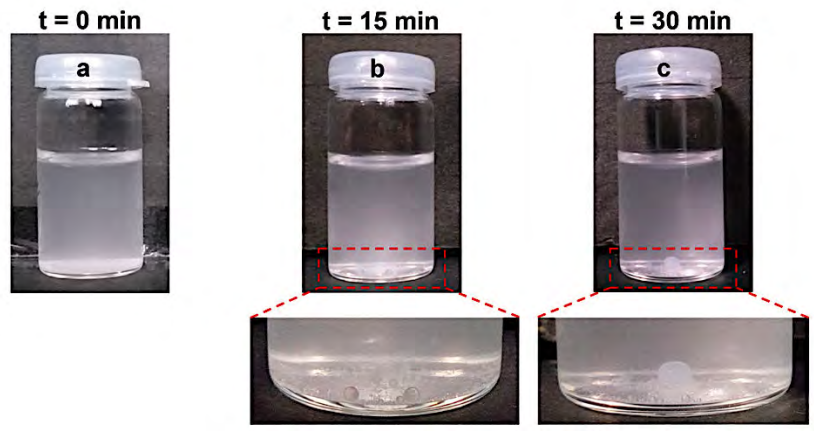


Figure 2.33. Visual image of bare E7 emulsion immediately after preparation (a), after storage 15 minutes and (c) 30 minutes respectively. Adapted from (Aery et al., 2023).

The stability of the liquid crystal microdroplet can also be verified under an optical optical microscope (Sofi & Dhara, 2019). Figure 2.34 shows the time variation of 5CB microdroplet diameters in PDMS. In PDMS, the droplet diameter decreases rapidly non-linearly. For example, the 70 μm microdroplet reduces to 10 μm in 2 hours represented by the red dot in Figure 3.24. Other microdroplet size follows the same trends. This trend indicates the instability of droplets in the PDMS medium.

05-4506832 pustaka.upsi.edu.my Perpustakaan Tuanku Bainun Kampus Sultan Abdul Jalil Shah PustakaTBainun ptbupsi

05-4506832 pustaka.upsi.edu.my Perpustakaan Tuanku Bainun Kampus Sultan Abdul Jalil Shah PustakaTBainun ptbupsi

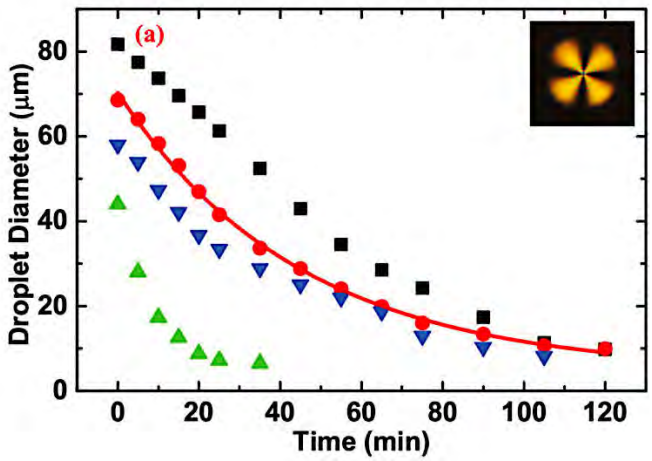


Figure 2.34. Variation of the diameter of 5CB microdroplets with time dispersed in PDMS. (Inset) Polarized optical microscope image of microdroplet with defects. Adapted from (Sofi & Dhara, 2019).

This study provides a qualitative method to determine liquid crystal stability by monitoring the diameter change over time. The limitation of this study is that it depends on the visual observation under a polarized optical microscope and is not quantitative. In addition, the 5CB microdroplet is dispersed in PDMS. The 5CB microdroplet stability might be different in water. There is a need to quantitatively study the microdroplet stability using light transmission to measure accurately.

2.20 Nematic Liquid Crystal Microdroplet Optical Trap

The underlying event in optical trapping is the interaction of optical forces. Optical forces result from the conservation of linear momentum in light-matter interactions, which attract the liquid crystal microdroplet toward the laser spot due to the difference in the refractive index between the liquid crystal microdroplet and its surrounding medium (Donato et al. 2016). As a result, angular momentum is transferred, causing

05-4506832 pustaka.upsi.edu.my Perpustakaan Tuanku Bainun Kampus Sultan Abdul Jalil Shah PustakaTBainun ptbupsi

05-4506832 pustaka.upsi.edu.my Perpustakaan Tuanku Bainun Kampus Sultan Abdul Jalil Shah PustakaTBainun ptbupsi

optical reaction torques on the trapped liquid crystal microdroplets (Donato et al., 2016; Yang et al., 2008). Optical trapping confines birefringence liquid crystal microdroplets dispersed in the water while the light polarization state induces molecular reconfigurations, forming conoscopic structures and microdroplet rotation (Usman et al., 2012). This event initiates the possibility of optical trapping. Previous research on liquid crystal dynamic behavior under various laser power, sizes, and polarization has reported optical manipulation of liquid crystal (Murazawa et al., 2006; Phanphak & Pattanaporkratana, 2014; T-thienprasert, Limtrakul, Zentgraf, & Chattham, 2019). Optical trapping of nematic (Brasselet, 2008; Usman et al., 2011), smectic (Murazawa et al., 2006; Usman et al., 2012), cholesteric (Smalyukh et al., 2007; Yang et al., 2008) and prior researchers have investigated lyotropic liquid crystal (Iwashita & Tanaka, 2003) to demonstrate trapping behavior and molecular reconfiguration. Liquid crystals are unique because they can respond to light polarization, and their molecules tend to orient according to the light polarization state. This change can be observed under a cross-polarized view. The position of liquid crystal droplets during trapping or rotational motion at definite light polarization can be employed to describe the dynamics of liquid crystal optical trapping.

Previous researchers reported the establishment of optical trapping of liquid crystals in the form of microdroplets in the water medium. Optical manipulation of the liquid crystal in the form of microdroplets was reported (Juodkazis et al., 1999). This study reported the observation of the trapped E44 droplet under optical trapping based on linearly and circularly polarized laser beams. The finding shows that linearly polarized light could control the angular reorientation of trapped liquid crystal droplets.

05-4506832 pustaka.upsi.edu.my Perpustakaan Tuanku Bainun Kampus Sultan Abdul Jalil Shah PustakaTBainun ptbupsi

05-4506832 pustaka.upsi.edu.my Perpustakaan Tuanku Bainun Kampus Sultan Abdul Jalil Shah PustakaTBainun ptbupsi

Figure 2.35 shows that the alignment of the liquid crystal droplet can be controlled by rotating the polarization of the incident beam using a half-wave plate.

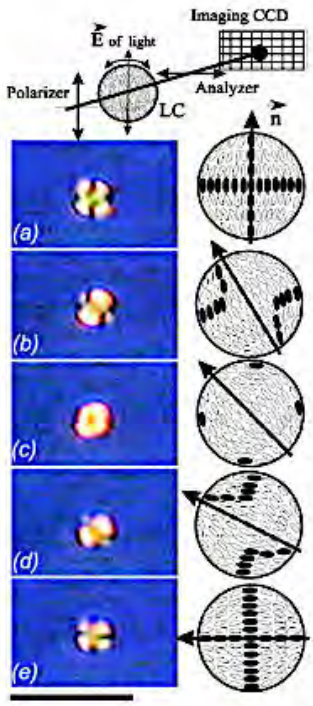


Figure 2.35. The schematic representation of polarization control of the incident trapping beam, the liquid crystal droplet was aligned according to the plane of polarization of the incident beam as shown in (a) to (e) (scale bar: 10 µm). Adapted from (Juodkazis et al., 1999).

Figure 2.35 shows the angle-controlled alignment of a liquid crystal droplet by plane-polarized irradiation. Polar alignment is indicated when the light passes through a polarizer-droplet analyzer, thereby scattering the light (shown schematically on the right in Figure 2.35). The area where it is marked with dark ellipses in the schematic drawing indicates that the passing light is not scattered. Figure 2.35 (e) shows that by controlling the polarization of the incident beam, the liquid crystal droplet is aligned to the plane of polarization of the incident beam. This can be done by rotating the angle of the half-wave plate.

05-4506832 pustaka.upsi.edu.my Perpustakaan Tuanku Bainun Kampus Sultan Abdul Jalil Shah PustakaTBainun ptbupsi

05-4506832 pustaka.upsi.edu.my Perpustakaan Tuanku Bainun Kampus Sultan Abdul Jalil Shah PustakaTBainun ptbupsi

Besides that, the effect of the circular polarization on the single liquid crystal droplet was also studied. They found that the single liquid crystal droplet spun under circularly polarized light, as shown in Figure 2.36.

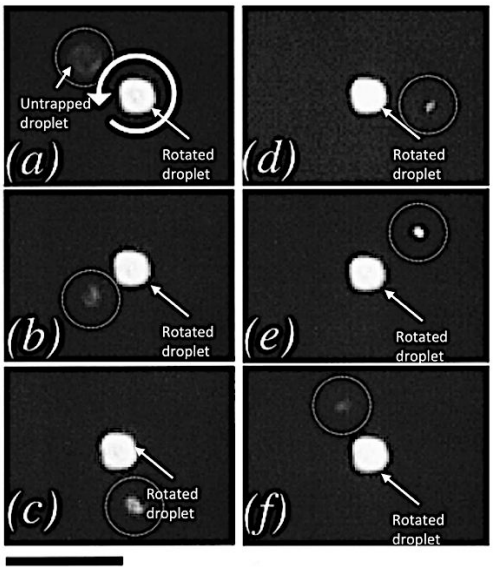


Figure 2.36. (a)-(e) shows the spinning of the rotation of the liquid crystal droplet by circularly polarized light. Scale bar: 10 µm. Adapted from (Juodkazis et al., 1999).

A spinning single liquid crystal microdroplet illuminated by the circularly polarized laser beam is presented in Figure 2.36. Figure 2.36 (a)-(e) shows the sequential images of the single liquid crystal microdroplet spinning. The spinning of the liquid crystal microdroplet was verified by observing the untrapped small particle orbiting the trapped liquid crystal microdroplet.

In brief, Juodkazis et al. (1999), reported that the alignment inside the liquid crystal could be aligned using a linearly polarized laser beam by changing the angle of the half-wave plate. In addition, it was demonstrated that the circularly polarized laser irradiation on the liquid crystal microdroplet could trap it and cause it to be rotated.

05-4506832 pustaka.upsi.edu.my Perpustakaan Tuanku Bainun Kampus Sultan Abdul Jalil Shah PustakaTBainun ptbupsi

05-4506832 pustaka.upsi.edu.my Perpustakaan Tuanku Bainun Kampus Sultan Abdul Jalil Shah PustakaTBainun ptbupsi

Although the effect of a linearly and circularly polarized laser beam could be used to manipulate the internal configuration and rotate the liquid crystal microdroplet, optical measurements such as optical stiffness were not reported. Besides, the range of size of liquid crystal microdroplets that could be trapped and rotated was lacking information.

In addition, the effect of circularly polarized tweezers on liquid crystal droplets was studied (Murazawa, Juodkazis, & Misawa, 2005). Figure 2.37 shows evidence of a single radial 5CB rotation under a circularly polarized laser beam.

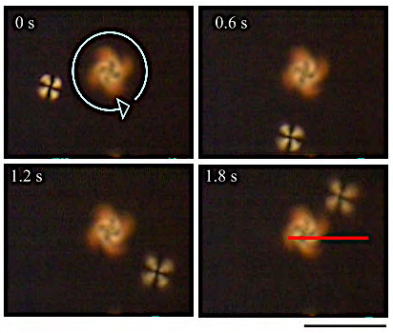


Figure 2.37. Spinning radial 5CB droplet at 310 mW dragged floating droplet into orbiting motion. Scale bar, 10 µm. Adapted from (Murazawa, Juodkazis, & Misawa, 2005).

Figure 2.37 shows the trapped radial 5CB droplet spinning under circularly polarized light at high laser power (P = 310 mW) under a cross-polarized view. The marked arrow at t = 0 s indicates the spinning of the radial 5CB droplet. It could be seen that the nearby particle close to the trapped radial 5CB droplet was changing the position accordingly at t = 0.6 s until t = 1.8 s. The rotation of the nearby particle confirms the spinning of this radial 5CB droplet. The spinning of the bipolar and radial 5CB was further investigated by studying the exposure of several 5CB droplet sizes to the circularly polarized laser beam. The bipolar 5CB droplets of 1.9 µm, 2.5 µm, and

05-4506832 pustaka.upsi.edu.my Perpustakaan Tuanku Bainun Kampus Sultan Abdul Jalil Shah PustakaTBainun ptbupsi

05-4506832 pustaka.upsi.edu.my Perpustakaan Tuanku Bainun Kampus Sultan Abdul Jalil Shah PustakaTBainun ptbupsi

3.2 µm were introduced to the circularly polarized laser beam in a specific laser power up to 360 mW. Meanwhile, for the radial 5CB droplet, several selected sizes, such as 4.8 µm, 5.4 µm 6.7 µm, and 7.8 µm, were also irradiated with a circular laser beam up to 440 mW laser power to study the droplet rotation. Next, the spinning of the bipolar and radial 5CB droplets of different sizes trapped under a circularly polarized laser beam is compared by gradually increasing the laser power, as shown in Figure 2.38.

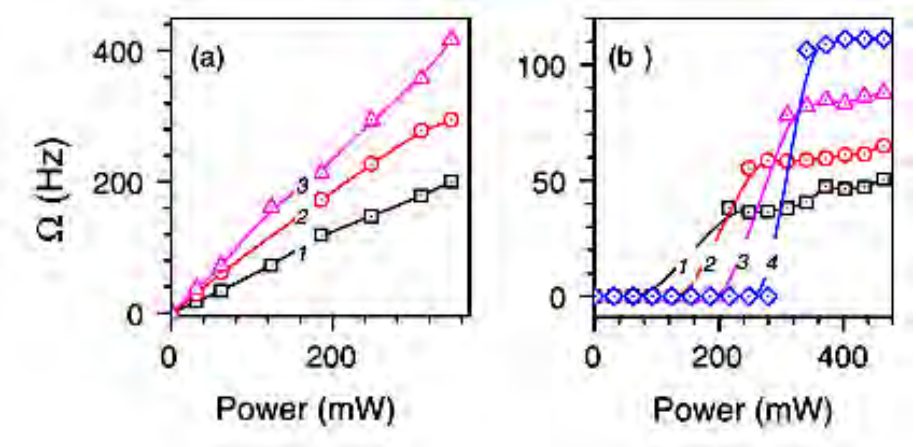


Figure 2.38. (a) Graph of rotation frequency, ω, of bipolar CB5 droplets against laser-power for diameters 3.2 µm (1), 2.5 µm (2), and 1.9 µm (3). (b) Graph of the rotation frequency of radial-5CB droplets against power for diameters 7.8 µm (1), 6.7 µm (2), 5.4 µm (3), and 4.8 µm (4). The lines act as guides for the eye. Adapted from (Murazawa, Juodkazis, & Misawa, 2005).

Figure 2.38 (a) shows the graph of the rotational frequency of the trapping of bipolar 5CB droplets of diameters 3.2 µm (1), 2.5 µm (2), and 1.9 µm (3) under a circularly polarized laser beam at varied laser power. At the same time, Figure 2.38 (b) shows the graph of the rotation frequency of the trapping of radial 5CB droplets of diameter 7.8 µm (1), 6.7 µm (2), 5.4 µm (3), and 4.8 µm (4) under a circularly polarized laser beam at varied laser power. In the context of bipolar droplet rotation, Figure 2.38 (a) shows that in the bipolar 5C droplet, the 3.2 µm droplet has the lowest spinning

05-4506832 pustaka.upsi.edu.my Perpustakaan Tuanku Bainun Kampus Sultan Abdul Jalil Shah PustakaTBainun ptbupsi

05-4506832 pustaka.upsi.edu.my Perpustakaan Tuanku Bainun Kampus Sultan Abdul Jalil Shah PustakaTBainun ptbupsi

frequency while the 1.9 µm droplet has the highest spinning frequency. Notably, the bipolar 5CB droplet in the range of the sizes shown in Figure 2.38 (a) spins at all the laser power used. The lowest laser power to spin the bipolar 5CB droplets was ~ 20 mW. The smallest bipolar 5CB droplets that managed to be trapped was 1.9 µm. The experiment results highlight that the spinning frequency of a bipolar 5CB droplet is proportional to the applied laser power beam and decreases with the droplet diameter. There was a slight difference in the case of exposing the radial 5CB droplets to the circularly polarized laser beam. The radial structure of the 5CB droplet exhibits negligibly small birefringence, causing the angular momentum transfer mechanism from light to the droplet to be unique compared to bipolar droplets (Murazawa, Juodkazis, & Misawa, 2005). It was observed that when the lower laser power was applied, the radial 5CB droplet did not spin. When the laser power was slowly increased to higher, the radial 5CB droplet started to shake with an intermittent spinning pattern. Figure 2.38 (b) shows that the radial 5CB droplets only rotated when the higher laser power was used. The even rotation frequency was achieved when using strong laser tweezing power. The smallest radial 5CB droplet of 4.8 µm rotated faster at very high laser power compared to the large radial 5CB droplet of 7.8 µm. It is attractive to observe that the larger radial 5CB droplet could be spinning at the lower laser power compared to the smaller radial 5CB droplet. The smallest laser power to rotate a radial 5CB droplet of 7.8 µm was ~ 200 mW. The experiment results highlight that the spinning frequency of radial 5CB is proportional to the applied laser power beam and decreased with the droplet diameter.

In short, the findings of Murazawa et al. (2005), showed that the rotation frequency of the trapped 5CB droplet of bipolar and radial are proportionate with the

05-4506832 pustaka.upsi.edu.my Perpustakaan Tuanku Bainun Kampus Sultan Abdul Jalil Shah PustakaTBainun ptbupsi

05-4506832 pustaka.upsi.edu.my Perpustakaan Tuanku Bainun Kampus Sultan Abdul Jalil Shah PustakaTBainun ptbupsi

laser power used. Meanwhile, the rotation frequency reduced with the increase of 5CB droplet size. The angular momentum transfer was different in the case of bipolar and radial 5CB. Despite demonstrating the rotation of bipolar and radial 5CB microdroplets, no optical stiffness measurement was done on the trapped droplet studied. The size of the trapped bipolar and radial microdroplets was bigger from the range of 1.9 to 7.8 μm. The laser power used to study the rotation frequency of the 5CB droplet used was so higher and stronger, up to 440 mW. The information on the rotational frequency of droplet sizes less than 1.9 μm was lacking. It is interesting to present the trapping of the bipolar and radial 5CB droplet using the smallest size and smallest laser power.

Another experiment reported the reconfiguring of bipolar liquid crystal microdroplets (Usman et al., 2013). Figure 2.39 shows the observation of the trapped bipolar nematic 5CB under a linearly polarized laser beam.

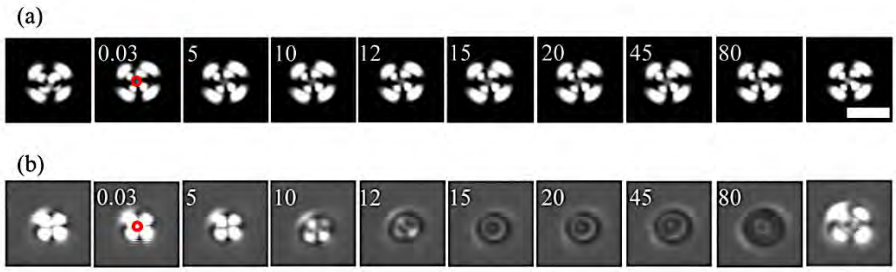


Figure 2.39. Sequences of the time evolution of POM images of an individual bipolar nematic 5CB droplet optically trapped by a linearly polarized trapping beam at (a) 130 mW (or 54 MW/cm2) and (b) 850 mW (or 360 MW/cm2). Adapted from (Usman et al., 2013).

Figures 2.39 (a) and (b) show the POM images of the individual ~2.5 μm nematic 5CB droplet under irradiation by the linearly polarized light beam at different laser power densities. The irradiation laser power in Figure 2.39 (a) was 130 mW or 54 MW/cm^2. Meanwhile, in Figure 2.39 (b), the irradiation laser power used was 850 mW

05-4506832 pustaka.upsi.edu.my Perpustakaan Tuanku Bainun Kampus Sultan Abdul Jalil Shah PustakaTBainun ptbupsi

05-4506832 pustaka.upsi.edu.my Perpustakaan Tuanku Bainun Kampus Sultan Abdul Jalil Shah PustakaTBainun ptbupsi

or 360 MW/cm^2. A few tens of MW/cm^2 laser power can trap the droplet stably at the focal spot. Under the trapping condition, the Maltese cross pattern in Figure 2.39 (a) remains unchanged, indicating that the intrinsic configuration inside the droplet remains intact.

Meanwhile, as the laser power was increased to hundreds of MW/cm^2, the POM images in Figure 2.39 (b) were time-dependence. This is shown in Figure 2.39 (b); at 10 s, the Maltese cross pattern started to disappear and was replaced by the ring pattern from 15 s to 80 s when higher laser power was applied to the trapped nematic 5CB droplet. Typically, a small ring near the center and one or two larger concentric rings showed up clearly on time scales of seconds to a few tens of seconds, depending on the laser power. Such time evolution of POM images indicates unambiguously that reordering inside the optically trapped droplet takes place under the high power of the laser beam. Next, the effect of the circularly polarized laser beam on the trapped 5CB droplet at different laser power densities was also investigated, as shown in Figures 2.40 (a), (b) and (c).

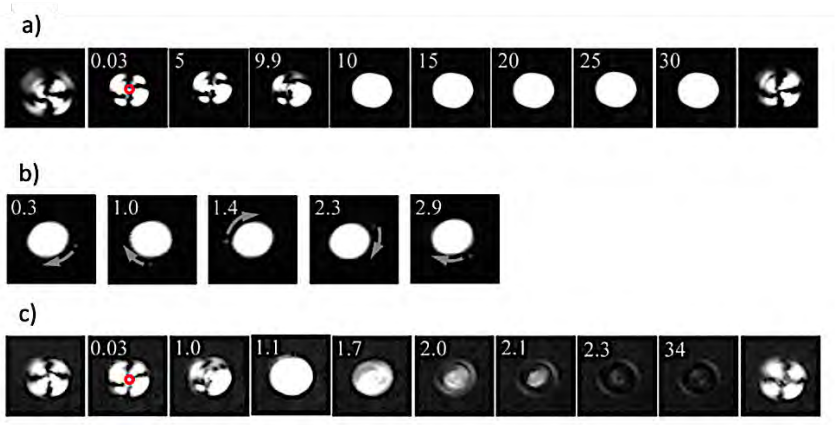


Figure 2.40. Sequences of the time evolution of POM images of an individual bipolar nematic 5CB droplet optically trapped by a circularly (left-handed) polarized laser beam (a) at laser power 460 mW or 190 MW/cm^2, (b) an orbit of a tiny droplet around the rotating optically trapped droplet (the time is in seconds after the droplet starts to rotate), and (c) at laser power 940 mW or 390 MW/cm^2 (Usman et al., 2013).

05-4506832 pustaka.upsi.edu.my Perpustakaan Tuanku Bainun Kampus Sultan Abdul Jalil Shah PustakaTBainun ptbupsi

05-4506832 pustaka.upsi.edu.my Perpustakaan Tuanku Bainun Kampus Sultan Abdul Jalil Shah PustakaTBainun ptbupsi

Figure 2.40 (c)-(e) illustrates the POM images of 5CB droplets of a size of ~3.5 μm trapped at different laser power densities. The 5CB droplet appeared as a full-bright circular area when the low laser power was applied for optical trapping in the POM images, as shown in Figure 2.40 (c). The full-bright circular area represents the high-speed rotating 5CB droplet, giving a uniform aspect to the snapshot of the crossed-polarization light imaging. The rotation of a single 5CB droplet was proved by the orbiting of a tiny droplet around the rotating droplet, as shown in Figure 2.40 (d). The full-bright circular area was observed temporarily at higher laser power for optical trapping of 5CB droplets, indicating that the droplet rotation was discontinued. Figure 2.40 (e) shows that the full-bright circular area disappeared and was replaced by a darker circular ring similarly to that observed during the 5CB droplet trapped by a linearly polarized laser at higher laser power. This characteristic' shows that the droplet's reordering occurs at higher laser power, and no rotation was observed at the reordering state. The laser power used affects the reordering inside the trapped 5CB droplet, and light polarization controls the dynamic of the trapped 5CB droplet.

In short, Usman et al. (2013), show the optical trapping of a bipolar 5CB droplet introduced to the linearly and circularly polarized laser beam. The bipolar 5CB droplet of ~2.5 μm could be stably trapped under a linearly polarized laser beam when the laser power used was 130 mW. It was found that the intense laser beam of the linearly polarized laser beam at 850 mW caused the bright spot of the trapped bipolar 5CB droplet to destroy or diminish. In the context of the circularly polarized laser beam, the bipolar 5CB of ~ 3.5 μm rotated when it was trapped by the linearly polarized laser beam at 460 mW. At a strong laser power applied ~940 mW, the rotation of the bipolar 5CB was fastest; the bright spot circular area disappeared and was replaced with the

05-4506832 pustaka.upsi.edu.my Perpustakaan Tuanku Bainun Kampus Sultan Abdul Jalil Shah PustakaTBainun ptbupsi

05-4506832 pustaka.upsi.edu.my Perpustakaan Tuanku Bainun Kampus Sultan Abdul Jalil Shah PustakaTBainun ptbupsi

darker ring. From this observation, at higher laser power affects the Maltase cross pattern of the trapped bipolar 5CB droplet at higher laser power use. The intense laser power used introduces the reordering inside the trapped 5CB droplet. This study is significant in showing the different dynamic effects when the linearly polarized and circularly polarized was introduced to a single trapped bipolar 5CB droplet. The higher laser power used affects the reordering inside the 5CB droplet. This study focused on observing the dynamics of the trapped 5CB droplet under linearly and circularly polarized light and the dependency of laser power on the 5CB droplet's internal configuration. However, the quantitative measurement of the optical stiffness of the trapped 5CB microdroplet was not reported. Besides that, the laser power to trap a single bipolar microdroplet optically was higher, ranging from 130 mW to 940 mW.

The optical trapping of a nematic liquid crystal microdroplet was further investigated by changing the light polarization. The dynamic behavior of the 5CB microdroplet under low laser power was observed (Phanphak et al., 2014). Based on the experiment result, the radial nematic liquid crystal microdroplet under linearly polarized trapping was always pushed slightly off-center, as shown in Figure 2.41. Energy minimization is the main reason that causes the radial nematic liquid crystal microdroplet to be slightly off-center. The minimum energy between the liquid crystal director and optical field interaction happens when the LC director is parallel to the optical electric field or polarization of light according to this equation:

$$f_{op} = -\frac{\varepsilon_{\perp}}{8\pi}E^2 - \frac{\Delta\varepsilon\,\langle\left(\left(\hat{n}\cdot\vec{E}\right)^2\right)\rangle}{8\pi} \tag{2.26}$$

05-4506832 pustaka.upsi.edu.my Perpustakaan Tuanku Bainun Kampus Sultan Abdul Jalil Shah PustakaTBainun ptbupsi

05-4506832 pustaka.upsi.edu.my Perpustakaan Tuanku Bainun Kampus Sultan Abdul Jalil Shah PustakaTBainun ptbupsi

where $\varepsilon_{\perp}$ is the dielectric constant perpendicular to the director axis, $\Delta\varepsilon$ is the dielectric anisotropy, $\hat{n}$ is the liquid crystal director and $\vec{E}$ is the optical electric field.

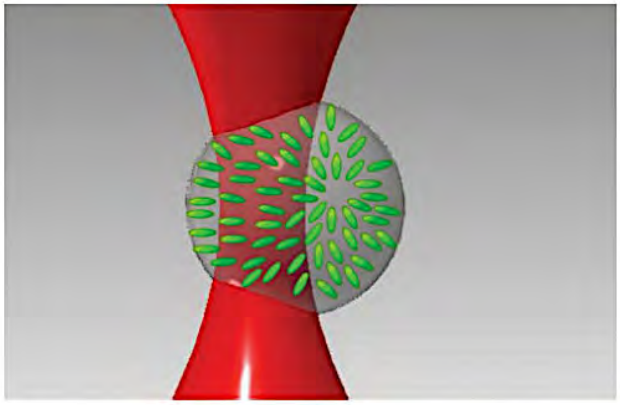


Figure 2.41. The trapping location of the radial nematic liquid crystal (green rods) droplet shifted away from the droplet center under a linearly polarized light-trapping laser (red beam) (Phanphak et al., 2014).

Figure 2.41 shows that the trapping location of the radial nematic liquid crystal droplet was shifted from the droplet center under a linearly polarized trapping laser. Notably, the linearly polarized laser beam caused the off-center trapping of the radially nematic liquid crystal microdroplet.

Meanwhile, the effect of the various laser powers on the radial liquid crystal microdroplet was also investigated. The observation of the trapped liquid crystal microdroplet at various laser powers is shown in Figure 2.42.

05-4506832 pustaka.upsi.edu.my Perpustakaan Tuanku Bainun Kampus Sultan Abdul Jalil Shah PustakaTBainun ptbupsi

05-4506832 pustaka.upsi.edu.my Perpustakaan Tuanku Bainun Kampus Sultan Abdul Jalil Shah PustakaTBainun ptbupsi

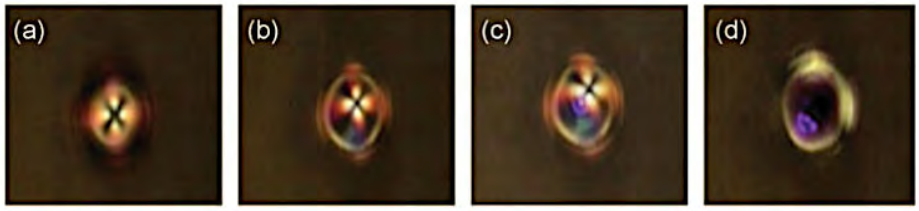


Figure 2.42. A radial nematic liquid crystal droplet of 11.5 μm in diameter under the linearly polarized light optical trap of the following power: (a) without laser, (b) 28 mW, (c) 130 mW, (d) 246 mW. Adapted from (Phanphak et al., 2014).

The linearly polarized laser beam was used to trap a single radial liquid crystal microdroplet of size 11.5 μm in diameter at different laser power, as shown in Figure 2.42. The initial image of the radial liquid crystal microdroplet when the laser was turned off is shown in Figure 2.42 (a). When the laser power was turned on and increased to 28 mW (low laser power), the radial liquid crystal microdroplet was trapped by the laser focus slightly off-center. However, the internal configurational of the trapped liquid crystal microdroplet was still intact and unchanged. The laser power was then increased to 130 mW, and the observed off-center distance was increased, as shown in Figure 2.42 (c). Despite that, the internal configuration was still present, and deformation was observed. Next, the laser trapping power was increased to 246 mW. The 246 mW laser power was too strong and caused the trapped radial liquid crystal microdroplet deformation, as shown in Figure 2.42 (d). No more extended optical pattern can be observed at this time as the internal configuration inside the liquid crystal microdroplet had fully deformed when the higher laser power was applied.

The effect of the elliptically polarized light on the trapped radial nematic liquid crystal microdroplet was also investigated. Figure 2.43 shows the trapped radial liquid

05-4506832 pustaka.upsi.edu.my Perpustakaan Tuanku Bainun Kampus Sultan Abdul Jalil Shah PustakaTBainun ptbupsi

05-4506832 pustaka.upsi.edu.my Perpustakaan Tuanku Bainun Kampus Sultan Abdul Jalil Shah PustakaTBainun ptbupsi

crystal microdroplet by an elliptically polarized laser beam at a different elliptical angle (χ).

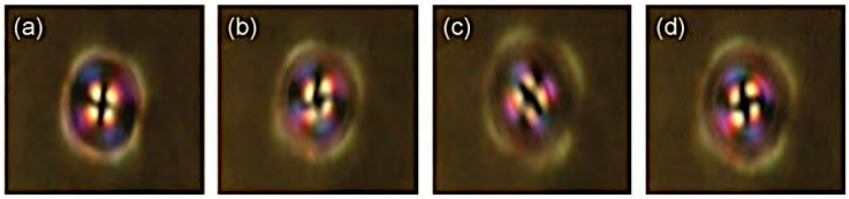


Figure 2.43. A radial nematic liquid crystal microdroplet of 16.8 µm in diameter under 28 mW elliptical polarize optical light trap of the following elliptical angle: (a) without laser, (b) $\chi = 18^{\circ}$, (c) $\chi = 30^{\circ}$ and (d) $\chi = 45^{\circ}$. Adapted from (Phanphak et al., 2014).

Figure 2.43 shows the observation of the dynamic rotational study of the trapped radial nematic liquid crystal microdroplet under an elliptically polarized laser beam at a different elliptical angle. The initial observation of the radial nematic liquid crystal microdroplet when the laser was turned on, is shown in Figure 2.43 (a). No rotation was observed as the trapping laser was off. When the laser beam was turned on, and the elliptical angle was adjusted until ($\chi = 18^{\circ}$), the trapped radial NLC microdroplet initiated the rotation. Hence, the 18° elliptical angle is the threshold angle for rotating the trapped radial nematic liquid crystal microdroplet. The elliptical angle was further increased to ($\chi = 30^{\circ}$), as shown in Figure 2.43 (c). As the elliptical angle was at 18°, the rotation became less stable. As the elliptical angle increased to ($\chi = 45^{\circ}$), where the elliptically polarized light had completely changed to the circularly polarized light, Figure 2.43 (d) observed the most stable rotation. The droplet size that can be rotated under low power optical trap was varied from a few microns to 10 microns. The rotation was possible because the optical torques could overcome resistance, such as drag friction from the surroundings and internal elastic strength. The torque that initiates the rotation depends on the microdroplet size. A small-size microdroplet requires higher

05-4506832 pustaka.upsi.edu.my Perpustakaan Tuanku Bainun Kampus Sultan Abdul Jalil Shah PustakaTBainun ptbupsi

05-4506832 pustaka.upsi.edu.my Perpustakaan Tuanku Bainun Kampus Sultan Abdul Jalil Shah PustakaTBainun ptbupsi

torque to initiate the rotation because of higher molecular anchoring and binding strength.

To summarize the study by Phanphak et al. (2014), the observation of the radial nematic liquid crystal microdroplet illuminated and trapped by a linearly and circularly polarized laser beam was reported. When the linearly polarized laser beam trapped the nematic liquid crystal microdroplet, the radial nematic liquid crystal microdroplet was slightly off-center when the laser polarization state was linearly polarized. As a result, the radial microdroplet could preserve its internal configuration at low laser power but deform at higher laser power. A different dynamic was observed when the elliptical polarization laser beam was used to trap a single radial nematic liquid crystal microdroplet. An elliptically polarized optical trap initiates the rotation of a radial nematic liquid crystal microdroplet if the elliptical angle reaches the threshold angle to start rotating. The stable rotation was achieved when the elliptical angle 45° was equal to circularly polarized. Besides, the rotation speed might vary according to the microdroplet size; even though their study reports the dynamic observation of the effect of light polarization, which is linear and elliptical on the trapped radial 5CB microdroplet, the significant parameter related to the optical force such as optical stiffness was not reported.

Meanwhile, the reported size of the radial nematic liquid crystal microdroplet trapped using a linearly polarized laser beam was 11.5 μm at a laser power of 28 mW. Meanwhile, the reported size of the radial nematic liquid crystal microdroplet trapped using an elliptical polarized laser beam was 16.8 μm at a laser power of 28 mW. The

05-4506832 pustaka.upsi.edu.my Perpustakaan Tuanku Bainun Kampus Sultan Abdul Jalil Shah PustakaTBainun ptbupsi

05-4506832 pustaka.upsi.edu.my Perpustakaan Tuanku Bainun Kampus Sultan Abdul Jalil Shah PustakaTBainun ptbupsi

bigger size of the nematic liquid crystal microdroplet is unsuitable for actuating and sensing applications.

The optical trapping of the nematic liquid crystal microdroplet was also reported to study internal transition change (Oster et al., 2022; Shechter et al., 2020). The optical tweezers are used to hold a liquid crystal microdroplet while monitoring the changes in the internal configuration of the trapped nematic liquid crystal microdroplet. This study reported interesting transition changes inside the trapped liquid crystal when it was systematically exposed to varied concentrations of SDS concentration. The use of optical tweezers to hold the liquid crystal microdroplet was significant. In this study, the optical tweezers were primarily used to hold a single liquid crystal microdroplet during the transition when the surfactant concentration increased or decreased. Unfortunately, the significant parameter for the optical trapping, such as optical stiffness, was not performed. Furthermore, the dynamic effect of the trapped liquid crystal microdroplet was neglected throughout the experiment because the scope of the experiment focused on transitional change.

The effect of light polarization on the achiral nematic liquid crystal microdroplet was also investigated (Kiang-Ia et al., 2021). It was reported that it was possible to rotate the achiral nematic liquid crystal microdroplet under a linearly polarized tweezer (Kiang-Ia et al., 2021). Despite that, previous research showed that the radial nematic liquid crystal microdroplet was stably trapped with no rotation observed. Conversely, in their experiment, stable trapping was observed when the laser power applied to the trapped radial microdroplet was from 124 mW to 298 mW. A few moments after the

05-4506832 pustaka.upsi.edu.my Perpustakaan Tuanku Bainun Kampus Sultan Abdul Jalil Shah PustakaTBainun ptbupsi

05-4506832 pustaka.upsi.edu.my Perpustakaan Tuanku Bainun Kampus Sultan Abdul Jalil Shah PustakaTBainun ptbupsi

laser power was increased to 298 mW, the defect showed a rotation around the laser spot in a clockwise direction, as shown in Figure 2.44.

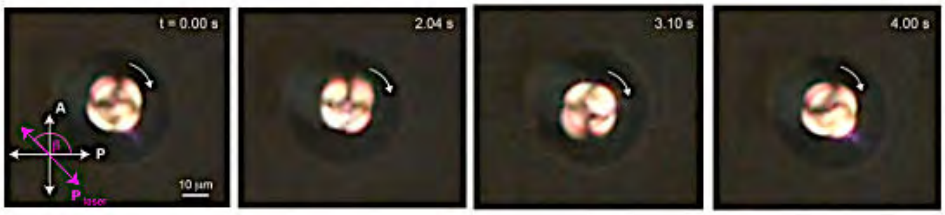


Figure 2.44. An NLC droplet was found rotating clockwise under a linearly polarized laser trap at laser power 298 mW. The laser polarization direction was set at an angle β = 135◦ to the horizontal. Adapted from (Kiang-Ia et al., 2021).

Increasing the laser power to 635 mW laser power caused the same 19 µm liquid crystal microdroplet to rotate counterclockwise, as shown in Figure 2.45. The condition explained that there was no temperature gradient when the droplet was trapped at the focal point. Thus, no rotation was observed. Meanwhile, by continually increasing the laser power, the droplet was levitated to the region above the focal point, and then reverse rotation appeared.

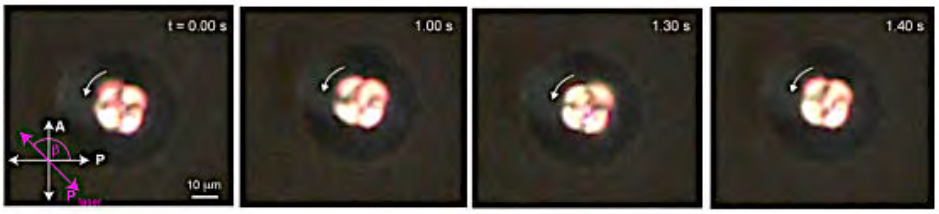


Figure 2.45. The same 19-µm NLC droplet in Figure 2.70 rotated in the reverse direction under the same linearly polarized laser trap at a higher laser power of 635 mW. Adapted from (Kiang-Ia et al., 2021).

05-4506832 pustaka.upsi.edu.my Perpustakaan Tuanku Bainun Kampus Sultan Abdul Jalil Shah PustakaTBainun ptbupsi

05-4506832 pustaka.upsi.edu.my Perpustakaan Tuanku Bainun Kampus Sultan Abdul Jalil Shah PustakaTBainun ptbupsi

The dependency of the rotation and microdroplet size was examined. The threshold of the power of the laser for the microdroplet clockwise and counterclockwise direction, along with microdroplet size, is shown in Figure 2.46.

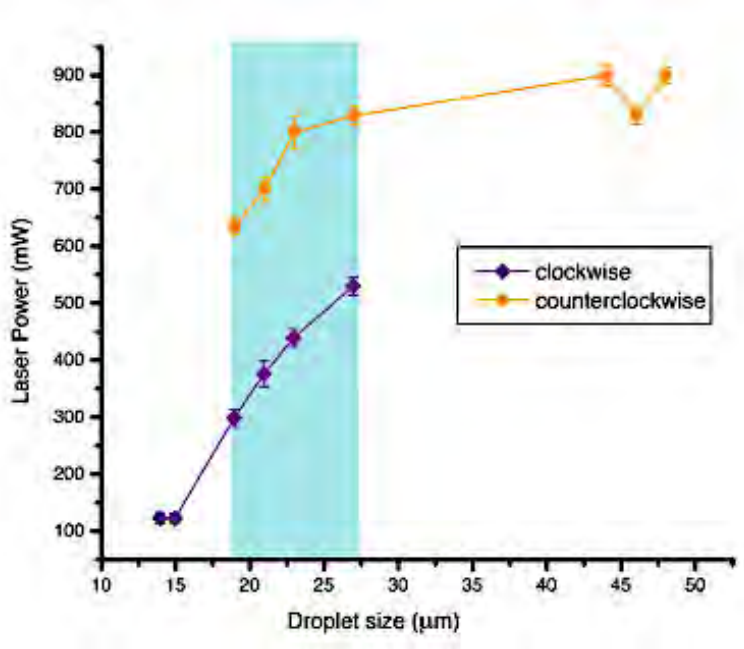


Figure 2.46. The graph of threshold laser power against droplet size clockwise and counterclockwise rotation. Adapted from (Kiang-Ia et al., 2021).

Figure 2.46 shows the graph of threshold laser power against droplet size clockwise and counterclockwise rotation. The ideal droplet sizes for rotating clockwise and counterclockwise ranged from 19 μm to 27 μm. However, it was found that if the microdroplet size was less than 19 μm, only clockwise rotation was observed. Below 19 μm, the size of the droplet was too tiny and rotated in the lower stable region below the focus of the laser. However, the tiny droplet was pushed out from the optical trap if the laser power was too high. For the droplet larger than 27 μm, the low laser power was insufficient to rotate the droplet; therefore, only counterclockwise rotation happened at the upper stable region.

05-4506832 pustaka.upsi.edu.my Perpustakaan Tuanku Bainun Kampus Sultan Abdul Jalil Shah PustakaTBainun ptbupsi

05-4506832 pustaka.upsi.edu.my Perpustakaan Tuanku Bainun Kampus Sultan Abdul Jalil Shah PustakaTBainun ptbupsi

In conclusion, the experiment showed that an achiral nematic liquid crystal droplet could form an asymmetric macroscopic structure under laser trapping, enough to generate Lehmann rotation under the heat gradient of a linearly polarized laser beam. Achiral nematic liquid crystal microdroplets could be rotated using a linearly polarized laser beam. However, the rotated achiral nematic liquid crystal droplet was in the range of 18 μm to 25 μm, which was very big. On top of that, the optical stiffness measurement was not performed despite the achiral nematic liquid crystal being successfully trapped by using a linearly polarized laser beam.

2.21 Nematic Liquid Crystal Microactuator

Microatuator is a micron-scale actuator that converts input energy (radiation, chemical, electrical) into mechanical energy. A microactuator creates a force that produces simple mechanical work or motion. The micrometer-sized particle can be optically rotated by light with its angular momentum. For example, a laser with a helical phase or circularly polarized light can extract the angular momentum of light absorption or birefringence properties due to the microparticles (Ito et al., 2012). The laser trapping beam plays essential roles, including confining the liquid crystal microdroplet, inducing internal molecular reconfiguration, and rotating within the focal spot of the trapping laser. Light can actuate liquid crystal microdroplets to form a rotated mechanical response under specific light polarization. The optical torque imparted to the liquid crystal microdroplet during the optical trap can be induced by wave plate behavior, light scattering, an absorption process, or optical realignment (Usman et al., 2012).

05-4506832 pustaka.upsi.edu.my Perpustakaan Tuanku Bainun Kampus Sultan Abdul Jalil Shah PustakaTBainun ptbupsi

05-4506832 pustaka.upsi.edu.my Perpustakaan Tuanku Bainun Kampus Sultan Abdul Jalil Shah PustakaTBainun ptbupsi

The successful use of circularly polarized light for precise switching control of liquid crystal micro-gears was demonstrated (Ito et al., 2012). A circularly polarized beam of 1064 nm was used to trap liquid crystal objects optically. Liquid crystal was made into liquid crystal micro-gears through a series of processes. Figure 2.47 shows the camera image of the microgear held by laser tweezers.

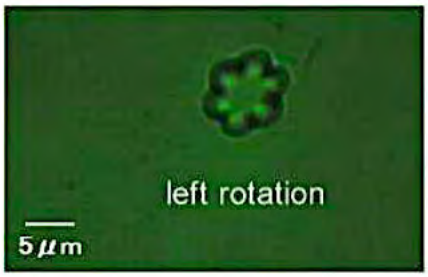


Figure 2.47. Optical micrograph of a micro-gear (r = 4 μm, h = 14 μm) rotating first to the left and then to the right under the control of the phase plate. Adapted with permission (Ito et al., 2012).

05-4506832 pustaka.upsi.edu.my Perpustakaan Tuanku Bainun Kampus Sultan Abdul Jalil Shah PustakaTBainun ptbupsi

The image of the micro-gear rotated left and right by controlling the phase plate of the P = 180 mW circularly polarized trapping beam is shown in Figure 2.47. At P = 180 mW, the liquid crystal micro-gear enables directional control of the optical rotation with a maximum frequency of 11 Hz, showing the superiority of the liquid crystal micromachine over micro rotors made of non-birefringent photocuring resins in terms of switching efficiency. In addition, the liquid crystal micro-gear acts as a rotating microactuator since circularly polarized light can precisely control the frequency and direction of rotation.

In short, optical trapping was successfully used to control and rotate the left and right of the micro-gear precisely. Despite the rotation control of the micro-gear, the optical stiffness measurement of the trapped micro-gear was not studied. The optical

05-4506832 pustaka.upsi.edu.my Perpustakaan Tuanku Bainun Kampus Sultan Abdul Jalil Shah PustakaTBainun ptbupsi

05-4506832 pustaka.upsi.edu.my Perpustakaan Tuanku Bainun Kampus Sultan Abdul Jalil Shah PustakaTBainun ptbupsi

stiffness information was significant in calibrating the optical trap strength. Even though the micro-gear can mimic the actuator's function, the micro-gear size was bigger.

In addition, the creation of a miniaturized and robust metalens-based optical tweezer system capable of rotating liquid crystal droplets to mimic the optical motor for future lab-on-chip applications was reported (T-thienprasert, Limtrakul, Zentgraf, & Chattham, 2019). Researchers performed an optical trap of microparticles using an optical setup with metalens, as shown in Figure 2.48.

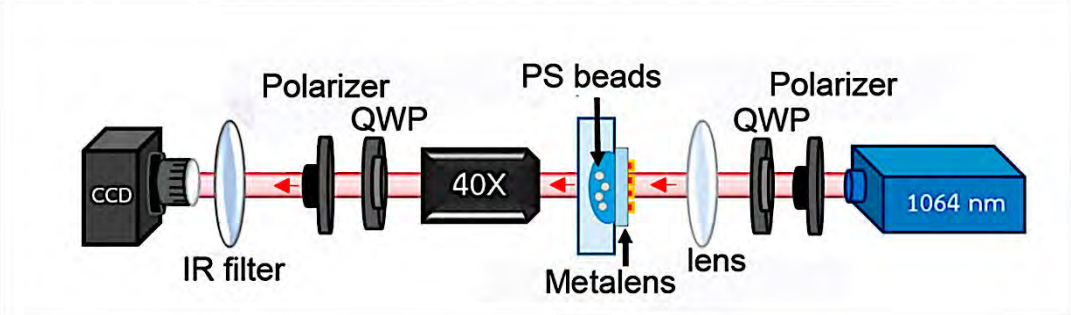


Figure 2.48. Experimental diagram of metalens-based optical tweezers. Adapted under the terms of the Creative Commons Attribution license (T-thienprasert et al., 2019).

This study used a 1064 wavelength, P = 30 mW CW laser, as the trapping laser source. Glan-Thompson polarizer and quarter wave plate were used to convert the linear beam into a circularly polarized laser beam. Figure 2.49 shows the successful nematic liquid crystal trapping using metalens-based tweezers.

05-4506832 pustaka.upsi.edu.my Perpustakaan Tuanku Bainun Kampus Sultan Abdul Jalil Shah PustakaTBainun ptbupsi

05-4506832 pustaka.upsi.edu.my Perpustakaan Tuanku Bainun Kampus Sultan Abdul Jalil Shah PustakaTBainun ptbupsi

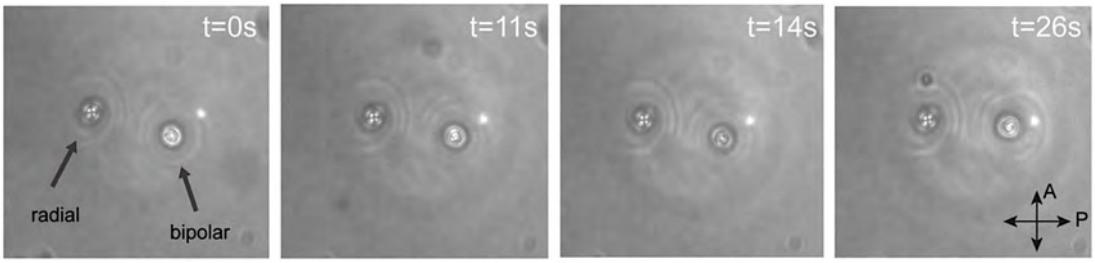


Figure 2.49. Trapped bipolar and radial nematic liquid crystal microdroplet at P = 30 mW by circularly polarized light. Adapted under the terms of the Creative Commons Attribution (T-thienprasert et al., 2019).

Figure 2.49 shows the trap of bipolar and radial liquid crystal microdroplets by metalens-based optical tweezers. The bipolar microdroplet showed an apparent rotation under circularly polarized light, as shown in Figure 2.49. The radial droplet structure remained due to its symmetrical configuration, while the bipolar droplet showed continuous rotation in the laser trap in Figure 2.49. Ultrathin metalens reflected the potential to replace the traditional lens for lab-on-chip application systems. The liquid-crystal microdroplet could be effectively integrated into the miniaturized optical tweezers, indicating the potential to act as an optical motor for microscopic systems to control motion and flow (T-thienprasert et al., 2019).

In short, T-thiemprasert et al. (2019), successfully created a miniaturized and robust metalens-based optical tweezer system capable of rotating liquid crystal droplets to mimic the optical motor for future lab-on-chip applications. The bipolar and radial 5CB were rotated under the irradiation of a circularly polarized laser beam by utilizing metalens-based polarized optical tweezers, which had a high potential to replace conventional lenses. Despite that, the details of the laser power used and the range of

05-4506832 pustaka.upsi.edu.my Perpustakaan Tuanku Bainun Kampus Sultan Abdul Jalil Shah PustakaTBainun ptbupsi

05-4506832 pustaka.upsi.edu.my Perpustakaan Tuanku Bainun Kampus Sultan Abdul Jalil Shah PustakaTBainun ptbupsi

liquid crystal microdroplets that could be trapped were not justified. On top of that, the optical stiffness of the trapped liquid crystal microdroplet was not studied.

In another study, it was reported that liquid crystal droplets were used to fabricate micrometer-sized cylinders that rotated in a circularly polarized optical trap to measure the viscosity of composite liquid crystal (Sanders et al., 2013a). In the same study, the rotation of the liquid crystal microdroplets was used to measure host media such as heavy water (Sanders et al. 2013).

Liquid crystal is a soft but brilliant material that responds to stimuli by adjusting its chemical and physical properties. The soft microactuator using a liquid crystal microdroplet is more flexible than a solid microactuator. LC polymers (LCPs) are used in the shape change system and are also known as crosslinked liquid crystal polymers (CLCPs) (Qin et al., 2021). LCPs can perform different deformation modes, including contraction and expansion, topographical deformation, bending, twisting, and rolling (Zhu et al., 2021). In particular, the soft liquid crystal microactuator is available by taking advantage of optical trapping.

2.22 Nematic Liquid Crystal Sensor

The liquid crystal is a transducer for detecting particular molecules or particles in a medium in sensing applications. The detection mechanism' is based on the sensor's contact with the targeted carrier in a medium (Popov, Piotr, Mann, Elizabeth, Jakli, 2017). The exciting properties, such as environmental response and striking optical

05-4506832 pustaka.upsi.edu.my Perpustakaan Tuanku Bainun Kampus Sultan Abdul Jalil Shah PustakaTBainun ptbupsi

05-4506832 pustaka.upsi.edu.my Perpustakaan Tuanku Bainun Kampus Sultan Abdul Jalil Shah PustakaTBainun ptbupsi

effects, made liquid crystals useful in sensor applications. The liquid crystal sensor mechanism is based on the director defect visualization when the extrapolation length is smaller than an object in the medium. Extrapolation length (b) is expressed as

$$b = \frac{K}{W} \tag{2.23}$$

where K is the director distortion elastic constant in the order of 1 to10 pN, and W is the anchoring strength typically found in the orders of 10^{-3} – 10^{-5} J.m^{-2} (Popov et al., 2017). The striking optical effect is formed and observed under polarized optical microscopy due to the liquid crystal orientation distortion above minimal size (b) (Popov et al., 2017).

05-4506832 pustaka.upsi.edu.my Perpustakaan Tuanku Bainun Kampus Sultan Abdul Jalil Shah PustakaTBainun ptbupsi

The thermotropic liquid crystal is immiscible in water. The thermotropic liquid crystal and analytes interact via a distinct liquid crystal water interface. As a result, the surface of the liquid crystal is exposed to contact with the target-carrying fluid. Commonly, the analytes remain outside the liquid crystal and are adsorbed on the surface of the liquid crystal. The liquid crystal molecules have a sensitive surface during contact with targeted molecules due to the delicate balance of bulk elastic deformations energy and surface anchoring energy of the director (Popov et al., 2017). Hence, chemical and biological sensing applications applied liquid crystal sensitivity as a transducer.

The light is modulated when passing liquid crystals because anisotropic molecules of liquid crystal exhibit a long-range order of the arrangement, and the liquid

05-4506832 pustaka.upsi.edu.my Perpustakaan Tuanku Bainun Kampus Sultan Abdul Jalil Shah PustakaTBainun ptbupsi

05-4506832 pustaka.upsi.edu.my Perpustakaan Tuanku Bainun Kampus Sultan Abdul Jalil Shah PustakaTBainun ptbupsi

crystals amplifies change. Figure 2.50 schematically shows the optical output signal generated by the sensor using a liquid crystal transducer.

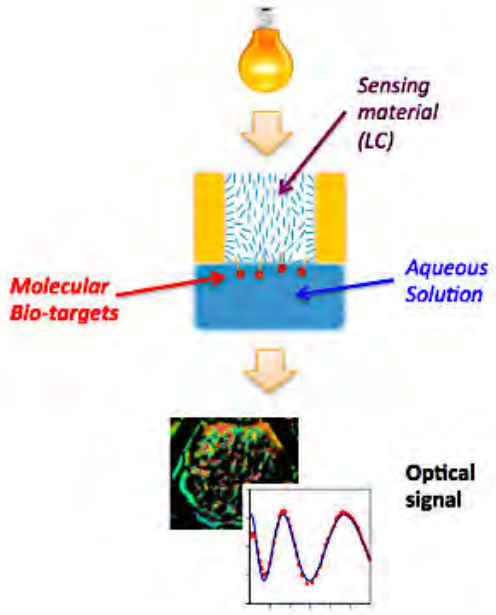


Figure 2.50. Schematic diagram of the sensor using liquid crystal (Popov et al., 2017).

05-4506832 pustaka.upsi.edu.my Perpustakaan Tuanku Bainun Kampus Sultan Abdul Jalil Shah PustakaTBainun ptbupsi

Figure 2.50 shows the simplified schematic of a sensor using liquid crystal. The transmission electron microscopy TEM-filled grid liquid crystal (middle) is exposed to targeted biomolecules in solution and is illuminated with light. The transmitted light produced the observable liquid crystal texture or quantitative optical signal image. The condenser collects, and the CCD camera records the transmitted light via liquid crystal. The anchored director on the two surface and bulk elastic properties decide the liquid crystal orientation in the cell. The variation of director orientation inside the cell influenced the sensor's optical response.

05-4506832 pustaka.upsi.edu.my Perpustakaan Tuanku Bainun Kampus Sultan Abdul Jalil Shah PustakaTBainun ptbupsi

05-4506832 pustaka.upsi.edu.my Perpustakaan Tuanku Bainun Kampus Sultan Abdul Jalil Shah PustakaTBainun ptbupsi

2.22.1 Microdroplet-Based Sensor

Liquid crystals in microdroplets can be a valuable transducer for detecting the analyte. Liquid crystal droplets are widely used in environmental and medical science as a high-sensitivity sensor (Niu et al., 2016). The liquid crystal is a promising optical biosensor because it has unique properties such as large birefringence and high sensitivity of the orientation of liquid crystal molecules to a tiny variation on the surface. Therefore, molecules occurring on the liquid crystal aqueous interface can be amplified and transduced to an optical signal. The naked eye can see this optical signal (change of structure of the optical pattern due to the change in molecule orientation) under polarized optical microscopy.

05-4506832 pustaka.upsi.edu.my Perpustakaan Tuanku Bainun Kampus Sultan Abdul Jalil Shah PustakaTBainun ptbupsi

Liquid crystal has lower water solubility, for example, 4-cyano-4'-pentylbiphenyl (5CB), which is 0.07 g/mL (Peddireddy et al., 2012). As a result, the liquid crystal has the highest tendency to form a microdroplet when it disperses in an aqueous medium, especially water. Liquid crystals are also immiscible in water. Due to the droplet-liquid interfacial tension, the immiscible liquid crystal in water spontaneously forms a spherical microdroplet (Usman et al., 2013). The droplet adopts bipolar, a bipolar molecular arrangement where the liquid crystal molecules align parallel to the droplet's surface without surfactant in the water. With the addition of a surfactant, the liquid crystal molecules adopt a radial molecular arrangement where they align perpendicularly to the surface of the microdroplet. These molecular arrangements are observable under polarized optical microscopy represented by optical patterns. The surface of the liquid crystal aqueous interface is so sensitive because it has a delicate balance between the director's bulk elastic deformation energy and

05-4506832 pustaka.upsi.edu.my Perpustakaan Tuanku Bainun Kampus Sultan Abdul Jalil Shah PustakaTBainun ptbupsi

05-4506832 pustaka.upsi.edu.my Perpustakaan Tuanku Bainun Kampus Sultan Abdul Jalil Shah PustakaTBainun ptbupsi

surface anchoring energy. The adsorbing of impurities on the surface of the liquid crystal microdroplet triggers the change of liquid crystal molecular arrangement. Because of its spherical geometry, the liquid crystal microdroplet's sensitivity is superior to that of the liquid crystal thin film. In spherical microdroplet form, liquid crystals have obtained a high surface area per volume ratio, are flexible, and are dispersed through the aqueous medium for high sensitivity detection. The liquid crystal microdroplet, especially using 5CB, has been widely used to detect different types of an analyte, such as cells, proteins, heavy metal ions, enzymes, viruses, and other particles. The conventional detection of the liquid crystal microdroplet-based sensor requires observation of the transition of molecular arrangement under a polarized optical microscope.

Some experiments have demonstrated the detection performed by the liquid crystal-based sensor in the form of microdroplets in an aqueous environment. For example, the detection of cholic acid by the liquid crystal microdroplet in the aqueous phosphate buffer solution (PBS) (Niu et al., 2016). The colic acid (CA) concentration was varied to investigate the slightest detection of CA in the sodium dodecyl sulfate (SDS) solution containing the SDS-laden liquid crystal droplets/aqueous surface, as shown in Figure 2.51. The increase in CA concentration caused the 5CB optical image to change from radial to bipolar configuration. The use of CA concentration (<5 μM) showed that the 5CB optical image remained in a radial configuration, as in Figure 2.51 (a). However, the CA concentration of (≥ 5 μm) a triggered the radial-to-bipolar transition and the corresponding liquid crystal optical image of the change from radial to bipolar configuration In Figure 2.51 (b). The increased CA concentration caused

05-4506832 pustaka.upsi.edu.my Perpustakaan Tuanku Bainun Kampus Sultan Abdul Jalil Shah PustakaTBainun ptbupsi

05-4506832 pustaka.upsi.edu.my Perpustakaan Tuanku Bainun Kampus Sultan Abdul Jalil Shah PustakaTBainun ptbupsi

more radial droplets to change to a bipolar configuration as shown in Figure 2.51 (b)-(d). Hence, 5 µM was the lowest CA concentration that the 5CB droplets could detect.

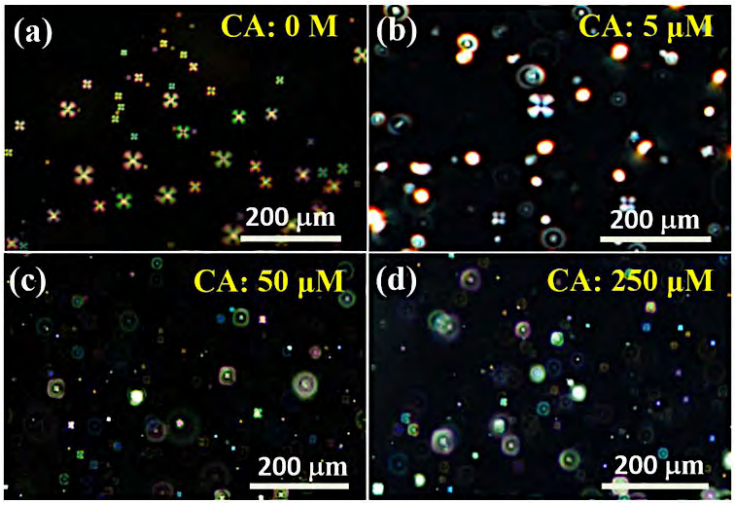


Figure 2.51. Liquid crystal droplet-based sensor for CA detection at varied concentrations. (a): 0 M; (b): 5 µM; (c): 25 µM; and (d): 50 µM. Scale bar: 200 µm. Adapted from (Niu et al., 2016).

05-4506832 pustaka.upsi.edu.my Perpustakaan Tuanku Bainun Kampus Sultan Abdul Jalil Shah PustakaTBainun ptbupsi

In brief, the nematic liquid crystal microdroplet anchored with an SDS solution could be a valuable sensor for detecting cholic acid (CA) in a PBS solution. It was highlighted that in this study, the performance of the dispersed liquid crystal droplet sensor in surfactant could achieve the detection limit of 5 µmol/L. Despite the successful detection of colic acid by the nematic liquid crystal microdroplet, colic acid (CA) detection required many nematic liquid crystal microdroplets. This indicated that the study could not control the number of microdroplets to detect CA. In addition, the size of the liquid crystal microdroplets used for the detection was enormous (in the range of 50 µm to 250 µm), so it was visible under a polarized optical microscope. However, the small liquid crystal microdroplet could not be observed under a polarized

05-4506832 pustaka.upsi.edu.my Perpustakaan Tuanku Bainun Kampus Sultan Abdul Jalil Shah PustakaTBainun ptbupsi

05-4506832 pustaka.upsi.edu.my Perpustakaan Tuanku Bainun Kampus Sultan Abdul Jalil Shah PustakaTBainun ptbupsi

optical microscope. The small liquid crystal microdroplets would have higher detection sensitivity than the bigger ones.

Besides that, liquid crystal microdroplets can be used to detect protein molecules such as an antibody (Lee et al., 2015). Therefore, Lee et al., (2015), developed a label-free biosensor based on the microdroplet, detecting IgG using AIgG-anchored liquid crystal microdroplets in a phosphate buffer saline (PBS) solution. The liquid crystals microdroplet was incubated with different concentrations of IgG for about 30 minutes, and the polarized optical microscopy images are shown in Figure 2.52. The addition of 10 ng mL^{-1} did not change the radial internal configuration of the liquid crystals microdroplets, as shown in Figure 2.52 (a). Therefore, the image was not changed for 10 ng mL^{-1}. However, when 20 ng mL^{-1} IgG was incubated with liquid crystals microdroplets, the transition from radial to bipolar configuration was observed, as shown in Figure 2.52 (b). Furthermore, the increasing IgG concentration up to 50 ng mL^{-1} caused the fraction of liquid crystal microdroplets showing transitional from radial to bipolar internal configuration was to increase, as shown in Figure 2.52 (c).

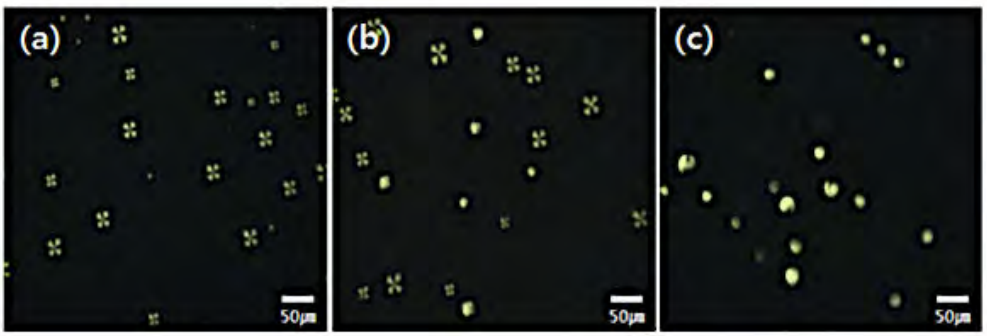


Figure 2.52. The images of AIgG-anchored LC microdroplets incubated in PBS) with varied IgG concentrations at fixed liquid crystal microdroplets density (9×10^3 microdroplets per mL) anchored with 5 $mgmL^{-1}$ of AIgG under polarized optical microscopy at 30 minutes contact time and room temperature. IgG concentration: (a) 10 ng ml^{-1}, (b) 20 ng ml^{-1}, and (c) 50 ng ml^{-1}. Adapted from (Lee et al., 2015).

05-4506832 pustaka.upsi.edu.my Perpustakaan Tuanku Bainun Kampus Sultan Abdul Jalil Shah PustakaTBainun ptbupsi

05-4506832 pustaka.upsi.edu.my Perpustakaan Tuanku Bainun Kampus Sultan Abdul Jalil Shah PustakaTBainun ptbupsi

To summarize, the conventional nematic liquid droplet sensor helps detect the targeted molecule in a bulk number of microdroplets. This showed that the antibodies' liquid crystal detection system uses 5CB liquid crystal emulsion prepared using folic acid conjugated block polymer in the presence of sodium dodecyl sulfate (SDS), which acts as the mediator of the configurational transitional. Conversely, there are a few limitations in the study reported (Lee et al., 2015). One limitation was that the liquid crystal microdroplets of various sizes (20 μm to 30 μm) used were larger for the sensing antibodies IgG and produced a naked visible eye signal image for observation under a polarized optical microscope. However, when the size of the liquid crystal microdroplet was 10 μm and lower, the image of liquid crystal microdroplets under polarized optical microscopy was invisible. Since the size of the liquid crystals microdroplets used in the study was significantly larger, the sensitivity of the microdroplet-based sensor is challenging to lower. In addition, this study used many liquid crystal microdroplets to detect the IgG, indicating that this study cannot manipulate and control the number of liquid crystal microdroplets for detection purposes.

The conventional nematic liquid crystal microdroplet-based sensor is proven to be effective in being used as a sensitive sensor because of its sensitive interface interaction with targeted molecules. The conventional nematic liquid crystal microdroplet-based sensor is based on the naked eye observation under optical microscopy, where the internal configurational change of the nematic liquid crystal microdroplet from bipolar to the radial state. Despite the detection limit of the excellent nematic liquid crystal microdroplet, the naked-eye observation of the transitional change has a disadvantage. The transitional change of the internal configuration of the nematic liquid crystal microdroplet is observable for bigger microdroplets. However,

05-4506832 pustaka.upsi.edu.my Perpustakaan Tuanku Bainun Kampus Sultan Abdul Jalil Shah PustakaTBainun ptbupsi

05-4506832 pustaka.upsi.edu.my Perpustakaan Tuanku Bainun Kampus Sultan Abdul Jalil Shah PustakaTBainun ptbupsi

the small microdroplet was challenging to observe. This issue can cause false judgment of the observer and affect the interpretation of the detection. To overcome this problem, the extra measurement using an optical signal or lasing technique can be used to increase the accuracy and sensitivity of the detection.

2.22.2 Whispering Gallery Mode (WGM) Sensing

The experiment using a Whispering Gallery Mode (WGM) lasing-based microdroplet sensor has been reported by several researchers. Humar and team investigated the application of Whispering Gallery Mode (WGM) lasing to detect surfactants using liquid crystal microdroplets (Humar & Muševič, 2011). The study presented a novel technique for detecting small concentrations of targeted molecules according to the spectra monitoring and changes in liquid crystal microdroplet WGMs. For instance, they found that the WGM lasing spectrum in micron-size nematic liquid crystal droplets changed with 0.3 mM sodium dodecyl sulfate (SDS) (Humar & Muševič, 2011).

In this experiment, the 5CB was performed as a homogenous light distributor emitter by dopping with fluorescence dye 7-diethylamino,4-benzophenoxazine-2-one (0.1 wt %, Nile Red, Sigma-Aldrich). The experiment setup is shown in Figure 2.53.

05-4506832 pustaka.upsi.edu.my Perpustakaan Tuanku Bainun Kampus Sultan Abdul Jalil Shah PustakaTBainun ptbupsi

05-4506832 pustaka.upsi.edu.my Perpustakaan Tuanku Bainun Kampus Sultan Abdul Jalil Shah PustakaTBainun ptbupsi

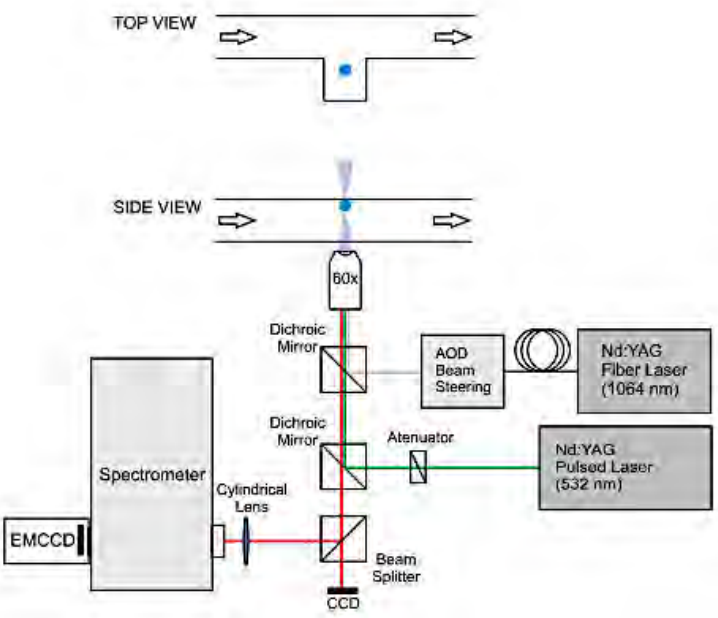


Figure 2.53. Experiment setup to monitor trapped 5CB light emission. Adapted from (Humar & Muševič, 2011).

An infrared laser beam of 1064 nm wavelength (Nd: YAG, Aresis) and an objective lens of 60× high numerical aperture water immersion objective were used to form an optical trap to trap a selected 5CB droplet. However, the 5CB droplet could not be trapped stably in 3 dimensions. Hence, the optical tweezers push the trapped 5CB droplet against the microchannel wall. The low laser power was used to trap a 5CB droplet as low as a typical 70 mW to avoid deforming or heating the droplet extensively. The laser power used for trapping was further reduced by trapping droplets not in the main channel but on the side of the blind leg of the T-channel, as shown in Figure 2.53.

The sensing characteristic of the nematic liquid crystal microdroplet was carefully examined under a non-polarized optical microscope, microscopic image under cross-polarizer, and light emission from the liquid crystal microdroplet. In addition, a selected 17 μm 5CB microdroplet was observed under an optical microscope, and the

05-4506832 pustaka.upsi.edu.my Perpustakaan Tuanku Bainun Kampus Sultan Abdul Jalil Shah PustakaTBainun ptbupsi

05-4506832 pustaka.upsi.edu.my Perpustakaan Tuanku Bainun Kampus Sultan Abdul Jalil Shah PustakaTBainun ptbupsi

SDS concentration was varied in the range of 0–2 mM. Figure 2.54 (a) shows the schematic structure of the 5CB droplet, Figure 2.54 (b) shows the image of the 5CB droplet under a non-polarize optical microscope, and Figure 2.54 (c) shows the image of the 5CB droplet under an optical microscope with a cross-polarizer. 5CB droplet remained in bipolar structure at 0 mM SDS concentration, as shown in the schematic diagram (Figure 2.54 (a)). The WGMs monitoring split indicated by the liquid crystal surface anchoring was not completely planar but slightly tilted.

The increase of SDS concentration from 0.2 mM to 2.0 mM changed the bipolar 5CB droplet to the radial configuration, as illustrated in Figure 2.54 (a)-(c). Meanwhile, the dependency of the light emission from 5CB microdroplets in water solution is described in Figure 2.54 (d). It could be seen that the emission light showed a significant difference when the 5CB microdroplet was in the bipolar phase, intermediate phase, and radial phase, as shown in Figure 2.54 (d). Interestingly, the chaotic region of the emission light was observed in the range of 0.3 mM to 0.4 mM SDS concentration. A detailed measurement was performed to study the chaotic change in the spectral that occurred for the SDS concentration range 0.3 mM to 0.4 mM. A 16 μm 5CB droplet performed the chaotic change in the spectra by changing the SDS concentration in 0.02 mM steps, as shown in Figure 2.54 (e). Figure 2.54 (e) shows that the broad spectral lines were present in the SDS solution's 0.3 mM to 0.4 mM range. However, the change in the position and width of the spectral lines were unpredictable and did not monotonically follow the increasing SDS concentration.

05-4506832 pustaka.upsi.edu.my Perpustakaan Tuanku Bainun Kampus Sultan Abdul Jalil Shah PustakaTBainun ptbupsi

05-4506832 pustaka.upsi.edu.my Perpustakaan Tuanku Bainun Kampus Sultan Abdul Jalil Shah PustakaTBainun ptbupsi

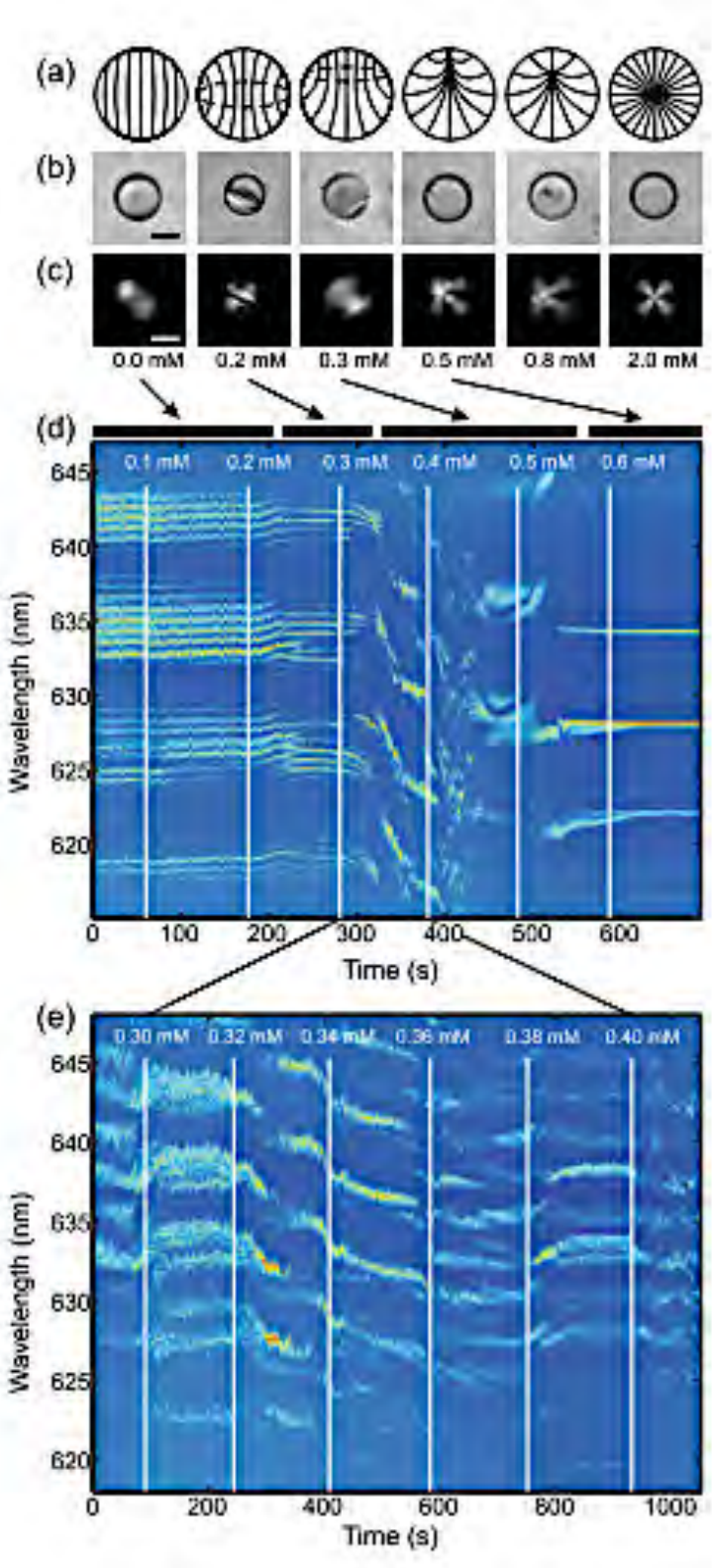


Figure 2.54. 5CB droplet structure (Figure 2.54 (a)), 5CB bright field microscopy images (Figure 2.54 (b)), and 5CB crossed polarization view images (Figure 2.54 (c)), the light emission concentration dependence of 5CB microdroplets in water (Figure 2.54 (d)-(e)). Adapted from (Humar & Muševič, 2011).

05-4506832 pustaka.upsi.edu.my Perpustakaan Tuanku Bainun Kampus Sultan Abdul Jalil Shah PustakaTBainun ptbupsi

05-4506832 pustaka.upsi.edu.my Perpustakaan Tuanku Bainun Kampus Sultan Abdul Jalil Shah PustakaTBainun ptbupsi

In short, Humar et al., (2011), demonstrated the monitoring of the internal configuration of liquid crystals based on WGMs' lasing. In this study, the transition change of the internal configuration from bipolar to radial inside the microdroplet was transduced to the optical signal via whispering gallery mode lasing. The dependency of liquid crystal orientation inside droplets on liquid crystal anchored at the surface supplies lasing spectra information on the molecule's adsorption process at the droplet interface. There were a few limitations of this study. This study used a single trapped nematic liquid crystal microdroplet of range between ~ 13 μm to ~ 17 μm as the probe of detection and sensing. The size of the nematic liquid crystal microdroplet was relatively larger for detecting the SDS molecules. The bigger liquid crystal microdroplet has a lower surface area per volume ratio, which reduces the detection limit. In addition, this study used optical tweezers to hold the nematic liquid crystal microdroplet' when exposed to the SDS solution's flow. The trapped liquid crystal was unstable and pushed toward the microchannel wall despite using optical tweezers to hold the liquid crystal microdroplet. This could cause the deformation in the trapped liquid crystal microdroplet's spherical shape and indirectly affect the measured optical signal. The trapped liquid crystal microdroplet should be free to preserve the optical signal accuracy. In addition, the optical signal of the trapped liquid crystal microdroplet in the context of the optical stiffness was neglected and not reported.

In addition, the application of liquid crystal microdroplet biosensors using Whispering Gallery Modes lasers was studied (Duan et al., 2019). The study demonstrates the heavy metal ion (HM) detection method by applying the Whispering Gallery Mode laser in a liquid crystal microdroplet biosensor. The nematic liquid crystal microdroplet is modified with a specific chemical to detect heavy metal ions.

05-4506832 pustaka.upsi.edu.my Perpustakaan Tuanku Bainun Kampus Sultan Abdul Jalil Shah PustakaTBainun ptbupsi

05-4506832 pustaka.upsi.edu.my Perpustakaan Tuanku Bainun Kampus Sultan Abdul Jalil Shah PustakaTBainun ptbupsi

The modification of the liquid crystal microdroplet involves its surface modification by doping with another chemical. In their experiment, the preparation of the liquid crystal microdroplet involved a solution of 1% (v/v) of the nematic 5CB in n-heptane mixed with dimethylaminostryl-4H-pyan (DCM, 0.01%). The sample mixture was sonicated and treated for 30 minutes to affirm uniformity. A silica capillary tube forms a tapered microtube of 7 µm diameter by the flame tapering method. Finally, a syringe pump was attached to the conical microtube's other end, dropping the 5CB sample. The different micro-droplet sizes were created by controlling the injection speed and pump operating time. The microdroplet in the 40 µm to 60 µm range was chosen for the sensor experiment. The pressure change in the microtube could lead to variations in droplet size and microdroplets hanging at the microtube end. The fabricated microtube generates one liquid crystal microdroplet each time in all experiments to facilitate WGM detection excitation. The test setup for the sensor experiment is shown in Figure 2.55.

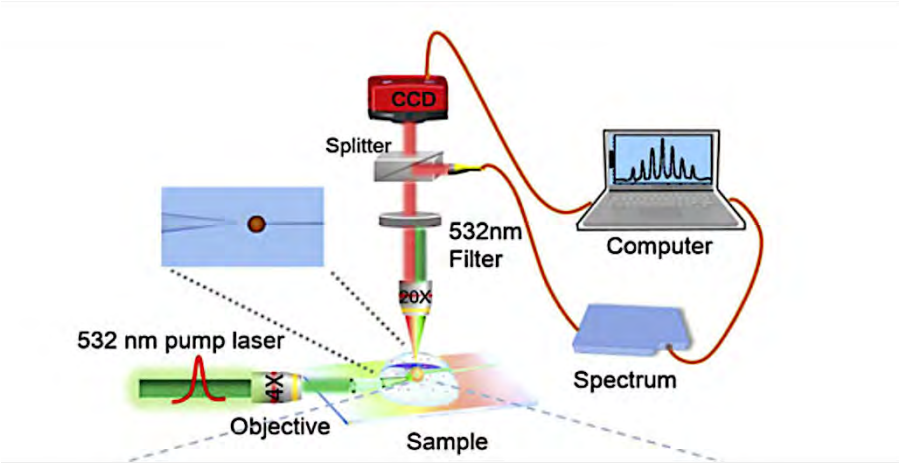


Figure 2.55. Illustration of the experimental setup for sensing. Adapted from (Duan et al., 2019).

05-4506832 pustaka.upsi.edu.my Perpustakaan Tuanku Bainun Kampus Sultan Abdul Jalil Shah PustakaTBainun ptbupsi

05-4506832 pustaka.upsi.edu.my Perpustakaan Tuanku Bainun Kampus Sultan Abdul Jalil Shah PustakaTBainun ptbupsi

Figure 2.55 (a) shows the series stearic acid-dope 5CB microdroplet of polarized optical microscope (POM) images exposed to 200 pM copper (II) chloride in PBS solution, and (b) corresponding lasing spectra of POM images. The exposure of the 200 pM of copper (II) chloride to acid-dope 5CB microdroplet; changes radial internal configuration (t = 0 s) to bipolar (t = 200 s) as shown in Figure 2.56 (a). In addition, the corresponding lasing spectra show that the spectra shifted to the right when observed in 200 s, as stated in Figure 2.56 (b). The POM image showed no significant changes from 120 s to 200 s, but lasing spectra detected these changes.

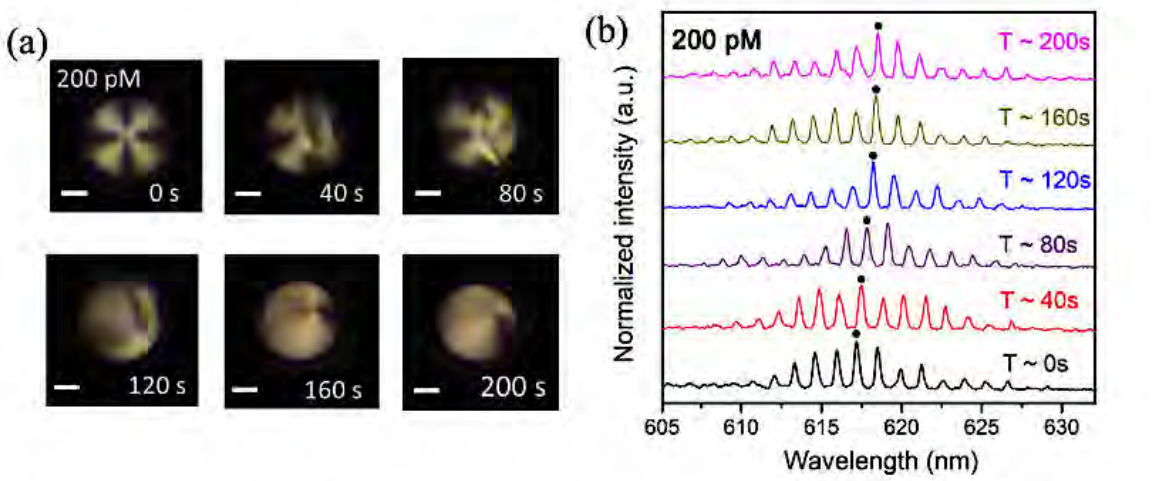


Figure 2.56. (a) The series stearic acid-dope 5CB microdroplet of polarized optical microscope (POM) images exposed to 200 pM copper (II) chloride in PBS solution at a specific time, (b) corresponding lasing spectra of POM images. Black dots represent the position of the WGM selected to monitor the spectral shifting of the droplet lasing emission. Scale bar: 20 µm. Adapted from (Duan et al., 2019).

This study used a single-doped liquid crystal as the detection probe, indicating that the number of liquid crystal microdroplets could be controlled compared to conventional liquid droplets that required many microdroplets. In addition, the doped liquid crystal microdroplet was suspended at the end of the

05-4506832 pustaka.upsi.edu.my Perpustakaan Tuanku Bainun Kampus Sultan Abdul Jalil Shah PustakaTBainun ptbupsi

05-4506832 pustaka.upsi.edu.my Perpustakaan Tuanku Bainun Kampus Sultan Abdul Jalil Shah PustakaTBainun ptbupsi

microtube in the detection solution sample. This indicated poor control and manipulation of the suspended liquid crystal microdroplet, and the liquid crystal microdroplet was inaccessible as it was physically attached to the end of the microtube. This indirectly affects the deformation of the spherical shape of the liquid crystal microdroplet. This deformation of the spherical shape of the suspended liquid crystal microdroplet directly affects the WGM signal. This problem can be solved by using optical tweezers, where the liquid crystal microdroplet can be held without physical contact, allowing control and manipulation of the liquid crystal microdroplet. Related to the sensitivity of liquid crystal droplet-based sensors, the size of the liquid crystal microdroplet used for detection ranged from 40 μm to 60 μm. The size of the liquid crystal microdroplet used for detection was larger. This, therefore, led to a reduction in the sensor detection limit. To solve this problem, a smaller droplet size of less than <10 μm increases sensor sensitivity.

Based on previous research, liquid crystals are widely used for sensing applications in thin films and microdroplets. The liquid crystal thin film-based sensor is less sensitive because the detection is limited to the targeted molecules on the surface of the medium in contact with the thin film layer. The liquid crystal microdroplet-based sensor is more sensitive in the form of microdroplets. The conventional liquid crystal-based microdroplet requires many microdroplets for detection, and the size of the microdroplet was varied. The liquid crystal microdroplet-based sensor is modified and combined with a lasing technique to increase its sensitivity and quantitative detection based on electrical signals. This significantly increases the sensitivity of the liquid crystal microdroplet. However, there are several issues in the liquid crystal

05-4506832 pustaka.upsi.edu.my Perpustakaan Tuanku Bainun Kampus Sultan Abdul Jalil Shah PustakaTBainun ptbupsi

05-4506832 pustaka.upsi.edu.my Perpustakaan Tuanku Bainun Kampus Sultan Abdul Jalil Shah PustakaTBainun ptbupsi

microdroplet-based sensor combined with lasing techniques such as WGM. The current liquid crystal microdroplet-based sensor detects the targeted particle using a single liquid crystal. The problem arose the liquid crystal microdroplet was attached to the glass slide or suspended at the end of the microtube in the sample medium. Because the liquid crystal is not free to move and is stuck to the glass slide or suspended to the microtube, the soft liquid crystal microdroplet cannot sustain its spherical shape, thus affecting the sensing and optical signal produced. Using optical tweezers to physically non-contact hold the microdroplet without deforming the liquid crystal microdroplet shape would help to increase the sensitivity of the liquid crystal-based sensor. Besides, the optical signal of the optical tweezers can be used as an alternative to the WGM technique in quantifying the chemical reaction at the interface of the liquid crystal sensor. Another issue for the current liquid crystal microdroplet-based sensor is the size of the liquid crystal microdroplet used for sensing applications. The current range of liquid crystal microdroplet-based sensors is ~ 13 μm to 60 μm, which are larger. This significantly reduces the sensitivity of the liquid crystal microdroplet-based sensor.

2.23 Summary

This chapter discussed the theory optical trapping. The theory of calibrating optical tweezers and previous optical trapping on solid particles and liquid microdroplets was discussed. In addition, the theory of liquid crystals was also discussed. The previously described liquid crystals in the form of microdroplets have been extensively discussed. Finally, the use of liquid crystals in microactuators and biosensors was also discussed in this chapter.

05-4506832 pustaka.upsi.edu.my Perpustakaan Tuanku Bainun Kampus Sultan Abdul Jalil Shah PustakaTBainun ptbupsi

05-4506832 pustaka.upsi.edu.my Perpustakaan Tuanku Bainun Kampus Sultan Abdul Jalil Shah PustakaTBainun ptbupsi

Table 2.2

Advantages and disadvantages of previous research.

Previous Research	Advantage	Disadvantage
Microdroplet Production (Niu et al., 2016).	• Create a 5CB microdroplet ranging from 60 µm to 250 µm. • Microdroplet size reduced with stirring time (6-240 s).	• Stirring technique generate larger 5CB microdroplet >10 µm. • The medium of dispersion is PBS.
Microdroplet Production (Adamow et al., 2017).	• Create dye-doped 5CB microdroplets ranging from 34.17 µm to 4.79 µm. • Create microdroplets using sonication. • Microdroplet size reduced with sonication time (10-30 minutes).	• No information on the average size from 0-10 minutes. • The medium of dispersion is a 9% PVA-water solution.

(*continue*)

05-4506832 pustaka.upsi.edu.my Perpustakaan Tuanku Bainun Kampus Sultan Abdul Jalil Shah PustakaTBainun ptbupsi

05-4506832 pustaka.upsi.edu.my Perpustakaan Tuanku Bainun Kampus Sultan Abdul Jalil Shah PustakaTBainun ptbupsi

Table 2.2 (*continue*)

Previous Research	Advantage	Disadvantage
Microdroplet Production (Shechter et al., 2020).	• Create a 5CB microdroplet by agitation and flicking the culture tube. • Study the effect of varied SDS concentration on droplet diameter and internal configuration	• No information on the change in microdroplet size with time. • The production technique of 5CB is too simple and not systematic.
Microdroplet Production (Oster et al., 2022).	• Create a 5CB microdroplet by mechanical agitation. • Study the PEG-C10 molecules on the 5CB internal configuration.	• No information on the 5CB microdroplet changes with time. • No detailed information on mechanical agitation was used.

(*continue*)

05-4506832 pustaka.upsi.edu.my Perpustakaan Tuanku Bainun Kampus Sultan Abdul Jalil Shah PustakaTBainun ptbupsi

05-4506832 pustaka.upsi.edu.my Perpustakaan Tuanku Bainun Kampus Sultan Abdul Jalil Shah PustakaTBainun ptbupsi

Table 2.2 (*continue*)

Previous Research	Advantage	Disadvantage
Microdroplet Production (Duan et al., 2019).	• Create stearic acid-doped 5CB microdroplet by microtube technique. • Better size control • Size from 30 µm to 80 µm.	• Microdroplet size larger > 10 µm • The technique is complex.
Microdroplet Stability (Aery et al., 2023).	• The E17 microdroplet stabilizes for 15 minutes of observation before sinking.	• Visual observation of the naked eye.
Microdroplet Stability (Sofi & Dhara, 2019).	• 5CB microdroplet size in PDMS medium decreased after a 2-hour observation.	• Visual observation under a polarized optical microscope.
Microdroplet Optical Trapping (Juodkazis et al., 1999).	• E44 microdroplet orientation and polarization control of 3.3 µm, laser power ~ 1 W.	• Focus on qualitative observation. • No optical stiffness studies.

(*continue*)

05-4506832 pustaka.upsi.edu.my Perpustakaan Tuanku Bainun Kampus Sultan Abdul Jalil Shah PustakaTBainun ptbupsi

05-4506832 pustaka.upsi.edu.my Perpustakaan Tuanku Bainun Kampus Sultan Abdul Jalil Shah PustakaTBainun ptbupsi

Table 2.2 (*continue*)

Previous Research	Advantage	Disadvantage
Microdroplet Optical Trapping (Murazawa, Juodkazis, & Misawa, 2005).	• Rotation of bipolar and radial 5CB microdroplet (size from 1.9-7.8 µm and laser power 31-467 mW) • Rotation increases with laser power and reduce with size.	• Focus on rotational study. • No optical stiffness studies.
Microdroplet Optical Trapping (Usman et al., 2013).	• Polarization control of bipolar 5CB microdroplet • Microdroplet size (~ 2.5 µm & 3.5 µm • Laser power used from130 mW-940 mW • Ambiguous configuration at high laser power.	• Focus on the observation. • No optical stiffness studies.

(*continue*)

05-4506832 pustaka.upsi.edu.my Perpustakaan Tuanku Bainun Kampus Sultan Abdul Jalil Shah PustakaTBainun ptbupsi

05-4506832 pustaka.upsi.edu.my Perpustakaan Tuanku Bainun Kampus Sultan Abdul Jalil Shah PustakaTBainun ptbupsi

Table 2.2 (*continue*)

Previous Research	Advantage	Disadvantage
Microdroplet Optical Trapping (Phanphak et al., 2014).	• Polarization control and effect of laser power on the trapped 5CB microdroplet. • Higher laser power destroys internal configuration. • Rotation faster when elliptical angle = 45º • Laser power used: 28-246 mW. • Size ~11.5 to 16.8 µm.	• Qualitative observation of 5CB trapping. • No optical stiffness was studied.
Microdroplet Optical Trapping (Shechter et al., 2020).	• A single 5CB was trapped to observed transition configuration changes due to SDS exposure.	• No optical stiffness measured. • Visual observation of transition change of the trapped 5CB microdroplet.

(*continue*)

05-4506832 pustaka.upsi.edu.my Perpustakaan Tuanku Bainun Kampus Sultan Abdul Jalil Shah PustakaTBainun ptbupsi

05-4506832 pustaka.upsi.edu.my Perpustakaan Tuanku Bainun Kampus Sultan Abdul Jalil Shah PustakaTBainun ptbupsi

Table 2.2 (*continue*)

Previous Research	Advantage	Disadvantage
Microdroplet Optical Trapping (Kiang-Ia et al., 2021).	• Rotation of achiral nematic LC microdroplet (5CB) trapped by linearly polarized light. • Laser power used: 124 mW to 298 mW. • Size ~ 15-50 µm • 18-17 µm microdroplet could rotate clockwise and counterclockwise.	• Qualitative observation of 5CB microdroplet trapping. • No optical stiffness was studied.
Microdroplet Optical Trapping (Oster et al., 2022).	• The trapping of a single 5CB microdroplet exposed to PEG-C10 surfactant.	• Focus on the transitional change if the trap 5CB microdroplet. • No optical stiffness measurement performed.

(*continue*)

05-4506832 pustaka.upsi.edu.my Perpustakaan Tuanku Bainun Kampus Sultan Abdul Jalil Shah PustakaTBainun ptbupsi

05-4506832 pustaka.upsi.edu.my Perpustakaan Tuanku Bainun Kampus Sultan Abdul Jalil Shah PustakaTBainun ptbupsi

Table 2.2 (*continue*)

Previous Research	Advantage	Disadvantage
Microactuator (Ito et al., 2012).	• Rotated micro-gear by circularly polarized. • Laser power used was 180 mW and size (r = 4 μm and h = 14 μm). • The resulted rotation frequency was 11 Hz.	• Focus on the rotational study of microgear. • No optical stiffness was measured.
Microactuator ((T-thienprasert et al., 2019).	• The rotation of bipolar and radial 5CB droplets mimics an optical motor. • Laser power used: 30 mW.	• Focus on the qualitative observation and rotational control. • No optical stiffness was measured.
Microsensing (Niu et al., 2016).	• Detect Cholic Acid (CA). • Radial 5CB changes to bipolar 5CB when introduced to 5 μM of CA.	• Visual observation of transition change. • Required many microdroplets indicated poor control.

(*continue*)

05-4506832 pustaka.upsi.edu.my Perpustakaan Tuanku Bainun Kampus Sultan Abdul Jalil Shah PustakaTBainun ptbupsi

05-4506832 pustaka.upsi.edu.my Perpustakaan Tuanku Bainun Kampus Sultan Abdul Jalil Shah PustakaTBainun ptbupsi

Table 2.2 (*continue*)

Previous Research	Advantage	Disadvantage
Microsensing (Lee et al., 2015).	• Detect IgG • Radial 5CB change to bipolar 5CB when introduced to 20 ng mL^{-1}.	• Visual observation of transition change. • Required many microdroplets indicated poor control.
Microsensing (Humar & Muševič, 2011).	• A single detection of SDS molecules by dye-doped 5CB microdroplet based on WGM. • The bipolar 5CB change to radial indicated the presence of SDS. • Change in emission spectra of 5CB microdroplet when transition from bipolar to radial.	• Poor control of 5CB microdroplet because of instability of trapping to hold. • Microdroplet size for observation and detection was bigger (~13-17 μm).

(*continue*)

05-4506832 pustaka.upsi.edu.my Perpustakaan Tuanku Bainun Kampus Sultan Abdul Jalil Shah PustakaTBainun ptbupsi

05-4506832 pustaka.upsi.edu.my Perpustakaan Tuanku Bainun Kampus Sultan Abdul Jalil Shah PustakaTBainun ptbupsi

Table 2.2 (*continue*)

Previous Research	Advantage	Disadvantage
Microsensing (Duan et al., 2019).	• A single detection of heavy metal ions by dye-doped 5CB microdroplet based on WGM. • The radial 5CB microdroplet changed to bipolar visually. • The wavelength shifts of the spectral due to the transition change from radial to bipolar.	• Poor control of the 5CB microdroplet because the droplet was hanging at the end of the microtube. • The size of the 5CB microdroplet used for detection was bigger (40-60 μm).

This study deals with the problem of formulation of the 5CB microdroplet in terms of distribution size and stability, the qualitative optical trapping of 5CB microdroplet, micro-control of 5CB microdroplet trapping with translational and polarization control and the issue of LC-based sensor in terms of quantitative and sensitive of detection.

05-4506832 pustaka.upsi.edu.my Perpustakaan Tuanku Bainun Kampus Sultan Abdul Jalil Shah PustakaTBainun ptbupsi

05-4506832 pustaka.upsi.edu.my Perpustakaan Tuanku Bainun Kampus Sultan Abdul Jalil Shah PustakaTBainun ptbupsi

CHAPTER 3

METHODOLOGY

05-4506832 pustaka.upsi.edu.my Perpustakaan Tuanku Bainun Kampus Sultan Abdul Jalil Shah PustakaTBainun ptbupsi

3.1 Introduction

Chapter 3 describes the methodology of the study. The methodology of the study consists of five main parts. The first part of the methodology discusses the assembly of the modular optical tweezers (OTKB/M), including calibrating the alignment and quadrant photo-diode (QPD). In the second part of the methodology, the preparation of the 5CB microdroplet suspension solution in water is discussed. The third part dealt with the optical capture of a single 5CB microdroplet in water using a linearly and circularly polarized laser beam in water. The trapping dynamics, rotation, translation, and micro-control of the 5CB microdroplet capture process were discussed. The fourth

05-4506832 pustaka.upsi.edu.my Perpustakaan Tuanku Bainun Kampus Sultan Abdul Jalil Shah PustakaTBainun ptbupsi

05-4506832 pustaka.upsi.edu.my Perpustakaan Tuanku Bainun Kampus Sultan Abdul Jalil Shah PustakaTBainun ptbupsi

part discussed the analysis of the corner frequency (f_c), and angular speed (ω) of the trapped single 5CB microdroplet in water. Finally, the last section explains the method to demonstrate the trapping mechanism of the trapped 5CB microdroplet exposed to the CTAB solution by analyzing the displacement variance (σ^2) of the (QPD) signals.

3.2 Research Flow Chart

Figure 3.1 illustrates the research flowchart in this study. In the first phase, the (OTKB/M) parts were assembled, optically aligned, and calibrated. After completion of the optical tweezers alignment, the performance test was performed to affirm stable and perfectly functional tweezers by trapping polystyrene microbead in water at a definite range of optical power density.

In the second phase, the 5CB microdroplets suspension of bipolar and radial was produced by sonication 5CB, deionized water, and CTAB at a specified ratio. The distribution size (r) of 5CB microdroplet suspension was inspected under an optical microscope and measured by ImageJ software. The stability of 5CB microdroplet suspension was examined by UV-Vis spectroscopy.

In the third phase, a single 5CB microdroplet was optically trapped by linearly and circularly polarized light with the control of a quarter-and-half wave plate. The dynamic of optically trapped 5CB microdroplets by linear and circularly polarized laser was visually studied. Forth phase, the size of the microdroplet (r), corner frequency

05-4506832 pustaka.upsi.edu.my Perpustakaan Tuanku Bainun Kampus Sultan Abdul Jalil Shah PustakaTBainun ptbupsi

05-4506832 pustaka.upsi.edu.my Perpustakaan Tuanku Bainun Kampus Sultan Abdul Jalil Shah PustakaTBainun ptbupsi

(f_c), and angular speed (ω) were determined using ImageJ, OSCal and OriginLab software.

The last phase of the experiment is to prove the sensing mechanism of the trapped 5CB microdroplet by studying internal configurational change and the corresponding QPD optical signal. The single trapped bipolar 5CB microdroplet was exposed to CTAB solution, the configurational change from bipolar to radial was visually recorded, and the QPD signal was analyzed to determine displacement variance (σ^2).

05-4506832 pustaka.upsi.edu.my Perpustakaan Tuanku Bainun Kampus Sultan Abdul Jalil Shah PustakaTBainun ptbupsi
05-4506832 pustaka.upsi.edu.my Perpustakaan Tuanku Bainun Kampus Sultan Abdul Jalil Shah PustakaTBainun ptbupsi

05-4506832 pustaka.upsi.edu.my Perpustakaan Tuanku Bainun Kampus Sultan Abdul Jalil Shah PustakaTBainun ptbupsi

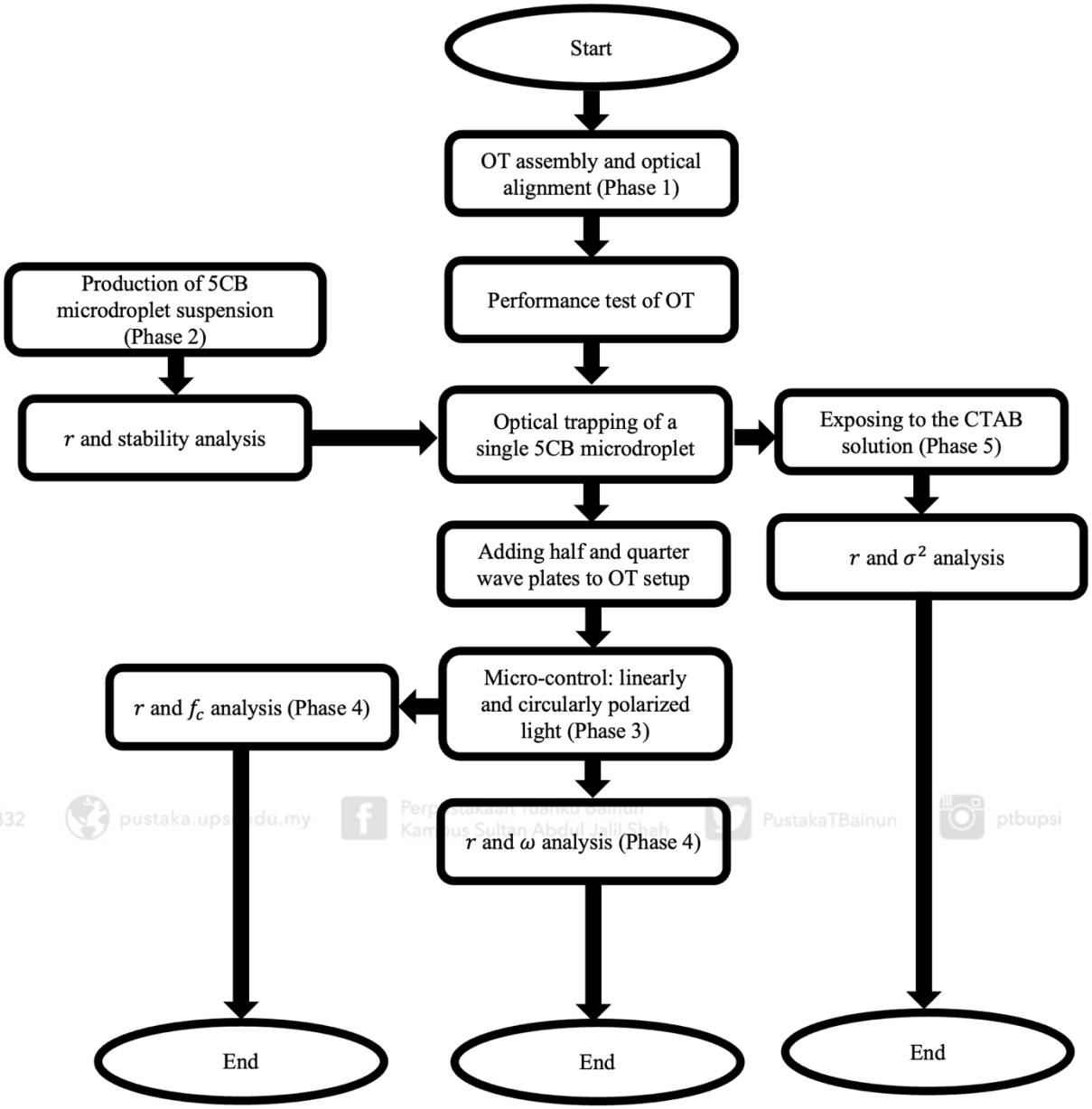


Figure 3.1. The research flowchart.

05-4506832 pustaka.upsi.edu.my Perpustakaan Tuanku Bainun Kampus Sultan Abdul Jalil Shah PustakaTBainun ptbupsi

05-4506832 pustaka.upsi.edu.my Perpustakaan Tuanku Bainun Kampus Sultan Abdul Jalil Shah PustakaTBainun ptbupsi

3.3 Optical Tweezers System [Phase 1]

Thorlabs' optical trapping system, the OTKB/M, available in the Applied Optics Laboratory, Faculty of Science and Mathematics, Universiti Pendidikan Sultan Idris, was used in this study. The system comprises components such as a sample positioning stage, white light LED, condenser, objective lens, beam expander, back focal plane detection module, CCD camera, fiber collimator, stage controller, and a (QPD), piezo stage, and laser diode controller. Figure 3.2 shows the (OTKB/M).

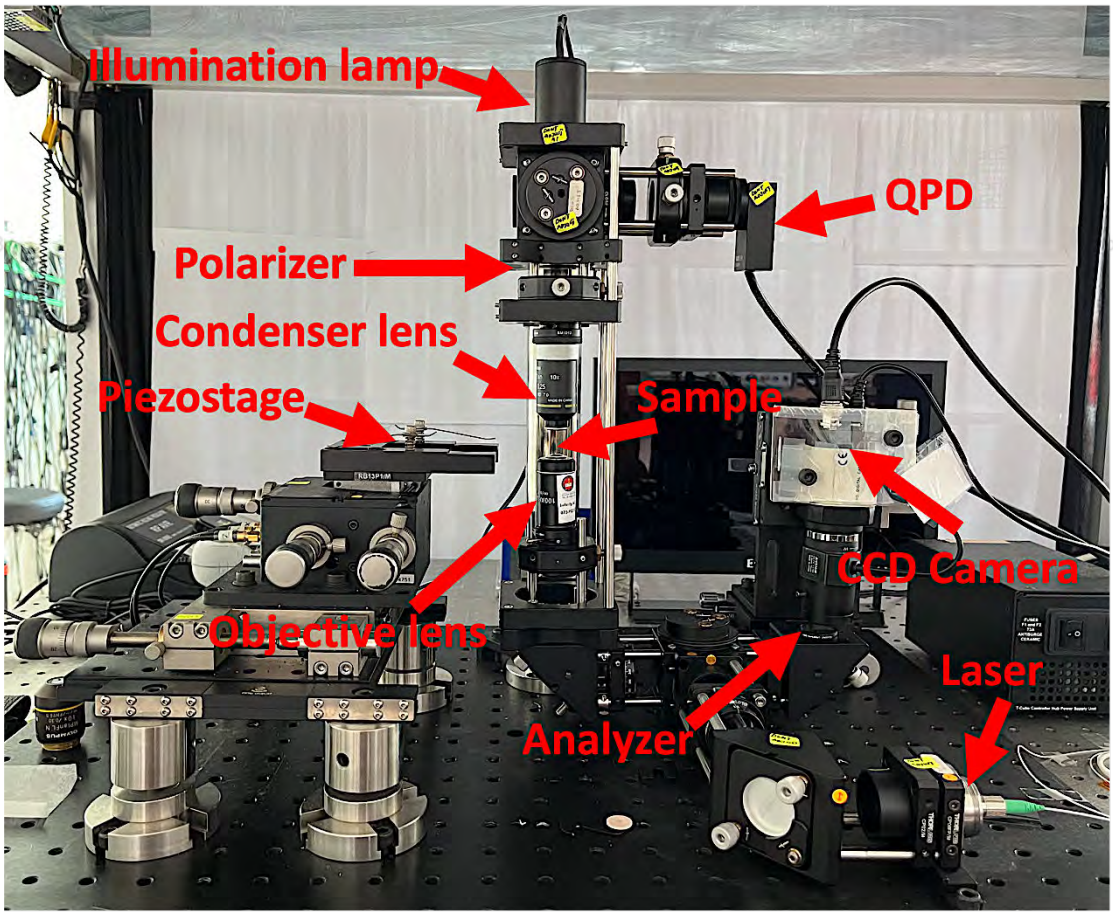


Figure 3.2. The actual (OTKB/M) system.

05-4506832 pustaka.upsi.edu.my Perpustakaan Tuanku Bainun Kampus Sultan Abdul Jalil Shah PustakaTBainun ptbupsi

05-4506832 pustaka.upsi.edu.my Perpustakaan Tuanku Bainun Kampus Sultan Abdul Jalil Shah PustakaTBainun ptbupsi

Figure 3.2 illustrates the actual image of the OTKB/M system used in this study. OTKB/M must be combined part by part, as it comes in separate modular blocks. An observation module, a trap module, and a detection module are the three main modules that make up the OTKB/M system. A trapping laser module refers to a basic optical trapping structure. An observation module views the trapped particle. The last module is the detection module. This module recorded the captured particle's movement and served as data storage.

OTKB/M must be calibrated before use. Proper laser alignment in optical tweezers is required to get the trapped bead's correct, accurate, and logical signal. Misalignment of the laser can cause it to lose power, making it less efficient for trap purposes. In addition, misalignment of the laser tweezers will affect the signal detected by the position detection device, the (QPD). To ensure the optical tweezers are correctly aligned, the Advanced Positioning Technologies (APTs) user software was used to display the laser spot position on the QPD. The laser beam is correctly aligned when the dot is in the center of the QPD. Each module consists of components that perform specific functions. Table 3.1 lists the components for each module.

05-4506832 pustaka.upsi.edu.my Perpustakaan Tuanku Bainun Kampus Sultan Abdul Jalil Shah PustakaTBainun ptbupsi

05-4506832 pustaka.upsi.edu.my Perpustakaan Tuanku Bainun Kampus Sultan Abdul Jalil Shah PustakaTBainun ptbupsi

Table 3.1

Module and Component of OTKB

Module	Component
Trapping	Laser driver
	Laser diode
	Dichroic mirror
	Beam expander
	Objective lens
	Condenser lens
	Piezostage
Observation	CCD camera
	LED illuminator
Detection	QPD position sensor
	Oscilloscope

05-4506832 pustaka.upsi.edu.my Perpustakaan Tuanku Bainun Kampus Sultan Abdul Jalil Shah PustakaTBainun ptbupsi

3.3.1 Trapping Module

Figure 3.3 shows the (OTKB/M) schematic diagram. The trapping module comprises a pigtail laser diode with a wavelength of 976 nm. The laser beam is collimated by a collimator and expanded by beam expansion. The beam expansion laser beam was directed to the dichroic mirror. The dichroic mirror acts as a reflector and beam adjuster, ensuring the laser beam reflects off the laser source. The laser beam reflected by the dichroic mirror was then directed to the objective lens. The objective lens (type 100× oil immersion, 1.25 numerical aperture (NA), 0.23 mm working distance (WD)) focuses the deflected laser beam onto the sample chamber positioned on the

05-4506832 pustaka.upsi.edu.my Perpustakaan Tuanku Bainun Kampus Sultan Abdul Jalil Shah PustakaTBainun ptbupsi

05-4506832 pustaka.upsi.edu.my Perpustakaan Tuanku Bainun Kampus Sultan Abdul Jalil Shah PustakaTBainun ptbupsi

piezo stage. The sample was controlled in the x-, y-, and z- directions by piezo stages (Thorlabs, MAX311D/M). The piezo stage was controlled by APTs User Software (a bundle software from Thorlabs). A condenser lens was used for this function to collimate the laser from the test sample toward the QPD, a condenser lens was used for this function. The scattered laser due to the inclusion of a particle in the test sample was detected by QPD. Then QPD sent the data to the oscilloscope. The trapped particle was illuminated with white light, and a CCD camera observed its image.

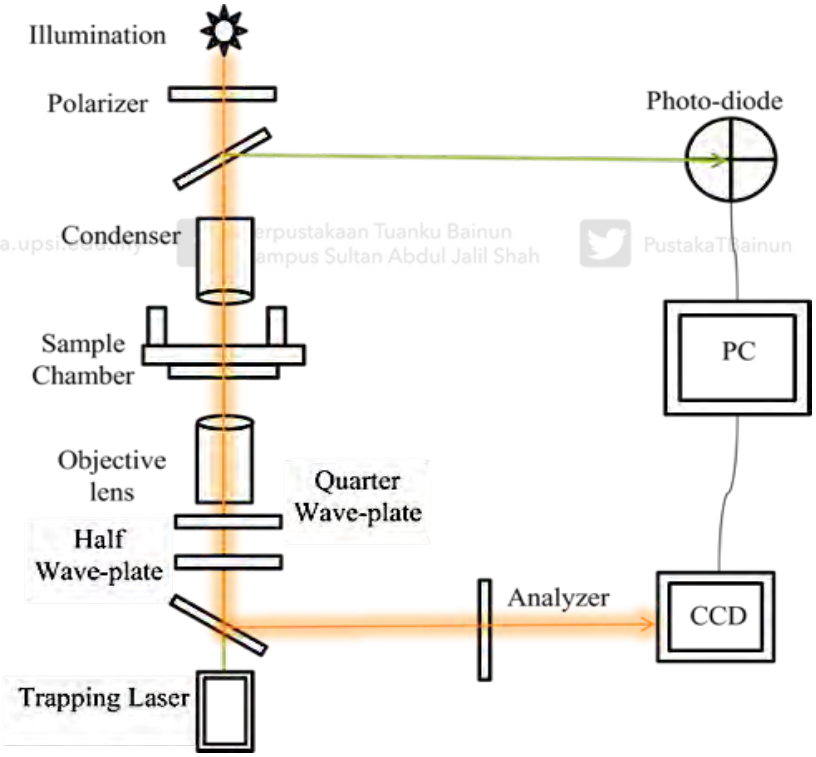


Figure 3.3. OTKB/M schematic diagram for optical trapping.

Control of trapped particles due to optical trapping is critical. The trapped particle can be manipulated and controlled by a piezostage component. The actual image of the piezostage is shown in Figure 3.4.

05-4506832 pustaka.upsi.edu.my Perpustakaan Tuanku Bainun Kampus Sultan Abdul Jalil Shah PustakaTBainun ptbupsi

05-4506832 pustaka.upsi.edu.my Perpustakaan Tuanku Bainun Kampus Sultan Abdul Jalil Shah PustakaTBainun ptbupsi

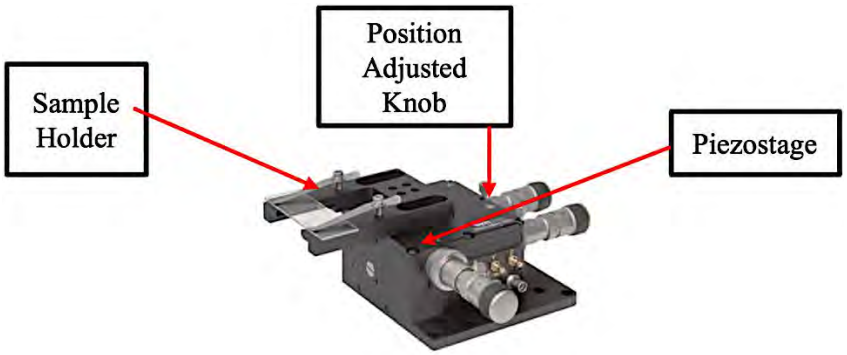


Figure 3.4. The snapshot of piezostage with labeled components.

Piezostage is one of the essential blocks in the capture module of optical tweezers. Piezostage mobilizes the sample holder that holds the test sample in a specific direction on the nanometer scale. Specifically, the piezo stage controlled the sample holder in three directions: *x*, *y*, and *z*. Piezostage motion range was 4 mm and 0.5 mm/rev resolution using the coarse adjustment with knob motion range ~ 300 µm with 50 µm/rev resolution per axis.

Piezostage can be manually controlled via a rotary position adjustment knob for three axes. However, manually adjusting the position control can result in a systematic error by applying additional forces and vibrations to the sensitive sample. The added force was vibration or shock during manual adjustment of the position knob. The piezostage can be virtually controlled with APT's user software, which requires calibration. The piezo stage was moved 1 µm for each applied drive voltage of 4 V. Therefore, the conversion factor as a reference for the three-axis displacement-stress profile was constant at 0.25 µm/V.

Furthermore, this study used a 976 nm wavelength infrared laser diode, single-mode, 14-pin butterfly module laser (Axcel Photonics). The wavelength of this diode

05-4506832 pustaka.upsi.edu.my Perpustakaan Tuanku Bainun Kampus Sultan Abdul Jalil Shah PustakaTBainun ptbupsi

05-4506832 pustaka.upsi.edu.my Perpustakaan Tuanku Bainun Kampus Sultan Abdul Jalil Shah PustakaTBainun ptbupsi

was 976 nm with a threshold current of 44 mA. Figure 3.5 shows the image of the butterfly laser diode.

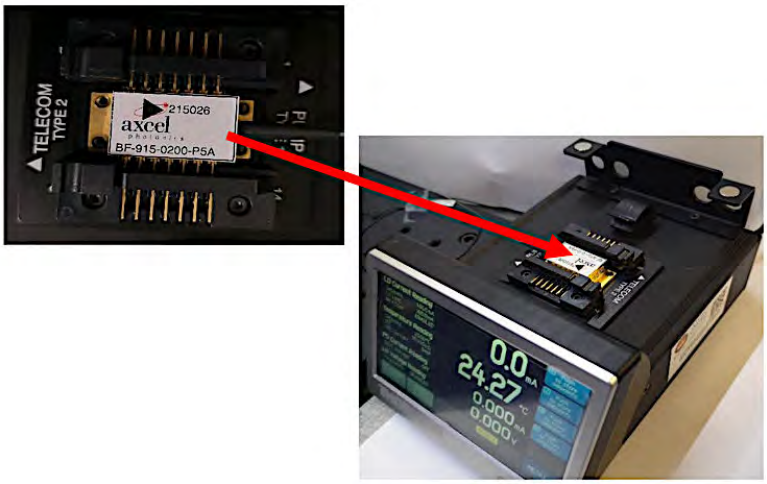


Figure 3.5. The actual image of the butterfly laser diode used as the trapping laser source.

05-4506832 pustaka.upsi.edu.my Perpustakaan Tuanku Bainun Kampus Sultan Abdul Jalil Shah PustakaTBainun ptbupsi

The compact laser diode driver has a temperature controller and bracket for butterfly housing (Thorlabs, CLD 1015) that controls the current feeding to the laser diode. In addition, the compact laser diode driver enabled power control in terms of current (mA). The driver interface is shown in Figure 3.6.



Figure 3.6. The image of a compact laser diode driver for controlling laser diode power.

05-4506832 pustaka.upsi.edu.my Perpustakaan Tuanku Bainun Kampus Sultan Abdul Jalil Shah PustakaTBainun ptbupsi

05-4506832 pustaka.upsi.edu.my Perpustakaan Tuanku Bainun Kampus Sultan Abdul Jalil Shah PustakaTBainun ptbupsi

Since the compact laser diode driver delivers the laser power as a current, it is essential to calibrate the current-power relationship dependency. Therefore, the laser power calibration measurement was required. In order to convert laser power from current to watts, a physical measurement must be performed. Therefore, a power meter (Thorlabs, model PM130D) measured the laser power output at the objective lens pupil. The actual image of the optical power meter used is shown in Figure 3.7.



Figure 3.7. The image of the laser power meter used in current-to-power calibration.

The laser current supplied relationship concerning the laser diode power was studied. After entering the objective lens, the current supplied to the laser and laser power output relationship was investigated by adjusting the input current from the laser diode driver, and the optical power meter measured the power. The laser diode constantly supplied independent laser current ranging from 50 mA to 250 mA in 20 mA increments. At the position after the beam entered the objective lens, the corresponding laser power output was measured. The average value was obtained by repeating the measurement three times. The relationship between the current supplied to the laser diode and the corresponding laser power is illustrated in Figure 3.8. The laser power and the current showed a linear relationship, represented by the equation

$P = 0.3979I - 17.697.$

05-4506832 pustaka.upsi.edu.my Perpustakaan Tuanku Bainun Kampus Sultan Abdul Jalil Shah PustakaTBainun ptbupsi

05-4506832 pustaka.upsi.edu.my Perpustakaan Tuanku Bainun Kampus Sultan Abdul Jalil Shah PustakaTBainun ptbupsi

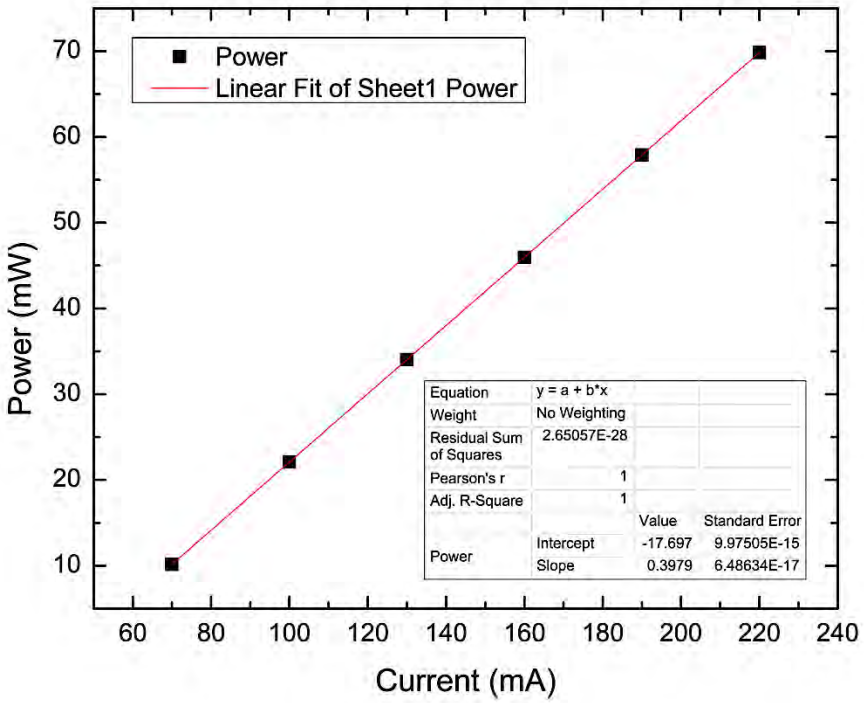


Figure 3.8. The plot of laser power (P) versus laser current (I) for calibrating the trapping laser in front of the objective lens.

The power density of the laser can be determined when the current-to-power ratio has been calibrated. This study defines power density as the laser power per unit area. The trapping laser diameter (d) was 1.1 µm. The calculation of the laser power density could be done by substituting the measured laser power and dividing by the area of the laser focal spot according to Equation 3.1

$$P = \frac{W}{\pi r^2} \tag{3.1}$$

05-4506832 pustaka.upsi.edu.my Perpustakaan Tuanku Bainun Kampus Sultan Abdul Jalil Shah PustakaTBainun ptbupsi

05-4506832 pustaka.upsi.edu.my Perpustakaan Tuanku Bainun Kampus Sultan Abdul Jalil Shah PustakaTBainun ptbupsi

where P represents optical power density, W represents laser power, and r represents the radius of the laser trapping trap spot. Table 3.2 lists the current, power, and power density used in this investigation.

Table 3.2

List of used laser current, power, and power density.

Current, I (mA)	Power, W (mW)	Power Density, P (MW/cm^2)
70	10.6	1.1
100	23.6	2.3
130	36.6	3.6
160	49.6	4.8
190	62.6	6.1
220	75.6	7.3

05-4506832 pustaka.upsi.edu.my Perpustakaan Tuanku Bainun Kampus Sultan Abdul Jalil Shah PustakaTBainun ptbupsi

The calculated laser power density for 70 mA, 100 mA, 130 mA, 160 mA, 190 mA, and 250 mA as 1.1 MW/cm^2, 2.3 MW/cm^2, 3.6 MW/cm^2, 4.8 MW/cm^2, 6.1 MW/cm^2 and 7.3 MW/cm^2 as listed in Table 3.2.

The following essential component in the trapping module is the objective lens. In optical trapping, the objective lens focuses the laser beam to a focal point. The objective lens with a high numerical aperture (NA) produces strong optical power compared to the lower objective lens with a low numerical aperture (NA). In addition, an objective lens with a high numerical aperture (NA) typically has a short working distance, which must be considered when preparing a suitable thickness

05-4506832 pustaka.upsi.edu.my Perpustakaan Tuanku Bainun Kampus Sultan Abdul Jalil Shah PustakaTBainun ptbupsi

05-4506832 pustaka.upsi.edu.my Perpustakaan Tuanku Bainun Kampus Sultan Abdul Jalil Shah PustakaTBainun ptbupsi

of the cell chamber. This study fixed the objective lens type throughout the experiment to ensure that only the laser power and microdroplet size affect the trapped particle's corner frequency and optical stiffness. The actual image of the objective lens used for optical trapping is shown in Figure 3.9. For the optical trapping process, an oil immersion type objective lens (100× magnification, 1.25 (NA), and 0.23 working distance (WD) was used.



Figure 3.9. A 100× magnification, 1.25 NA, 0.23 mm WD oil immersion objective.

3.3.2 Observation Module

The observation module works to display the trapped particle in the test sample. Therefore, when the sample test was placed on the sample holder of the piezostage, the sample test was ready for the trapping process and observation under an inverted microscope as shown in Figure 3.10. The image of the trapped particle was illuminated by white light from the illuminator.

05-4506832 pustaka.upsi.edu.my Perpustakaan Tuanku Bainun Kampus Sultan Abdul Jalil Shah PustakaTBainun ptbupsi

05-4506832 pustaka.upsi.edu.my Perpustakaan Tuanku Bainun Kampus Sultan Abdul Jalil Shah PustakaTBainun ptbupsi

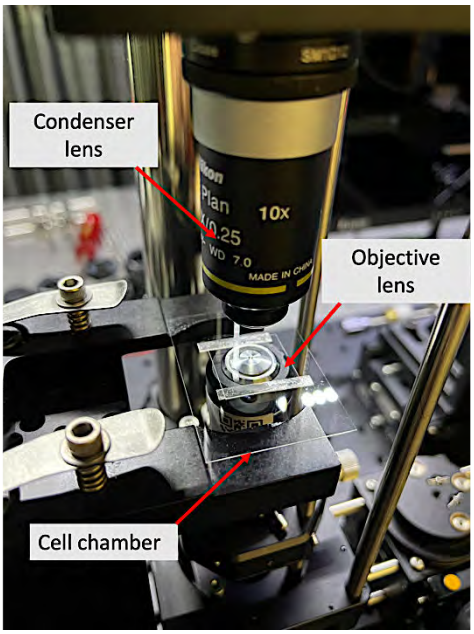


Figure 3.10. Test cell under observation.

The tightly focused laser beam caused the particle suspended in the sample chamber to be trapped. This study used a CCD camera (800TVL 1/3" CCD Digital Industry Microscope Camera BNC Camera, Brand: HAYEAR) to record the image and live video of the trapped particle. The CCD camera was directly linked to the PC; therefore, the image of the trapped bead could be displayed on the PC. Figure 3.11 illustrates the snapshot live display of the CCD camera on the PC.

05-4506832 pustaka.upsi.edu.my Perpustakaan Tuanku Bainun Kampus Sultan Abdul Jalil Shah PustakaTBainun ptbupsi

05-4506832 pustaka.upsi.edu.my Perpustakaan Tuanku Bainun Kampus Sultan Abdul Jalil Shah PustakaTBainun ptbupsi



Figure 3.11. The live image of the CCD camera is displayed on the PC.

The next step was determining the calibration between pixel to micrometer of the image the CCD camera shows. A specific objective lens was used for the optical trapping application, and this objective lens produced an image of different resolutions, magnifications, and views. Hence, the calibration was significant in determining the size (r) of the trapped particle. In this study, the (OTKB/M) used 100× magnification 1.25 Numerical Aperture (NA) and an immersion oil-type objective lens. Hence, calibration must be performed to ensure that the post-analysis of the image is precise and accurate.

The clear image of the micro ruler under the objective was recorded by a CCD camera and uploaded to the ImageJ software for the calibration process to determine the conversion factor pixel to the micrometer. The uploaded micro calibration ruler image in the ImageJ software is illustrated in Figure 3.12.

05-4506832 pustaka.upsi.edu.my Perpustakaan Tuanku Bainun Kampus Sultan Abdul Jalil Shah PustakaTBainun ptbupsi

05-4506832 pustaka.upsi.edu.my Perpustakaan Tuanku Bainun Kampus Sultan Abdul Jalil Shah PustakaTBainun ptbupsi

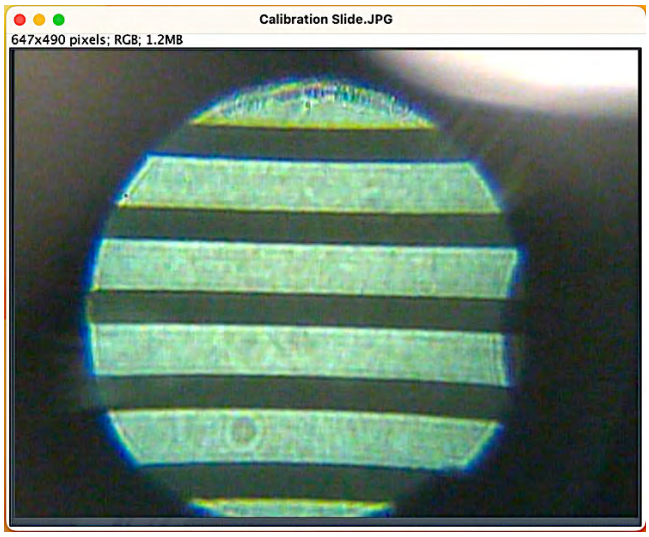


Figure 3.12. The front panel of the uploaded image of the calibration slide micro ruler in the ImageJ software.

Then, a straight line was drawn perpendicularly between the two consecutive scales, representing the micro ruler's distance, as shown in Figure 3.13. The distance between the two consecutive scales was 10 µm.

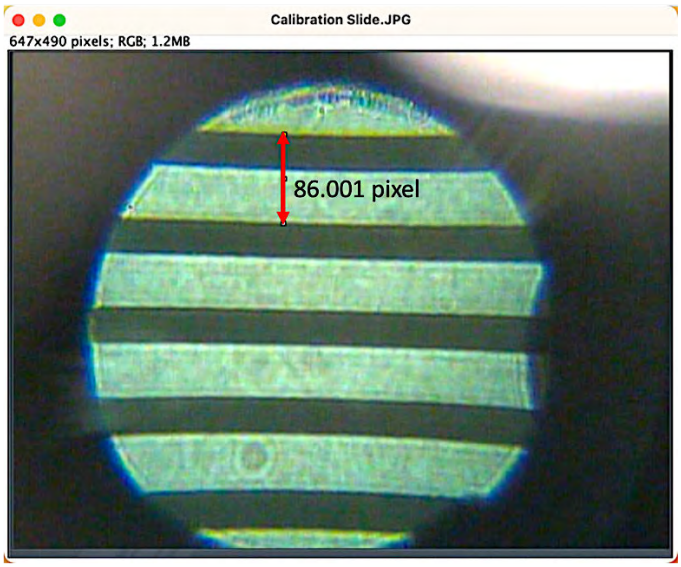


Figure 3.13. The snapshot of the ImageJ front panel shows the straight-line measurement to determine the distance between two consecutive scales in pixels.

05-4506832 pustaka.upsi.edu.my Perpustakaan Tuanku Bainun Kampus Sultan Abdul Jalil Shah PustakaTBainun ptbupsi

05-4506832 pustaka.upsi.edu.my Perpustakaan Tuanku Bainun Kampus Sultan Abdul Jalil Shah PustakaTBainun ptbupsi

The straight-line measurement option in ImageJ showed that the distance between two consecutive scales in pixels was 86.001. Therefore, the measurement was repeated ten times to find the average distance in the pixels. The summarization of the ten measurements made to find the average distance in the pixels is shown in Table 3.3.

Table 3.3

Measurement of length in unit pixels by ImageJ.

Label	Measurement	Length (pixels)
	1	86.000
	2	86.000
	3	86.000
	4	85.000
	5	85.000
	6	87.000
	7	86.000
	8	86.000
	9	87.000
	10	86.001
Mean		86.000
Standard Deviation		0.667

From Table 3.3, the average distance of the two consecutive scales measured was 86.000 ± 0.667 pixels. Therefore, a 10 μm distance was equal to 86.000 pixels. The resulting conversion factor was 8.6 pixels per micrometer. Using the obtained

05-4506832 pustaka.upsi.edu.my Perpustakaan Tuanku Bainun Kampus Sultan Abdul Jalil Shah PustakaTBainun ptbupsi

05-4506832 pustaka.upsi.edu.my Perpustakaan Tuanku Bainun Kampus Sultan Abdul Jalil Shah PustakaTBainun ptbupsi

conversion factors, measurements such as distribution size or the individual size of the particle using the specific objective lens can be performed and measured.

3.3.3 Detection Module

The detection module detects the trapped particle's motion, vibration, or trajectory. While trapping a single particle, the particle was confined to the laser trap focus. The vibration of the trapped particle at the trap laser focus caused the stable laser trap intensity to be disrupted and scattered. The scattered trap laser beam contained information about the trajectory and position of the trapped particle at a specific time. In other words, the scattered trap laser beam's fluctuation was correlated to the trapped particle's trajectory. Hence, the particle motion can be analyzed using the position detector signal. This information was significantly essential to calculate f_c and k_T. Therefore, a position detector sensor was required to collect and record the scattered trap laser beam of the trapped particle. The position detector used in this study was a QPD. The QPD collected the scattered trap laser beam and converted it to the electrical signal (voltage). Figure 3.14. illustrates the QPD (PDQ80A, Brand: Thorlabs) used for position sensing in OTKB/M.

05-4506832 pustaka.upsi.edu.my Perpustakaan Tuanku Bainun Kampus Sultan Abdul Jalil Shah PustakaTBainun ptbupsi

05-4506832 pustaka.upsi.edu.my Perpustakaan Tuanku Bainun Kampus Sultan Abdul Jalil Shah PustakaTBainun ptbupsi



Figure 3.14. A QPD (PDQ80A, Thorlabs) is used for position sensing in OTKB/M.

The most important part of calibrating OTKB/M is the alignment of the laser beam. The correct, accurate and logical signal from a single trapped particle can be assured through the proper alignment. The alignment process was performed by displaying the laser dot position on QPD through the APT user program, as shown in Figure 3.15. If the dot position is in the center of the QPD, the laser beam is correctly aligned.

05-4506832 pustaka.upsi.edu.my Perpustakaan Tuanku Bainun Kampus Sultan Abdul Jalil Shah PustakaTBainun ptbupsi

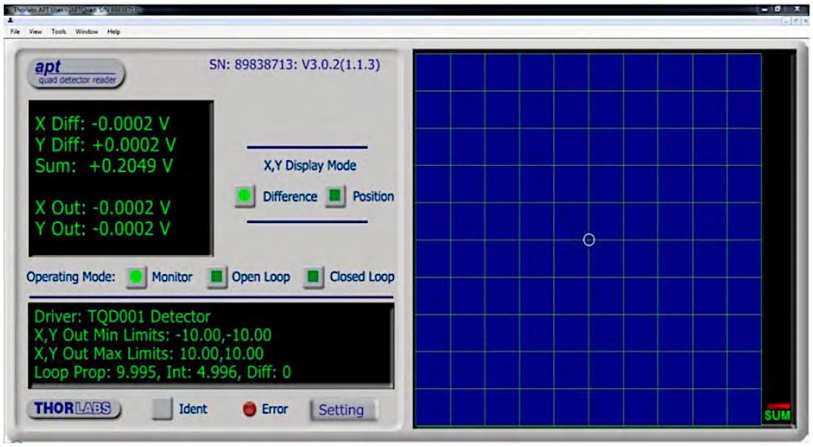


Figure 3.15. The laser alignment procedure displays the position of the laser spot on the QPD via the APT user program.

Figure 3.16 shows a schematic diagram for position detection in optical tweezers using QPD (PDQ80A, Thorlabs). The obtained QPD signal should be

05-4506832 pustaka.upsi.edu.my Perpustakaan Tuanku Bainun Kampus Sultan Abdul Jalil Shah PustakaTBainun ptbupsi

05-4506832 pustaka.upsi.edu.my Perpustakaan Tuanku Bainun Kampus Sultan Abdul Jalil Shah PustakaTBainun ptbupsi

optimized before the data acquisition process. The laser beam was aimed directly at the QPD without interruption to optimize the QPD signal. QPD consists of four sensitive and identical quadrants. These quadrants are light-sensitive sensors that respond to changes in the intensity of light focused on them. Figure 3.16. shows the illustration of the QPD schematic diagram.

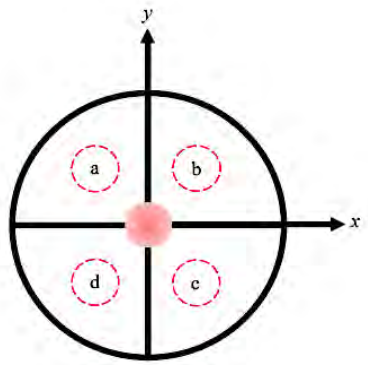


Figure 3.16. The QPD diagram with four quadrant labels labeled a, b, c, and d.

05-4506832 pustaka.upsi.edu.my Perpustakaan Tuanku Bainun Kampus Sultan Abdul Jalil Shah PustakaTBainun ptbupsi

Each quadrant on the QPD detects the photocurrent (a, b, c, and d) due to the focused beam. The position of the laser spot can be examined from the difference in the photocurrent. The normalized coordinates of the beam positions (X, Y) are represented by Equations 3.2 and 3.3.

$$X = \frac{(a+d)-(b+c)}{(a+b+c+d)} \tag{3.2}$$

$$Y = \frac{(a+b)-(d+c)}{(a+b+c+d)} \tag{3.3}$$

The four-quadrant sensors capture four equal photocurrents under the condition that the beam aimed at the center of the QPD is perfectly symmetrical. If the condition is met, the ray coordinates in the APT user program indicate (X, Y) = (0,0). The change

05-4506832 pustaka.upsi.edu.my Perpustakaan Tuanku Bainun Kampus Sultan Abdul Jalil Shah PustakaTBainun ptbupsi

05-4506832 pustaka.upsi.edu.my Perpustakaan Tuanku Bainun Kampus Sultan Abdul Jalil Shah PustakaTBainun ptbupsi

in photocurrent is detected when the beam is deflected away from the center, causing the coordinate to change accordingly. The dichroic mirror was used to adjust the light captured by the QPD to stay as close to (0,0) as possible when the laser was on to ensure the QPD signal was optimized.

During the experiment, without placing any sample, the laser beam was adjusted and fixed at the center of the QPD and (X, Y) = (0, 0). However, when the optical tweezers trap the particle, the previous QPD alignment might misalign. Therefore, it is essential to adjust the laser beam position to the center again by adjusting the dichroic mirror until the beam coordinates almost (X, Y) = (0, 0) again. This step is critical to ensure that the collected signal from the QPD is in the Lorentzian form and can be fitted with the Lorentzian Fitting, especially when using the PSD method.

05-4506832 pustaka.upsi.edu.my Perpustakaan Tuanku Bainun Kampus Sultan Abdul Jalil Shah PustakaTBainun ptbupsi

This quadrant photodiode was sensitive to detect light intensity changes toward the sensor's center at QPD. The collected scattered laser beam due to the trapped bead at the focal of the laser spot was detected by QPD. The QPD converted the scattered laser beam into voltage (Volt). As a result, three signals can be obtained: differential (*x* and *y*-signals) and *sum* signals. The differential signals represent the bead motion in the lateral *x* and *y* axes, while the *sum* represents the sum of the bead motion in the *x* and *y* direction. The scattered laser beam due to the trapped bead was converted to a voltage signal by the QPD and transferred to the oscilloscope. The QPD was connected to an oscilloscope (Yokogawa DL6054), as shown in Figure 3.17, to obtain its electrical signal. The example of the voltage signal of the trapped particle is illustrated in Figure 3.17. The oscilloscope division scale was set to 100 ms/division for the *x*-division and 100 mV/division for the *y*-division for channel 1 and channel 2, which were connected

05-4506832 pustaka.upsi.edu.my Perpustakaan Tuanku Bainun Kampus Sultan Abdul Jalil Shah PustakaTBainun ptbupsi

05-4506832 pustaka.upsi.edu.my Perpustakaan Tuanku Bainun Kampus Sultan Abdul Jalil Shah PustakaTBainun ptbupsi

to the QPD x and y voltage signals. For analysis f_c and k_T, the differential electrical signal of the y data was acquired at a rate of 250 kilo samples/second. The procedure to save the oscilloscope data to the USB drive varies depending on the oscilloscope one uses. In our experiment, the QPD waveform data was saved by pressing File> Save > Waveform> Save Exec based on our oscilloscope model.



Figure 3.17. Voltage waveform display on the Yokogawa DL6054 digital oscilloscope.

Figure 3.17 shows the voltage waveform display on the Yokogawa DL6054 digital oscilloscope. The data was kept in ASCII (American Standard Code for Information Interchange) file format. In addition, a USB flash drive was used to transfer this data to the PC for post-analysis.

05-4506832 pustaka.upsi.edu.my Perpustakaan Tuanku Bainun Kampus Sultan Abdul Jalil Shah PustakaTBainun ptbupsi

05-4506832 pustaka.upsi.edu.my Perpustakaan Tuanku Bainun Kampus Sultan Abdul Jalil Shah PustakaTBainun ptbupsi

3.3.4 Optical Tweezers Performance Test

The optical tweezers were performed by optically trapping 1and 2-micron polystyrene microbeads in water. The trapping stability and the range of suitable laser power density were determined. The single polystyrene microbead was trapped using a linearly polarized laser beam at laser optical power density ranging from 1.1 to 7.3 MW/cm^2. The polystyrene microspheres were used to calibrate the optical trap before measuring the liquid crystal microdroplet. For each optical laser power density, corner frequency (f_c) and the optical stiffness (k_T) of 1 μm and 2 μm polystyrene microspheres were determined.

Figure 3.18 shows the graph of corner frequency (f_c) against laser optical power density (P) for optically trapped polystyrene microbeads in water. In contrast, Figure 3.19 shows the graph of optical stiffness (k_T) against laser optical power density (P) for optically trapped polystyrene microbeads in water. f_c showed a consistent increase with the increasing optical laser power density for both 1 μm and 2 μm polystyrene microbeads used. The k_T followed the same trend as the f_c. The increasing trends show that the optical tweezer was a stable trap and working properly. The optical tweezers were ready to test the f_c and k_T of the 5CB microdroplet.

05-4506832 pustaka.upsi.edu.my Perpustakaan Tuanku Bainun Kampus Sultan Abdul Jalil Shah PustakaTBainun ptbupsi

05-4506832 pustaka.upsi.edu.my Perpustakaan Tuanku Bainun Kampus Sultan Abdul Jalil Shah PustakaTBainun ptbupsi

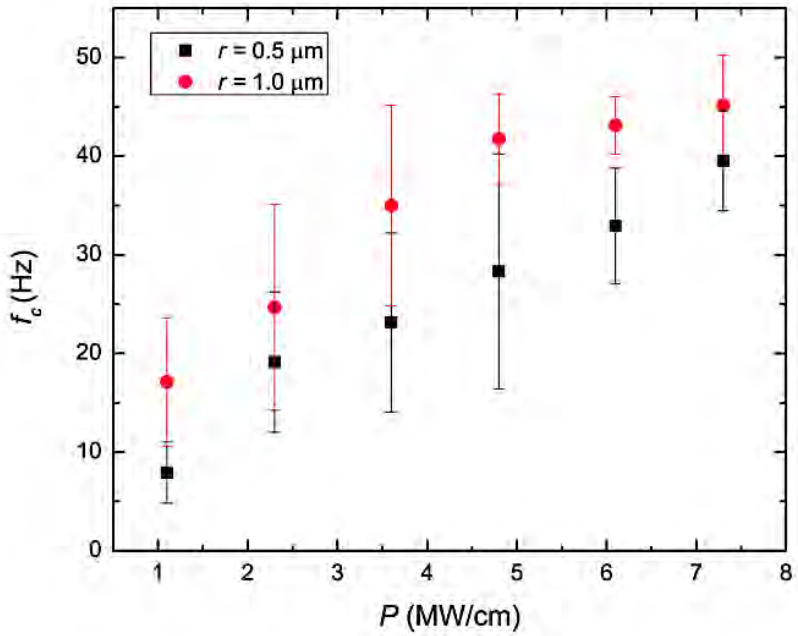


Figure 3.18. The graph of corner frequency (f_c) against laser optical power density (P) for optically trapped polystyrene microbeads in water.

05-4506832 Perpustakaan Tuanku Bainun ptbupsi

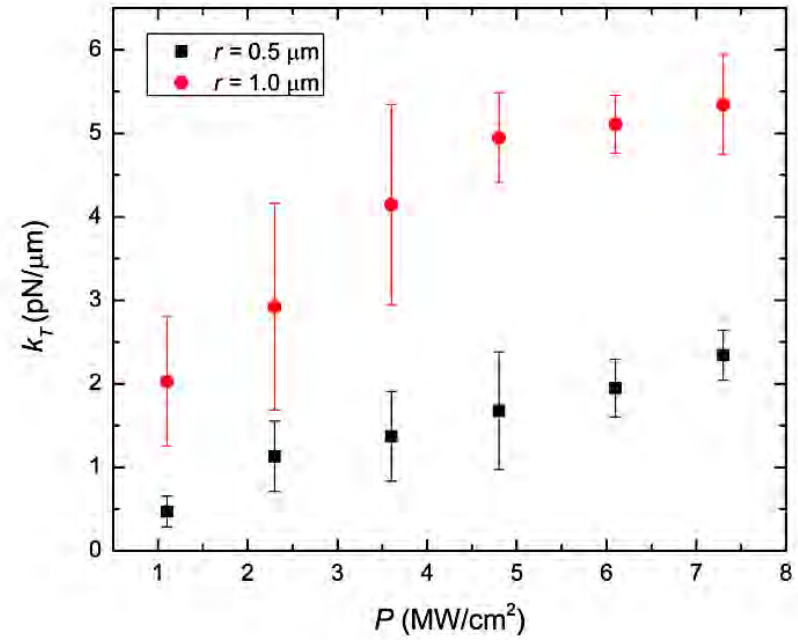


Figure 3.19. The graph of optical stiffness (k_T) against laser optical power density (P) for optically trapped polystyrene microbeads in water.

05-4506832 pustaka.upsi.edu.my Perpustakaan Tuanku Bainun Kampus Sultan Abdul Jalil Shah PustakaTBainun ptbupsi

05-4506832 pustaka.upsi.edu.my Perpustakaan Tuanku Bainun Kampus Sultan Abdul Jalil Shah PustakaTBainun ptbupsi

3.4 Preparation of 5CB Microdroplet Solution [Phase 2]

Preparing 5CB microdroplet suspension in the water requires a specific mixing ratio of liquid 5CB, deionized water, and surfactant (CTAB or SDS). The density of 5CB is 1.008 g/mL. 5CB has lower water insolubility which is 0.07 mg/L; thus, it can produce 5CB microdroplets in the water. The production of the 5CB with a specific internal configuration (bipolar or radial) depends on the addition of surfactant. The surfactant modifies and anchors the surface of the 5CB microdroplet and causes the liquid crystal molecules to align in a perpendicular (radial configuration) or parallel (bipolar) configuration concerning the 5CB spherical boundary. The typical schematic diagram of the bipolar and radial internal configuration of the 5CB microdroplet is illustrated in Figure 3.20.

05-4506832 pustaka.upsi.edu.my Perpustakaan Tuanku Bainun Kampus Sultan Abdul Jalil Shah PustakaTBainun ptbupsi

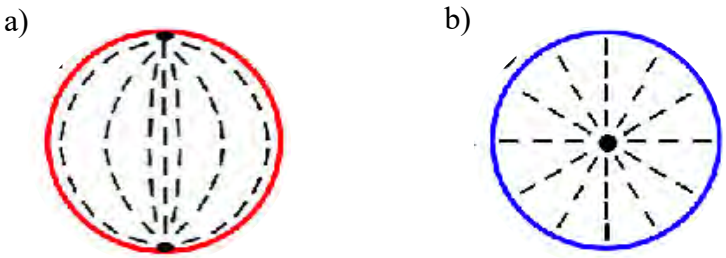


Figure 3.20. The schematic diagram of the 5CB internal configuration (a) bipolar and (b) radial.

5CB has refractive indices such as ordinary refractive index (n_0: 1.57) and extraordinary refractive index (n_e: 1.71). 5CB refractive indices are higher than water (n_w: 1.33), which is the medium of microdroplets for the optical trapping process. The detailed procedure to produce a 5CB microdroplet solution will be explained in the next sub-topic.

05-4506832 pustaka.upsi.edu.my Perpustakaan Tuanku Bainun Kampus Sultan Abdul Jalil Shah PustakaTBainun ptbupsi

05-4506832 pustaka.upsi.edu.my Perpustakaan Tuanku Bainun Kampus Sultan Abdul Jalil Shah PustakaTBainun ptbupsi

The 5CB microdroplet can be prepared by vertexing, sonication, homogenization, hand stirring, microfluidic and encapsulation (Concellón, 2023; Wang et al., 2017). In this study, the sonication technique was chosen to generate a 5CB microdroplet suspension solution. The possible reason is that the sonication technique is the most straightforward technique and require small sample size, as low as ~ 100 μL, to produce 5CB microdroplets of ~ 100 nm to 10 μm (Concellón, 2023). Optical trapping experiment only uses minimal sample volume ~ 5-10 μL sample volume. Vertexing and homogenization produce bigger microdroplets ~ 1-100 μm, while microfluidic and encapsulation techniques are complex process and time-consuming for microdroplet production (Concellón, 2023; Wang et al., 2017). This also includes the production of the microdroplet using a microtube, which is also complex and generates bigger microdroplets (>10 μm) (Duan, Hao, et al., 2020; Duan, Li, et al., 2020; Yan et al., 2017). The bigger microdroplet is inert to the pico-newton optical force of optical tweezers; hence, smaller microdroplet (<1-3 μm) range size is suitable to be used for optical manipulation. In this study, deionized water is used as the medium because water is the simplest and basic liquid.

3.4.1 Bipolar 5CB Microdroplet Solution Preparation

In this research, 0.5 μl of a liquid 4-cyano-4'-pentylbiphenyl (5CB) (Sigma Aldrich, CAS-No. 40817-08-1) was pipette in 2 mL plastic vials containing 1.0, 1.5, and 2.0 mL of deionized water (18.2 Ωm^{-1}) respectively to prepare 5CB microdroplet suspension with bipolar internal configuration. Figure 3.21 shows the purchased 4-cyano-4'-

05-4506832 pustaka.upsi.edu.my Perpustakaan Tuanku Bainun Kampus Sultan Abdul Jalil Shah PustakaTBainun ptbupsi

05-4506832 pustaka.upsi.edu.my Perpustakaan Tuanku Bainun Kampus Sultan Abdul Jalil Shah PustakaTBainun ptbupsi

pentylbiphenyl (5CB) in a glass bottle. The 5CB is a liquid at room temperature, as seen in Figure 3.21.



Figure 3.21. The snapshot of purchased 4-cyano-4'-pentylbiphenyl (5CB) in a glass bottle.

5CB microdroplet suspension obtains a bipolar t internal configuration when it is dispersed in deionized water. Furthermore, the 5CB microdroplet was prepared at room temperature (22°C), the ideal temperature for 5CB microdroplet suspension to obtain the nematic phase. The schematic diagram of the bipolar 5CB microdroplet suspension solution production is summarized in Figure 3.22.

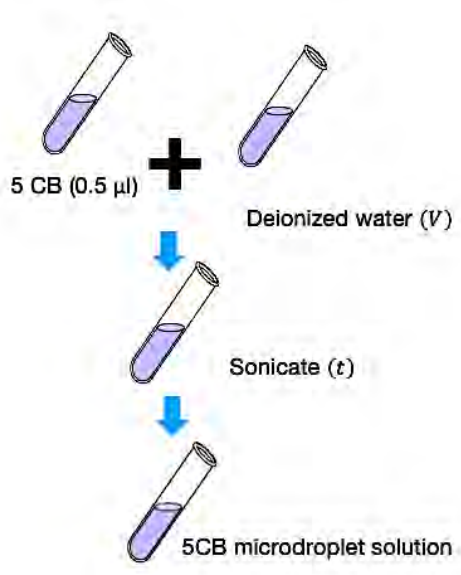


Figure 3.22. The schematic diagram of bipolar 5CB microdroplet suspension solution production.

05-4506832 pustaka.upsi.edu.my Perpustakaan Tuanku Bainun Kampus Sultan Abdul Jalil Shah PustakaTBainun ptbupsi

05-4506832 pustaka.upsi.edu.my Perpustakaan Tuanku Bainun Kampus Sultan Abdul Jalil Shah PustakaTBainun ptbupsi

The 0.5 µL liquid 5CB and deionized water mixture in a 2 mL vial were shaken using a test tube shaker for 30 s to facilitate the microdroplet generation process and prevent the liquid 5CB from sticking at the bottom of the vial. Then, the ultrasonic bath (GT Sonic, VGT-1620QTD) was used to sonicate the mixture of the liquid 5CB and the deionized water to produce a homogenous 5CB microdroplet suspension. Figure 3.23. illustrates the sonication of the mixture of the liquid 5CB and deionized water, and it was immersed in the water for the sonication process to produce 5CB microdroplet suspension.



Figure 3.23. The snapshot of the sonication process of liquid 5CB and deionized water mixture to produce a 5CB microdroplet suspension solution.

A tweezer held the sample vial containing the mixture at 45° (estimated using protractor) and fully immersed in the water for sonication, as shown in Figure 3.23. The sonication time was varied from 1.0, 2.0, 3.0, and 10.0 minutes to examine the effect of the sonication time on the generated size of bipolar 5CB microdroplet suspension. Due to the sonication process, the cloudy color suspension was formed when 5CB

05-4506832 pustaka.upsi.edu.my Perpustakaan Tuanku Bainun Kampus Sultan Abdul Jalil Shah PustakaTBainun ptbupsi

05-4506832 pustaka.upsi.edu.my Perpustakaan Tuanku Bainun Kampus Sultan Abdul Jalil Shah PustakaTBainun ptbupsi

microdroplet suspension was mixed homogenously in deionized water. The sonication process breaks down the large 5CB microdroplet size into smaller sizes. Due to the fact that 5CB has lower water solubility, thus the formation of the 5CB microdroplet was possible. Figure 3.24 shows the mixture of liquid 5CB and deionized water (a) before and (b) after the sonication process.

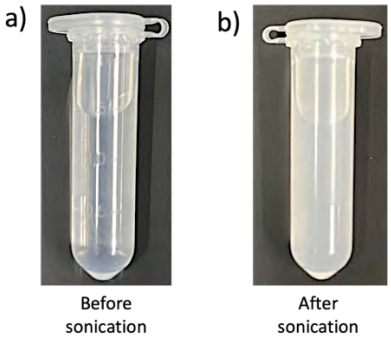


Figure 3.24. The snapshot of the mixture of the liquid 5CB and deionized water (a) before and (b) after the sonication process. The cloudy solution was formed after sonication, indicating the formation of the 5CB microdroplet suspension.

05-4506832 pustaka.upsi.edu.my Perpustakaan Tuanku Bainun Kampus Sultan Abdul Jalil Shah PustakaTBainun ptbupsi

Then about 5 µL of the solution was added to the sample chamber with a micropipette. Figure 3.25 (a) shows the sample chamber constructed from a sandwiching glass slide with two strips of double-sided tape. A glass coverslip (Matsunami, #0, thickness <0.12 mm) was used to cover the sample in the sample chamber and subsequently form a chamber with a thickness of about 150 µm. The thickness of the cell chamber was performed using an vernier caliper. The thickness of the glass slide and cover glass was initially measured. The space that form in between the glass slide and coverslip assembled with double-sided tape was obtained by measuring the whole completed cell chamber and subtracting with the thickness of the glass slide and coverslip. Figure 3.25 (b)-(c) shows the picture of the finished sample chamber and the side view used for experiments and applications with optical traps.

05-4506832 pustaka.upsi.edu.my Perpustakaan Tuanku Bainun Kampus Sultan Abdul Jalil Shah PustakaTBainun ptbupsi

05-4506832 pustaka.upsi.edu.my Perpustakaan Tuanku Bainun Kampus Sultan Abdul Jalil Shah PustakaTBainun ptbupsi

The 5CB microdroplet suspension solution that filled the finished cell chamber could now be observed and examined under the optical microscope. Finally, the cell chamber was positioned on the intended sample stage of the optical microscope.

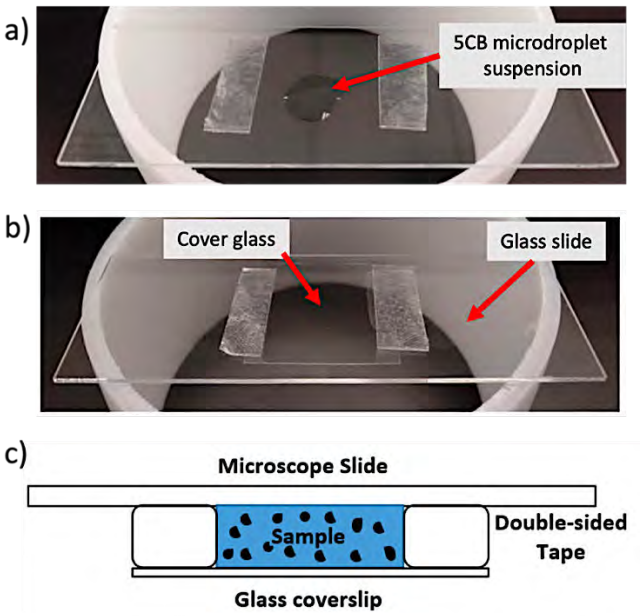


Figure 3.25. The image of the cell chamber (a) the 5CB microdroplet suspension was dropped on the glass slide, (b) the cover glass was assembled to the glass slide with two strips of double-sided tape, and (c) the schematic diagram of the cell chamber.

3.4.2 Radial 5CB Microdroplet Solution Preparation

The preparation of the radial 5CB microdroplet suspension in the water slightly differs from the bipolar 5CB microdroplet suspension. The surfactant is required to modify and anchor the surface of the 5CB microdroplet to produce 5CB microdroplet suspension with radial internal configuration. There was an initially necessary procedure to produce radial 5CB microdroplets, which was to determine the minimum Centrimonium Bromide (CTAB) volume to change all the bipolar 5CB microdroplets

05-4506832 pustaka.upsi.edu.my Perpustakaan Tuanku Bainun Kampus Sultan Abdul Jalil Shah PustakaTBainun ptbupsi

05-4506832 pustaka.upsi.edu.my Perpustakaan Tuanku Bainun Kampus Sultan Abdul Jalil Shah PustakaTBainun ptbupsi

to radial 5CB microdroplets. This was done by adding several CTAB solutions of 2% g/mL (w/v) concentration of varied volume to the 2 mL bipolar 5CB microdroplet suspension solution of increment 5 µL. The CTAB Critical Micelle Concentration (CMC) to trigger the transition of bipolar to radial configuration of 5CB microdroplet is 13 µM (Murazawa, Juodkazis, & Misawa, 2005; Murazawa, Juodkazis, Matsuo, et al., 2005a). The prepared 2% g/mL (w/v) of CTAB solution is equal to 54877 µM more than CTAB CMC (13 µM) to generate radial 5CB microdroplet. The radial 5CB microdroplet suspension formation was observed and determined under an optical polarized microscope. Figure 3.26 shows the snapshot of the bipolar 5CB microdroplet suspension solution exposed to the different volumes of CTAB solution.

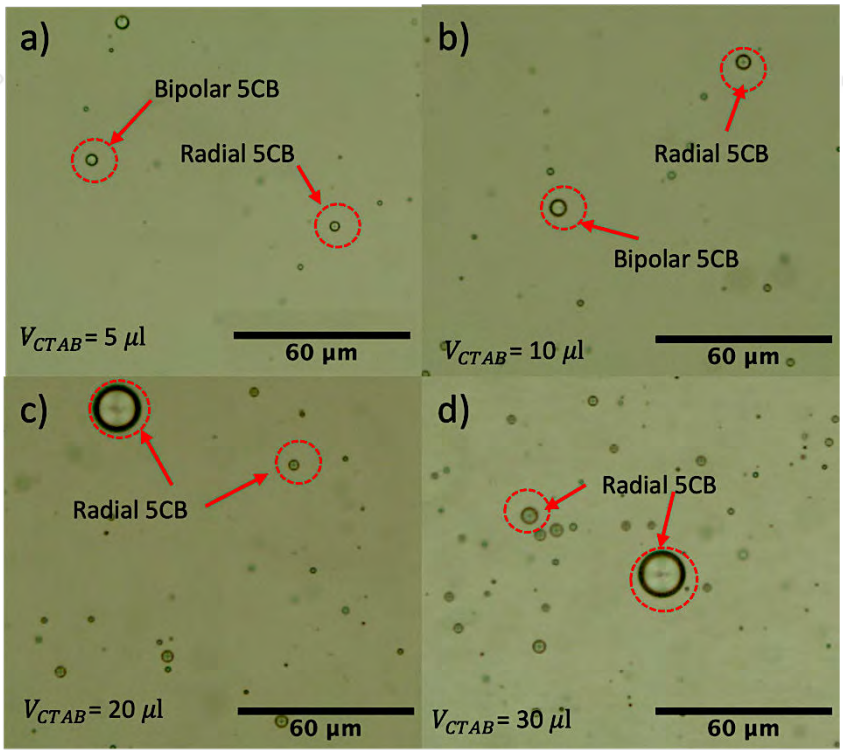


Figure 3.26. The effect of the CTAB solution volume on the formation of the radial 5CB microdroplet suspension.

05-4506832 pustaka.upsi.edu.my Perpustakaan Tuanku Bainun Kampus Sultan Abdul Jalil Shah PustakaTBainun ptbupsi

05-4506832 pustaka.upsi.edu.my Perpustakaan Tuanku Bainun Kampus Sultan Abdul Jalil Shah PustakaTBainun ptbupsi

Figure 3.26 highlights the effect of the CTAB solution of 2 % (w/v) of a different volume exposed to the bipolar 5CB microdroplet in 2 mL of deionized water. Figure 3.26 (a) shows the 5CB microdroplet suspension in water exposed to 5 µL of CTAB solution. It could be observed that a mixed composition of the bipolar and radial internal configurations existed together. Then, Figure 3.26 (b) shows the 5CB microdroplet suspension in water that was exposed to the 10 µl of CTAB solution. The composition of the 5CB microdroplet exhibited both bipolar and radial configurations when observed under an optical microscope. Then the CTAB solution volume added to the 5CB microdroplet suspension was increased to 20 µL as shown in Figure 3.26 (c). All the 5CB microdroplets observed under the optical microscope showed radial internal configuration when the 5CB microdroplet was exposed to 20 µL CTAB solution volume. Next, the 5CB microdroplet suspension was added with 30 µL of CTAB solution, and the microscopic image of the 5CB microdroplet suspension is shown in Figure 3.26 (d). It was observed that when 30 µL CTAB solution volume was used, all the 5CB microdroplets exhibited radial internal configuration. Based on this observation, the minimum CTAB volume of 2% g/mL (w/v) should be used to ensure all the 5CB microdroplets in 2 mL of deionized water were 20 µL. Below the 20 µL volume of CTAB, the 5CB microdroplet exists in both a bipolar and radial configuration.

First, 0.5 µL of the liquid 5CB was pipette in the clean 2 mL plastic vials containing 1.0, 1.5, and 2.0 ml of deionized water to prepare 5CB microdroplet suspension with the radial internal configuration. Next, a 20 µL of CTAB of 2% (w/v) concentration solution was pipette to the mixture of the liquid 5CB and deionized water to generate 5CB microdroplet suspension. The mixture was then shaken for 30 s to

05-4506832 pustaka.upsi.edu.my Perpustakaan Tuanku Bainun Kampus Sultan Abdul Jalil Shah PustakaTBainun ptbupsi

05-4506832 pustaka.upsi.edu.my Perpustakaan Tuanku Bainun Kampus Sultan Abdul Jalil Shah PustakaTBainun ptbupsi

avoid a liquid 5CB stick at the bottom of the vial and dispersed in the mixture. The schematic diagram of the summarization procedure for radial 5CB microdroplet suspension solution is shown in Figure 3.27.

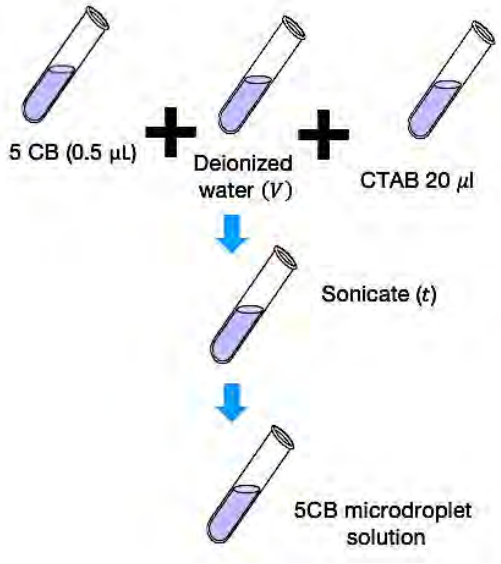


Figure 3.27. The schematic diagram summarizes the production of the radial 5CB microdroplet suspension solution.

An ultrasonic bath (GT Sonic, VGT-1620QTD) was used to sonicate the mixture of the liquid 5CB, deionized water, and CTAB solution to produce a homogenous 5CB microdroplet suspension of radial internal configuration. The sonication time was varied from 1.0, 2.0, 3.0, and 10.0 minutes to examine the effect of the sonication time on the size of the 5CB microdroplet formed.

05-4506832 pustaka.upsi.edu.my Perpustakaan Tuanku Bainun Kampus Sultan Abdul Jalil Shah PustakaTBainun ptbupsi

05-4506832 pustaka.upsi.edu.my Perpustakaan Tuanku Bainun Kampus Sultan Abdul Jalil Shah PustakaTBainun ptbupsi

3.4.3 5CB Microdroplet Observation by Optical Microscopy

An optical microscope is essential for viewing and observing the sample in the cell chamber. This study used the Inverted Metallurgical Microscope GX51 from Olympus to observe the 5CB microdroplets' dynamic and size. This microscope uses a 20× magnification and 0.9 numerical aperture (NA) air-type objective lens. The actual image of the Inverted Metallurgical Microscope GX51 used in the experiment is shown in Figure 3.28.

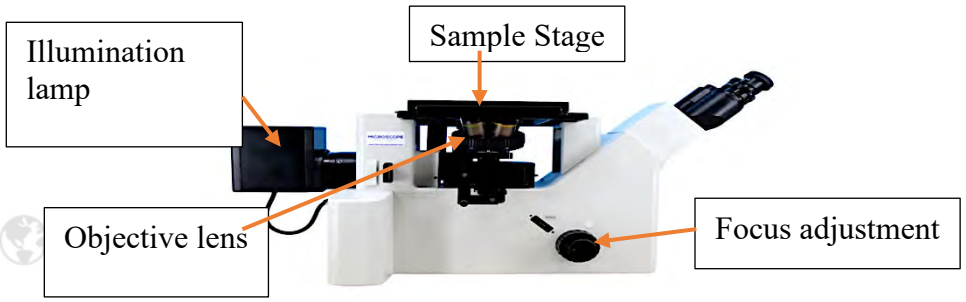


Figure 3.28. The actual image of the Inverted Metallurgical Microscope GX51 for observing and viewing purposes.

The procedure for using the Inverted Metallurgical Microscope was easy. First, the sample chamber was placed on the sample stage. Then, the illumination lamp was turned on so that light illuminated the sample. Finally, use the focus adjustment to focus the image of the 5C microdroplets until the image of the sample is visible and apparent. The schematic diagram of the Inverted Metallurgical Microscope GX51 is shown in Figure 3.29.

05-4506832 pustaka.upsi.edu.my Perpustakaan Tuanku Bainun Kampus Sultan Abdul Jalil Shah PustakaTBainun ptbupsi

05-4506832 pustaka.upsi.edu.my Perpustakaan Tuanku Bainun Kampus Sultan Abdul Jalil Shah PustakaTBainun ptbupsi

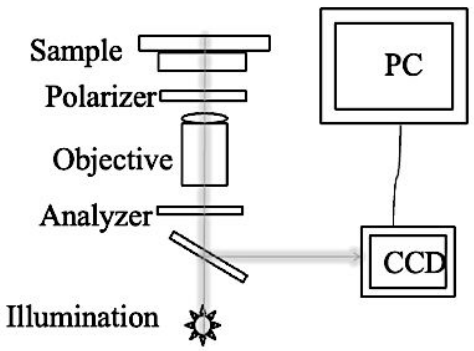


Figure 3.29. The schematic diagram of the Inverted Metallurgical Microscope GX51.

The image of the sample was then recollected by the objective lens and passed through the analyzer before being reflected by the dichroic mirror to the CCD camera. The CCD camera recorded the image of the sample and live video at the focus plane. The recorded image and video were saved in PNG and MKV files for post-analysis.

05-4506832 pustaka.upsi.edu.my Perpustakaan Tuanku Bainun Kampus Sultan Abdul Jalil Shah PustakaTBainun ptbupsi

An example of the sample image in which the 5CB microdroplet suspension solution is at the specific focal plane is illustrated in Figure 3.30. Several circular images indicated the 5CB droplets of various sizes dispersed in the dispersion medium (water). The focus adjustment can be adjusted to obtain the precise image of the particle (5CB) microdroplet images. In addition, the microscope stage can be moved in x and y directions to the observed particle at a different location. The image must be calibrated before analysis can be done. The calibration of the image will be explained in the next section.

05-4506832 pustaka.upsi.edu.my Perpustakaan Tuanku Bainun Kampus Sultan Abdul Jalil Shah PustakaTBainun ptbupsi

05-4506832 pustaka.upsi.edu.my Perpustakaan Tuanku Bainun Kampus Sultan Abdul Jalil Shah PustakaTBainun ptbupsi

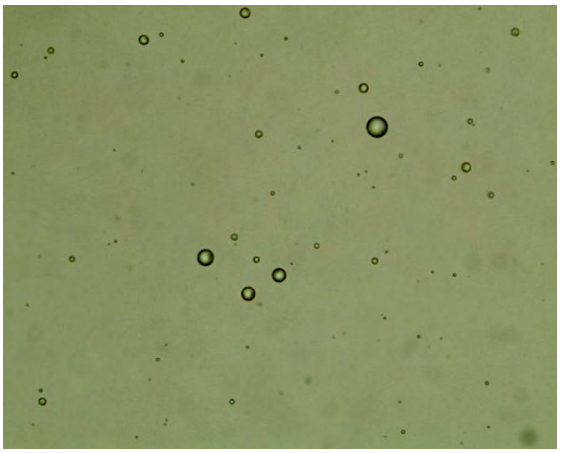


Figure 3.30. The actual particles (5CB microdroplet images) are seen at the specific focal plane.

3.4.4 Image J Optical Microscope Calibration

05-4506832 pustaka.upsi.edu.my Perpustakaan Tuanku Bainun Kampus Sultan Abdul Jalil Shah PustakaTBainun ptbupsi

Before any measurement, calibration of the pixel to micrometer of the image by ImageJ software is critical. First, the user must find the distance correlation between the unit pixel and the meter. The failure to calibrate ImageJ software will cause inaccurate measurements. Clicking the ImageJ program icon will open the front panel of the ImageJ software. For example, the front panel of the ImageJ software is shown in Figure 3.31.



Figure 3.31. Front Panel of ImageJ software.

05-4506832 pustaka.upsi.edu.my Perpustakaan Tuanku Bainun Kampus Sultan Abdul Jalil Shah PustakaTBainun ptbupsi

05-4506832 pustaka.upsi.edu.my Perpustakaan Tuanku Bainun Kampus Sultan Abdul Jalil Shah PustakaTBainun ptbupsi

Typically, for an optical microscope, the image of the calibration slide can be used to calibrate the ImageJ software. Then upload the captured image of the calibration slide by dragging it to the front panel of ImageJ software. The image of the calibration slide viewed using an air-type objective lens (0.45 NA and 20× magnification) is shown in Figure 3.32 (a) and the front panel of an uploaded image of the calibration slide ruler in ImageJ software in Figure (b).

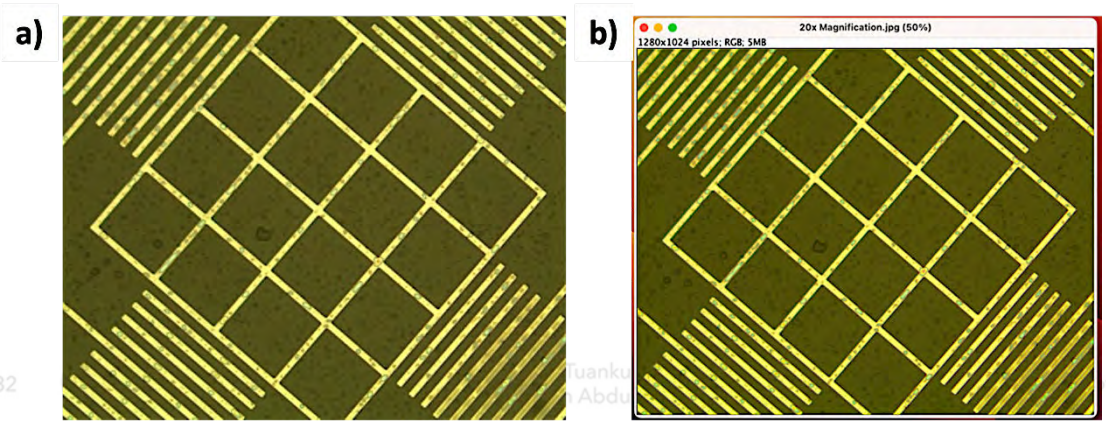


Figure 3.32. (a) The image of the calibration slide ruler was observed under an inverted optical microscope (20× objective lens), (b) the front panel of an uploaded image of the calibration slide ruler in ImageJ software.

The straight-line measurement function can be selected from the front panel of the ImageJ software, as shown in Figure 3.33.



Figure 3.33. The snapshot of the straight-line measurement function is labeled with a dashed circle.

05-4506832 pustaka.upsi.edu.my Perpustakaan Tuanku Bainun Kampus Sultan Abdul Jalil Shah PustakaTBainun ptbupsi

05-4506832 pustaka.upsi.edu.my Perpustakaan Tuanku Bainun Kampus Sultan Abdul Jalil Shah PustakaTBainun ptbupsi

The given distance between the two scales of the calibration scale ruler is 10 µm. Then, the distance of the calibration ruler scale was measured using the straight-line option in the ImageJ software to find the distance in unit pixels, as shown in Figure 3.33. To make this process easier, the image of the calibration slide ruler was zoomed out (150 % from the actual image) to make measurement easy and efficient, as illustrated in Figure 3.34.



Figure 3.34. The zoomed Figure 3.32 (b) to demonstrates the Measurement of the distance between two scales of calibration ruler by a straight-line measurement. The obtained length was 40.608 pixels.

A straight-line option measured the distance between the two scales on the calibration ruler, as shown in Figure 3.34. The measurement showed that the distance was 40.608 pixels. Ten distance measurements were performed to find the average value. The measurement made by the ImageJ software is illustrated in Table 3.4.

05-4506832 pustaka.upsi.edu.my Perpustakaan Tuanku Bainun Kampus Sultan Abdul Jalil Shah PustakaTBainun ptbupsi

05-4506832 pustaka.upsi.edu.my Perpustakaan Tuanku Bainun Kampus Sultan Abdul Jalil Shah PustakaTBainun ptbupsi

Table 3.4

Measurement of length in unit pixels by ImageJ.

Label	Measurement	Length (pixels)
	1	41.231
	2	41.773
	3	40.608
	4	39.051
	5	40.460
	6	40.460
	7	41.231
	8	39.051
	9	40.361
	10	41.231
Mean		40.546
Standard Deviation		0.909

05-4506832 pustaka.upsi.edu.my Perpustakaan Tuanku Bainun Kampus Sultan Abdul Jalil Shah PustakaTBainun ptbupsi

The average distance between the two scales of the calibration ruler was 40.546 ± 0.909 pixels. The distance of the two scales in meters was 10 μm, and the distance in the pixels was 40.546 pixels, so the calibration factor was 4.0546 pixels/μm.

05-4506832 pustaka.upsi.edu.my Perpustakaan Tuanku Bainun Kampus Sultan Abdul Jalil Shah PustakaTBainun ptbupsi

05-4506832 pustaka.upsi.edu.my Perpustakaan Tuanku Bainun Kampus Sultan Abdul Jalil Shah PustakaTBainun ptbupsi

3.4.5 ImageJ Distribution Size (r) Measurement

The previous section has described the procedure to obtain the calibration factor pixel per micrometer when the 0.45 NA, 20× air type objective lens. The calibration factor measured was 4.0546 pixel/μm and was used to measure the distribution size (r) of the 5CB microdroplets using ImageJ software. The measurement was referred to the ImageJ User Guide (Ferreira & Rasband, 2012).

In order to use ImageJ software for distribution size measurement of the 5CB microdroplet, the image of the 5CB microdroplet under the focus of the optical microscope at a definite focal plane was recorded and saved in the format of PNG or jpeg. The sample of uncalibrated 5CB microdroplets image under the polarized microscope is shown in Figure 3.35 (a). The image of the 5CB microdroplets under the polarized microscope must be calibrated before ImageJ software can analyze the distribution size. To start with, the image of the 5CB microdroplet was imported to the ImageJ software, and the front panel of the 5CB microdroplet image is shown in Figure 3.35 (b).

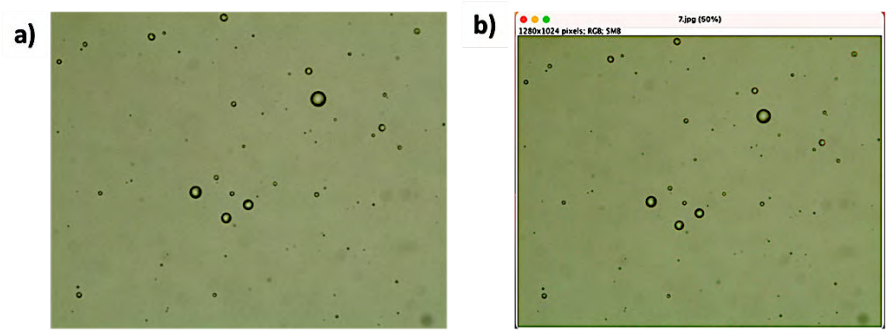


Figure 3.35. The snapshot of the (a) uncalibrated 5CB microdroplet image under an optical microscope and (b) front panel of uploaded 5CB microdroplets images by ImageJ software.

05-4506832 pustaka.upsi.edu.my Perpustakaan Tuanku Bainun Kampus Sultan Abdul Jalil Shah PustakaTBainun ptbupsi

05-4506832 pustaka.upsi.edu.my Perpustakaan Tuanku Bainun Kampus Sultan Abdul Jalil Shah PustakaTBainun ptbupsi

Then, the uploaded 5CB microdroplet image was calibrated with the previous calibration factor. Next, calibrate the uploaded 5CB microdroplets image; it can be done by clicking the analyze function and selecting the set scale option as shown in Figure 3.36 (a). The click of the set scale function will pop up the front panel for the set scale, as shown in Figure 3.36 (b).

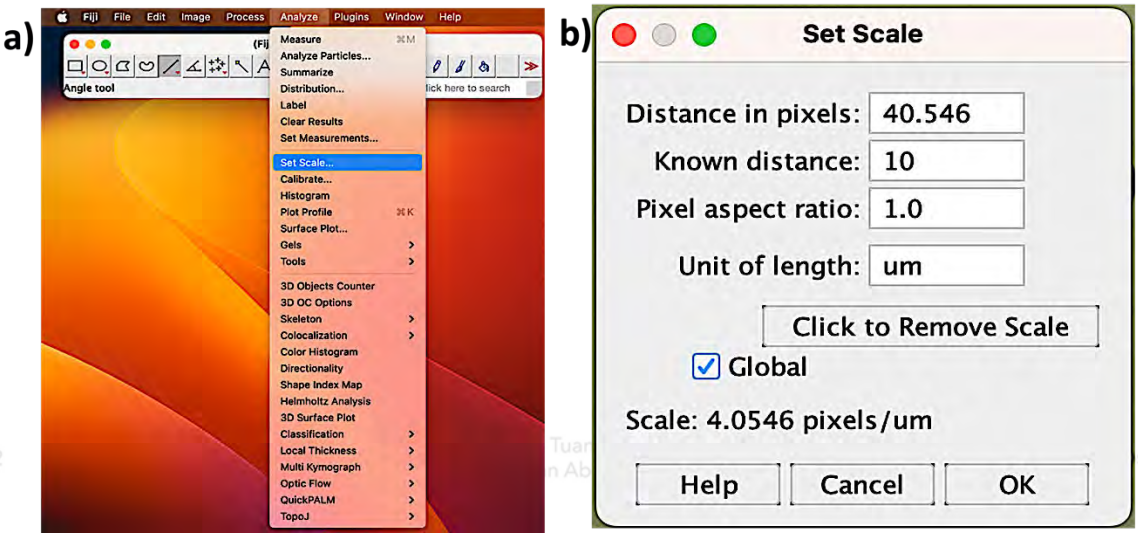


Figure 3.36. (a) Front panel for analysis and set scale function, (b) set scale front panel for calibration.

In the set scale front panel, fill in the distance in pixels as 40.546, known distance as 10 µm, pixel aspect ratio was set to 1.0, and the unit of length in micrometer (µm). Then, once the OK button was clicked, the image was calibrated and ready for distribution size analysis.

To measure the distribution size of the 5CB microdroplet, the calibrated 5CB microdroplets image must be converted to an 8-bits image. Figure 3.37 (a) shows the

05-4506832 pustaka.upsi.edu.my Perpustakaan Tuanku Bainun Kampus Sultan Abdul Jalil Shah PustakaTBainun ptbupsi

05-4506832 pustaka.upsi.edu.my Perpustakaan Tuanku Bainun Kampus Sultan Abdul Jalil Shah PustakaTBainun ptbupsi

front panel for conversion of an 8-bit image and (b) the resulting 5CB microdroplet image after 8-bit conversion.

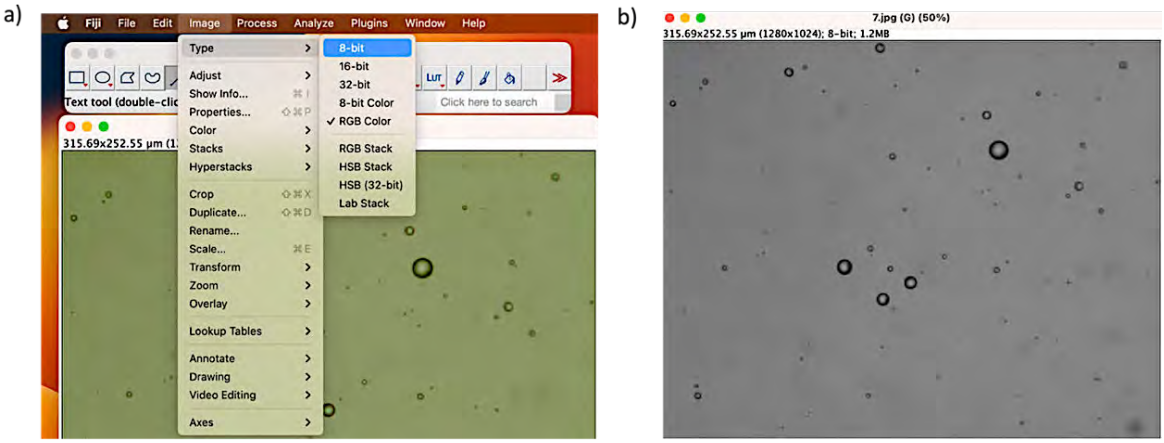


Figure 3.37. (a) Front panel for 8-bit image conversion and (b) image of 5CB microdroplets after 8-bit conversion.

To convert the 5CB microdroplets image to an 8-bit image, click the image and 8-bit option as shown in Figure 3.37 (a). The image is converted to an 8-bit image because the threshold measurement can only recognize images in 8-bit. As a result, the 5CB microdroplets turned grayscale images, as shown in Figure 3.37 (b). The image of the 5CB microdroplet was further modified by applying the bandpass filter and referred to the ImageJ User Guide (Ferreira & Rasband, 2012). The function of the bandpass filter is to enhance the image and the structure of the 5CB microdroplets (Ferreira & Rasband, 2012). Figure 3.38 (a) shows the front panel to impose the bandpass filter, (b) FFT Bandpass Filter settings, and (c) the front panel of the 5CB microdroplet image imposed with the FFT Bandpass Filter.

05-4506832 pustaka.upsi.edu.my Perpustakaan Tuanku Bainun Kampus Sultan Abdul Jalil Shah PustakaTBainun ptbupsi

05-4506832 pustaka.upsi.edu.my Perpustakaan Tuanku Bainun Kampus Sultan Abdul Jalil Shah PustakaTBainun ptbupsi

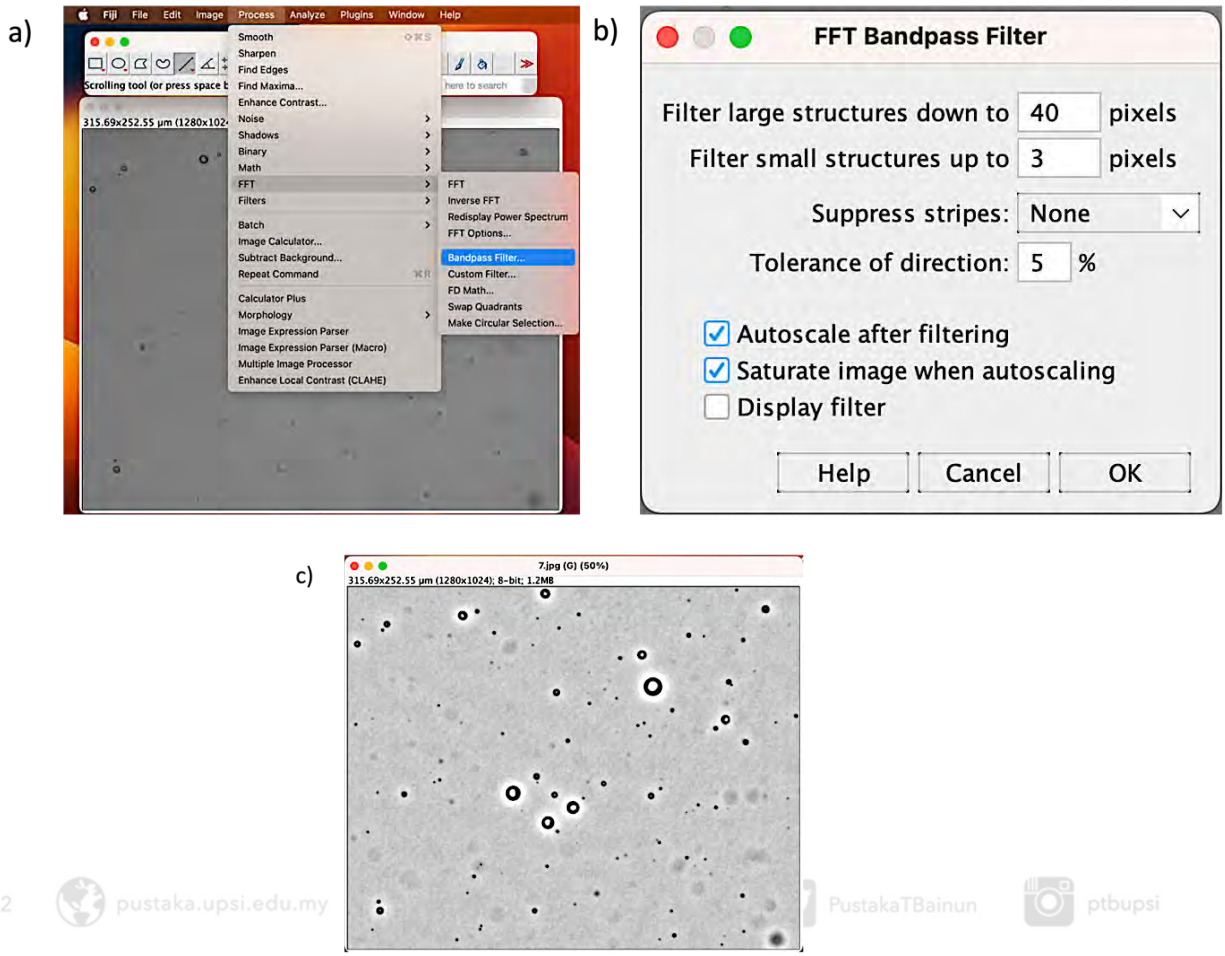


Figure 3.38. The snapshot of the ImageJ front panel (a) front panel to impose bandpass filter, (b) FFT bandpass filter setting, and (c) the resulting image of the FFT bandpass filter imposed on the 5CB microdroplet image.

To impose the FFT bandpass filter, click the Process, choose the FFT function, and then click Bandpass filter, as shown in Figure 3.38 (a). The popup window of the FFT Bandpass filter setting is shown in Figure 3.38 (b). The default setting of the FFT Bandpass filter consists of a large filter structure down to 40 pixels, a small filter structure up to 3 pixels, a suppress stripe set to none, and the tolerance of direction was 5% (Ferreira & Rasband, 2012). The result of the 5CB microdroplet image after imposing with an FFT Bandpass filter is shown in Figure 3.38 (c). The structure and the circularity of the 5CB microdroplet become enhanced and contrast with the

05-4506832 pustaka.upsi.edu.my Perpustakaan Tuanku Bainun Kampus Sultan Abdul Jalil Shah PustakaTBainun ptbupsi

05-4506832 pustaka.upsi.edu.my Perpustakaan Tuanku Bainun Kampus Sultan Abdul Jalil Shah PustakaTBainun ptbupsi

surrounding environment based on the default setting used. If the sample structure is complex, small, or irregular, the setting in Figure 3.38 (b) can be adjusted according to the complexity of the sample. This is significant to facilitate the auto measurement of 5CB microdroplet size in the later process. The distribution sizes could be measured once the FFT Bandpass filter was applied to the 5CB microdroplet image.

Next, the 5CB microdroplet image finished undergoing the FFT Bandpass filter and was ready for distribution size measurement. Then, go to the ImageJ front panel, and click the Image option, as shown in Figure 3.39 (a). This resulted in a series of display choices. First, choose the Adjust option and click threshold, as shown in Figure 3.39 (a). Next, the front panel of the threshold was displayed when the Threshold option was clicked, as shown in Figure 3.39 (b).

05-4506832 pustaka.upsi.edu.my Perpustakaan Tuanku Bainun Kampus Sultan Abdul Jalil Shah PustakaTBainun ptbupsi

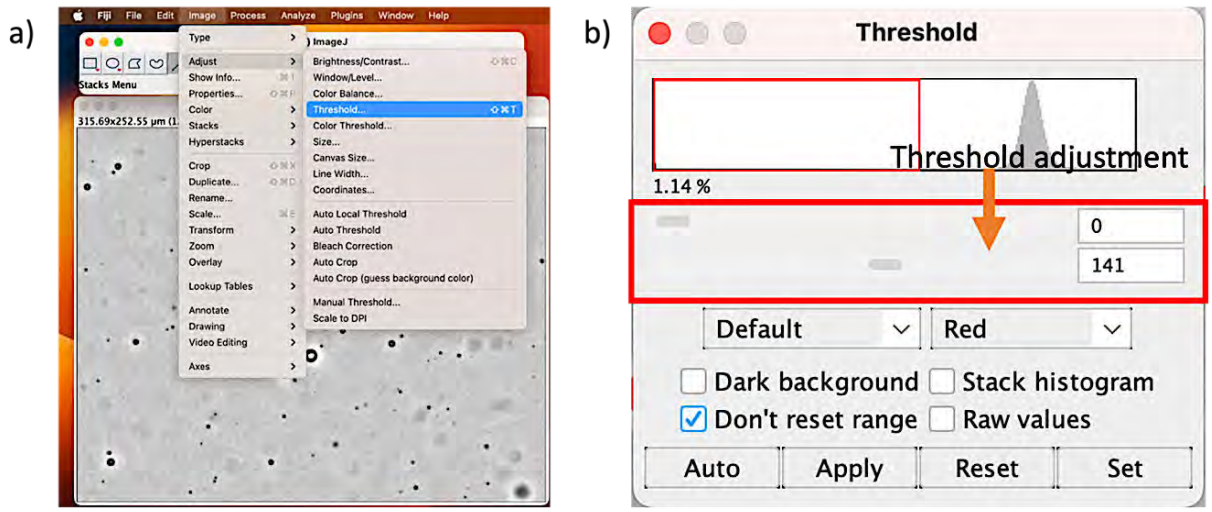


Figure 3.39. The snapshot of the (a) front panel for the Threshold option and (b) front panel for the "Threshold" setting.

The "Threshold" front panel is shown in Figure 3.39 (b). The ImageJ software automatically suggested the threshold setting. If the suggested threshold value is not

05-4506832 pustaka.upsi.edu.my Perpustakaan Tuanku Bainun Kampus Sultan Abdul Jalil Shah PustakaTBainun ptbupsi

05-4506832 pustaka.upsi.edu.my Perpustakaan Tuanku Bainun Kampus Sultan Abdul Jalil Shah PustakaTBainun ptbupsi

suitable for measurement (if the threshold function highlights the intended particle incorrectly), the threshold value can be adjusted manually. The threshold setting can be adjusted by dragging the threshold or writing the required threshold value. The threshold function was to highlight the shape of 5CB droplets that needed to be measured. Figure 3.40 (a) shows the ImageJ automatic threshold highlighting the visible 5CB microdroplet with the red color. Only the highlighted 5CB microdroplets will be measured in size. The ImageJ will not measure the unhighlighted microdroplet. Once the user satisfaction with the suggested threshold or manually adjusts the threshold, click the apply button to apply the threshold on the 5CB microdroplet image. As a result, the confirmed 5CB microdroplets' front panel will be displayed, as shown in Figure 3.40 (b). Only the white 5CB microdroplet was measured, and the black surrounding was the subtracted background to avoid interference with the measurement.

05-4506832 pustaka.upsi.edu.my Perpustakaan Tuanku Bainun Kampus Sultan Abdul Jalil Shah PustakaTBainun ptbupsi

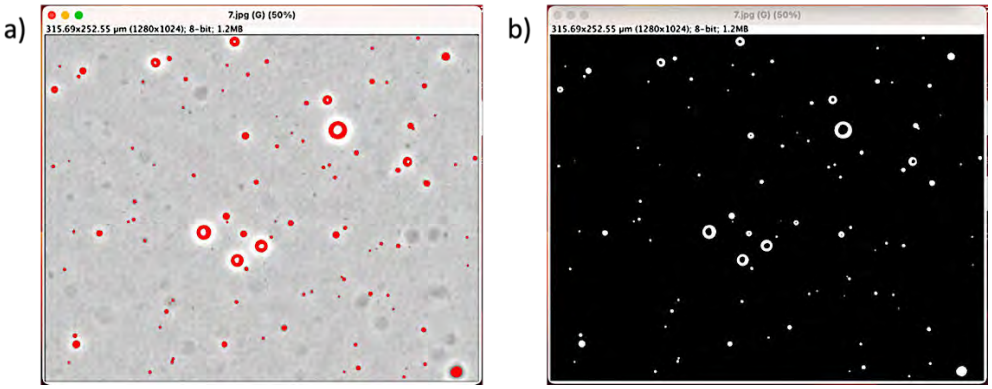


Figure 3.40. (a) ImageJ automatic threshold highlighting the visible 5CB microdroplet with the red color, (b) the image of 5CB microdroplet after threshold measurement made by ImageJ.

After finishing the threshold part, the last step was the distribution measurement size. To measure the distribution size of the 5CB microdroplets, click the Analyze

05-4506832 pustaka.upsi.edu.my Perpustakaan Tuanku Bainun Kampus Sultan Abdul Jalil Shah PustakaTBainun ptbupsi

05-4506832 pustaka.upsi.edu.my Perpustakaan Tuanku Bainun Kampus Sultan Abdul Jalil Shah PustakaTBainun ptbupsi

option from the ImageJ front panel. Then, choose the Analyze Particle option as shown in Figure 3.41 (a). Clicking the Analyzer Particle option caused the Analyze Particle front panel to pop up, as shown in Figure 3.41 (b).

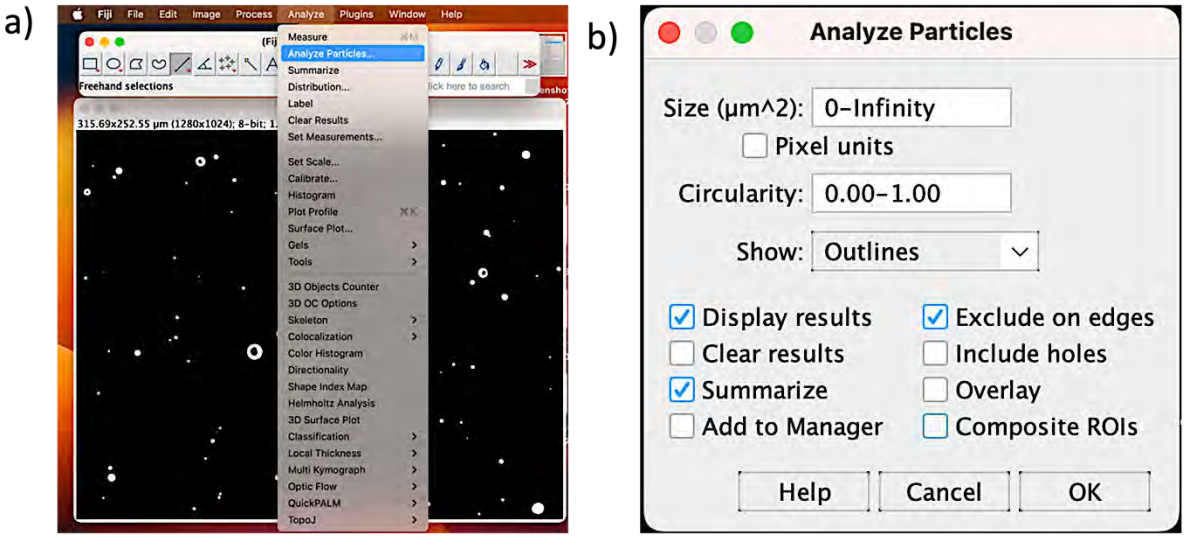


Figure 3.41. (a) ImageJ front panel view for Analyze Particle option, Figure 3.41 (b) The front panel of Analyze Particles popup.

The measurement set was displayed on the front view of Analyze Particles, as shown in Figure 3.41 (b). The setting was set as size (0 to infinity, default setting), circularity (shape), 0 means not circle while 1 means most circle (0.00-1.00), and show (users set this to Outlines). Tick the display results, summarize and exclude on edges and click OK.

The measurement of each 5CB microdroplet on the 5CB microdroplet image was labeled and outlined and shown in Figure 3.42 (a). All the 5CB microdroplets that were previously highlighted with threshold were measured in this section. The total number of the microdroplets measured and the area of each of the 5CB microdroplets

05-4506832 pustaka.upsi.edu.my Perpustakaan Tuanku Bainun Kampus Sultan Abdul Jalil Shah PustakaTBainun ptbupsi

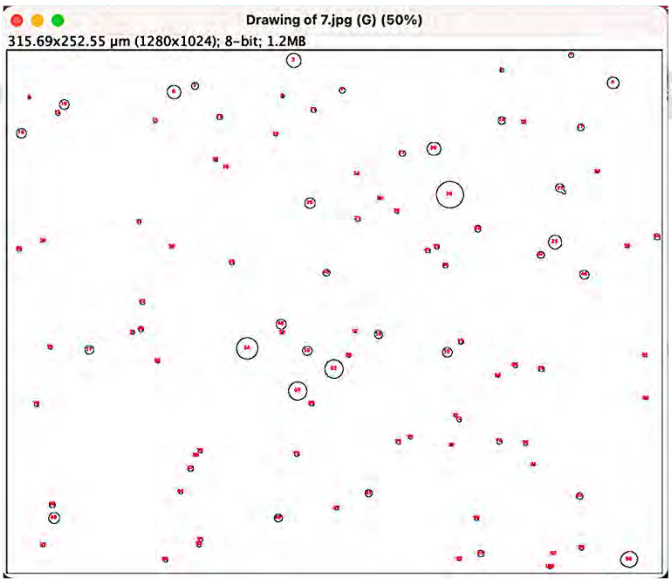
05-4506832 pustaka.upsi.edu.my Perpustakaan Tuanku Bainun Kampus Sultan Abdul Jalil Shah PustakaTBainun ptbupsi

was recorded and tabulated in the Table, as shown in Figure 3.42 (b). The ImageJ did not directly measure the diameter or the radius of the 5CB microdroplet, but it measured the area of each of the 5CB microdroplets. However, the ImageJ summarizes the measurement's total area and standard deviation. The radius of the 5CB microdroplet can be calculated using the equation

$$r = \sqrt{\left(\frac{A}{\pi}\right)} \tag{3.4}$$

where A is the area of the circle, and r is the circle's radius.

a)



b)

	Label	Area
1		4.380
2		32.908
3		2.798
4		24.696
5		8.698
6		29.562
7		6.022
8		2.190
9		1.399
10		16.910
11		4.562
12		3.893

Figure 3.42. (a) Outlines the measured 5CB microdroplet area, and (b) the tabulated number and area of each measured 5CB microdroplet.

The data of the 5CB microdroplets area can be further analyzed to obtain the radius or post-statistics analysis. In this study, ten frames of 5CB microdroplet images

05-4506832 pustaka.upsi.edu.my Perpustakaan Tuanku Bainun Kampus Sultan Abdul Jalil Shah PustakaTBainun ptbupsi

05-4506832 pustaka.upsi.edu.my Perpustakaan Tuanku Bainun Kampus Sultan Abdul Jalil Shah PustakaTBainun ptbupsi

were taken at the same focus plane, and the average of the 5CB microdroplet radius was determined.

3.4.6 5CB Microdroplet Stability Measurement

The measurement of the microdroplet suspension stability and sustainability are significant to estimate how long the suspension produced can remain to disperse, not sink, avoid coalescence, and decrease the microdroplets after a specific monitoring time. This measurement can be done by using UV-VIS spectroscopy. The estimation of the microdroplet can be examined by observing the signal change of the UV-VIS spectral for a certain period. UV-VIS is one of the alternative techniques that can be used to study microdroplet suspension and stability in water. This study used UV-Vis spectroscopy (Agilent 8453 Optics) to determine 5CB microdroplet stability.

For UV-Vis measurement, bipolar 5CB microdroplet solution was pipetted in the cuvette for inspection of absorbance spectra. The absorbance spectra were monitored for 1 hour with 5-minute increments. The same procedure was repeated for radial 5CB microdroplet solution. Figure 3.43 shows the schematic diagram of the cuvette filled with 1.8 mL of 5CB microdroplet suspension solution for UV-Vis inspection.

05-4506832 pustaka.upsi.edu.my Perpustakaan Tuanku Bainun Kampus Sultan Abdul Jalil Shah PustakaTBainun ptbupsi

05-4506832 pustaka.upsi.edu.my Perpustakaan Tuanku Bainun Kampus Sultan Abdul Jalil Shah PustakaTBainun ptbupsi

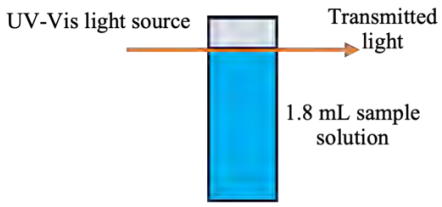


Figure 3.43. Schematic diagram of the 5CB microdroplet suspension (1.8 mL) for stability inspection by UV-Vis spectroscopy.

The absorbance peak of the 5CB microdroplet suspension sample at different times was compared to determine its stability. The stability measurement is based how long the 5CB microdroplet can remain and sustained at its position. If the 5CB microdroplet was stable, the absorbance peak should be constant. However, if the absorbance peak changed, that indicated instability. It is important to quantify how much the absorbance peak changes through 1 hour monitoring time. This is because the time for the optical process depends on how long the 5CB microdroplet can suspend in the sample. The absorbance percentage change ($\Delta A_{\%}$) was calculated by equation

$$\Delta A_{\%} = \left| \frac{A_i - A_f}{A_f} \right| \times 100 \tag{3.5}$$

where A_i is the initial absorbance and A_f is the final absorbance.

3.5 The 5CB Microdroplet Micro-Control [Phase 3]

First, 0.5 µL of the 5CB microdroplet suspension solution was filled into a cell chamber. The sample chamber consisted of the bipolar 5CB microdroplets suspension placed on the piezostage of the Modular Optical Tweezers (OTKB/M) for the optical trapping

05-4506832 pustaka.upsi.edu.my Perpustakaan Tuanku Bainun Kampus Sultan Abdul Jalil Shah PustakaTBainun ptbupsi

05-4506832 pustaka.upsi.edu.my Perpustakaan Tuanku Bainun Kampus Sultan Abdul Jalil Shah PustakaTBainun ptbupsi

process in the water. The *z*-adjusted knob of the piezostage, which controlled the focal view, was adjusted until the free-moving 5CB microdroplets could be seen on the PC's live display of the CCD camera. After the image of the 5CB microdroplets was visible, turn on the trapping laser power to trap a single 5CB microdroplet in the water. A single bipolar 5CB microdroplet of different radii (r), at varied optical power density (P) was trapped using a linearly polarized laser beam to find the dependency of corner frequency and optical power density.

The size (r) of the trapped bipolar 5CB microdroplet was measured by ImageJ software. The CCD camera recorded the image of the single optical trapping of the bipolar 5CB microdroplet. The polarizer and analyzer were crossed to form a cross-polarized view to confirm the trapping of the 5CB microdroplet and examine the microdroplet's internal configuration during the optical trapping performed. The same procedure was repeated for the optical trapping of several sizes of radial 5CB microdroplets.

3.5.1 Microdroplet Internal Configuration Control

In order to study the orientation control of the trapped 5CB microdroplet, the half-wave plate was installed in the path of the trapping laser beam. In the context of our experiment, the half-wave plate (Thorlabs, WPH10M-980 - Ø1" Zero-Order Half-Wave Plate, SM1-Threaded Mount, $\lambda = 980$ nm) was used to manipulate linearly polarized laser beam direction. The actual image of the used half-wave plate was

05-4506832 pustaka.upsi.edu.my Perpustakaan Tuanku Bainun Kampus Sultan Abdul Jalil Shah PustakaTBainun ptbupsi

05-4506832 pustaka.upsi.edu.my Perpustakaan Tuanku Bainun Kampus Sultan Abdul Jalil Shah PustakaTBainun ptbupsi

illustrated in Figure 3.44 (a) the half-wave plate and (b) the schematic diagram showing the position of the half-wave plate inserted in the optical path of the optical tweezers setup.

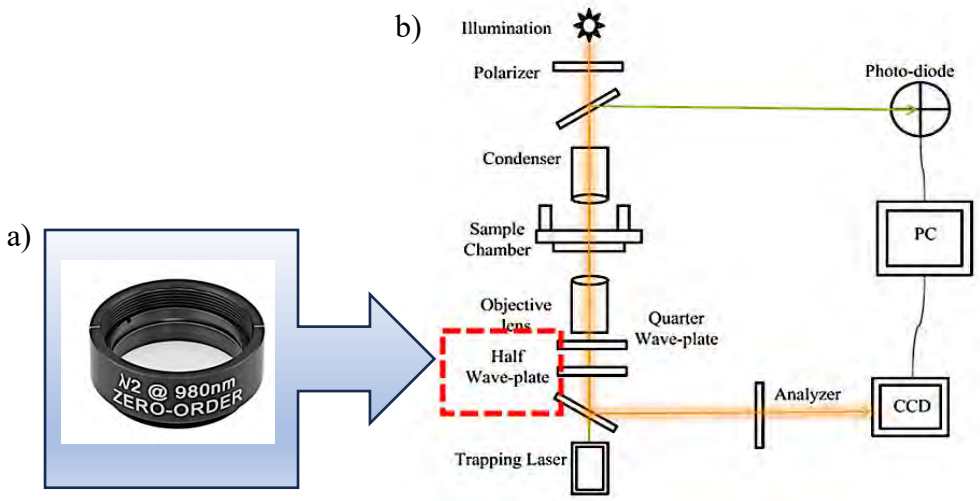


Figure 3.44. (a) The actual image of the half-wave plate and (b) the position of the half-wave plate inserted in the optical path of the optical tweezers setup.

The half-wave plate was set to perpendicular (θ: 0°), identical to the direction of linearly polarized light in a perpendicular direction. The rotation of the half-wave plate angle was in the range of θ: 0° − 360°, changing the direction of the linear polarized laser beam accordingly. Figure 3.45, the schematic diagram showing that the half-wave plate was oriented to angle θ, to the incoming perpendicular direction linearly polarized laser beam produced a horizontal linearly polarized laser beam to angle 2θ.

05-4506832 pustaka.upsi.edu.my Perpustakaan Tuanku Bainun Kampus Sultan Abdul Jalil Shah PustakaTBainun ptbupsi

05-4506832 pustaka.upsi.edu.my Perpustakaan Tuanku Bainun Kampus Sultan Abdul Jalil Shah PustakaTBainun ptbupsi

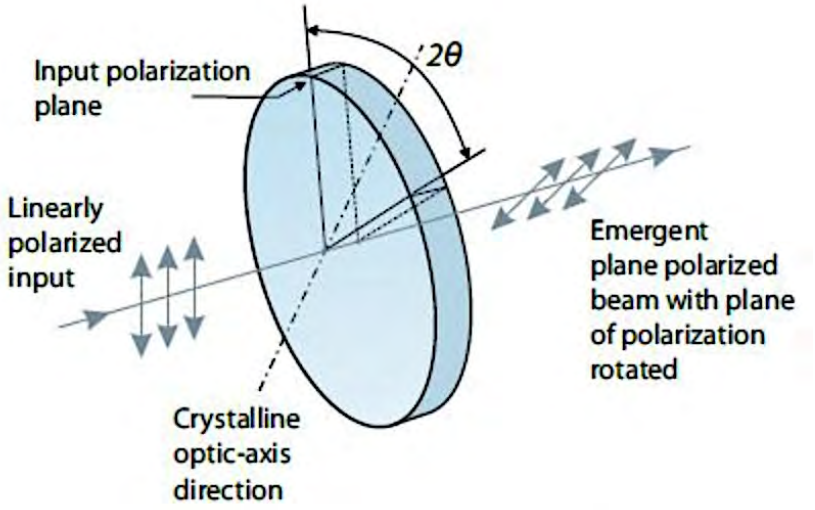


Figure 3.45. The schematic diagram shows the half-wave plate was oriented to angle θ, to the incoming perpendicular direction linearly polarized laser beam produced a horizontal linearly polarized laser beam to angle 2θ. Adapted from Standa Photonics.

After aligning the half-wave plate's fast axis with the perpendicular linearly polarized light, the optical tweezers were ready to study the orientation control of the 5CB microdroplet. First, the single 5CB microdroplet was trapped by a linearly polarized laser beam at a specific laser power. Then, the orientation control of the 5CB microdroplet was performed by slowly adjusting the angle of the half-wave plate starting from $\theta = 0^{o}$ until $\theta = 180^{o}$ with an increment of 30^{o}. The effect of the linearly polarized laser direction on the internal configuration inside the trapped 5CB microdroplet was observed under optical microscopy and cross-polarized view. The CCD camera recorded the image of the trapped 5CB microdroplet internal configuration orientation change and displayed it live on the PC.

05-4506832 pustaka.upsi.edu.my Perpustakaan Tuanku Bainun Kampus Sultan Abdul Jalil Shah PustakaTBainun ptbupsi

05-4506832 pustaka.upsi.edu.my Perpustakaan Tuanku Bainun Kampus Sultan Abdul Jalil Shah PustakaTBainun ptbupsi

3.5.2 5CB Microdroplet Rotational Control

To study the rotatability of the trapped single 5CB microdroplet in water, the linearly polarized laser beam was replaced with the circularly polarized laser beam. To investigate the rotatability of the trapped single 5CB microdroplet, a quarter wave plate was installed in the path of the trapping laser beam. This study used a quarter wave plate (WPQ10M-980 - Ø1" Zero-Order Quarter-Wave Plate, SM1-Threaded Mount, $\lambda = 980$ nm) which functions to convert a linearly polarized laser beam to the circularly polarized laser beam. The actual image of the used quarter wave-plate was illustrated in Figure 3.46 (a) the quarter-wave plate, and (b) the schematic diagram showed the position of the quarter-wave plate inserted in the optical path of the optical tweezers setup.

05-4506832 pustaka.upsi.edu.my ptbupsi

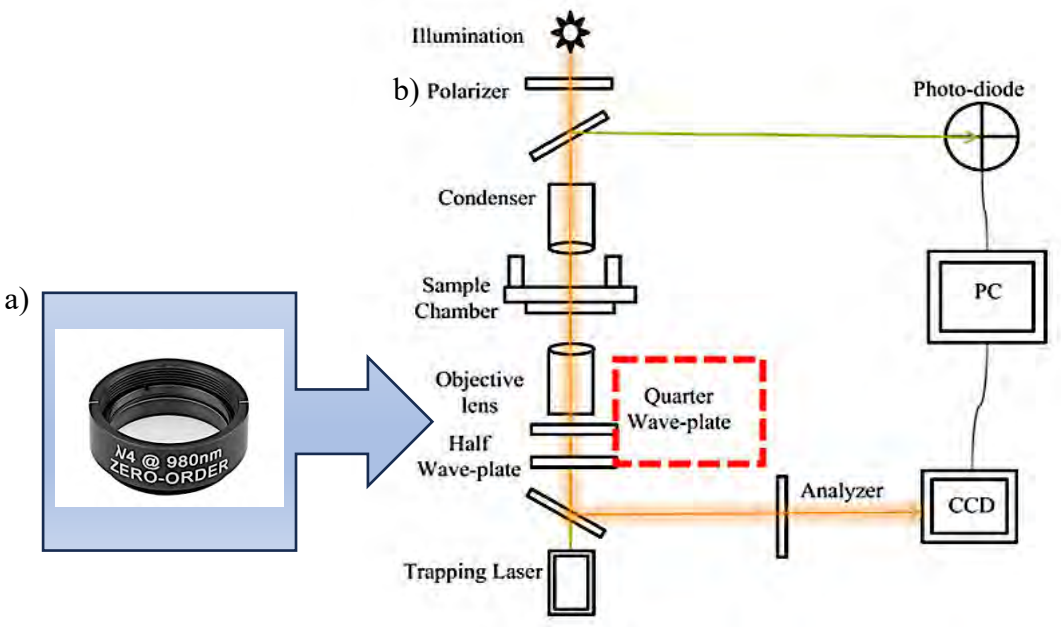


Figure 3.46. (a) The actual image of the quarter wave-plate and (b) the position of the quarter-wave plate inserted in the optical path of the optical tweezers setup.

05-4506832 pustaka.upsi.edu.my Perpustakaan Tuanku Bainun Kampus Sultan Abdul Jalil Shah PustakaTBainun ptbupsi

05-4506832 pustaka.upsi.edu.my Perpustakaan Tuanku Bainun Kampus Sultan Abdul Jalil Shah PustakaTBainun ptbupsi

The quarter-wave plate was set to perpendicular ($\theta: 0°$), identical to the direction of linearly polarized light in a perpendicular direction. The rotation of the quarter-wave plate angle was in the range of $\theta: 0° - 360°$, changing the polarization from linear, elliptical, and circular accordingly. The rotation of quarter-wave plate angle ($\theta: 0° - 360°$) changed the light polarization; $\theta: 0° =$ linearly polarized, $\theta: 10º - 44° =$ elliptically polarized, and $\theta: 45° =$ circularly polarized. Figure 3.47. the schematic diagram of the quarter-wave plate oriented to angle θ = 45º, to the incoming perpendicular direction linearly polarized laser beam, produced a circularly polarized laser beam. The relative orientation of the quarter-wave plate at 45°, either to the right or left, to the central axis of the initial polarization state of the incident linearly polarized laser established right and left circular polarization.

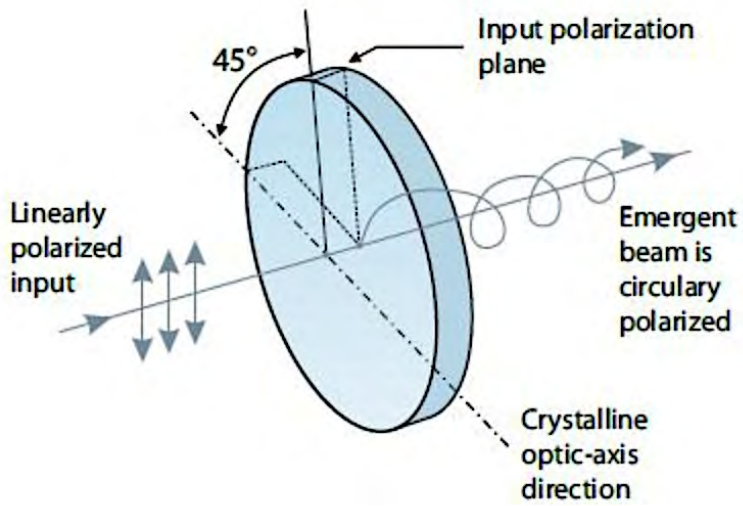


Figure 3.47. The schematic diagram shows the quarter wave-plate was oriented to angle θ = 45º, to the incoming perpendicular direction linearly polarized laser beam produced a left-handed circularly polarized laser beam. Adapted from Standa Photonics.

After aligning the fast axis of the quarter-wave plate 45º to the linearly polarized laser beam, the resulting polarization was circularly polarized and ready for the optical

05-4506832 pustaka.upsi.edu.my Perpustakaan Tuanku Bainun Kampus Sultan Abdul Jalil Shah PustakaTBainun ptbupsi

05-4506832 pustaka.upsi.edu.my Perpustakaan Tuanku Bainun Kampus Sultan Abdul Jalil Shah PustakaTBainun ptbupsi

trapping process. The circularly polarized laser beam trapped the single 5CB microdroplet, and the rotation of the trapped 5CB microdroplet was observed under an optical microscope and in a cross-polarization view. The 5CB rotated when irradiated and trapped by the circularly polarized laser beam because the light carries angular momentum. The optical laser power used to trap and rotate a single 5CB microdroplet optically was varied to study the effect on the rotatability, specifically angular speed. Next, the CCD camera captured the image of the trapped 5CB microdroplet to measure the r. As the trapped 5CB microdroplet rotated, the QPD signal reading was recorded for each trapped 5CB microdroplet video.

3.5.3. Translation and Polarization Control

05-4506832 pustaka.upsi.edu.my Perpustakaan Tuanku Bainun Kampus Sultan Abdul Jalil Shah PustakaTBainun ptbupsi

The translation and micro-control of the trapped single 5CB microdroplet in the water by definite laser polarization were investigated. In this stage, the optically trapped 5CB microdroplet was controlled in two degrees of freedom: (1) translation and (2) polarization control. The piezostage controlled the translation of the trapped 5CB microdroplet in water via APT's User Software. The interface of the APT's User Software is shown in Figure 3.48. Meanwhile, the polarization of the laser beam was controlled by the half-wave plate and quarter-wave plate.



Figure 3.48. The snapshot of the APT's User Software interface to control the translation of the piezostage.

05-4506832 pustaka.upsi.edu.my Perpustakaan Tuanku Bainun Kampus Sultan Abdul Jalil Shah PustakaTBainun ptbupsi

05-4506832 pustaka.upsi.edu.my Perpustakaan Tuanku Bainun Kampus Sultan Abdul Jalil Shah PustakaTBainun ptbupsi

The first part of the translational and micro-control was to simultaneously study the translation of the trapped 5CB microdroplet and the polarization control of the linearly polarized laser beam. The CCD camera recorded the translation of the trapped 5CB microdroplet and the effect of the retrapping. Figure 3.49 shows the schematic diagram of the translation of the trapped particle by the piezostage control. The trapped 5CB microdroplet was translated to the right and left by controlling the voltage supplied to the piezostage via APT's User Software.

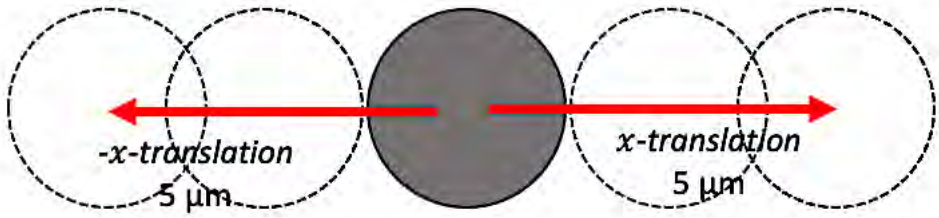


Figure 3.49. The schematic diagram of the translation of the trapped particle by the piezostage control.

A linearly polarized laser beam initially trapped a single 5CB microdroplet. The trapped 5CB microdroplet was translated 5 μm to the right when the 20 V voltage was supplied to the piezostage using APT's User software. Figure 3.50 shows the front panel of the APT's User to translate the piezostage to 5 µm translation to the right.

05-4506832 pustaka.upsi.edu.my Perpustakaan Tuanku Bainun Kampus Sultan Abdul Jalil Shah PustakaTBainun ptbupsi

05-4506832 pustaka.upsi.edu.my Perpustakaan Tuanku Bainun Kampus Sultan Abdul Jalil Shah PustakaTBainun ptbupsi

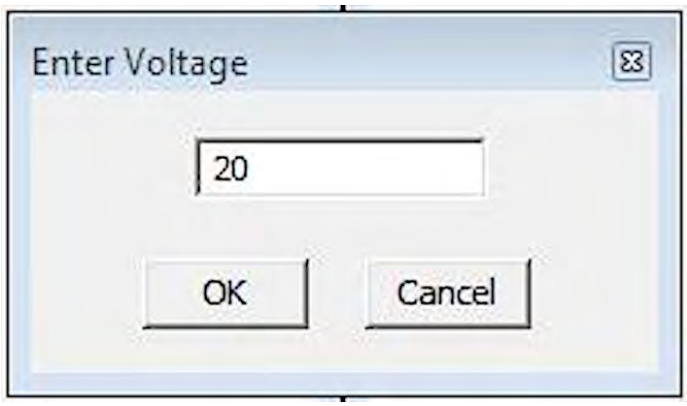


Figure 3.50. The front panel of the APT's User translates the piezostage 5 μm to the right.

After the trapped 5CB microdroplet was displaced to the right, the displaced trapped 5CB microdroplet was displaced from the trap spot. However, after a few times, the displaced 5CB microdroplet was again attracted to the optical trap. Then, the trapped 5CB microdroplet was translated 5 μm to the left when the voltage input to the piezostage was set to 0 V and caused the trapped 5CB microdroplet to displace from the trap spot.

The displaced 5CB microdroplet reattracted to the trap spot after a specific monitoring time or could be escaped. The trajectory of the whole translation, right and left, was recorded by the CCD camera, and the trajectory of the translation and trapping was analyzed using Tracker Software.

The same procedure was repeated by changing the linearly polarized laser beam to the circularly polarized laser beam. Figure 3.51 shows the schematic diagram of the translation and micro-control of the trapped 5CB microdroplet under a circularly polarized laser beam.

05-4506832 pustaka.upsi.edu.my Perpustakaan Tuanku Bainun Kampus Sultan Abdul Jalil Shah PustakaTBainun ptbupsi

05-4506832 pustaka.upsi.edu.my Perpustakaan Tuanku Bainun Kampus Sultan Abdul Jalil Shah PustakaTBainun ptbupsi

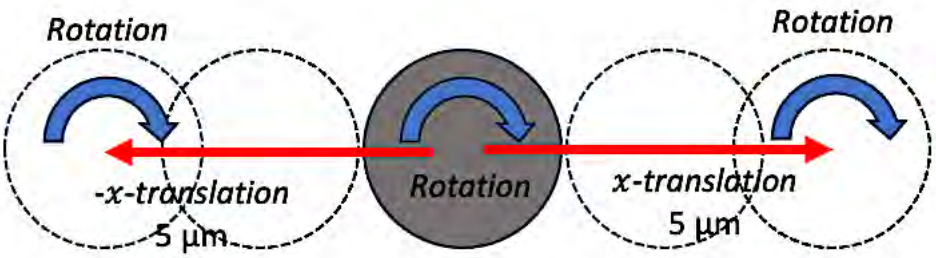


Figure 3.51. The schematic diagram of the translation and micro-control of the trapped 5CB microdroplet under a circularly polarized laser beam. The trapped 5CB microdroplet was rotated when the laser beam trapped it.

3.5.4 Trajectory Analysis of 5CB Microdroplet

The translation and micro-control of the trapped 5CB microdroplet by the linearly and circularly polarized were monitored under the polarized optical microscope, and the CCD camera recorded the translation video. The video of the translational and micro-control of the trapped 5CB microdroplet under linear and circular polarization was analyzed by using Tracker Software. This study used the tracker software to track the position along the *x*-direction of the translated and micro-control of the trapped 5CB microdroplet under a linearly and circularly polarized laser beam.

To start tracking the motion of the trapped 5CB microdroplet in terms of translational and micro-control under linearly and circularly polarized laser beam, the video of the trapped 5CB microdroplet was imported to the Tracker Software. Figure 3.52 shows the front panel of the Tracker Software to import the recorded video of the trapped 5CB microdroplet.

05-4506832 pustaka.upsi.edu.my Perpustakaan Tuanku Bainun Kampus Sultan Abdul Jalil Shah PustakaTBainun ptbupsi

05-4506832 pustaka.upsi.edu.my Perpustakaan Tuanku Bainun Kampus Sultan Abdul Jalil Shah PustakaTBainun ptbupsi

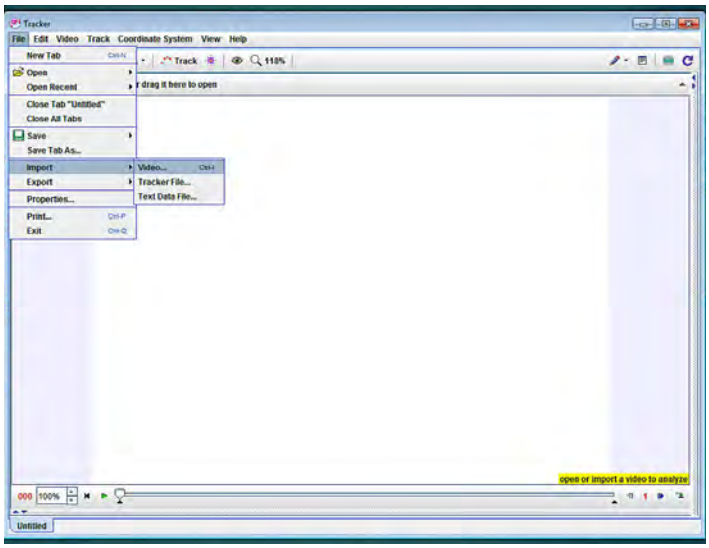


Figure 3.52. The screenshot of the Tracker Software to import the recorded video of the trapped 5CB microdroplet.

After the recorded video of the trapped 5CB microdroplet was loaded into the Tracker Software, the loaded recorded video of the trapped 5CB microdroplet was calibrated with calibrated stick function and set to 2 μm. The center of the 5CB microdroplet was set as the origin, and the axis function was added as guidance. The initial and final frames could be set according to the observer's preferences depending on how much the tracking position data wants to be extracted from the recorded video. Figure 3.53 shows the front panel display of the Tracker Software, indicating the calibration of the recorded video of the trapped 5CB microdroplet. Then the calibration was finished.

05-4506832 pustaka.upsi.edu.my Perpustakaan Tuanku Bainun Kampus Sultan Abdul Jalil Shah PustakaTBainun ptbupsi

05-4506832 pustaka.upsi.edu.my Perpustakaan Tuanku Bainun Kampus Sultan Abdul Jalil Shah PustakaTBainun ptbupsi

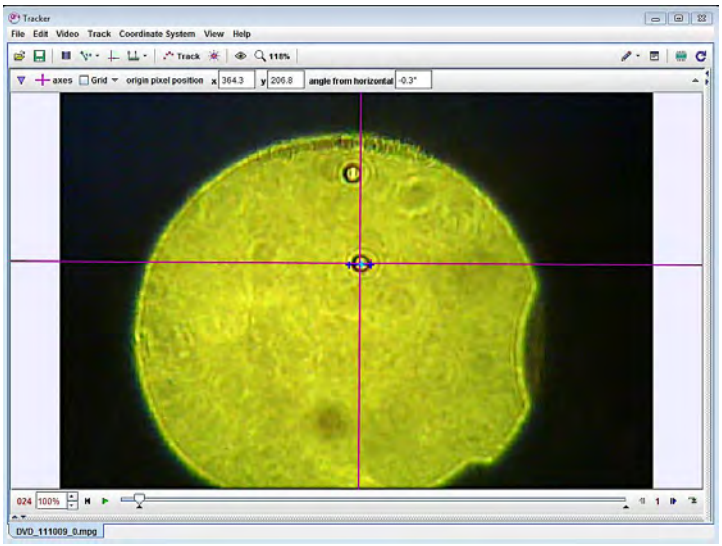


Figure 3.53. The snapshot of the calibrated recorded video of the trapped 5CB microdroplet by the Tracker Software.

After the trapped 5CB microdroplet video was calibrated, the tracking process was followed. Click the "Track" icon on the front panel of the Tracker Software and choose the point mass function, as shown in Figure 3.54. After clicking the point mass function, the user must mark the particle that must be tracked. This can be done by clicking "shift," "control," and right-clicking on the intended interest particles. To make the analysis and extraction of the position trajectory more convenient, the Autotracker function provides a more straightforward tracking method.

05-4506832 pustaka.upsi.edu.my Perpustakaan Tuanku Bainun Kampus Sultan Abdul Jalil Shah PustakaTBainun ptbupsi

05-4506832 pustaka.upsi.edu.my Perpustakaan Tuanku Bainun Kampus Sultan Abdul Jalil Shah PustakaTBainun ptbupsi

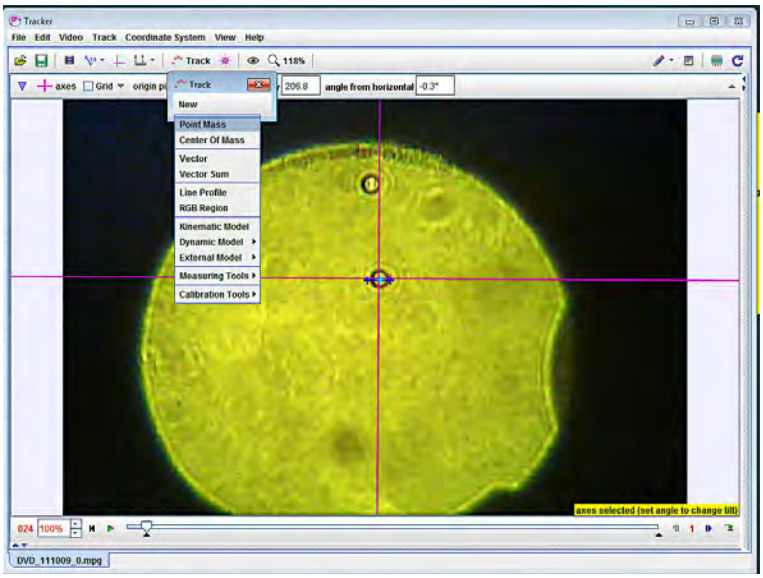


Figure 3.54. The snapshot of the Tracker Software interface demonstrated the tracking procedure on the respected interest particle.

The interface of the Autotracker is illustrated in Figure 3.55. An additional front panel corresponds to the Autotracker popup when the user clicks the Autotracker function. Clicking the search button on the Autotracker front panel automatically tracked the marked particle trajectory concerning the number of frames set constraint.

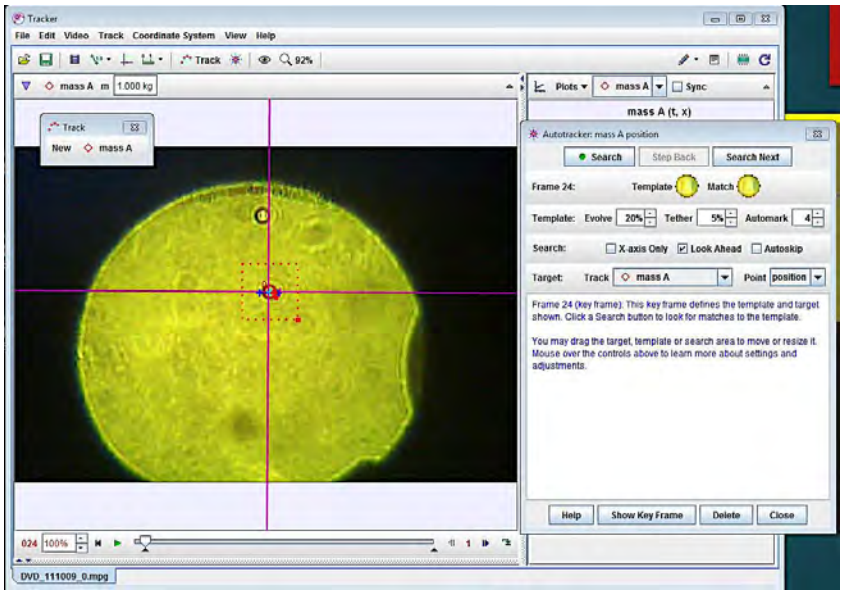


Figure 3.55. The snapshot of the Tracker Software's main front panel and the Autotracker function's front panel.

05-4506832 pustaka.upsi.edu.my Perpustakaan Tuanku Bainun Kampus Sultan Abdul Jalil Shah PustakaTBainun ptbupsi

05-4506832 pustaka.upsi.edu.my Perpustakaan Tuanku Bainun Kampus Sultan Abdul Jalil Shah PustakaTBainun ptbupsi

The data of the tracked particle by the Autotracker function was analyzed and illustrated on the right side of the main front panel of the Tracker Software, as shown in Figure 3.56. Figure 3.56 shows that the trapped particle was displaced to the right.

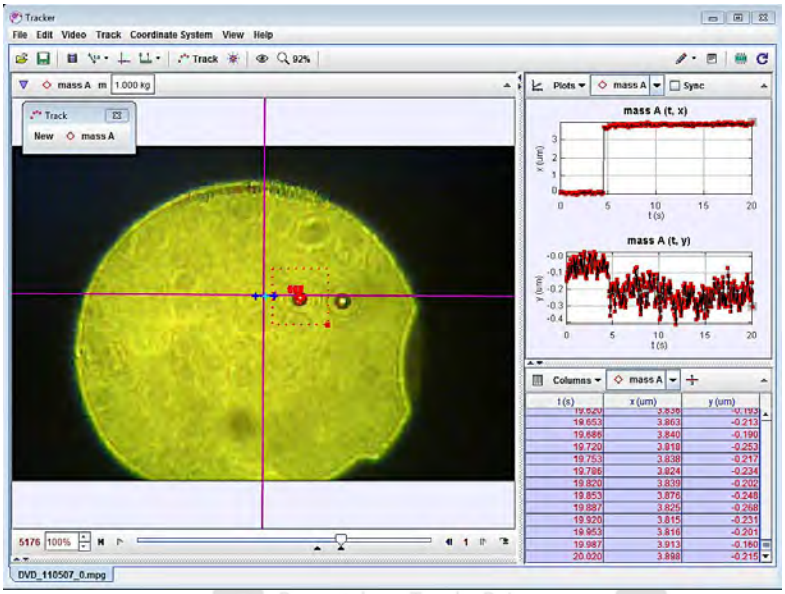


Figure 3.56. The snapshot of the Tracker Software, on the right side, shows the result of the tracked particle presented in the form of graph position in the *x*-direction and *y*-direction against time.

The graph shown in Figure 3.56 was enlarged and shown in Figure 3.57. The corresponding *x*-direction trajectory to the translation of the trapped particle is shown in Figure 3.57.

05-4506832 pustaka.upsi.edu.my Perpustakaan Tuanku Bainun Kampus Sultan Abdul Jalil Shah PustakaTBainun ptbupsi

05-4506832 pustaka.upsi.edu.my Perpustakaan Tuanku Bainun Kampus Sultan Abdul Jalil Shah PustakaTBainun ptbupsi



Figure 3.57. The snapshot of the trajectory data from the translation of the trapped particle.

The data of the trajectory of the translated trapped particle could be saved by copying the data into an Excel document. The Tracker software provides a valuable method to track the position of the trapped particle.

05-4506832 pustaka.upsi.edu.my Perpustakaan Tuanku Bainun Kampus Sultan Abdul Jalil Shah PustakaTBainun ptbupsi

3.6 Corner Frequency (f_c) and Angular Speed (ω) Measurement [Phase 4]

3.6.1 Corner Frequency (f_c) Flowchart Analysis

Figure 3.58 illustrates a series of flowchart analyses of radius (r), and corner frequency (f_c), using ImageJ and a custom-made program Optical Tweezers Calculator (OSCal). First, a single 5CB microdroplet is trapped in water. The image of the trapped 5CB microdroplet was snapped and recorded by a CCD camera. QPD recorded the trapped 5CB microdroplet signal via an oscilloscope. The image of the trapped 5CB microdroplet was uploaded in ImageJ software for r analysis. Next, the QPD signal of the trapped 5CB microdroplet collected from the oscilloscope required editing by using

05-4506832 pustaka.upsi.edu.my Perpustakaan Tuanku Bainun Kampus Sultan Abdul Jalil Shah PustakaTBainun ptbupsi

05-4506832 pustaka.upsi.edu.my Perpustakaan Tuanku Bainun Kampus Sultan Abdul Jalil Shah PustakaTBainun ptbupsi

Excel so that it could be read by the OSCal software algorithm during the uploading process. Lastly, the fitting process was performed to determine the average data f_c based on the *Y-Power spectrum*. Based on the average data f_c obtained from the OSCal software, the relationship between corner frequency, laser power density, and radius of the 5CB microdroplet could be shown by plotting the graph of corner frequency versus laser power density.

05-4506832 pustaka.upsi.edu.my Perpustakaan Tuanku Bainun Kampus Sultan Abdul Jalil Shah PustakaTBainun ptbupsi
05-4506832 pustaka.upsi.edu.my Perpustakaan Tuanku Bainun Kampus Sultan Abdul Jalil Shah PustakaTBainun ptbupsi

05-4506832 pustaka.upsi.edu.my Perpustakaan Tuanku Bainun Kampus Sultan Abdul Jalil Shah PustakaTBainun ptbupsi

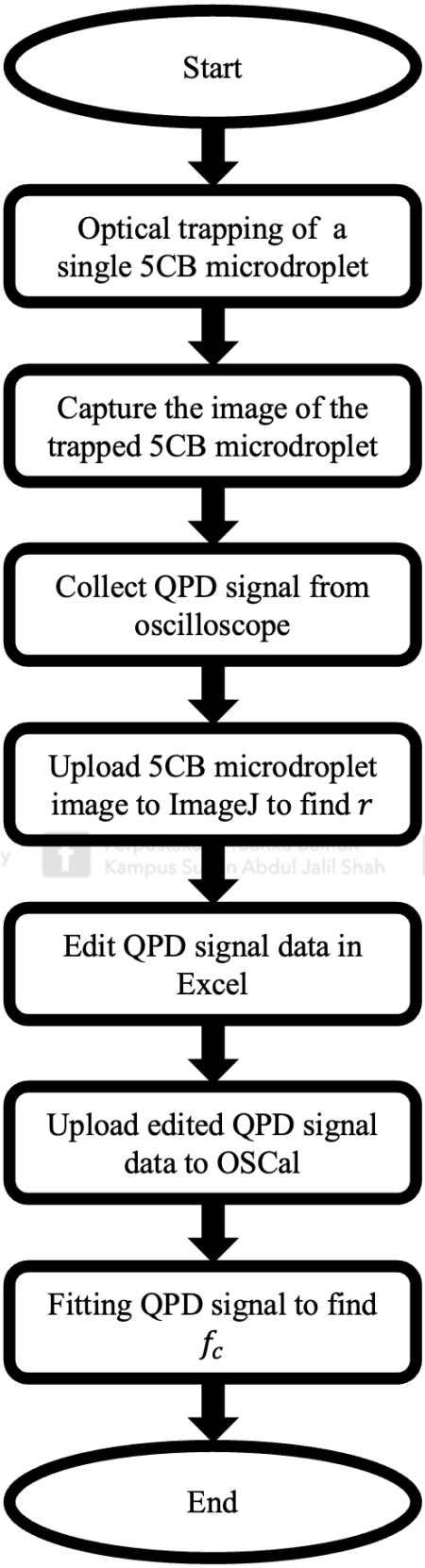


Figure 3.58. The flowchart for measuring 5CB microdroplet radius (r) and corner frequency (f_c) using the ImageJ program and OSCal program.

05-4506832 pustaka.upsi.edu.my Perpustakaan Tuanku Bainun Kampus Sultan Abdul Jalil Shah PustakaTBainun ptbupsi

05-4506832 pustaka.upsi.edu.my Perpustakaan Tuanku Bainun Kampus Sultan Abdul Jalil Shah PustakaTBainun ptbupsi

3.6.2 5CB Microdroplet Radius (r) Measurement

The trapped 5CB microdroplet size (r) was measured immediately after the optical trapping of a single 5CB microdroplet was successful. After optical tweezers managed to trap a single 5CB microdroplet, the image of the 5CB microdroplet was snapped by the CCD camera. The selected image of the trapped 5CB microdroplet was uploaded to ImageJ software. The ImageJ software measures the size (r) of the optically trapped 5CB microdroplet. Figure 3.59 shows the uploaded and calibrated image of the trapped 5CB microdroplet in the ImageJ software.

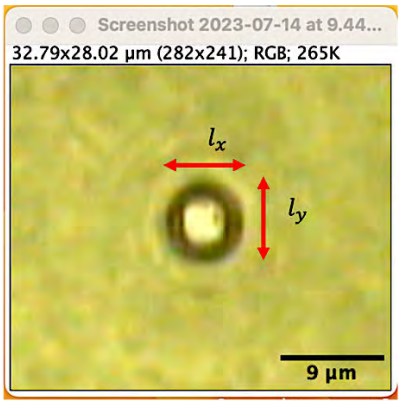


Figure 3.59. The snapshot of the ImageJ Software front panel showed the uploaded and calibrated image of the trapped 5CB microdroplet.

The conventional technique to measure r could be done by measuring the trapped 5CB microdroplet length in the x- and y-plane, as shown in Figure 3.64. However, this measurement was done manually and might cause deviation. To minimize the deviation from the manual measurement, the 5CB microdroplet size (r) was measured automatically using the Threshold function provided by the ImageJ software. The Threshold function automatically measures the area of the trapped 5CB

05-4506832 pustaka.upsi.edu.my Perpustakaan Tuanku Bainun Kampus Sultan Abdul Jalil Shah PustakaTBainun ptbupsi

05-4506832 pustaka.upsi.edu.my Perpustakaan Tuanku Bainun Kampus Sultan Abdul Jalil Shah PustakaTBainun ptbupsi

microdroplet and accurately measures the 5CB microdroplet size. To do this measurement, the image of the trapped 5CB microdroplet in Figure 3.59, initially in RGB image, was converted to an 8-bit image. Figure 3.60 shows the converted RGB image of Figure 3.60 to the 8-bit image.

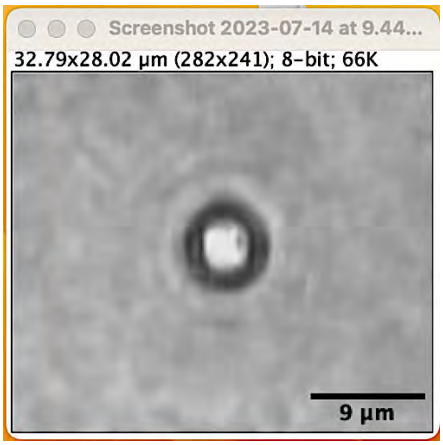


Figure 3.60. The snapshot of the converted trapped 5CB microdroplet RGB image in Figure 3.59 to 8-bit.

05-4506832 pustaka.upsi.edu.my Perpustakaan Tuanku Bainun Kampus Sultan Abdul Jalil Shah PustakaTBainun ptbupsi

Then the threshold of the trapped 5CB microdroplet in Figure 3.60 was adjusted by clicking the Image > Adjust > Threshold on the ImageJ front panel. The clicking of the threshold function resulted in the display of the Threshold front panel and the corresponding threshold measured panel, as shown in Figure 3.61 (a) and (b).

05-4506832 pustaka.upsi.edu.my Perpustakaan Tuanku Bainun Kampus Sultan Abdul Jalil Shah PustakaTBainun ptbupsi

05-4506832 pustaka.upsi.edu.my Perpustakaan Tuanku Bainun Kampus Sultan Abdul Jalil Shah PustakaTBainun ptbupsi

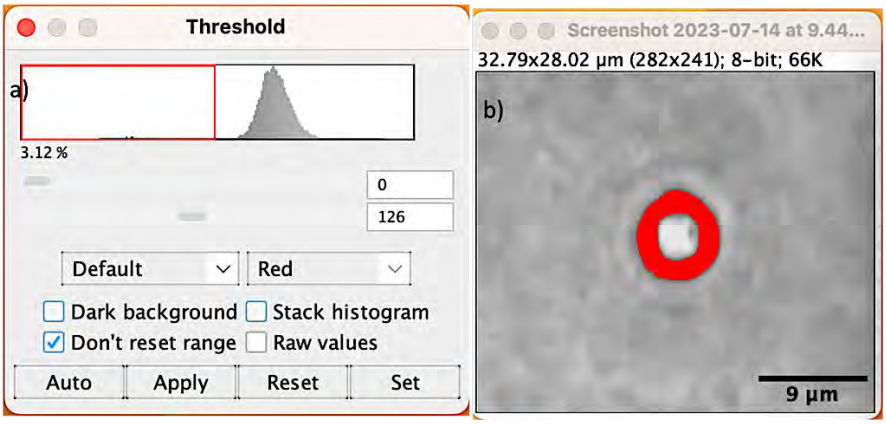


Figure 3.61. (a) The snapshot of the Threshold front panel and (b) the corresponding display of the threshold measured on the trapped 5CB microdroplet image.

Figure 3.61 (a) shows the auto threshold set and detected by the ImageJ software to measure the area of the trapped 5CB microdroplet. The user could adjust the threshold according to their preferences. Still, in this study, because the trapped 5CB microdroplet image was clear and high resolution, the auto threshold was enough to measure the area of the trapped 5CB microdroplet correctly. Then, once the user is satisfied with the suggested threshold by the ImageJ software, click the "Apply" button. Next, click the Analyze button, Analyze Particles button and click OK to measure and obtain the area of the trapped 5CB microdroplet. Figure 3.62 shows (a) the front panel of the image of the trapped 5CB microdroplet measured according to the set threshold and (b) the front panel to analyze the area of the trapped 5CB microdroplet by ImageJ software.

05-4506832 pustaka.upsi.edu.my Perpustakaan Tuanku Bainun Kampus Sultan Abdul Jalil Shah PustakaTBainun ptbupsi

05-4506832 pustaka.upsi.edu.my Perpustakaan Tuanku Bainun Kampus Sultan Abdul Jalil Shah PustakaTBainun ptbupsi

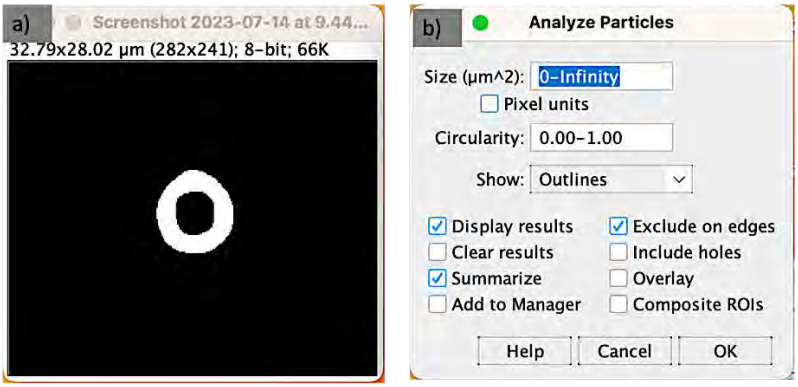


Figure 3.62. (a) The snapshot of the image of the trapped 5CB microdroplet measured according to the set threshold in Figure 3.76 and (b) The snapshot of the Analyze Particles front panel to measure the area of the trapped 5CB microdroplet.

The area of the trapped 5CB microdroplet was measured when the OK button in Figure 3.62 was clicked. Figure 3.63 shows (a) the snapshot of the front panel of the measured image of the trapped 5CB microdroplet and (b) the snapshot of the results of the area of the measured image of the trapped 5CB microdroplet done by ImageJ software.

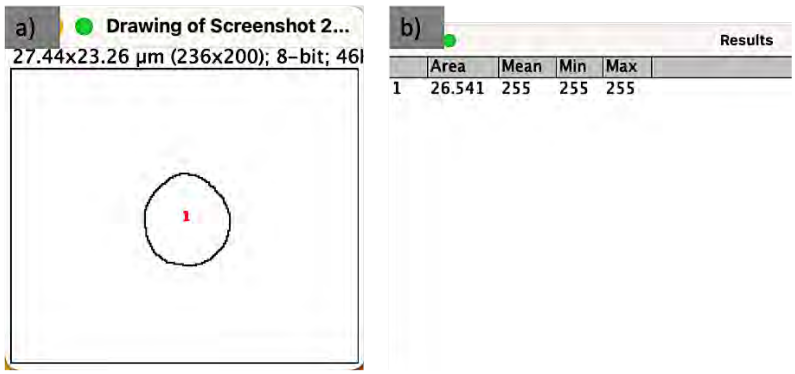


Figure 3.63. (a) The snapshot of the front panel shows the measured area of the trapped 5CB microdroplet image by ImageJ software. Figure 3.63 (b) The snapshot front panel shows the result of the area measured of the trapped 5CB microdroplet image by ImageJ Software.

05-4506832 pustaka.upsi.edu.my Perpustakaan Tuanku Bainun Kampus Sultan Abdul Jalil Shah PustakaTBainun ptbupsi

05-4506832 pustaka.upsi.edu.my Perpustakaan Tuanku Bainun Kampus Sultan Abdul Jalil Shah PustakaTBainun ptbupsi

The area of the trapped 5CB microdroplet measured by the Image Software was 26.541 μm^2. The area of the trapped 5CB microdroplet (A) is related to the microdroplet size (r) by the equation

$$r = \sqrt{\left(\frac{A}{\pi}\right)} \tag{3.4}$$

Hence, the trapped 5CB microdroplet radius (r) obtained using ImageJ software was 2.9 μm. The same step was repeated to measure the different sizes of the trapped 5CB microdroplet. This measurement provides consistent measurement and minimizes the deviation from manual measurement. For better understanding, measuring the size (r) of the trapped 5CB microdroplet is important. The size of the trapped 5CB microdroplet (r) is related to the parameter between f_c and k_T. The size of the trapped 5CB microdroplet (r), f_c and k_T are related by the equation

$$k_T = 2\pi\gamma_0 f_c \tag{2.17}$$

where $\gamma_0 = 6\pi\eta r$, η : surrounding medium viscosity, and r : 5CB microdroplet radius.

3.6.3 Corner Frequency (f_c) Analysis

The QPD signal of the trapped 5CB microdroplet was saved by oscilloscope in the American Standard Code for Information Interchange (ASCII) file. A USB drive was

05-4506832 pustaka.upsi.edu.my Perpustakaan Tuanku Bainun Kampus Sultan Abdul Jalil Shah PustakaTBainun ptbupsi

05-4506832 pustaka.upsi.edu.my Perpustakaan Tuanku Bainun Kampus Sultan Abdul Jalil Shah PustakaTBainun ptbupsi

used to transfer the File from the oscilloscope to the PC. Figure 3.64 shows that the File was modified in Excel before being uploaded to OSCal.

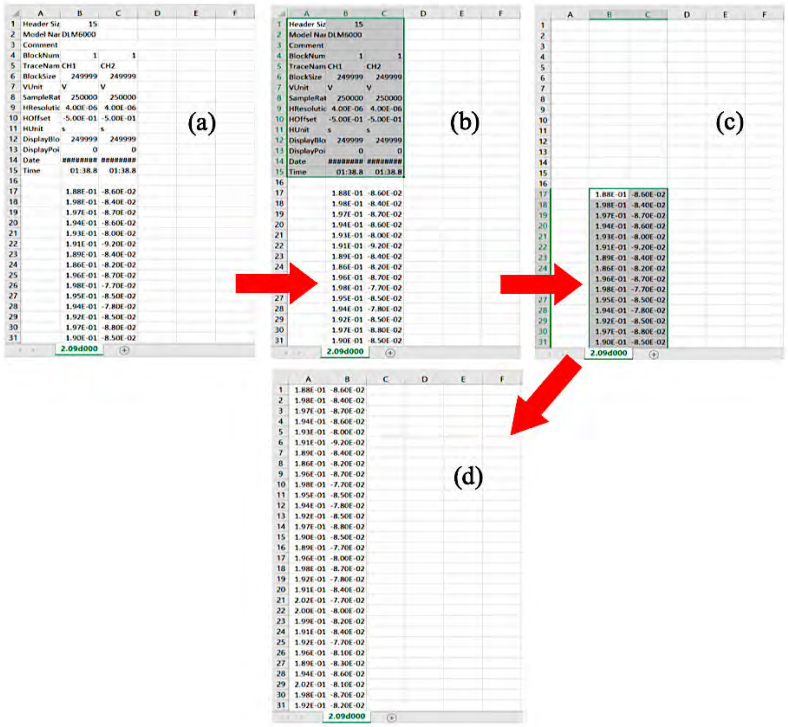


Figure 3.64. Process of deleting headers inside Columns A1 to C15 of the signal data in Excel.

The header inside columns A1 to C5 was deleted and replaced with signal data. OSCal only reads and accepts signal data in columns A (x-value) and B (y-value). The data was then uploaded to OSCal software developed by Yunus (H. Wang et al., 2011). Power Spectrum Density Module from OSCal software was used to calculate f_c and k_T. Figure 3.65 illustrates the OSCal interface. The default sampling duration was 1 s and can be changed according to user preferences.

05-4506832 pustaka.upsi.edu.my Perpustakaan Tuanku Bainun Kampus Sultan Abdul Jalil Shah PustakaTBainun ptbupsi

05-4506832 pustaka.upsi.edu.my Perpustakaan Tuanku Bainun Kampus Sultan Abdul Jalil Shah PustakaTBainun ptbupsi

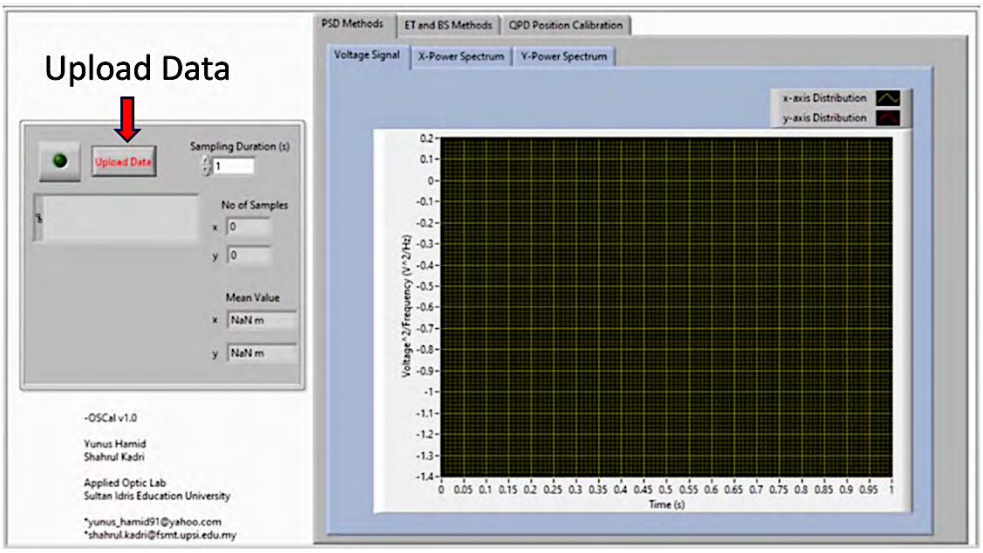


Figure 3.65. The interface of OSCal without any voltage signal data.

The modified File was uploaded to OSCal software by clicking the Upload Data button, as shown in Figure 3.65. The user was required to select the File to be read by the OSCal software.

05-4506832 pustaka.upsi.edu.my Perpustakaan Tuanku Bainun Kampus Sultan Abdul Jalil Shah PustakaTBainun ptbupsi

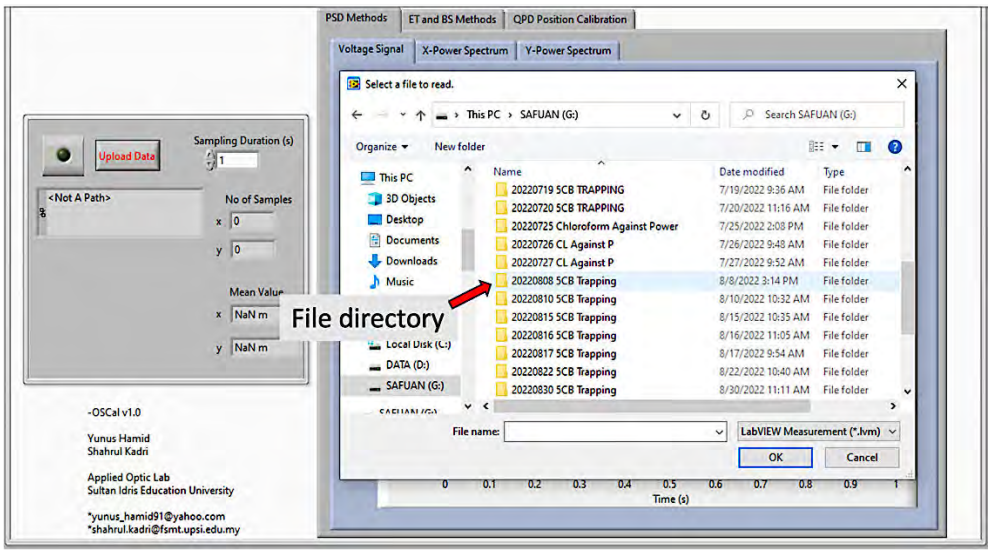


Figure 3.66. Selecting the directory of the data stored in the USB drive.

05-4506832 pustaka.upsi.edu.my Perpustakaan Tuanku Bainun Kampus Sultan Abdul Jalil Shah PustakaTBainun ptbupsi

05-4506832 pustaka.upsi.edu.my Perpustakaan Tuanku Bainun Kampus Sultan Abdul Jalil Shah PustakaTBainun ptbupsi

For instance, clicking “20220808 5CB Trapping Folder” displayed a series of CSV files containing modified QPD signal data of 5CB microdroplet trapping, as shown in Figure 3.66. Clicking a specific CSV file and OK caused OSCal software to read the selected File.

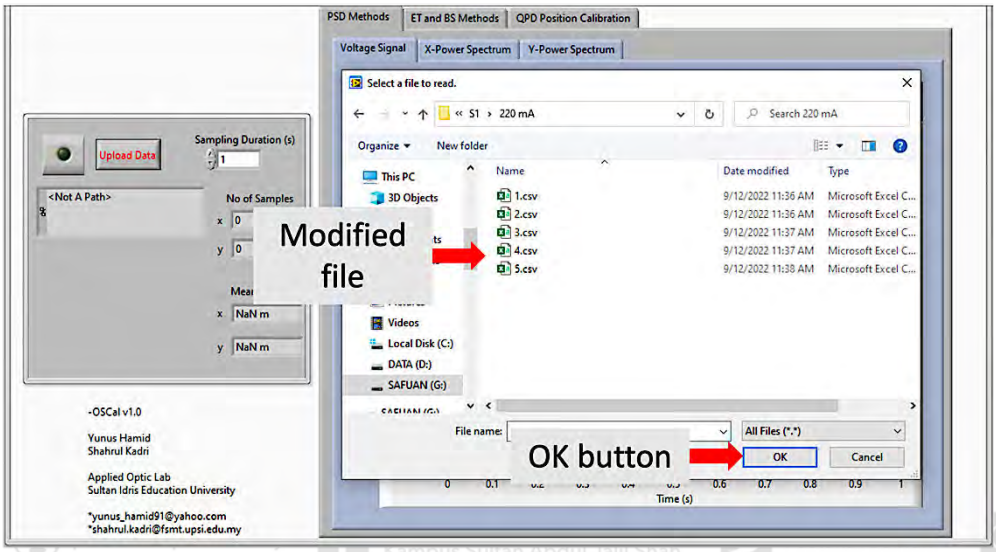


Figure 3.67. Data selection to upload into OSCal software.

The clicking of OK resulted in the displayed QPD signal of the trapped 5CB microdroplet, as shown in Figure 3.68. Two QPD signals were displayed on the OSCal interface; a yellow *x*-voltage signal and a *y*-voltage signal.

05-4506832 pustaka.upsi.edu.my Perpustakaan Tuanku Bainun Kampus Sultan Abdul Jalil Shah PustakaTBainun ptbupsi

05-4506832 pustaka.upsi.edu.my Perpustakaan Tuanku Bainun Kampus Sultan Abdul Jalil Shah PustakaTBainun ptbupsi

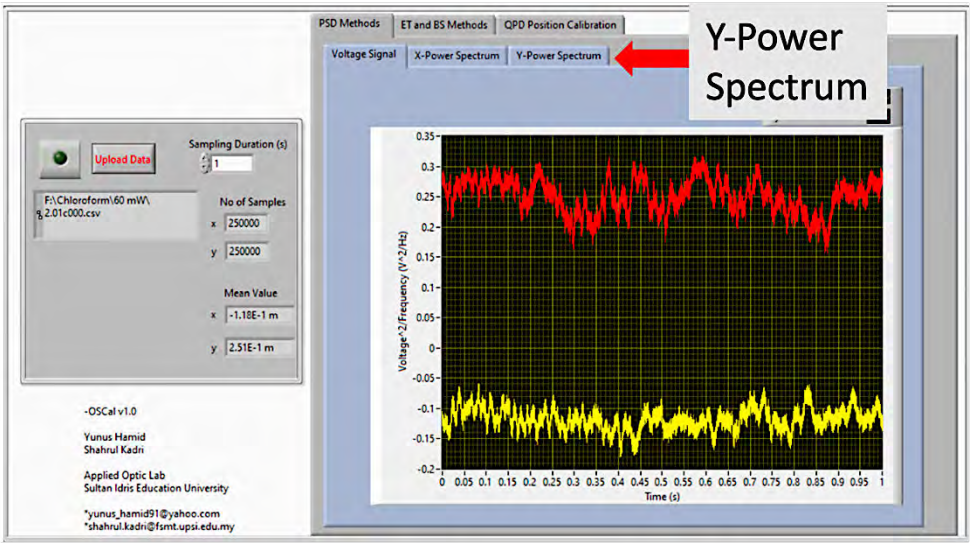


Figure 3.68. The QPD voltage signal is displayed in the OSCal interface.

The Power Density Spectrum (PSD) interface was displayed when the Y-Power Spectrum tab was clicked in Figure 3.68. The interface of the Y-Power Spectrum is illustrated in Figure 3.69. f_c and k_T analysis required only one dimensional to justify the confinement and trap strength. Hence, the measurement was performed on the *y-axis* data in this study. Fourier transforms (FT) convert time domain signals into frequency domain signals. FT was imposed on the QPD voltage signal, resulting in power spectrum density.

05-4506832 pustaka.upsi.edu.my Perpustakaan Tuanku Bainun Kampus Sultan Abdul Jalil Shah PustakaTBainun ptbupsi

05-4506832 pustaka.upsi.edu.my Perpustakaan Tuanku Bainun Kampus Sultan Abdul Jalil Shah PustakaTBainun ptbupsi

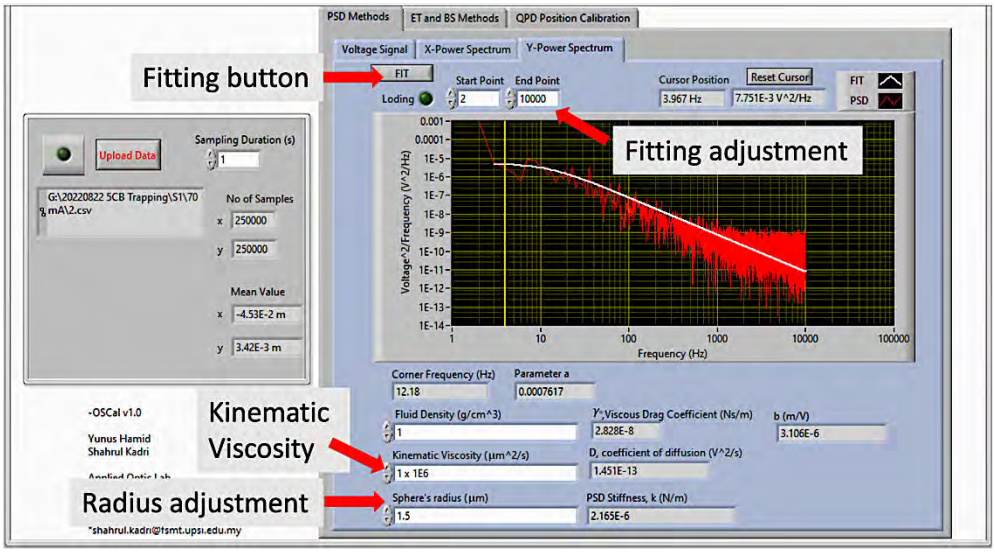


Figure 3.69. OSCal interface for Y-Power Spectrum of 3.0 μm 5CB microdroplet.

The are several important things that users must take into account. The starting fitting point, 5CB microdroplet radius, kinematic viscosity, and temperature are essential parameters while using OSCal software and could be adjusted according to user experimental conditions. The fitting start point depends on the user's preferences. For example, the fitting start point used in Figure 3.69 was 2 – 10000 Hz. The radius of the trapped 5CB was 1.5 μm. The water kinetic viscosity at 25 ° was 1×10^{-6} $\mu m^{-2}/s$. Once all the parameters were set accordingly, the fit button was clicked to start fitting the power spectrum, as represented by the white line in Figure 3.69.

Figure 3.70 shows the power spectrum fitted with Lorentzian fitting. For optical trapping, the Fourier transform of its trapped time-domain signal will come out as exponential decay function or bell-shaped curve addressed as the Lorentzian profile. The calculated f_c and k_T for 1.5 μm 5CB microdroplet was 12.18 Hz and 2.165×10^{-6} N/m. The fitting process was repeated with different fitting start points to find the average f_c and k_T.

05-4506832 pustaka.upsi.edu.my Perpustakaan Tuanku Bainun Kampus Sultan Abdul Jalil Shah PustakaTBainun ptbupsi

05-4506832 pustaka.upsi.edu.my Perpustakaan Tuanku Bainun Kampus Sultan Abdul Jalil Shah PustakaTBainun ptbupsi

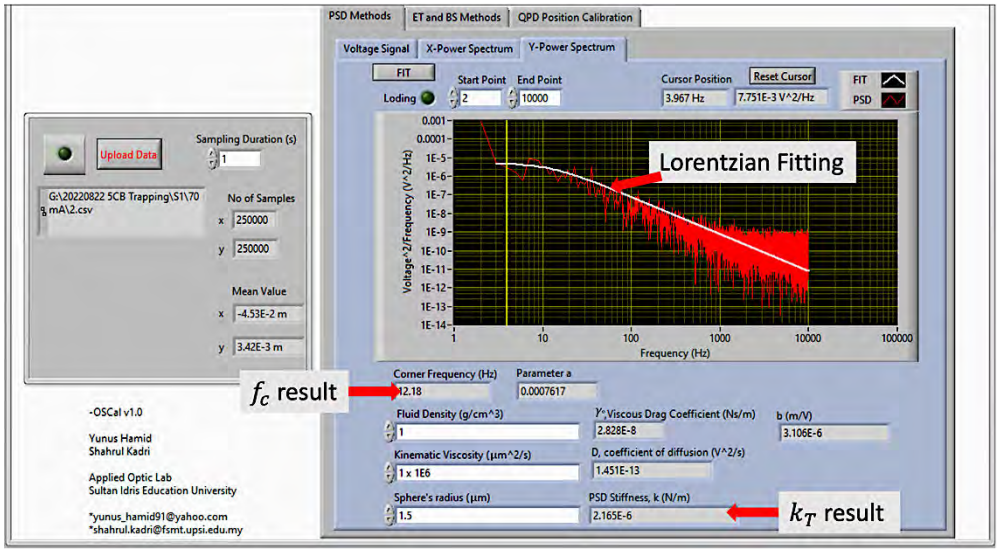


Figure 3.70. The result of the power spectrum fitted with Lorentzian fitting.

3.6.4. Angular Speed (ω) Measurement

Figure 3.71 shows the rotatability analysis of trapped 5CB microdroplets. The circularly polarized laser beam from the half and quarter wave plate trapped a 5CB microdroplet in water. The trapping using circularly polarized light resulted in microdroplet rotation. The image and the optical signal of the rotated 5CB microdroplet were recorded and collected by the CCD camera and QPD. The radius (r) of the trapped 5CB microdroplet was determined using ImageJ. The angular speed (ω) was determined by analyzing the QPD signal of the rotating 5CB microdroplet.

05-4506832 pustaka.upsi.edu.my Perpustakaan Tuanku Bainun Kampus Sultan Abdul Jalil Shah PustakaTBainun ptbupsi

05-4506832 pustaka.upsi.edu.my Perpustakaan Tuanku Bainun Kampus Sultan Abdul Jalil Shah PustakaTBainun ptbupsi

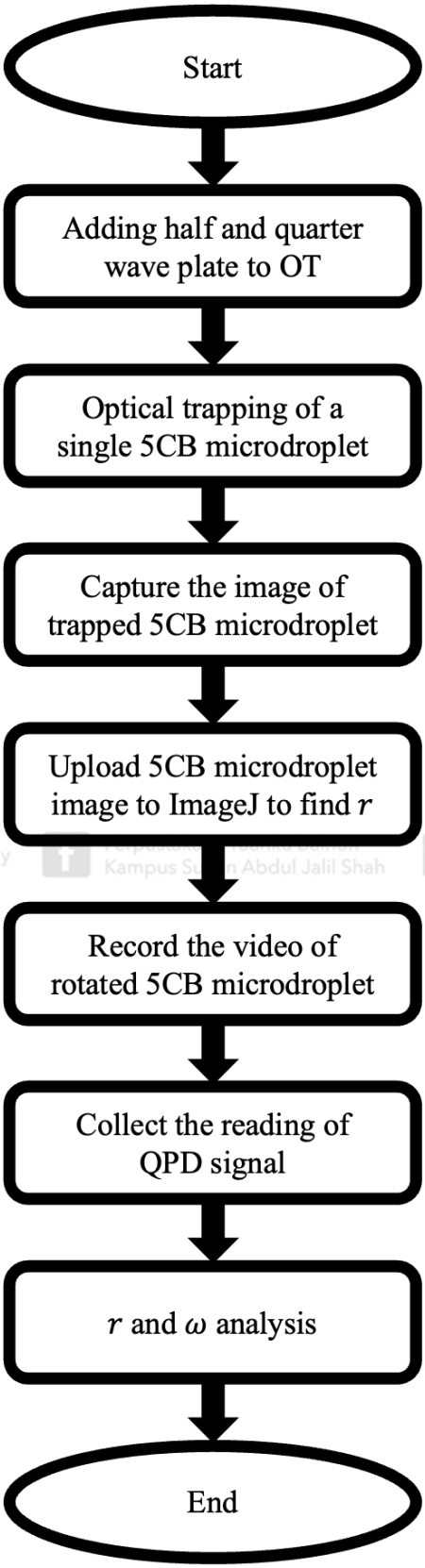


Figure 3.71. The flowchart for the rotatability of trapped 5CB microdroplet analysis.

05-4506832 pustaka.upsi.edu.my Perpustakaan Tuanku Bainun Kampus Sultan Abdul Jalil Shah PustakaTBainun ptbupsi

05-4506832 pustaka.upsi.edu.my Perpustakaan Tuanku Bainun Kampus Sultan Abdul Jalil Shah PustakaTBainun ptbupsi

3.6.5 5CB Microdroplet Angular Speed (ω) Analysis

The circularly polarized laser beam trapped and rotated a 5CB microdroplet in water. ImageJ software measured r of the trapped 5CB microdroplet using the previously described procedure in section 3.6.2. Then, the angular speed (ω) of rotating 5CB microdroplets was quantified based on the QPD signal analysis. The QPD signal records the 5CB microdroplet rotating signal for 1 s. The light polarization direction was in line with the y-axis. Therefore, only the y-axis QPD signal was analyzed. Figure 3.72 shows the graph of QPD signal voltage against time for rotating 5CB microdroplets.

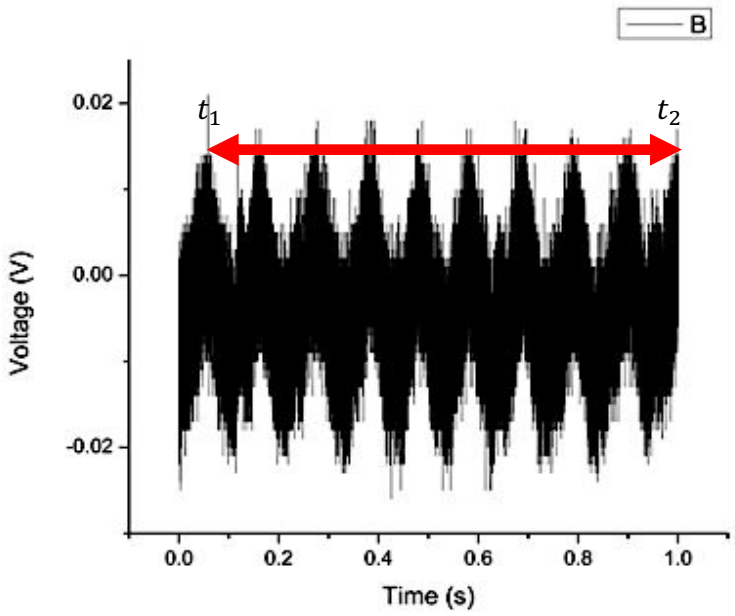


Figure 3.72. The graph is plotted from the QPD signal to determine the average time for a complete 2π rotation.

The average time (t_{avg}) to complete 2π rotation was calculated from peak to peak time (t_1 and t_2) and number of complete rotation f by using equation

05-4506832 pustaka.upsi.edu.my Perpustakaan Tuanku Bainun Kampus Sultan Abdul Jalil Shah PustakaTBainun ptbupsi

05-4506832 pustaka.upsi.edu.my Perpustakaan Tuanku Bainun Kampus Sultan Abdul Jalil Shah PustakaTBainun ptbupsi

$$t_{avg} = \frac{(t_2 - t_1)}{f} \tag{3.6}$$

and the 5CB microdroplet angular speed (ω) was calculated using the equation

$$\omega = \frac{2\pi}{t_{avg}} \tag{3.7}$$

3.7 Microdroplet Trapping in CTAB Solution [Phase 5]

The flowchart of the optical trapping of a single 5CB Microdroplet in CTAB solution is shown in Figure 3.73. The experiment was started by trapping a single bipolar 5CB microdroplet. The initial configuration and QPD signal of the trapped 5CB microdroplet was recorded. Then, the CTAB solution was introduced to the trapped bipolar 5CB microdroplet. Next, the CCD camera and QPD record the internal configuration and optical signal inside the trapped 5CB microdroplet. The ImageJ software measured the r of the 5CB microdroplet. The displacement variance was calculated and analyzed from the QPD signal obtained.

05-4506832 pustaka.upsi.edu.my Perpustakaan Tuanku Bainun Kampus Sultan Abdul Jalil Shah PustakaTBainun ptbupsi

05-4506832 pustaka.upsi.edu.my Perpustakaan Tuanku Bainun Kampus Sultan Abdul Jalil Shah PustakaTBainun ptbupsi

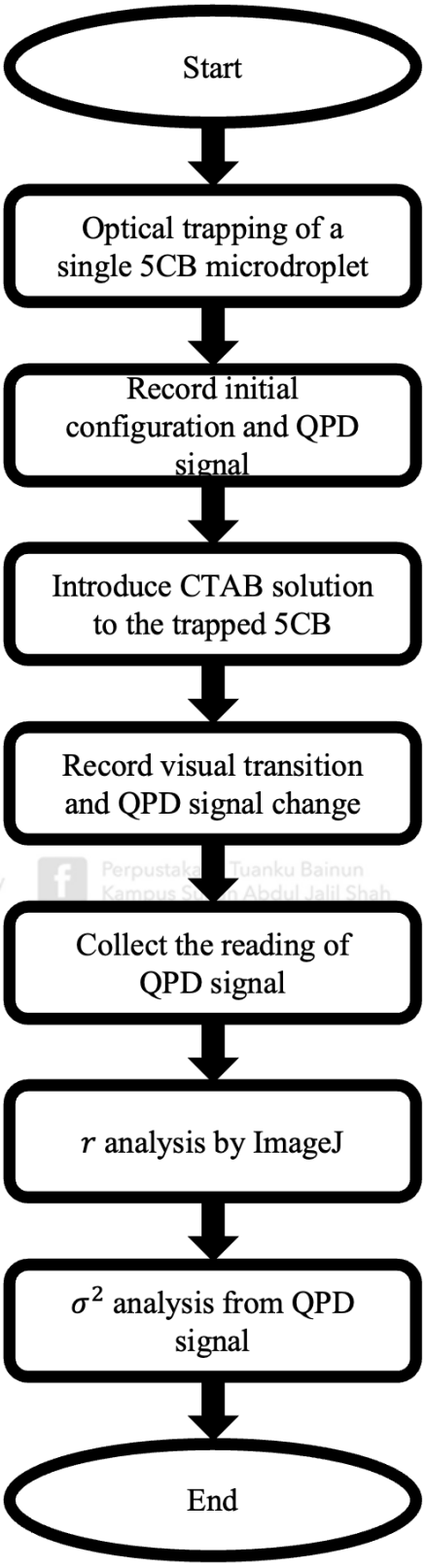


Figure 3.73. The flow chart of the optical trapping of a single 5CB microdroplet in CTAB solution.

05-4506832 pustaka.upsi.edu.my Perpustakaan Tuanku Bainun Kampus Sultan Abdul Jalil Shah PustakaTBainun ptbupsi

05-4506832 pustaka.upsi.edu.my Perpustakaan Tuanku Bainun Kampus Sultan Abdul Jalil Shah PustakaTBainun ptbupsi

3.7.1. 5CB Microdroplet Trapping in CTAB Solution

This experiment required a specially made cell chamber for the optical trapping process. Hence, a micro cover glass from Matsunami with a dimension 35 mm x 50 mm was sandwiched with another cover glass of 20 mm x 20 mm. A double-sided tape was used to attach and assemble the two cover glasses. The schematic diagram of the cell chamber (a) top view, (b) side view, and (c) the actual image is shown in Figure 3.74.

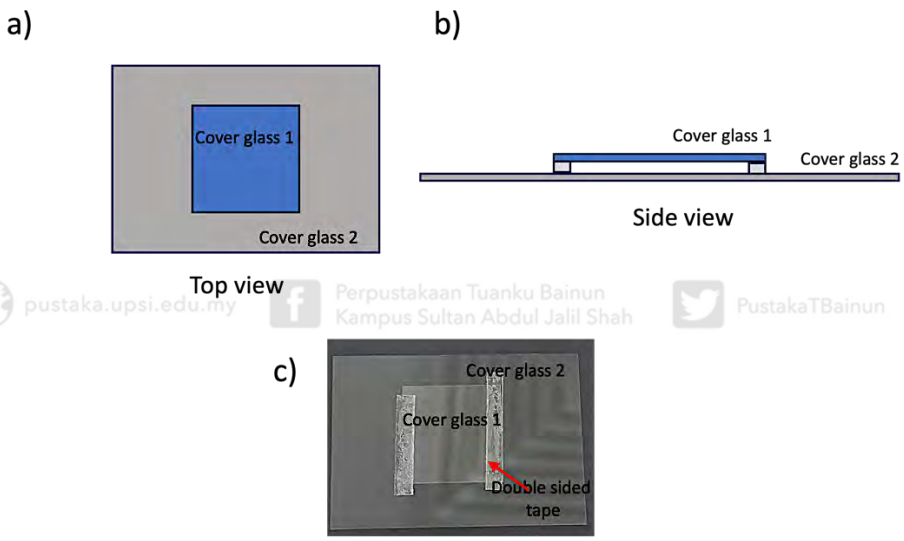


Figure 3.74. The schematic diagram of the cell chamber (a) top view and (b) side view. The actual image of the cell chamber is shown in (c).

Next, the cell chamber was filled with 10 µl of diluted 5CB microdroplet solution and was placed on the piezostage to be viewed under a CCD camera. The *z*-adjusted knob of the piezostage was adjusted to obtain the focal plane of the cell chamber. Once the focal plane was found, the *x* and *y-adjusted* knob of the piezostage was adjusted to find the free-moving 5CB microdroplet in the sample chamber. The 5CB microdroplet must be free moving and cannot be stuck to the cover glass wall. A

05-4506832 pustaka.upsi.edu.my Perpustakaan Tuanku Bainun Kampus Sultan Abdul Jalil Shah PustakaTBainun ptbupsi

05-4506832 pustaka.upsi.edu.my Perpustakaan Tuanku Bainun Kampus Sultan Abdul Jalil Shah PustakaTBainun ptbupsi

near-infrared laser beam of 976 nm wavelength with a linear polarization was used to trap a single 5CB microdroplet in the water. The single trapped 5CB microdroplet focal plane was adjusted until the CCD camera captured a clear, sharp image of the 5CB and displayed it on the PC for observation. Once the trapping was stable, a cross-polarization view was performed to determine the internal configuration of the trapped 5CB microdroplet. The internal configuration of the trapped 5CB microdroplet must exhibit bipolar internal configuration, which was verified by observing the 5CB under a cross-polarization view. The initial bipolar internal configuration was captured and recorded by the CCD camera to compare it with the final internal configuration once the surfactant solution was introduced to the trapped 5CB microdroplet. The QPD detected the initial QPD signal of the trapped 5CB microdroplet and

The next step was to introduce the CTAB solution to the trapped 5CB microdroplet. Hence, a 20 μL of the CTAB solution having 10^{-3} g/mL concentration was carefully dropped using a micro syringe at the edge of the cell chamber containing trapped bipolar 5CB microdroplet, as shown in Figure 3.75. This process was so critical because the trapped bipolar 5CB microdroplet was displaced from the trap spot if the process of dropping the CTAB solution was not performed carefully and slowly.

05-4506832 pustaka.upsi.edu.my Perpustakaan Tuanku Bainun Kampus Sultan Abdul Jalil Shah PustakaTBainun ptbupsi

05-4506832 pustaka.upsi.edu.my Perpustakaan Tuanku Bainun Kampus Sultan Abdul Jalil Shah PustakaTBainun ptbupsi

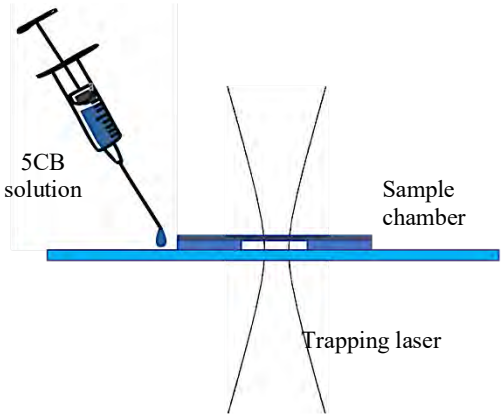


Figure 3.75. Schematic diagram of adding CTAB solution to the sample chamber edge.

Figure 3.75 shows the schematic diagram of introducing the CTAB solution to containing the trap 5CB microdroplet to the cell chamber. The CTAB solution dropped at the edge of the cell chamber was slowly diffused when it came into contact with the diluted 5CB microdroplet solution in the cell chamber. The bipolar internal configuration of the trapped 5CB microdroplet was monitored using a cross-polarized view, and the image was recorded by the CCD camera and displayed on the PC. At the same time, the scattered signal of the trapped 5CB microdroplet was detected by the QPD, and the signal was displayed and recorded by the oscilloscope. The transition change of the bipolar internal configuration of the trapped 5CB microdroplet was monitored continuously via cross-polarized view and optical signal change until the trapped 5CB microdroplet was utterly changed to the radial internal configuration. The visual monitoring of the internal configuration of the trapped 5CB microdroplet was continued and stopped when the radially internal configuration of the trapped 5CB microdroplet formed. The visual change in the internal configuration was recorded and compared with the initial and final states. In the meantime, the QPD signal of the transition change from bipolar to the radial internal configuration of the trapped 5CB

05-4506832 pustaka.upsi.edu.my Perpustakaan Tuanku Bainun Kampus Sultan Abdul Jalil Shah PustakaTBainun ptbupsi

05-4506832 pustaka.upsi.edu.my Perpustakaan Tuanku Bainun Kampus Sultan Abdul Jalil Shah PustakaTBainun ptbupsi

microdroplet was analyzed to determine the trajectory change when the transition happened.

3.7.2 Displacement Variance (σ_2) Analysis

The 5CB microdroplet radius was measured using the procedure in section 3.6.2. The trajectory of the trapped particle by the optical tweezers contains information about the strength of the optical force. The trajectory of the trapped particle in a region of weak optical force confinement covers a broad position distribution, indicating that the trapped particle was held weakly by the optical force. Meanwhile, the trajectory of the trapped particle in a region of strong optical force produces a sharp position distribution, indicating that the trapped particle is held tightly by the optical force. The trajectory of the trapped particle can be used as a parameter to determine the strength of the optical force. There is a direct relationship between the trajectory of the trapped particle and the optical force. The displacement variance (σ^2) is related to the trajectory along the *y*-axis by the equation

$$(\sigma)^2 =< \left(y - y_{avg}\right)^2 > \tag{2.9}$$

where σ^2 is the displacement variance, y is the position of the trapped particle along the and y_{avg} is the average position of the trapped particle along the *y*-axis. The optical force is related to the trajectory of the trapped particle by the equation

05-4506832 pustaka.upsi.edu.my Perpustakaan Tuanku Bainun Kampus Sultan Abdul Jalil Shah PustakaTBainun ptbupsi

05-4506832 pustaka.upsi.edu.my Perpustakaan Tuanku Bainun Kampus Sultan Abdul Jalil Shah PustakaTBainun ptbupsi

$$k_T = \frac{k_B T}{(\sigma)^2} \tag{2.11}$$

wherek_T is the optical stiffness, k_B is the Boltzmann constant, T is the temperature and σ^2 is the displacement variance.

From equation 2.6, if the displacement variance increases, the optical stiffness is weaker, directly reflecting the weak optical force. Meanwhile, the decrease in the displacement variance indicated the strong optical stiffness, which reflects the stronger optical force. Displacement variance is another parameter that can be used to determine the strength of the optical force other than calculating the corner frequency (f_c).

In the experiment context, the single 5CB microdroplet of definite internal configuration was trapped at specific laser power, and the QPD collected the scattered laser trapping signal.

05-4506832 pustaka.upsi.edu.my Perpustakaan Tuanku Bainun Kampus Sultan Abdul Jalil Shah PustakaTBainun ptbupsi

05-4506832 pustaka.upsi.edu.my Perpustakaan Tuanku Bainun Kampus Sultan Abdul Jalil Shah PustakaTBainun ptbupsi

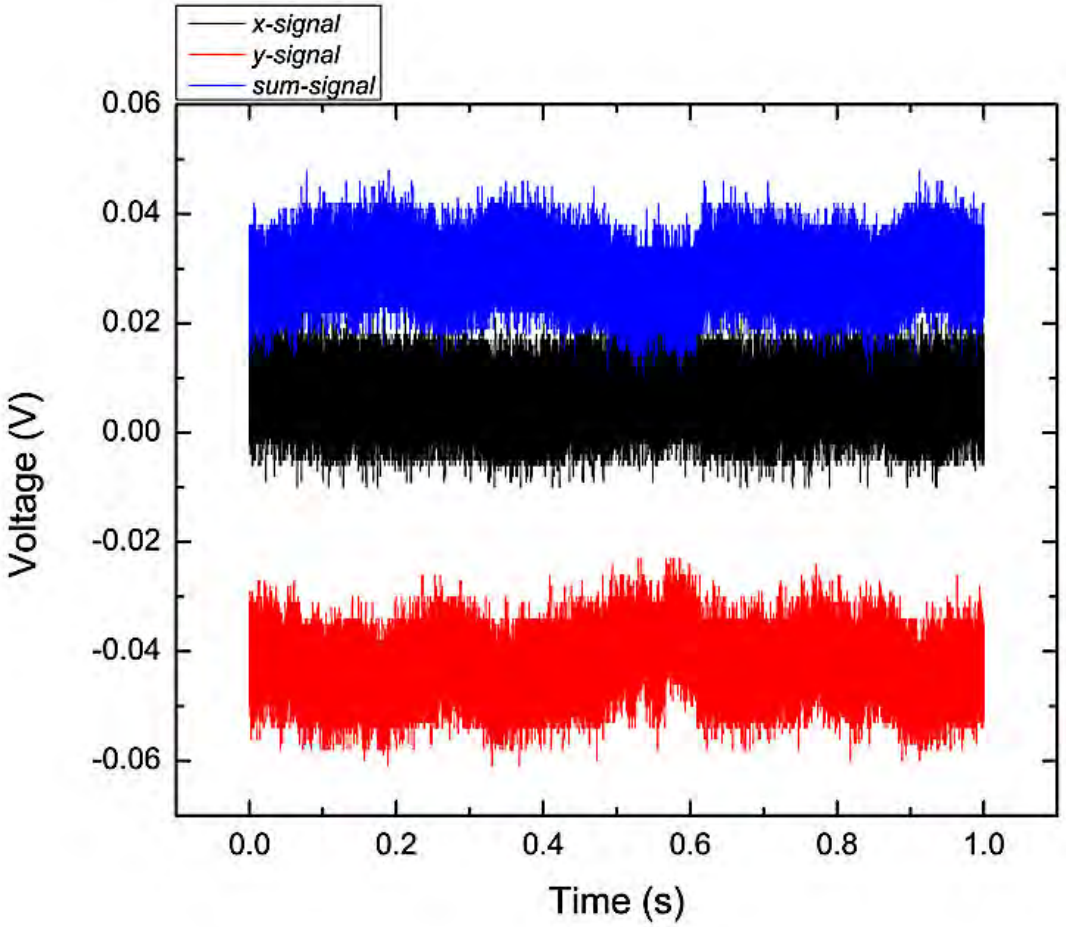


Figure 3.76. The graph of voltage against time represents the trajectory of the trapped single 5CB microdroplet in water.

The QPD recorded three types of signals: *x*-signal, *y*-signal, and sum signal, as shown in Figure 3.76. All three signals were taken and recorded to justify the displacement variance of the trapped particle during the transition change of the trapped 5CB microdroplet from bipolar to radial. The raw data of the trajectory was pasted and sorted in an Excel document. The displacement variance was calculated using the variance function in the Excel data analysis function.

05-45068
05-4506832 pustaka.upsi.edu.my Perpustakaan Tuanku Bainun Kampus Sultan Abdul Jalil Shah PustakaTBainun ptbupsi

05-4506832 pustaka.upsi.edu.my Perpustakaan Tuanku Bainun Kampus Sultan Abdul Jalil Shah PustakaTBainun ptbupsi

3.8. Summary

This chapter describes the experimental work of this research. The research started with the optical tweezer's assembly and alignment, 5CB microdroplet suspension preparation, optical trapping of a single 5CB microdroplet using linear and circular polarized light, micro-control of trapped 5CB, analysis of corner frequency, f_c, angular speed ω, and displacement variance σ of the trapped 5CB microdroplet.

05-4506832 pustaka.upsi.edu.my Perpustakaan Tuanku Bainun Kampus Sultan Abdul Jalil Shah PustakaTBainun ptbupsi
05-4506832 pustaka.upsi.edu.my Perpustakaan Tuanku Bainun Kampus Sultan Abdul Jalil Shah PustakaTBainun ptbupsi

05-4506832 pustaka.upsi.edu.my Perpustakaan Tuanku Bainun Kampus Sultan Abdul Jalil Shah PustakaTBainun ptbupsi

CHAPTER 4

RESULTS AND DISCUSSION

05-4506832 pustaka.upsi.edu.my Perpustakaan Tuanku Bainun Kampus Sultan Abdul Jalil Shah PustakaTBainun ptbupsi

4.1 Introduction

This chapter describes the experimental results obtained from this study. The first part discusses the formulation of the 5CB microdroplet suspension, distribution size (r), and stability. The observation of the optical trapping of bipolar and radial 5CB microdroplets was discussed thoroughly in the second part of this chapter. The corner frequency, f_c and angular speed (ω) of 5CB microdroplet optical trapping in water at different optical power densities (P) and sizes (r) are discussed. The last part of this chapter discusses the observation of the transitional change of the internal configuration

05-4506832 pustaka.upsi.edu.my Perpustakaan Tuanku Bainun Kampus Sultan Abdul Jalil Shah PustakaTBainun ptbupsi

05-4506832 pustaka.upsi.edu.my Perpustakaan Tuanku Bainun Kampus Sultan Abdul Jalil Shah PustakaTBainun ptbupsi

from bipolar to radial and the QPD optical signal of the trapped bipolar 5CB microdroplet to radial by the exposure to CTAB solution.

4.2 The Production of 5CB Microdroplet Suspension

The production of the 5CB microdroplet suspension in water was formulated for two types of internal configuration. This study formulated the production of the bipolar and radial 5CB microdroplet suspension in water. The 5CB microdroplet suspension in water was produced by mixing deionized water, liquid 5CB, and surfactant. Then, the mixture was sonicated for a specific time to produce a 5CB microdroplet with bipolar and radial internal configuration. The sonication technique was used primarily to generate the 5CB microdroplet suspension in water. The generated 5CB microdroplet suspension, whether in a bipolar or radial configuration, was studied in terms of its distribution size and stability for optical trapping applications. The effect of the sonication time on the generated 5CB microdroplet size (r) was investigated. The stability and the sustainability of the 5CB microdroplet suspension in water were determined and monitored for 1-hour.

4.2.1 Effect of Sonication Time on the Size of 5CB Microdroplet

The first objective of this research is to formulate the production of 5CB microdroplets within a suitable range to be optically trapped. This study involves the production of

05-4506832 pustaka.upsi.edu.my Perpustakaan Tuanku Bainun Kampus Sultan Abdul Jalil Shah PustakaTBainun ptbupsi

05-4506832 pustaka.upsi.edu.my Perpustakaan Tuanku Bainun Kampus Sultan Abdul Jalil Shah PustakaTBainun ptbupsi

5CB microdroplets with bipolar and radial internal configurations. This was done by controlling the volume of liquid 5CB and deionized water mixed to form the 5CB microdroplet suspension and sonication time.

The effect of sonication time on the distribution size of the 5CB microdroplet form and its stability in water was investigated in this study. The freshly prepared 5CB microdroplet suspension of 5 µL volume was filled in a clean cell chamber. The effect of sonication time on the size of the generated 5CB microdroplets was examined by placing the sample on an optical microscope. The size distribution (r) was analyzed to obtain the average sample size after a given sonication time. The ImageJ software was used to determine the distribution size (r) of the 5CB microdroplet suspension concerning sonication time. Figures 4.1 and 4.2 show the observation image obtained from the optical microscope for bipolar and radial sonication at 1, 2, 3, and 10 minutes. The sonication time was selected in the range of 1, 2, 3 and 10 minutes to avoid the heating effect on the 5CB microdroplet due to the sonication process. A longer sonication process increases the temperature of water and destroys the 5CB nematic phase.

Figure 4.1 shows the snapshots of bipolar 5CB microdroplet suspension under optical microscopy sonicated at (a) t = 1 minute, (b) t = 2 minutes, (c) t = 3 minutes, and (d) t = 10 minutes for V_{H2O} = 1 mL. The inset shows the internal configuration of the bipolar 5CB microdroplet. Based on Figure 4.1 (a), the size of the bipolar 5CB microdroplet suspension was relatively larger when the mixture of liquid 5CB and deionized water was sonicated for 1 minute. When the sonication time was increased from 2 to 10 minutes, as shown in Figure 4.1 (b)-(c), the size of the 5CB microdroplet

05-4506832 pustaka.upsi.edu.my Perpustakaan Tuanku Bainun Kampus Sultan Abdul Jalil Shah PustakaTBainun ptbupsi

05-4506832 pustaka.upsi.edu.my Perpustakaan Tuanku Bainun Kampus Sultan Abdul Jalil Shah PustakaTBainun ptbupsi

was relatively decreased accordingly based on the visual observation. The sonication process dispersed the liquid 5CB in the water, which coalesces the dispersed 5CB to form a microdroplet. The microdroplet can break off and form smaller microdrops (Asadinezhad et al., 2019). Hence, a longer sonication time can result in a smaller microdroplet (Adamow et al., 2017; Asadinezhad et al., 2019).

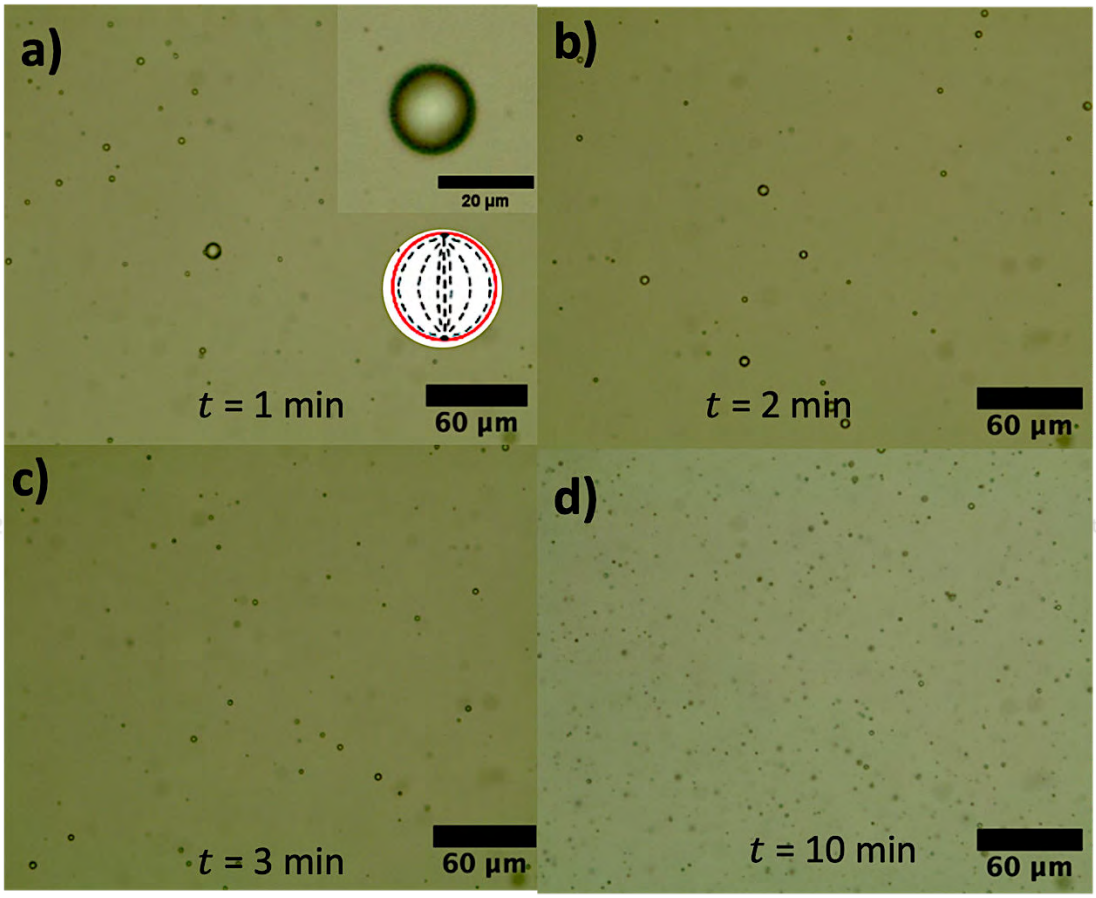


Figure 4.1. The snapshots of bipolar 5CB microdroplet suspension under optical microscopy sonicated at (a) t = 1 minute, (b) t = 2 minutes, (c) t = 3 minutes, and (d) t = 10 minutes for V_{H2O} = 1 mL. The inset shows the internal configuration of the bipolar 5CB microdroplet.

Besides that, the formation of the radial 5CB microdroplet suspension was also observed under the optical microscope. Figure 4.2 shows the snapshots of radial 5CB microdroplet suspension under optical microscopy sonicated at (a) t = 1 minute, (b) t = 2 minutes, (c) t = 3 minutes, and (d) t = 10 minutes for V_{H2O} = 1 mL. The inset shows

05-4506832 pustaka.upsi.edu.my Perpustakaan Tuanku Bainun Kampus Sultan Abdul Jalil Shah PustakaTBainun ptbupsi

05-4506832 pustaka.upsi.edu.my Perpustakaan Tuanku Bainun Kampus Sultan Abdul Jalil Shah PustakaTBainun ptbupsi

the internal configuration of the radial 5CB microdroplet. The size of the radial 5CB microdroplet formed and observed at 1 minute sonication time was relatively bigger, as shown in Figure 4.2 (a). At the same time, as the sonication time was increased from 2 minutes to 10 minutes, the size of the radial 5CB microdroplet was significantly reduced visually, as shown in Figure 4.2 (b)-(d).

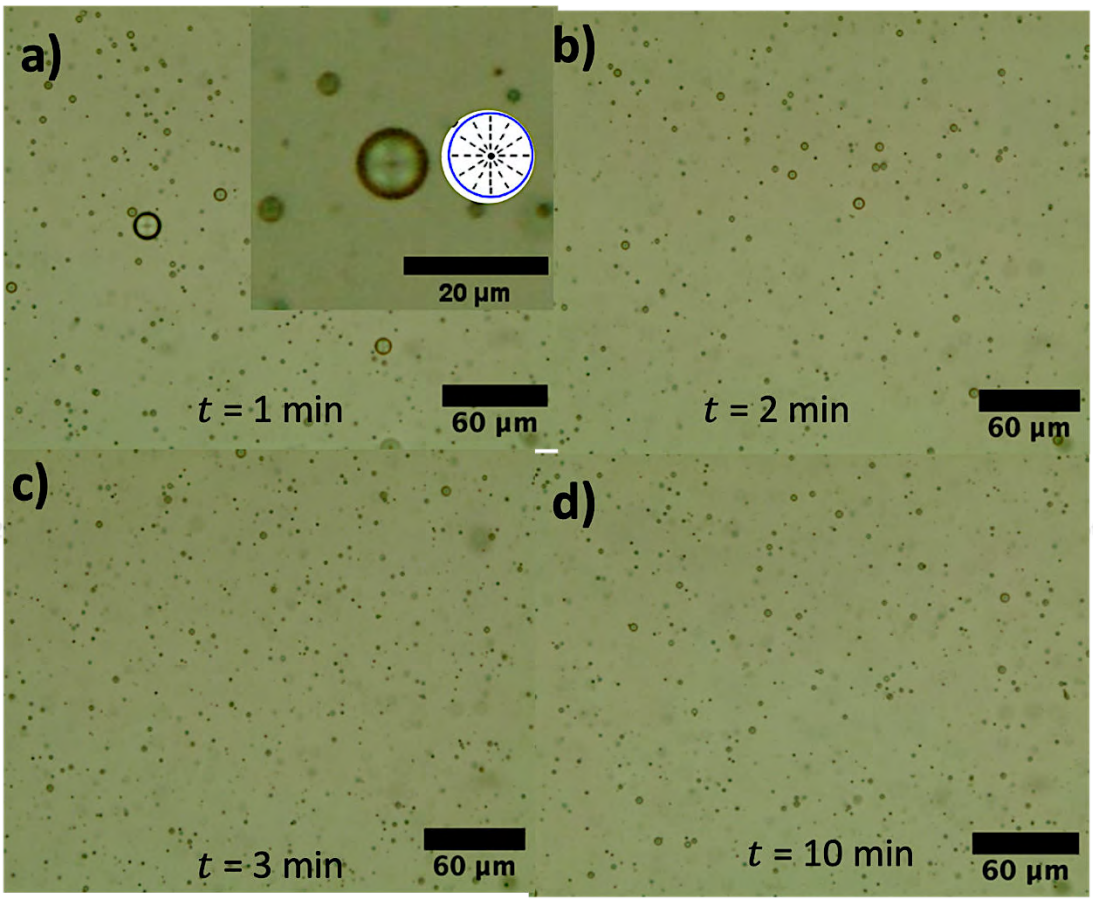


Figure 4.2. The snapshots of bipolar 5CB microdroplet suspension under optical microscopy sonicated at (a) t = 1 minute, (b) t = 2 minutes, (c) t = 3 minutes, and (d) t = 10 minutes for V_{H2O} = 1 mL. The inset shows the internal configuration of the radial 5CB microdroplet.

The effect of sonication time during solution preparation on the size of microdroplets in water was studied. Figure 4.3 shows the graph of the average radius of 5CB microdroplets, r, measured after sonication for a specific time, (a) bipolar and (b) radial.

05-4506832 pustaka.upsi.edu.my Perpustakaan Tuanku Bainun Kampus Sultan Abdul Jalil Shah PustakaTBainun ptbupsi

05-4506832 pustaka.upsi.edu.my Perpustakaan Tuanku Bainun Kampus Sultan Abdul Jalil Shah PustakaTBainun ptbupsi

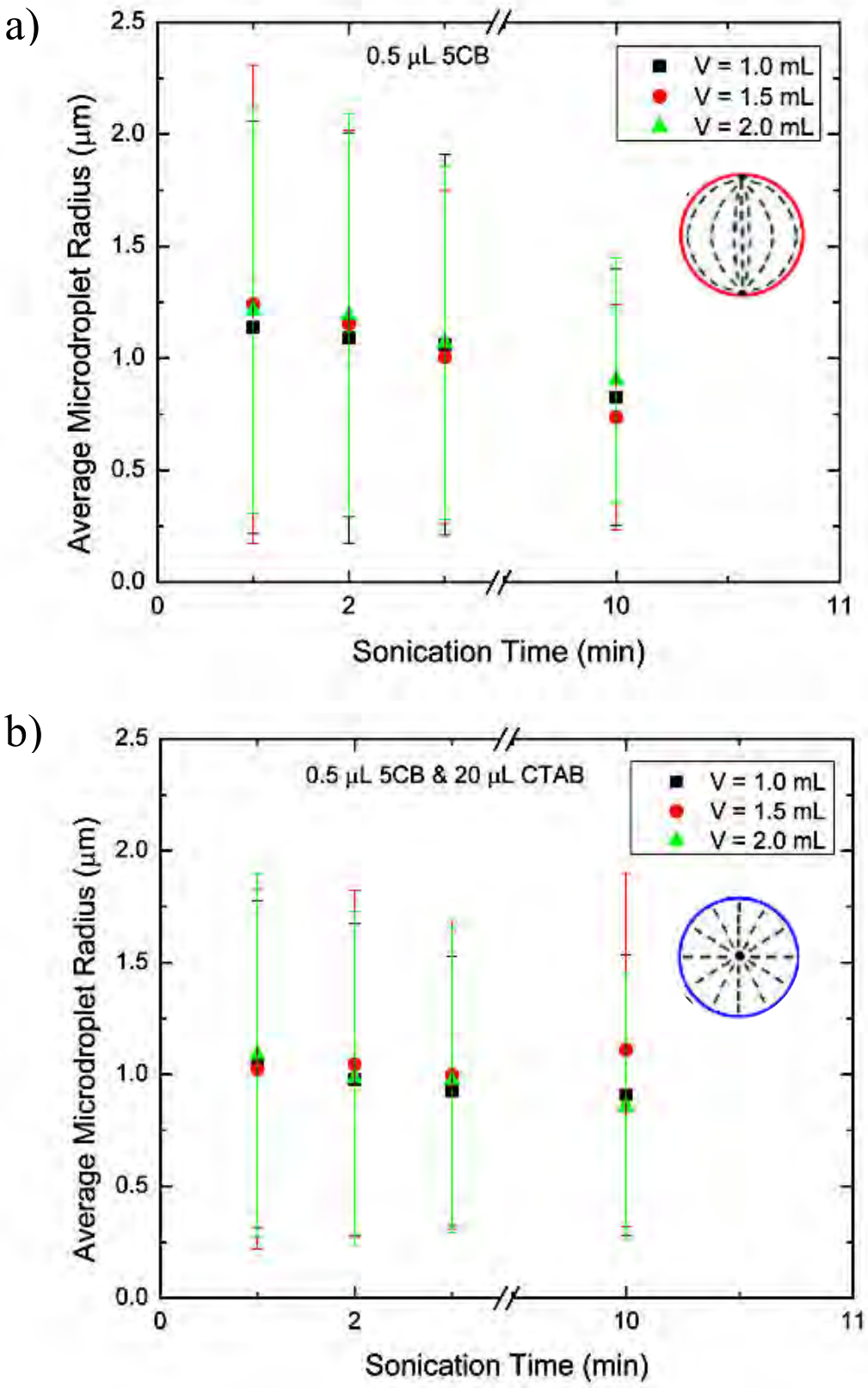


Figure 4.3. The average radius r, of 5CB microdroplets versus sonication time for (a) bipolar and (b) radial.

05-4506832 pustaka.upsi.edu.my Perpustakaan Tuanku Bainun Kampus Sultan Abdul Jalil Shah PustakaTBainun ptbupsi

05-4506832 pustaka.upsi.edu.my Perpustakaan Tuanku Bainun Kampus Sultan Abdul Jalil Shah PustakaTBainun ptbupsi

Based on Figure 4.3 (a), r shows no apparent change from the sonication time of 1.0 to 3.0 minutes for the suspension of bipolar 5CB microdroplets for 1.0, 1.5 and 2.0 mL deionized water volume used. This trend of no apparent change in r was in alignment when the sonication time was studied from 0.5 to 4 minutes of chloroform microdroplet (Yeng et al., 2023). The possible reason is that the short sonication time supplies smaller shear forces exerted to break down microdroplets into smaller sizes (Asadinezhad et al., 2019). However, when sonication was increased from 3 to 10 minutes, r showed a significant size reduction; when the sonication time longer, it generated higher shear forces to break down large microdroplets into smaller droplets (Asadinezhad et al., 2019). This trend is in alignment with the average chloroform microdroplet size using sonication time from 4 to 10 minutes (Yeng et al., 2023) and the average size of gelation emulsion sonicated from 3 to 9 minutes (Li et al., 2023). The same trend was obtained for the 5CB radial microdroplet suspension in Figure 4.3 (b), except for 1.5 mL deionized water sample volume. r shows an increment from 3 to 10 minutes for radial 5CB microdroplet in Figure 4.3 (b). This trend is similar to the gelatin emulsion size sonicated from 12-15 minutes (Li et al., 2023). The possible reason for the increasing in size is due to the reduction of emulsifier adsorption on the droplet surface, which causes microdroplet recoalescence (Asadinezhad et al., 2019). The emulsifier works to prevent the merging of microdroplets, but longer sonication causes its reduction (Urbanski et al., 2017).

In addition, the variation in the r size distribution also narrowed with increasing sonication time. The sonication process disperses the liquid 5CB in the water, which coalesces the dispersed 5CB to form a microdroplet. Microdroplets can

05-4506832 pustaka.upsi.edu.my Perpustakaan Tuanku Bainun Kampus Sultan Abdul Jalil Shah PustakaTBainun ptbupsi

05-4506832 pustaka.upsi.edu.my Perpustakaan Tuanku Bainun Kampus Sultan Abdul Jalil Shah PustakaTBainun ptbupsi

break off and form smaller microdroplets during the sonication process (Li et al., 2023). Therefore, a longer sonication time can result in smaller microdroplets, as Figures 4.1 and 4.2 show (Asadinezhad et al., 2019). This result guides the estimation of the desired microdroplet size production. Based on Figure 4.3 (a) and (b), a sonication time of 1 minute was sufficient to produce a large variation in the microdroplet size. Therefore, the size of the microdroplet can be chosen within the prepared solution for a specific purpose. In addition, 2 ml of deionized water samples produced the bipolar and radial 5CB microdroplet suspension with a dilute concentration. The dilute concentration of the bipolar and radial 5CB concentration is recommended for optical trapping applications where optical trapping only requires a single microdroplet. Too concentrated 5CB microdroplet suspension is unsuitable for optical trapping because the trap spot attracts too many 5CB microdroplets, interrupting the optical trapping process (Chen et al., 2022). In addition, the UV-Vis spectroscopy stability measurement needs a sample solution of diluted concentration to allow a significant amount of light pass through the sample and obtain the best absorbance signal (Nishii, 2021).

The distribution size (r) of the 5CB microdroplet suspension produced in this study was compared with the previously reported 5CB microdroplet using the sonication method. The comparison was made to compare the distribution size between pure 5CB microdroplet suspension and doped 5CB microdroplet suspension. Table 4.1 shows the comparison of the 5CB microdroplet average radius produced from sonication. Sample 1 consisted of the dye-doped 5CB microdroplet produced from the mixture of 5CB, deionized water, PVA and dye molecules (DCM, Coumarin 504,

05-4506832 pustaka.upsi.edu.my Perpustakaan Tuanku Bainun Kampus Sultan Abdul Jalil Shah PustakaTBainun ptbupsi

05-4506832 pustaka.upsi.edu.my Perpustakaan Tuanku Bainun Kampus Sultan Abdul Jalil Shah PustakaTBainun ptbupsi

Coumarin 540) (Adamow et al., 2017) and was compared with a 2 mL sample of bipolar and radial 5CB microdroplet solution.

Table 4.1

The comparison of 5CB microdroplet size produced from sonication.

Sample	1		2		3	
Material	5CB, deionized water, PVA, and dyes molecules (DCM, Coumarin 504, Coumarin 540) (Adamow et al., 2017).		5CB and deionized water (bipolar).		5CB, CTAB solution and deionized water (radial).	
Dispersion medium	9 % PVA-water solution		Deionized water		Deionized water	
	Time (min)	Average Radius (μm)	Time (min)	Average Radius (μm)	Time (min)	Average Radius (μm)
	10.0	34.17	1.0	1.21	1.0	1.09
	15.0	8.53	2.0	1.19	2.0	0.98
	20.0	8.13	3.0	1.07	3.0	0.97
	25.5	4.17	10.0	0.90	10.0	0.86

05-4506832 pustaka.upsi.edu.my Perpustakaan Tuanku Bainun Kampus Sultan Abdul Jalil Shah PustakaTBainun ptbupsi

According to Table 4.1, the sample 1 sonication time generated dye-doped 5CB microdroplets in the range of 10 to 30 minutes. The dye-doped 5CB microdroplet average radius reduced from 34.17 μm to 4.79 μm as the sonication increased from 10 minutes to 30 minutes. This shows that the average radius of a dye-doped 5CB

05-4506832 pustaka.upsi.edu.my Perpustakaan Tuanku Bainun Kampus Sultan Abdul Jalil Shah PustakaTBainun ptbupsi

05-4506832 pustaka.upsi.edu.my Perpustakaan Tuanku Bainun Kampus Sultan Abdul Jalil Shah PustakaTBainun ptbupsi

microdroplet decreases with increasing sonication time, as shown in Table 4.1. Despite that, there was no information on the microdroplet average radius for sonication time less than 10 minutes for sample 1. In sample 2, the sonication time increased from 1.0 minutes to 10.0 minutes, and the size of the 5CB microdroplet significantly reduced from 1.21 μm to 0.90 μm. In sample 3, the radius of the 5CB microdroplet decreased from 1.09 μm to 0.86 μm as the sonication time was increased from 1 minute to 10 minutes. The pure 5CB microdroplet has a similar trend to the dye-doped 5CB microdroplet, where the average size decreased with the increase of sonication time despite the dispersion medium being different. However, the average radius of pure 5CB microdroplets was relatively smaller compared to dye-doped 5CB microdroplets.

At 10 minutes of sonication time, Sample 1 produced a 5CB microdroplet of 34.17 μm radius. Meanwhile, at 10 minutes of sonication time, Sample 2 and Sample 3 produce 5CB microdroplet sizes of 0.90 μm and 0.86 μm, respectively. The 5CB microdroplet sizes produced by the Sample 2 and Sample 3 are 97.36% and 97.48% reductions compared to Sample 1. The possible reason why the average dye-doped 5CB microdroplet in the sample 1 was larger was due to the dispersion medium of 9 % PVA-water solution. The addition of 9 % PVA in deionized water reduces water viscosity and leads to a bigger size microdroplet form (Shafiei et al., 2023). Sample 2 and Sample 3 contain pure 5CB microdroplets dispersed in pure deionized water. The average 5CB microdroplet radius in Sample 3 was smaller than in Sample 2 because CTAB functions as a surfactant to disperse, stabilize and prevent coalescence, hence resulting in a smaller radius (Bartoš et al., 2022; Shafiei et al., 2023). Hence, our technique showed a smaller 5CB microdroplet production size.

05-4506832 pustaka.upsi.edu.my Perpustakaan Tuanku Bainun Kampus Sultan Abdul Jalil Shah PustakaTBainun ptbupsi

05-4506832 pustaka.upsi.edu.my Perpustakaan Tuanku Bainun Kampus Sultan Abdul Jalil Shah PustakaTBainun ptbupsi

4.2.2 5CB Microdroplet Suspension Stability in Water

After the distribution size (r) of the bipolar and radial 5CB microdroplet suspension was observed, the next step was to determine the stability of the bipolar and radial 5CB microdroplet suspension in water. The measurement of the stability of the bipolar and radial 5CB microdroplet suspension was conducted by using UV-Vis spectroscopy. The absorbance of the 5CB microdroplet suspension of bipolar and radial configuration was monitored and recorded to determine the stability of the microdroplet for 1-hour. The absorbance of the bipolar and radial 5CB microdroplet suspension in water was monitored every 5 minutes in increments time to determine stability and sustainability systematically.

05-4506832 Perpustakaan Tuanku Bainun ptbupsi

Figure 4.4 shows the absorption spectrum of a 5CB microdroplet solution. The arrow indicates the absorbance peak of interest to monitor the 5CB concentration along the light path of the cuvette (refer to Figure 3.43). The absorbance peak of the bipolar 5CB microdroplet suspension in water was monitored at a specific wavelength for 1 hour, as shown in Figure 4.4 (a) and (b). For example, the absorbance peak of the bipolar 5CB microdroplet suspension was higher at t = 0 minutes (the initial reading) compared to the absorbance at t = 60 minutes, as shown in Figure 4.4 (a). This is because the freshly sonicated sample was measured immediately under UV-Vis spectroscopy. The fresh sample contains a dispersion of 5CB microdroplets throughout the sample and the UV-Vis light path. As a result, the absorbance recorded was highest at t = 0 min. There was a significant drop in the bipolar 5CB microdroplet suspension between monitoring time t = 0 min and t = 60 min. The 5CB density is 1.008 g/cm^3 and the water density is 0.9970 g/cm^3 at room

05-4506832 pustaka.upsi.edu.my Perpustakaan Tuanku Bainun Kampus Sultan Abdul Jalil Shah PustakaTBainun ptbupsi

05-4506832 pustaka.upsi.edu.my Perpustakaan Tuanku Bainun Kampus Sultan Abdul Jalil Shah PustakaTBainun ptbupsi

temperature; hence, the 5CB microdroplet tends to sink over time. As a result, the decrease in the number of 5CB microdroplets along the UV-Vis light path due to sinking to the bottom of the cuvette and resulted in a decrease in absorbance. At the same time, the absorbance of the radial 5CB microdroplet suspension was also measured and monitored, as shown in Figure 4.4 (b). The absorbance signal of the radial 5CB microdroplet suspension showed the highest peak when the monitoring time was 0 minutes and the lowest when the monitoring time was 60 minutes. It was also observed that the wavelength peak shifted to the left due to the presence of CTAB in the radial 5CB microdroplet sample. A similar trend was observed when the copper nanoparticles were present in pure 5CB (Srivastava et al., 2023). The reduction of the absorbance at the peak wavelength of radial 5CB microdroplet suspension was similar to bipolar 5CB microdroplets.

05-4506832 pustaka.upsi.edu.my Perpustakaan Tuanku Bainun Kampus Sultan Abdul Jalil Shah PustakaTBainun ptbupsi
05-4506832 pustaka.upsi.edu.my Perpustakaan Tuanku Bainun Kampus Sultan Abdul Jalil Shah PustakaTBainun ptbupsi

05-4506832 pustaka.upsi.edu.my Perpustakaan Tuanku Bainun Kampus Sultan Abdul Jalil Shah PustakaTBainun ptbupsi

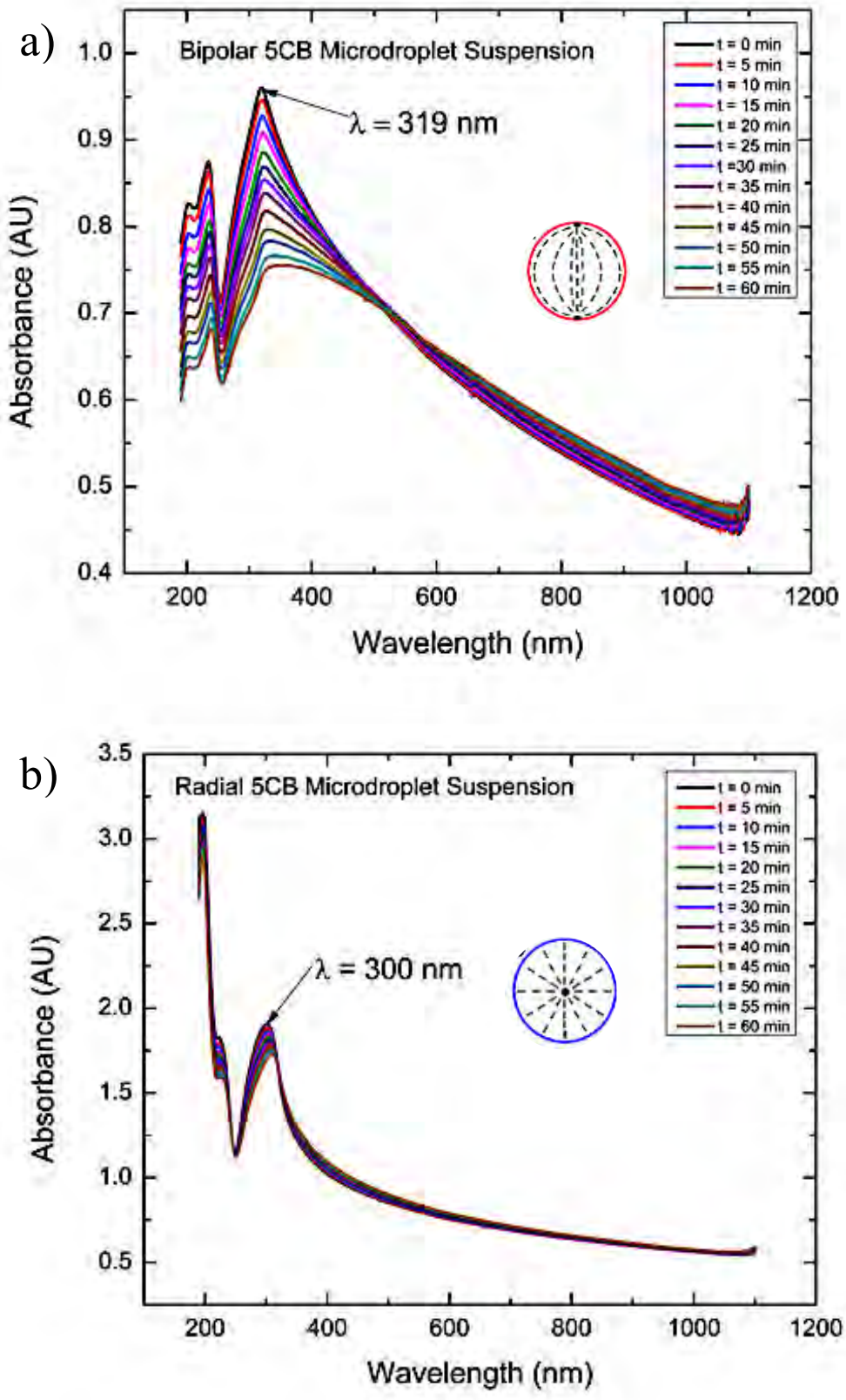


Figure 4.4. The absorption spectrum of 5CB for a 1-hour monitoring period.

05-4506832 pustaka.upsi.edu.my Perpustakaan Tuanku Bainun Kampus Sultan Abdul Jalil Shah PustakaTBainun ptbupsi

05-4506832 pustaka.upsi.edu.my Perpustakaan Tuanku Bainun Kampus Sultan Abdul Jalil Shah PustakaTBainun ptbupsi

The absorbance peak of the 5CB microdroplets in the microdroplet solution was observed for 1 hour to determine its stability. The microdroplets might sink or collapse to form smaller or combine to form larger microdroplets during the measurement period due to the difference in density of 5CB and deionized water. Figure 4.5 shows the graph of absorbance peak versus time in Figure 4.4 of 5CB versus time for (a) bipolar and (b) radial internal configuration. The absorbance percentage change was calculated by using Equation 3.5. During the 1-hour monitoring, there was a 22% and 11% reduction in bipolar and radial 5CB microdroplets within 1 hour along the measurement path, as shown in Figure 4.5. The absorbance of the 5CB microdroplet was compared with the absorbance of the chloroform microdroplet because both used UV-Vis spectroscopy to determine the microdroplet stability. It was reported that chloroform microdroplet absorbance dropped about 2% when it was monitored using UV-Vis spectroscopy for 1 hour (Yeng et al., 2023). This is because 2% of chloroform microdroplets sinking due to the small difference between chloroform (0.53 cP) and water (0.89 cP) viscosities (Yeng et al., 2023). The reduction trend was comparable with the reduction trend of the chloroform microdroplet stability in water using the UV-Vis inspection (Yeng et al., 2023). However, the reduction of the radial 5CB microdroplets' absorbance was less than that of the bipolar 5CB microdroplets. The possible reason is that CTAB changes the internal configuration and stabilizes the radial 5CB microdroplet (Bartoš et al., 2022; Urbanski et al., 2017; Yeng, Ayop, & Sasaki, 2022). On the other hand, the reduction was due to the sinking of the 5CB microdroplets at the bottom of the cuvette (Yeng et al., 2023). In addition, the absorption of 5CB was compared to water in Figure 4.6 (a) and compared to CTAB and water in Figure 4.6 (b).

05-4506832 pustaka.upsi.edu.my Perpustakaan Tuanku Bainun Kampus Sultan Abdul Jalil Shah PustakaTBainun ptbupsi

05-4506832 pustaka.upsi.edu.my Perpustakaan Tuanku Bainun Kampus Sultan Abdul Jalil Shah PustakaTBainun ptbupsi

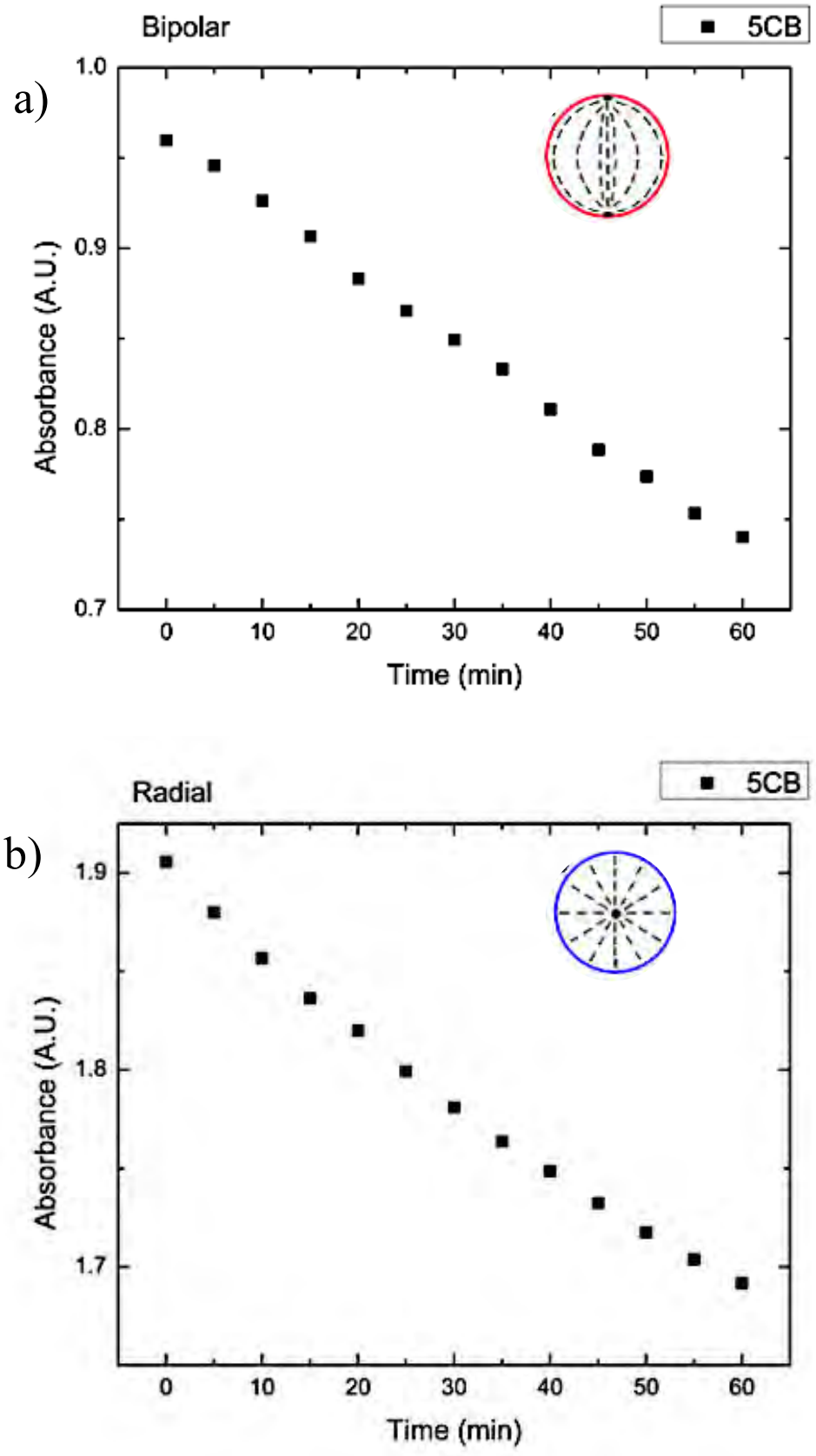


Figure 4.5. The graph of peak versus time is in Figure 4.4 for (a) bipolar and (b) radial 5CB microdroplet suspension in water.

05-4506832 pustaka.upsi.edu.my Perpustakaan Tuanku Bainun Kampus Sultan Abdul Jalil Shah PustakaTBainun ptbupsi

05-4506832 pustaka.upsi.edu.my Perpustakaan Tuanku Bainun Kampus Sultan Abdul Jalil Shah PustakaTBainun ptbupsi

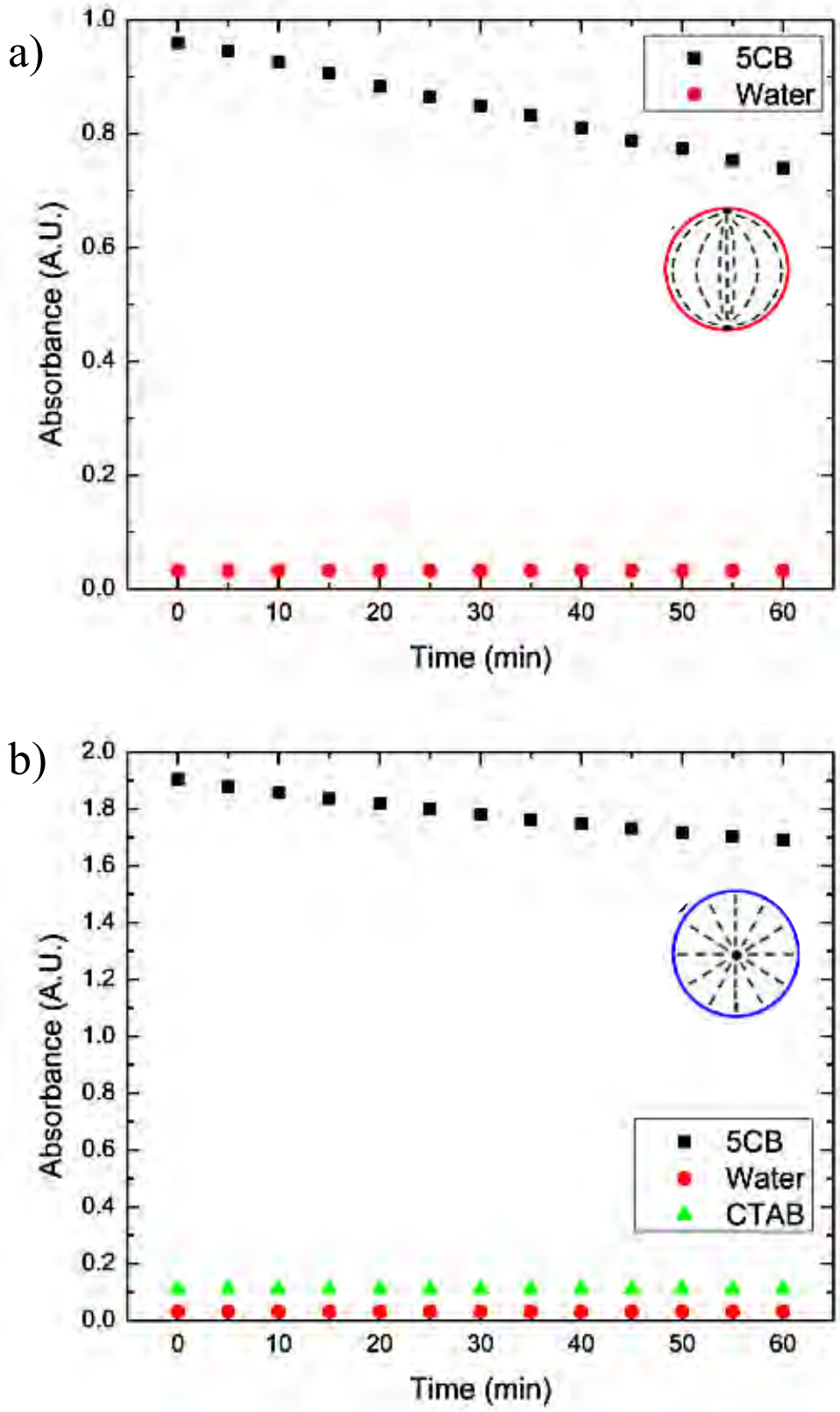


Figure 4.6. The graph of peak versus time in Figure 4.5 absorbance against time (a) bipolar 5CB and water, (b) radial 5CB, water, and CTAB.

05-4506832 pustaka.upsi.edu.my Perpustakaan Tuanku Bainun Kampus Sultan Abdul Jalil Shah PustakaTBainun ptbupsi

05-4506832 pustaka.upsi.edu.my Perpustakaan Tuanku Bainun Kampus Sultan Abdul Jalil Shah PustakaTBainun ptbupsi

Figure 4.6 (a) shows that the absorption of 5CB bipolar microdroplets is higher than that of water. This indicated that bipolar 5CB microdroplets were present in the water (Yeng et al., 2023). If water absorbance is higher than 5CB absorbance, that indicates the sample contains more water than 5CB. Thus, the 5CB bipolar microdroplet was stable in water for 1-hour of observation. Meanwhile, Figure 4.6 (b) shows that the absorption of radial 5CB microdroplets is higher than that of CTAB and water. This effect was like that of the 5CB bipolar microdroplet. This finding helps estimate how long 5CB microdroplets can sustain in water. In this study, the bipolar and radial 5CB microdroplet absorbance reduce to 22 % and 11%, respectively. This information can guide the researcher in planning the use of microdroplet-specific applications for 1-hour monitoring study. This means that during the optical trapping process, in the sample chamber containing 5CB microdroplet solution, there was less than a 22 % probability of the 5CB microdroplet to be sinking or stuck on the glass slide. For this amount of 22 % stability, the sample chamber could be used for 1 hour of trapping without the need to change or make a new sample regularly during the optical trapping process or other microdroplet application for 1-hour monitoring.

05-4506832 pustaka.upsi.edu.my Perpustakaan Tuanku Bainun Kampus Sultan Abdul Jalil Shah PustakaTBainun ptbupsi

4.3 Linearly Polarized Laser 5CB Microdroplet Trapping

Figure 4.7 shows the temporal image sequence of the 0.7 μm bipolar 5CB microdroplet captured into optical tweezers spot by the linearly polarized laser. In Figure 4.7, at t_1 = 1 s, there was a single free-moving bipolar 5CB microdroplet beyond the focal plane of view. When the laser trapping was turned on, the free-moving 5CB microdroplet was

05-4506832 pustaka.upsi.edu.my Perpustakaan Tuanku Bainun Kampus Sultan Abdul Jalil Shah PustakaTBainun ptbupsi

05-4506832 pustaka.upsi.edu.my Perpustakaan Tuanku Bainun Kampus Sultan Abdul Jalil Shah PustakaTBainun ptbupsi

slowly attracted to the trap spot represented by the red dash circle from the event t_1 = 1 s to t_3 = 4 s. This shows by the image of the 5CB microdroplet, which is initially out of focus and suddenly becomes clear and sharp as it approaches the trap spot. The bipolar 5CB microdroplet was captured stably at the trap spot at the event t_4 = 4 s to t_6 = 10 s at 0.2 MW/cm^2. The trapped single 5CB microdroplet showed a clear image as it get trapped at the center of the trap spot. In order to verify whether the trapped 5CB microdroplet was a bipolar 5CB microdroplet or radial 5CB, the cross-polarization view was performed. The bipolar internal configuration was shown at t_6 = 10 s using cross-polarization. The bright spot represents the signature visual for the bipolar internal configuration of the trapped 5CB microdroplet. The 5CB microdroplet escaped from the trap spot when the laser was off at t_7 = 14 s to t_8 = 15 s.

05-4506832 pustaka.upsi.edu.my Perpustakaan Tuanku Bainun PustakaTBainun ptbupsi

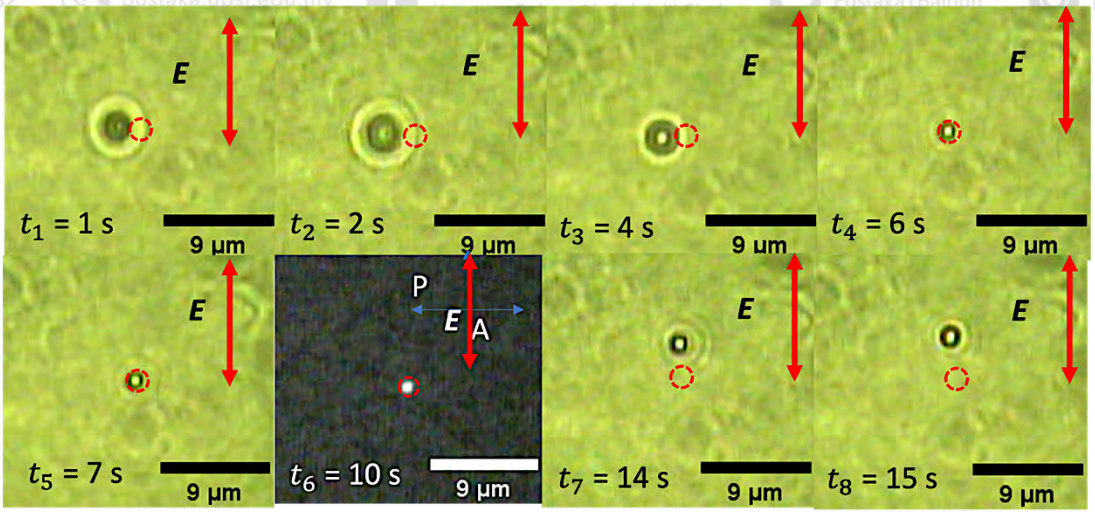


Figure 4.7. Image sequence of the 0.7 µm bipolar 5CB microdroplet capturing into optical tweezers trap (red dash circle) at 0.2 MW/cm^2. The red arrows indicate the polarization direction of the trapping laser.

Figure 4.8 shows the sequence image of the 1.0 µm radial 5CB microdroplet capturing event in the optical tweezers spot by linearly polarized laser. Initially, in

05-4506832 pustaka.upsi.edu.my Perpustakaan Tuanku Bainun Kampus Sultan Abdul Jalil Shah PustakaTBainun ptbupsi

05-4506832 pustaka.upsi.edu.my Perpustakaan Tuanku Bainun Kampus Sultan Abdul Jalil Shah PustakaTBainun ptbupsi

Figure 4.8, a free-moving radial 5CB microdroplet was in the water at t_1 = 1 s. The laser was turned on to start trapping a single radial 5CB microdroplet. The free-moving single radial 5CB microdroplet was attracted toward the trap spot labeled with a dash red circle from t_1 = 1 s to t_3 = 9 s. The optical force attracts the radial 5CB microdroplet toward the center of the trap spot. The radial 5CB microdroplet was successfully trapped in the laser trap spot from t_4 = 11 s to t_5 = 12 s at 0.2 MW/cm^2. The trapped radial 5CB microdroplet was confined in the trap spot and restricted from moving freely. The internal configuration of the trapped radial 5CB microdroplet was shown at t_6 = 13 s. The signature "Maltese crossed structure" bright spot indicated that the trapped 5CB microdroplet was radial 5CB. The radial 5CB microdroplet escaped the trap spot at t_7 = 27 s to t_8 = 28 s as the trapping laser was off.

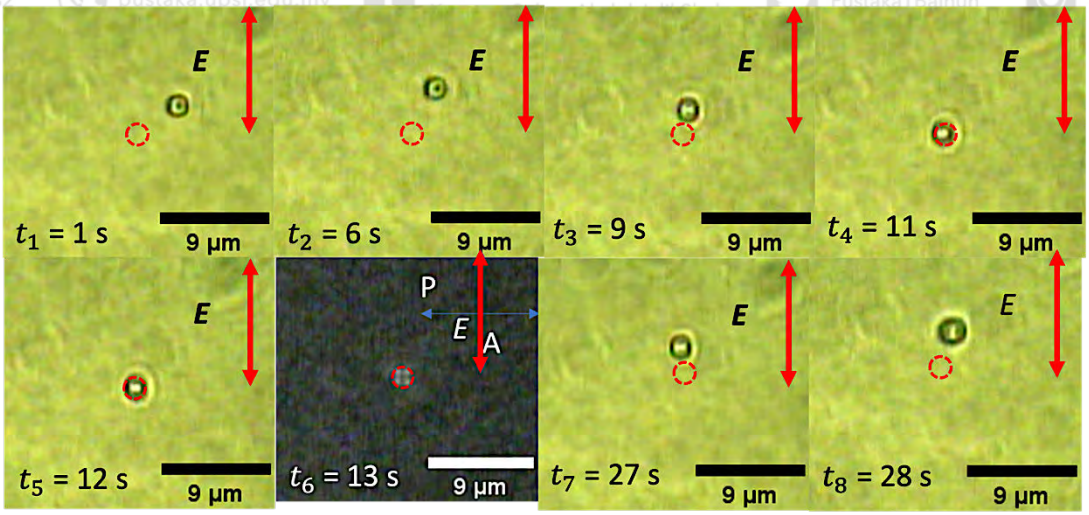


Figure 4.8. Image sequence of the 1.0 µm radial 5CB microdroplet capturing into optical tweezers trap (red dash circle) at 0.2 MW/cm^2. The red arrows indicate the polarization direction of the trapping laser.

These optical trapping events in Figures 4.7 and 4.8 showed the ability of the optical tweezers to attract and hold a single 5CB microdroplet at low power density (0.2 MW/cm^2). The trap spot creates an optical potential where the 5CB microdroplet is

05-4506832 pustaka.upsi.edu.my Perpustakaan Tuanku Bainun Kampus Sultan Abdul Jalil Shah PustakaTBainun ptbupsi

05-4506832 pustaka.upsi.edu.my Perpustakaan Tuanku Bainun Kampus Sultan Abdul Jalil Shah PustakaTBainun ptbupsi

attracted and confined. The result was part of a single 5CB microdroplet trapping of size range 0.6 μm to 0.37 μm within power density ranges from 0.2 MW/cm^2 to 7.3 MW/cm^2. In our optical tweezers setup, the lowest laser power to start trapping a single 5CB was 0.2 MW/cm^2. Optical trapping was impossible if the laser power was below 0.2 MW/cm^2 because this is the threshold laser power for trapping to occur. Below threshold laser power, no trapping occurred. Besides that, not all 5CB microdroplets could be trapped using optical tweezers. In this study, the smallest size of the 5CB microdroplet that could be trapped was 0.6 μm. The optical resolution of OTKB/M is ~ 0.5 μm and this is the limit of the OTKB/M to observe the particle. The optical trapping was challenging when the microdroplet size was less than 0.6 μm due to the limitation of optical resolution (~ 0.5 μm) because the microdroplet in the range of ~ 0.5 μm unclear, blurred and difficult to be distinguish and be viewed under optical tweezers. This caused the problem of identifying whether the microdroplet was 5CB or bubbles. Hence, the optical trapping could not be proceeded. In addition, trapping particles of size smaller than 0.5 μm is challenging especially at higher laser power, because the trapping becomes unstable and pushes out from the trap spot (Zhong et al., 2017). It was essential to successfully trap a single 5CB microdroplet stably before manipulation and micro-control could be done.

05-4506832 pustaka.upsi.edu.my Perpustakaan Tuanku Bainun Kampus Sultan Abdul Jalil Shah PustakaTBainun ptbupsi

05-4506832 pustaka.upsi.edu.my Perpustakaan Tuanku Bainun Kampus Sultan Abdul Jalil Shah PustakaTBainun ptbupsi

4.4 5CB Microdroplet Orientation Control

The orientation control of the trapped 5CB microdroplet under a linearly polarized laser beam was studied. Figure 4.9 shows the snapshot of a 2.0 μm bipolar 5CB microdroplet trapped by a linearly polarized laser beam of 0.2 MW/cm^2 at polarization direction, θ. The linearly polarized laser beam direction was slowly adjusted from θ = 0º until θ = 180º with a 30º increment, and the optical texture of the trapped 5CB microdroplet was observed using a CCD camera. Figure 4.9 shows the optical texture image of the trapped single 5CB microdroplet observed under bright field microscopy corresponding to the linearly polarized laser beam direction, θ. The red arrow represents the polarization direction of the linearly polarized laser beam. From Figure 4.9, the optical texture aligns according to the polarization direction represented by the red arrow. However, the bright microscope images could not clearly show the interaction between the internal configuration of bipolar 5CB and the polarization direction of the linearly polarized light, as shown in Figure 4.9. In order to justify the orientation control of the internal configuration of the trapped bipolar 5CB, which was aligned with the polarization direction of the linearly polarized laser beam, the cross-polarization view was required. Figure 4.10 shows the snapshot of a 2.0 μm bipolar 5CB microdroplet trap at 0.2 MW/cm^2 at varied polarization direction, θ, under the cross-polarized view. The texture of the trapped bipolar 5CB microdroplet was orientated according to the orientation as confirmed under a cross-polarization view, as shown in Figure 4.10.

05-4506832 pustaka.upsi.edu.my Perpustakaan Tuanku Bainun Kampus Sultan Abdul Jalil Shah PustakaTBainun ptbupsi

05-4506832 pustaka.upsi.edu.my Perpustakaan Tuanku Bainun Kampus Sultan Abdul Jalil Shah PustakaTBainun ptbupsi

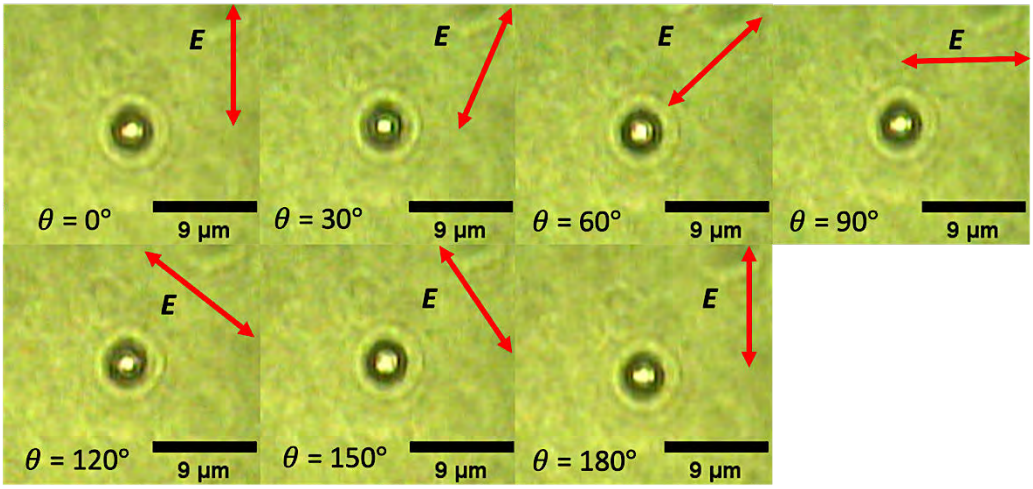


Figure 4.9. The snapshot of 2.0 μm bipolar 5CB microdroplet trap at 0.2 MW/cm^2 at varied polarization direction, θ. The red arrows indicate the polarization direction of the trapping laser.

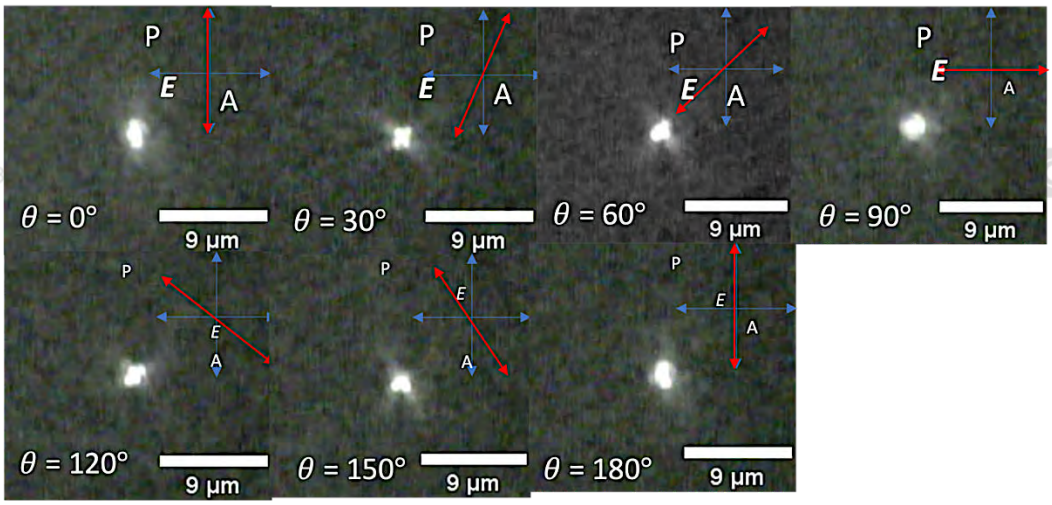


Figure 4.10. The snapshot of 2.0 μm bipolar 5CB microdroplet trap at 0.2 MW/cm^2 at varied polarization direction, θ under cross-polarized view. The red arrows indicate the polarization direction of the trapping laser.

Figure 4.10 shows the snapshot of 2.0 μm of bipolar 5CB microdroplet trap at 0.2 MW/cm^2 at varied polarization direction, θ under cross-polarization view. The bright spot showed the structure of the bipolar 5CB microdroplet trapped by the linearly polarized laser beam. As the polarization direction increased, the internal configuration changed inside the 5CB microdroplet oriented along the direction of the linearly

05-4506832 pustaka.upsi.edu.my Perpustakaan Tuanku Bainun Kampus Sultan Abdul Jalil Shah PustakaTBainun ptbupsi

05-4506832 pustaka.upsi.edu.my Perpustakaan Tuanku Bainun Kampus Sultan Abdul Jalil Shah PustakaTBainun ptbupsi

polarized direction, and this could be observed, as shown in Figure 4.10. This indicated that the internal configuration of the bipolar 5CB microdroplet responds and is influenced by the direction of laser polarization (Brasselet & Juodkazis, 2009).

Figure 4.11 shows the schematic diagram drawn to show the orientation of 5CB molecules inside the microdroplet oriented along the direction of the linearly polarized light. The direction of the laser spot is out from the page.

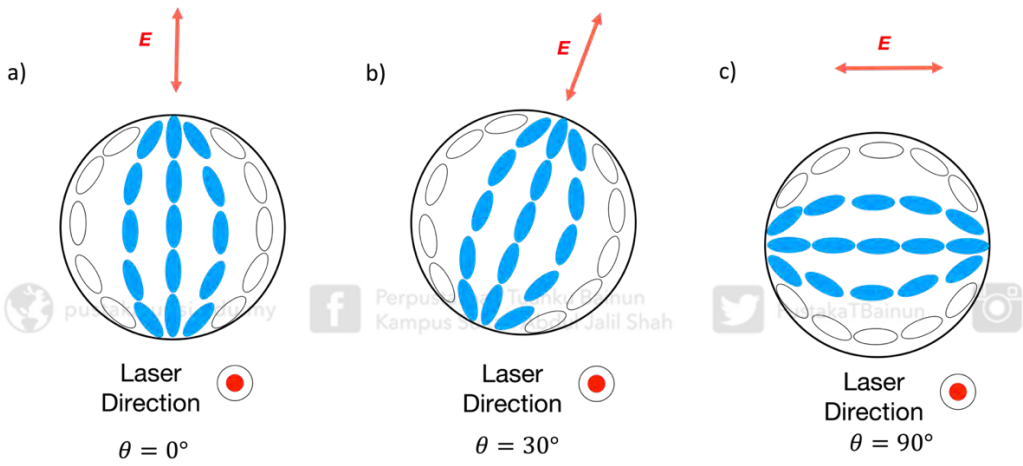


Figure 4.11. The schematic diagram of 5CB molecules orientation inside the microdroplet to the polarization direction of linearly polarized light. The red arrows indicate the polarization direction of the trapping laser.

Figure 4.11 (a) shows the 5CB molecules inside the microdroplet oriented at $\theta = 0^{o}$ along the polarization direction represented by the red arrow. The blue-shaded 5CB molecules are the bright spots of the bipolar 5CB that respond to the linearly polarized laser beam direction. The bright spot was due to the light scattering inside the bipolar 5CB microdroplet (Juodkazis et al., 1999). Then, Figure 4.11 (b) shows the orientation of the 5CB molecules when the linearly polarized laser beam was oriented to $\theta = 30^{o}$. It could be seen that the 5CB molecules also aligned according to the

05-4506832 pustaka.upsi.edu.my Perpustakaan Tuanku Bainun Kampus Sultan Abdul Jalil Shah PustakaTBainun ptbupsi

05-4506832 pustaka.upsi.edu.my Perpustakaan Tuanku Bainun Kampus Sultan Abdul Jalil Shah PustakaTBainun ptbupsi

polarization direction, as indicated by the red arrow. When the linearly polarized light direction was increased to θ = 90º, as shown by the red arrow in Figure 4.11 (c), the 5CB molecule changed the orientation to θ = 90º too. From Figures 4.9 and 4.10, the orientation of the bipolar 5CB molecules inside the microdroplet depends on the linearly polarized light direction. This concludes that the polarization direction could control the orientation of the 5CB molecules. The bipolar 5CB microdroplet has significance in birefringence (Δn) (Murazawa, Juodkazis, & Misawa, 2005). The birefringence (Δn) is correlated to the refractive index and the optical force of the laser beam (Tsuji et al., 2022). The significant value of birefringence contributed to the strong optical force effect on the liquid crystal molecules inside the 5CB microdroplet. This optical force caused the liquid crystal molecules to align along the polarization direction of the laser beam.

05-4506832 pustaka.upsi.edu.my Perpustakaan Tuanku Bainun Kampus Sultan Abdul Jalil Shah PustakaTBainun ptbupsi

Figure 4.12 shows the optical texture image of the trapped single 5CB microdroplet observed under bright field microscopy corresponding to the linearly polarized laser beam direction, θ. The red arrow represents the polarization direction of the linearly polarized laser beam. As the polarization direction of the linearly polarized laser beam used was increased, there was no change in the optical texture of the trapped radial 5CB microdroplet, as shown in Figure 4.12. For example, when the polarization direction increased from $\theta = 0$º to $\theta = 90$º, the bright field microscopic image of the trapped radial 5CB did not change the optical texture. This implied that the linearly polarized light direction change did not influence the 5CB molecules inside the radial 5CB microdroplet, θ (Brasselet & Juodkazis, 2009). In order to verify this observation, the trapped radial 5CB microdroplet was observed under a cross-polarization view, as shown in Figure 4.13.

05-4506832 pustaka.upsi.edu.my Perpustakaan Tuanku Bainun Kampus Sultan Abdul Jalil Shah PustakaTBainun ptbupsi

05-4506832 pustaka.upsi.edu.my Perpustakaan Tuanku Bainun Kampus Sultan Abdul Jalil Shah PustakaTBainun ptbupsi

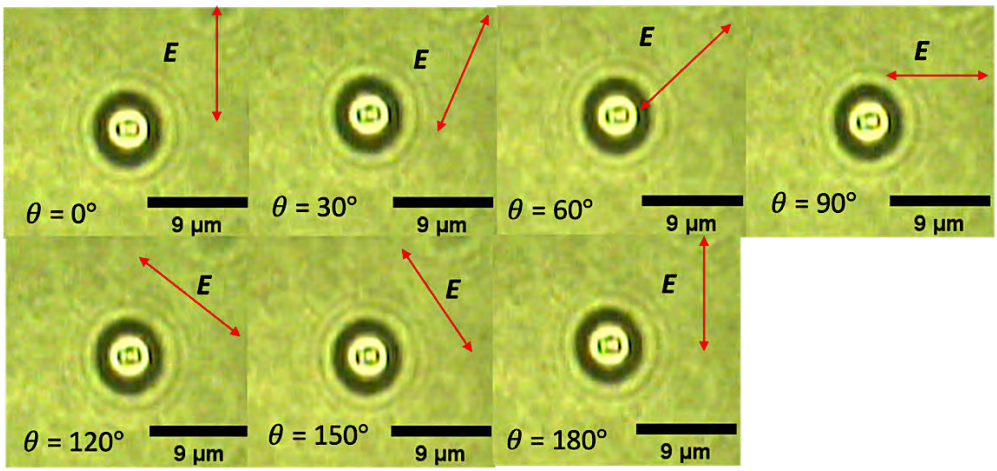


Figure 4.12. The snapshot of 3.3 µm radial 5CB microdroplet trap at 0.2 MW/cm^2 at varied polarization direction, θ. The red arrows indicate the polarization direction of the trapping laser.

The cross-polarization view was used to investigate further the effect of polarization direction change on the radial 5CB microdroplet internal configuration. Figure 4.13 shows the snapshot of a 3.3 µm radial 5CB microdroplet trapped by 0.2 MW/cm^2 laser at varied polarization direction, θ under a cross-polarized view. The bright spot with the Maltese cross structure represents the signature arrangement of 5CB molecules of radial 5CB microdroplet, as shown in Figure 4.13. The red arrow presents the linearly polarized direction. From Figure 4.13, as the polarization direction was increased, there was no change in the Maltese cross structure of the radial 5CB microdroplet. It could be seen that there was no change in the orientation of the Maltese cross structure when the polarization direction of the linearly polarized laser beam was systematically increased.

05-4506832 pustaka.upsi.edu.my Perpustakaan Tuanku Bainun Kampus Sultan Abdul Jalil Shah PustakaTBainun ptbupsi

05-4506832 pustaka.upsi.edu.my Perpustakaan Tuanku Bainun Kampus Sultan Abdul Jalil Shah PustakaTBainun ptbupsi

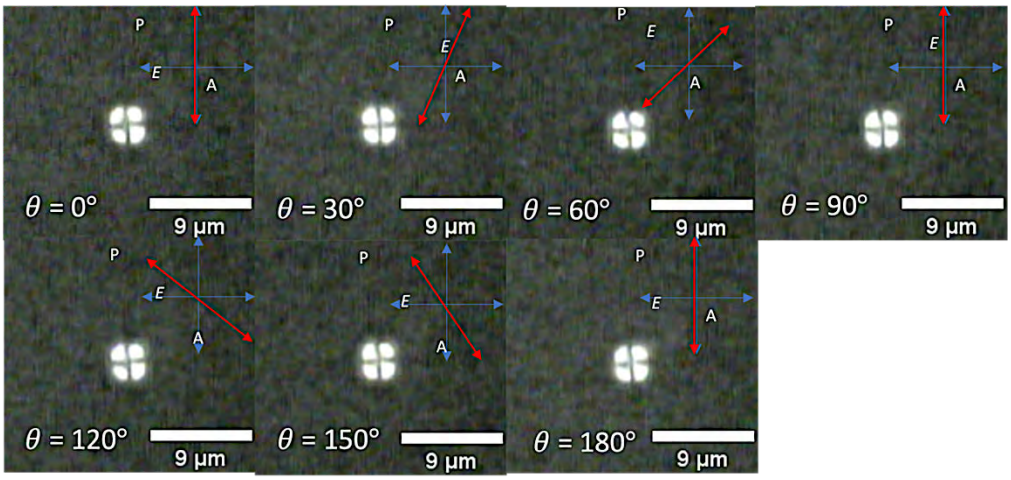


Figure 4.13. The snapshot of 3.3 μm radial 5CB microdroplet trap at 0.2 MW/cm^2 at varied polarization direction, θ under cross-polarized view. The red arrows indicate the polarization direction of the trapping laser.

Figure 4.14. shows the schematic diagram drawn to show the orientation of 5CB molecules inside the microdroplet oriented along the direction of the linearly polarized light. The direction of the laser spot is out from the page.

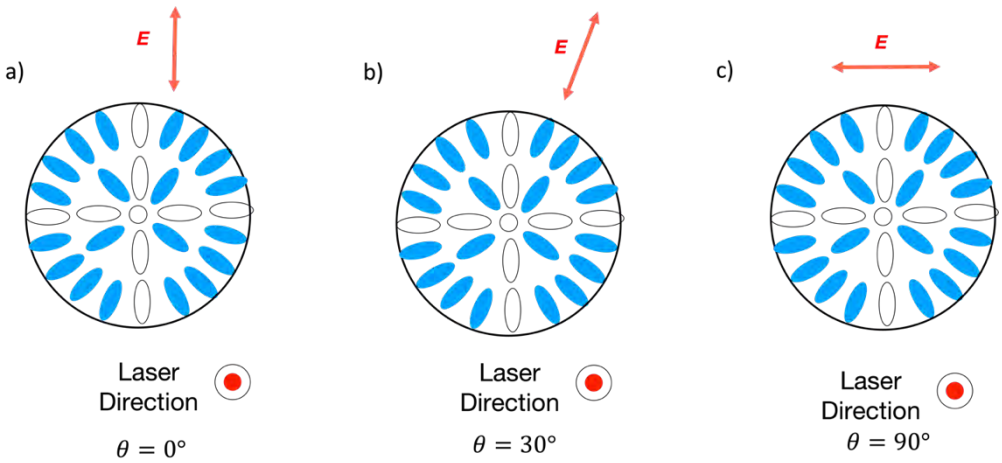


Figure 4.14. The schematic diagram of 5CB molecules orientation inside the microdroplet to the polarization direction of linearly polarized light. The red arrows indicate the polarization direction of the trapping laser.

Figure 4.14 (a) shows the orientation of 5CB molecules inside the radial 5CB

05-4506832 pustaka.upsi.edu.my Perpustakaan Tuanku Bainun Kampus Sultan Abdul Jalil Shah PustakaTBainun ptbupsi

05-4506832 pustaka.upsi.edu.my Perpustakaan Tuanku Bainun Kampus Sultan Abdul Jalil Shah PustakaTBainun ptbupsi

microdroplet not oriented along the linearly polarized laser beam at $\theta = 0^{o}$, presented by the red arrow. The blue shaded 5CB molecules are the bright spot of the radial 5CB that respond to the linearly polarized laser beam direction forming a Maltase cross pattern. The bright spot was due to the light scattering inside the radial 5CB microdroplet (Juodkazis et al., 1999). The liquid crystal molecules that align parallel and perpendicular to the polarizer and analyzer appear as black because light are blocked. However, the liquid crystal molecules that not align parallel or perpendicular to the polarizer and analyzer let light to pass through and appears as bright under cross-polarized view. Figure 4.14 (a) shows that the 5CB molecules were unaffected by the linearly polarized laser beam direction set at $\theta = 0^{o}$. As the polarization direction of the linearly polarized laser beam was further increased to $\theta = 30^{o}$, it could be seen that the 5CB molecules did not affect the polarization direction, as shown in Figure 4.14 (b). The orientation of the 5CB molecules in the radial 5CB microdroplet remained the same even when the polarization direction, θ, was increased to 90º, as shown in Figure 4.14 (c). Based on the result, the 5CB molecules inside the radial 5CB microdroplet were independent of the linearly polarized direction when the low laser power was used. It was reported that radial 5CB microdroplet has negligible birefringence due to the radial symmetry of its molecular arrangement and contributed to the strong elastic and viscoelastic forces of liquid crystal molecules (Murazawa, Juodkazis, Matsuo, et al., 2005). The small birefringence is correlated to a small refractive index and generates a weak optical force of the laser beam (Tsuji et al., 2022). This weak optical force is unable to overcome strong elastic and viscoelastic forces of liquid crystal molecules inside the radial 5CB microdroplet; hence, the alignment to the laser polarization was not possible as shown in Figures 4.12 and 4.13.

05-4506832 pustaka.upsi.edu.my Perpustakaan Tuanku Bainun Kampus Sultan Abdul Jalil Shah PustakaTBainun ptbupsi

05-4506832 pustaka.upsi.edu.my Perpustakaan Tuanku Bainun Kampus Sultan Abdul Jalil Shah PustakaTBainun ptbupsi

4.5 Rotatability of 5CB Microdroplet

The rotatability of the 5CB microdroplet was investigated by trapping a single bipolar 5CB microdroplet in the water using a circularly polarized laser beam. Figure 4.15 shows the snapshot of the rotated 2.1 µm bipolar 5CB microdroplet in the water by a circularly polarized laser trap spot at 1.1 MW/cm^2. The bipolar 5CB microdroplet was rotated clockwise from t_1= 1 s to t_4 = 4 s, as shown in Figure 4.15.

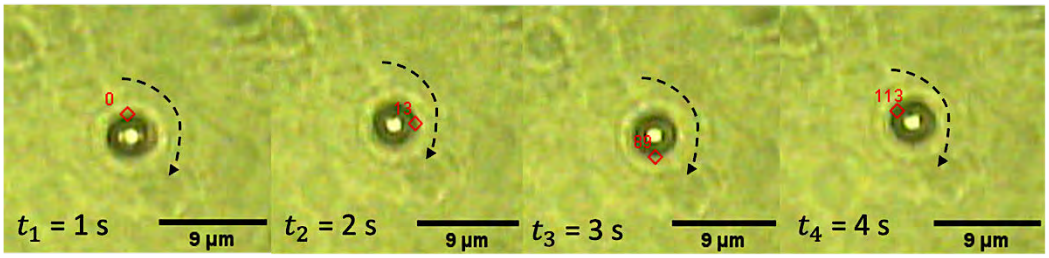


Figure 4.15. The snapshot of a rotated bipolar 5CB microdroplet of 2.1 µm diameter in water by a circularly polarized laser beam.

The bipolar 5CB microdroplet rotated in the optical trap or about its center, as shown in Figure 4.16 (a), and the typical QPD signal of the rotated 5CB microdroplet in Figure 4.16 (b). t is the time taken for a complete rotation peak to peak.

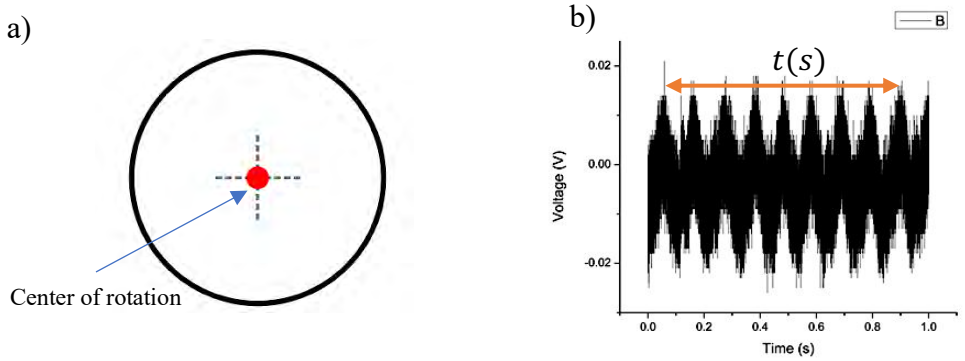


Figure 4.16. (a) Schematic diagram of bipolar 5CB microdroplet rotates in an optical trap and (b) QPD signal of the rotated 5CB microdroplet.

05-4506832 pustaka.upsi.edu.my Perpustakaan Tuanku Bainun Kampus Sultan Abdul Jalil Shah PustakaTBainun ptbupsi

05-4506832 pustaka.upsi.edu.my Perpustakaan Tuanku Bainun Kampus Sultan Abdul Jalil Shah PustakaTBainun ptbupsi

Similar to the bipolar 5CB microdroplet, the radial 5CB microdroplet could also be rotated. A single radial 5CB microdroplet of 2.9 µm was trapped stably and rotated in the water by a circularly polarized laser beam at 1.1 MW/cm^2. The snapshot of the rotated radial 5CB microdroplet was observed from t_1= 1 s to t_4 = 4 s, as shown in Figure 4.17.

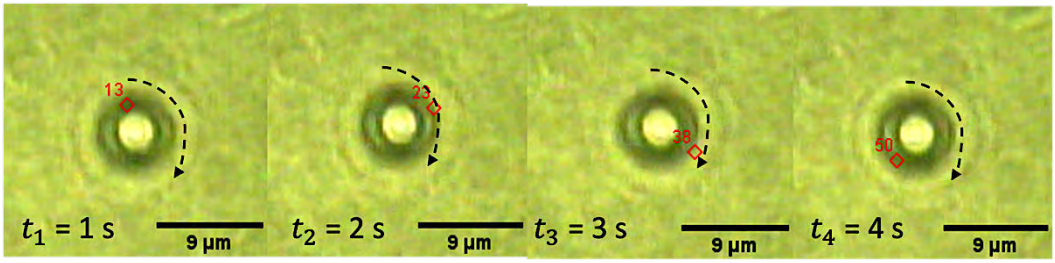


Figure 4.17. The snapshot of rotated radial 5CB microdroplet of 2.9 µm diameter in water by a circularly polarized laser beam.

05-4506832 pustaka.upsi.edu.my Perpustakaan Tuanku Bainun Kampus Sultan Abdul Jalil Shah PustakaTBainun ptbupsi

However, the rotation mechanism of the radial 5CB microdroplet differed from that of the bipolar 5CB microdroplet. The radial 5CB microdroplet rotates about a circle, as shown in Figure 4.18 (a) and (b), which is the typical QPD signal for a rotating 5CB microdroplet. t is the time taken for a complete rotation peak to peak.

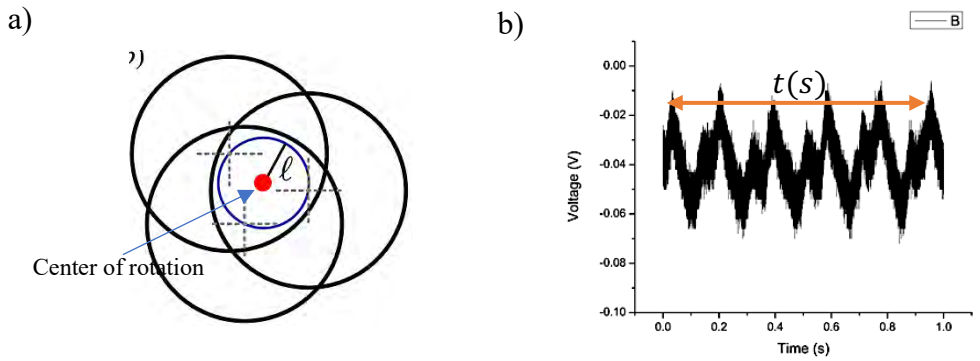


Figure 4.18. (a) The schematic diagram of a radial 5CB microdroplet rotates about a circle (b), which is the typical QPD signal of the rotating 5CB microdroplet.

05-4506832 pustaka.upsi.edu.my Perpustakaan Tuanku Bainun Kampus Sultan Abdul Jalil Shah PustakaTBainun ptbupsi

05-4506832 pustaka.upsi.edu.my Perpustakaan Tuanku Bainun Kampus Sultan Abdul Jalil Shah PustakaTBainun ptbupsi

The 5CB microdroplet of bipolar and radial configuration in Figures 4.15 and 4.17 rotated when they were exposed to the circularly polarized laser beam. The refraction of the circularly polarized going into and out from the 5CB microdroplet caused the angular momentum to change, and the change in angular momentum creates a reaction torque that rotates the 5CB microdroplet as shown in Figures 4.15 and 4.17 (Manzo et al., 2006; Wood et al., 2004). It was observed in Figures 4.15 and 4.17 that the bipolar 5CB rotated within the laser spot but radial 5CB rotated orbiting the laser spot (Sanders et al., 2013). This is because of the different birefringence between bipolar and radial 5CB microdroplets, which affects the transfer of angular momentum (Murazawa, Juodkazis, Matsuo, et al., 2005).

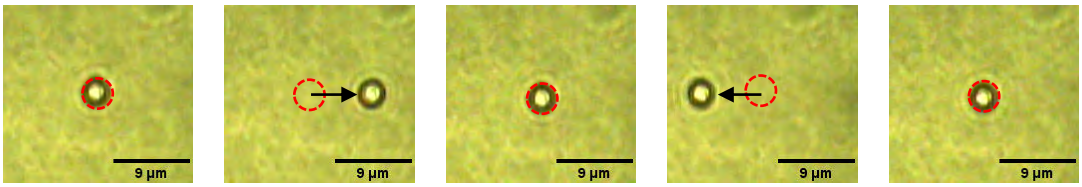
4.6 5CB Microdroplet Translational and Micro-control

05-4506832 pustaka.upsi.edu.my Perpustakaan Tuanku Bainun Kampus Sultan Abdul Jalil Shah PustakaTBainun ptbupsi

Besides, the single optical tweezers are used for single manipulation analysis after the particle is trapped. In this study, the optical tweezers can simultaneously translate and micro-control a single 5CB microdroplet in water. Figure 4.19 shows the translation and micro-control of a single 1.8 μm bipolar 5CB microdroplet by a linearly polarized laser beam at 0.2 MW/cm^2. The bipolar 5CB microdroplet could be trapped and translated simultaneously, as shown in Figure 4.19.

05-4506832 pustaka.upsi.edu.my Perpustakaan Tuanku Bainun Kampus Sultan Abdul Jalil Shah PustakaTBainun ptbupsi

05-4506832 pustaka.upsi.edu.my Perpustakaan Tuanku Bainun Kampus Sultan Abdul Jalil Shah PustakaTBainun ptbupsi

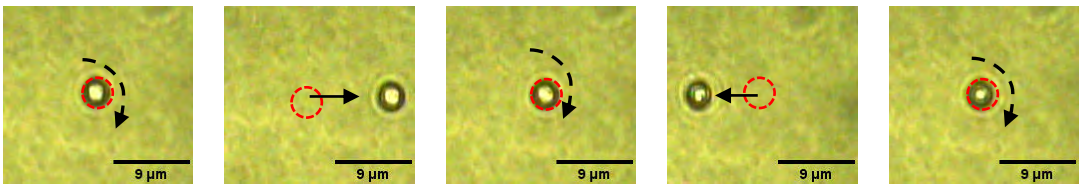


A, t_1 = 1 s B, t_2 = 10 s C, t_3 = 15 s D, t_4 = 25 s E, t_5 = 27 s

Figure 4.19. The translation and micro-control of a single 1.8 µm bipolar 5CB microdroplet by a linearly polarized laser beam at 0.2 MW/cm^2. A: The 5CB microdroplet was trapped in the optical trap at t_1= 1 s. B: The 5CB microdroplet translation 5 µm to the right at t_2 = 10 s. C: The 5CB microdroplet retrapped at t_3 = 15 s. D: The 5CB microdroplet translation 5 µm to the left at t_4 = 25 s. E: The 5CB microdroplet retrapped at t_5 = 27 s.

Figure 4.20 shows the translation and micro-control of a single 1.8 µm bipolar 5CB microdroplet by a circularly polarized laser beam at 0.2 MW/cm^2. The bipolar 5CB microdroplet could be translated and rotated micro-controlled simultaneously, as shown in Figure 4.20.

05-4506832 pustaka.upsi.edu.my Perpustakaan Tuanku Bainun Kampus Sultan Abdul Jalil Shah PustakaTBainun ptbupsi



A, t_1 = 1 s B, t_2 = 10 s C, t_3 = 13 s D, t_4 = 25 s E, t_5 = 28 s

Figure 4.20. The translation and micro-control of a single 1.8 µm bipolar 5CB microdroplet by a circularly polarized laser beam at 0.2 MW/cm^2. A: The 5CB microdroplet was trapped and rotated in the optical trap at t_1 = 1 s. B: The 5CB microdroplet translation 5 µm to the right at t_2 = 10 s. C: The 5CB microdroplet retrapped and rotated at t_3 = 13 s. D: The 5CB microdroplet translation 5 µm to the left at t_4 = 25 s. E: The 5CB microdroplet retrapped and rotated at t_5 = 28 s.

Figure 4.21 shows the *x*-axis trajectory of the trapped bipolar 5CB microdroplet in Figure 4.19 and Figure 4.20 at P = 0.2 and 1.1 MW/cm^2, respectively. Points A, C, and E show the trajectory of the trapped 5CB microdroplet, while points B and D showed the trajectory when the piezostage displaced the trapped 5CB microdroplet

05-4506832 pustaka.upsi.edu.my Perpustakaan Tuanku Bainun Kampus Sultan Abdul Jalil Shah PustakaTBainun ptbupsi

05-4506832 pustaka.upsi.edu.my Perpustakaan Tuanku Bainun Kampus Sultan Abdul Jalil Shah PustakaTBainun ptbupsi

from the trap spot in Figure 4.21 (a). As the laser power used increased, the time taken for the 5CB microdroplet to be retrapped (at points B and D) became shorter in Figure 4.21 (a) and (b). This indicated that bipolar 5CB microdroplets could strongly translate the intense tweezing and stable trapping without escape. A similar trend was seen for bipolar 5CB microdroplets trapped by circularly polarized light, as shown in Figure 4.21 (b).

05-4506832 pustaka.upsi.edu.my Perpustakaan Tuanku Bainun Kampus Sultan Abdul Jalil Shah PustakaTBainun ptbupsi

05-4506832 pustaka.upsi.edu.my Perpustakaan Tuanku Bainun Kampus Sultan Abdul Jalil Shah PustakaTBainun ptbupsi

05-4506832 pustaka.upsi.edu.my Perpustakaan Tuanku Bainun Kampus Sultan Abdul Jalil Shah PustakaTBainun ptbupsi

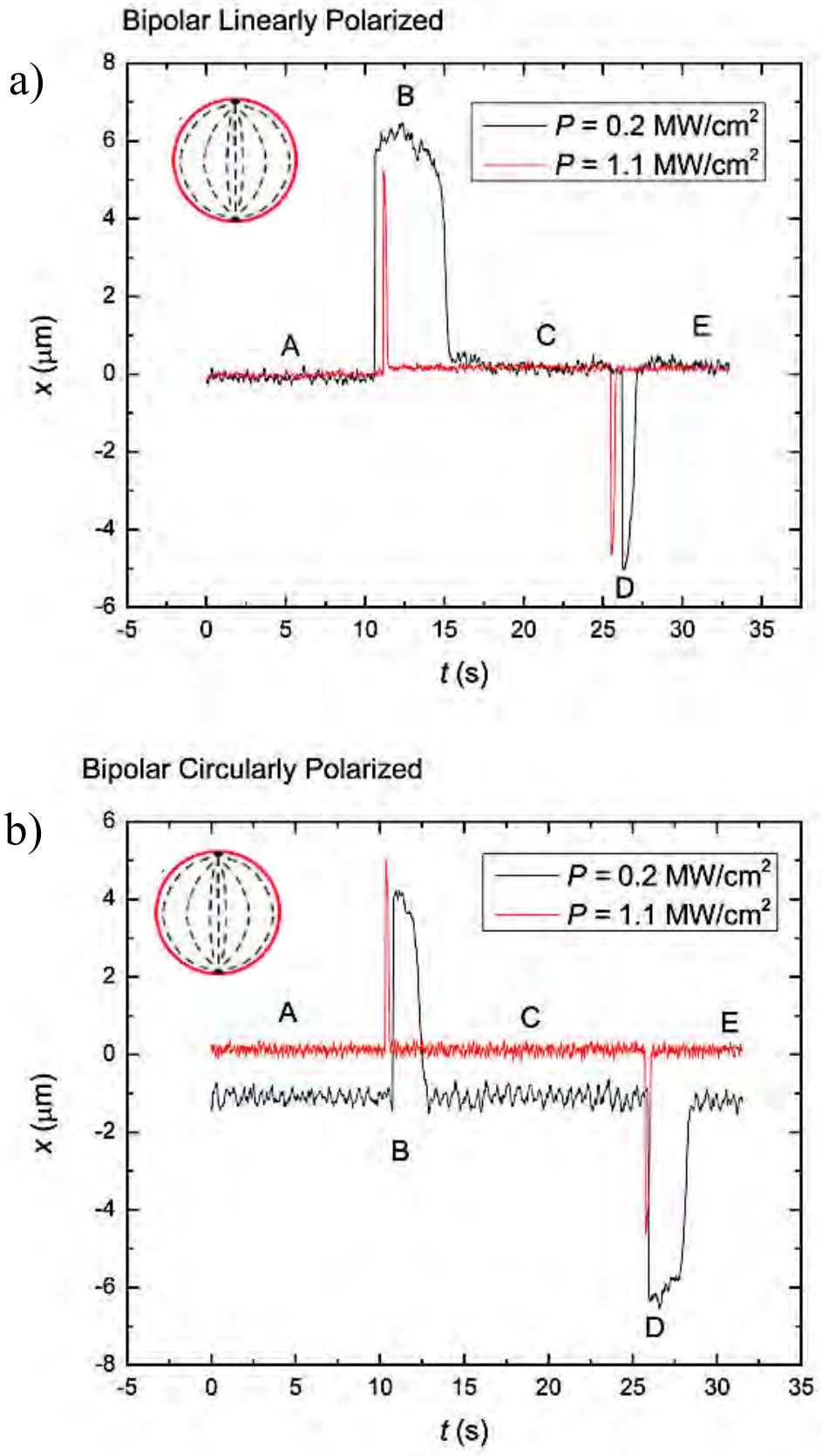
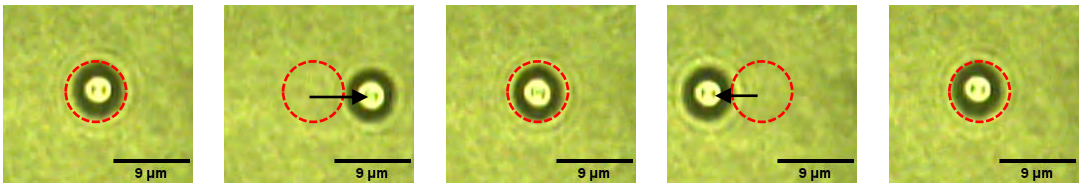


Figure 4.21. (a) The *x*-axis trajectory of the trapped bipolar 5CB microdroplet is in Figure 4.19 and (b) in Figure 4.20.

05-4506832 pustaka.upsi.edu.my Perpustakaan Tuanku Bainun Kampus Sultan Abdul Jalil Shah PustakaTBainun ptbupsi

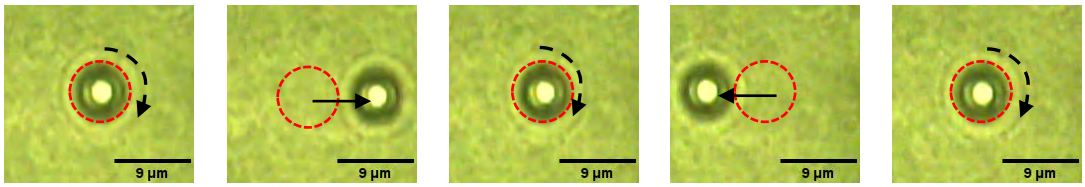
05-4506832 pustaka.upsi.edu.my Perpustakaan Tuanku Bainun Kampus Sultan Abdul Jalil Shah PustakaTBainun ptbupsi

The same procedure was repeated by translating and trapping a 3.3 μm radial 5CB microdroplet with a linearly and circularly polarized laser beam. Figure 4.22 shows the simultaneous translation and micro-control of a single 6.6 μm radial 5CB microdroplet by a linearly polarized laser beam, and Figure 4.23 by a circularly polarized laser beam at 0.2 MW/cm^2. The radial 5CB microdroplet could be translated and micro-controlled stably without escaping, as shown in Figure 29 and Figure 30.



A, t_1 = 1 s B, t_2 = 10 s C, t_3 = 11 s D, t_4 = 25 s E, t_5 = 28 s

Figure 4.22. The translation and micro-control of a single 3.3 μm radial 5CB microdroplet by a linearly polarized laser beam at 0.2 MW/cm^2. A: The 5CB microdroplet was trapped in the optical trap at t_1 = 1 s. B: The 5CB microdroplet translation 5 μm to the right at t_2 = 10 s. C: The 5CB microdroplet retrapped at t_3 = 11 s. D: The 5CB microdroplet translation 5 μm to the left at t_4 = 25 s. E: The 5CB microdroplet retrapped at t_5 = 28 s.



A, t_1 = 1 s B, t_2 = 10 s C, t_3 = 13 s D, t_4 = 25 s E, t_5 = 32 s

Figure 4.23. The translation and micro-control of a single 3.3 μm radial 5CB microdroplet by a circularly polarized laser beam at 0.2 MW/cm^2. A: The 5CB microdroplet was trapped and rotated in the optical trap at t_1 = 1 s. B: The 5CB microdroplet translation 5 μm to the right at t_2 = 10 s. C: The 5CB microdroplet retrapped and rotated at t_3 = 13 s. D: The 5CB microdroplet translation 5 μm to the left at t_4= 25 s. E: The 5CB microdroplet retrapped and rotated at t_5 = 32 s.

Figure 4.24 shows the *x*-axis trajectory of the trapped radial 5CB microdroplet in Figure 4.22 and Figure 4.23 at P = 0.2 and 1.1 MW/cm^2, respectively. Points A, C,

05-4506832 pustaka.upsi.edu.my Perpustakaan Tuanku Bainun Kampus Sultan Abdul Jalil Shah PustakaTBainun ptbupsi

05-4506832 pustaka.upsi.edu.my Perpustakaan Tuanku Bainun Kampus Sultan Abdul Jalil Shah PustakaTBainun ptbupsi

and E show the trajectory of the trapped 5CB microdroplet, while points B and D showed the trajectory when the piezostage displaced the trapped 5CB microdroplet from the trap spot in Figure 4.24 (a). Translating and rotating the trapped 5CB microdroplet's micro-control was possible under a circularly polarized light. The intense laser power caused the strong tweezing and translating of the radial 5CB microdroplet, as shown in Figure 4.24.

05-4506832 pustaka.upsi.edu.my Perpustakaan Tuanku Bainun Kampus Sultan Abdul Jalil Shah PustakaTBainun ptbupsi
05-4506832 pustaka.upsi.edu.my Perpustakaan Tuanku Bainun Kampus Sultan Abdul Jalil Shah PustakaTBainun ptbupsi

05-4506832 pustaka.upsi.edu.my Perpustakaan Tuanku Bainun Kampus Sultan Abdul Jalil Shah PustakaTBainun ptbupsi

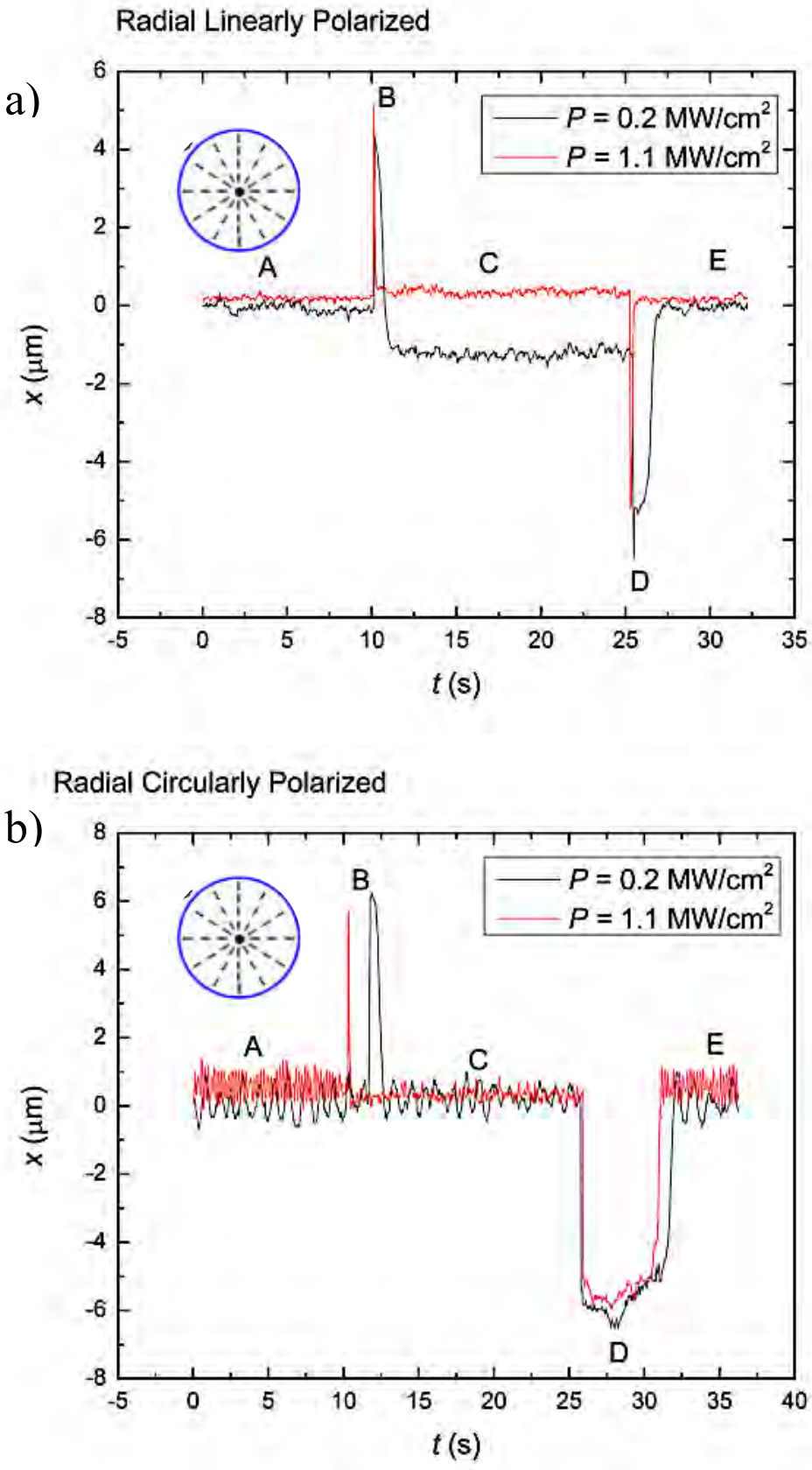


Figure 4.24. (a) The *x*-axis trajectory of the trapped radial 5CB microdroplet is in Figure 4.22 and (b) in Figure 4.23.

05-4506832 pustaka.upsi.edu.my Perpustakaan Tuanku Bainun Kampus Sultan Abdul Jalil Shah PustakaTBainun ptbupsi

05-4506832 pustaka.upsi.edu.my Perpustakaan Tuanku Bainun Kampus Sultan Abdul Jalil Shah PustakaTBainun ptbupsi

These results showed that the simultaneous translation and micro-control of a single 5CB microdroplet (bipolar or radial) could be realized by combining the piezostage positioning and light polarization (linear and circular).

4.7 Corner Frequency (f_c) Analysis

The most vital part of optical trapping is achieving stable trapping, where the trapped particle can be held optically trapped without escape. The optical stiffness (k_T) parameter measures the strength of the optical trap of the optical tweezers and the confinement of the trapped particle inside the trapping spot. f_c values were measured to quantify optical stiffness at specific optical power density (P) to justify the stiffness of the trap. f_c is related to k_T by equation

$$f_c = \frac{k_T}{2\pi\gamma_0} \tag{2.17}$$

where $\gamma_0 = 6\pi\eta r$. Based on the equation, f_c is proportionate to k_T. Calculating the f_c is enough to justify the strength of the confinement of the trapped 5CB microdroplet by the optical tweezers. k_T should be stronger for higher optical power density as long the gradient force is larger than the scattering force.

The dependency of the f_c with P was investigated. A single 5CB microdroplet of bipolar and radial of varied size was trapped by a linearly polarized laser beam at P = 1.1 MW/cm^2, 2.3 MW/cm^2, 3.6 MW/cm^2, 4.8 MW/cm^2, 6.1 MW/cm^2, and 7.3

05-4506832 pustaka.upsi.edu.my Perpustakaan Tuanku Bainun Kampus Sultan Abdul Jalil Shah PustakaTBainun ptbupsi

05-4506832 pustaka.upsi.edu.my Perpustakaan Tuanku Bainun Kampus Sultan Abdul Jalil Shah PustakaTBainun ptbupsi

MW/cm^2. Figure 4.25 shows the graph of corner frequency (f_c) versus optical power density (P) for (a) bipolar 5CB and (b) radial 5CB for several selected sizes. Figure 4.25 (a) and (b) illustrates that f_c increases with an increase of P as in Equation 2.2. The ratio of corner frequency (f_c) per microdroplet radius (r) was calculated to compare f_c of different microdroplet radius, r at different optical power densities, P. The data in Figure 4.25 was replotted in the context of corner frequency per microdroplet radius ($\frac{f_c}{r}$) versus optical power density (P) for (a) bipolar and (b) radial as shown in Figure 4.26.

05-4506832 pustaka.upsi.edu.my Perpustakaan Tuanku Bainun Kampus Sultan Abdul Jalil Shah PustakaTBainun ptbupsi
05-4506832 pustaka.upsi.edu.my Perpustakaan Tuanku Bainun Kampus Sultan Abdul Jalil Shah PustakaTBainun ptbupsi

05-4506832 pustaka.upsi.edu.my Perpustakaan Tuanku Bainun Kampus Sultan Abdul Jalil Shah PustakaTBainun ptbupsi

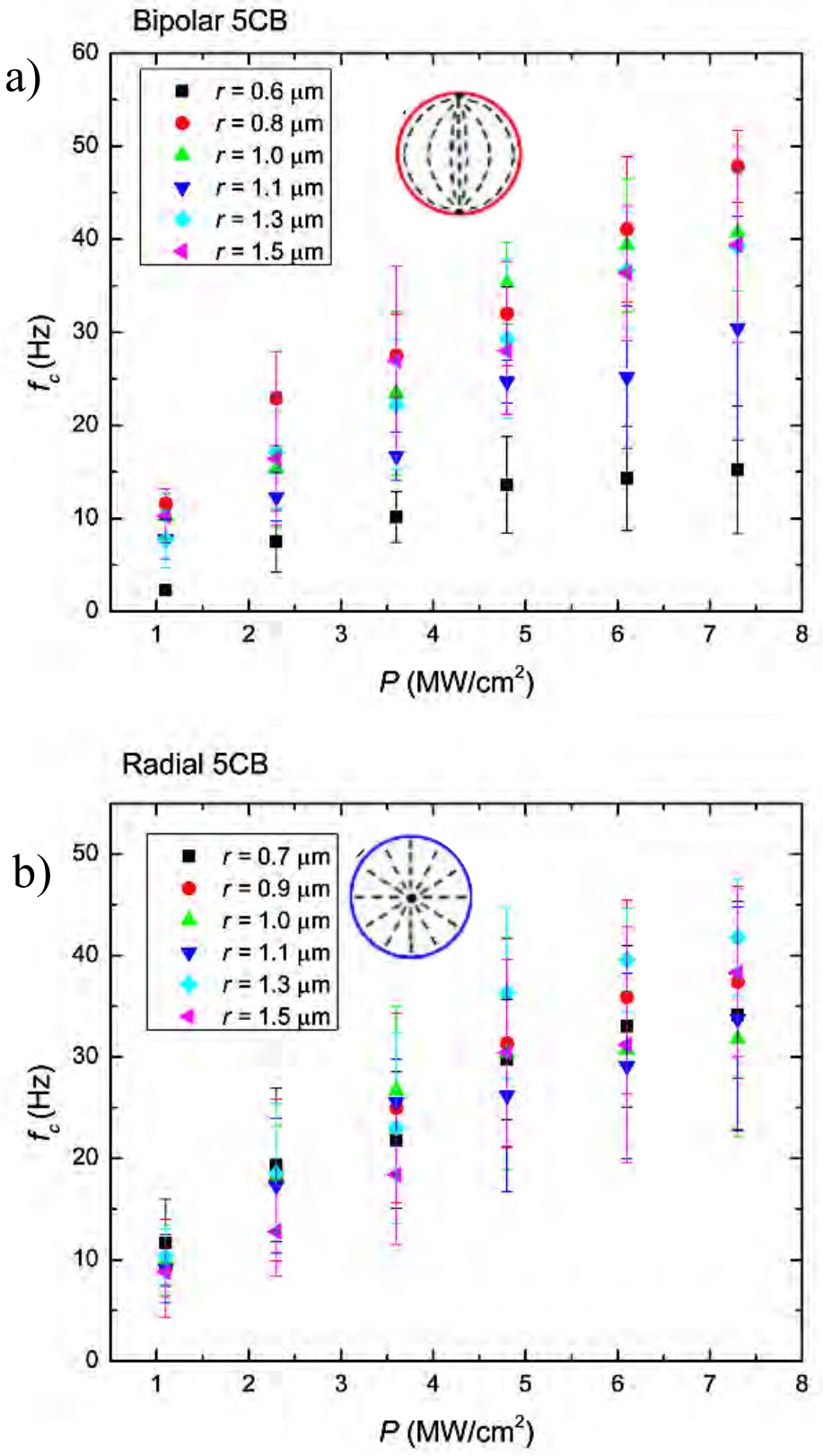


Figure 4.25. Graph of corner frequency (f_c) versus optical power density (P) for (a) bipolar and (b) radial.

05-4506832 pustaka.upsi.edu.my Perpustakaan Tuanku Bainun Kampus Sultan Abdul Jalil Shah PustakaTBainun ptbupsi

05-4506832 pustaka.upsi.edu.my Perpustakaan Tuanku Bainun Kampus Sultan Abdul Jalil Shah PustakaTBainun ptbupsi

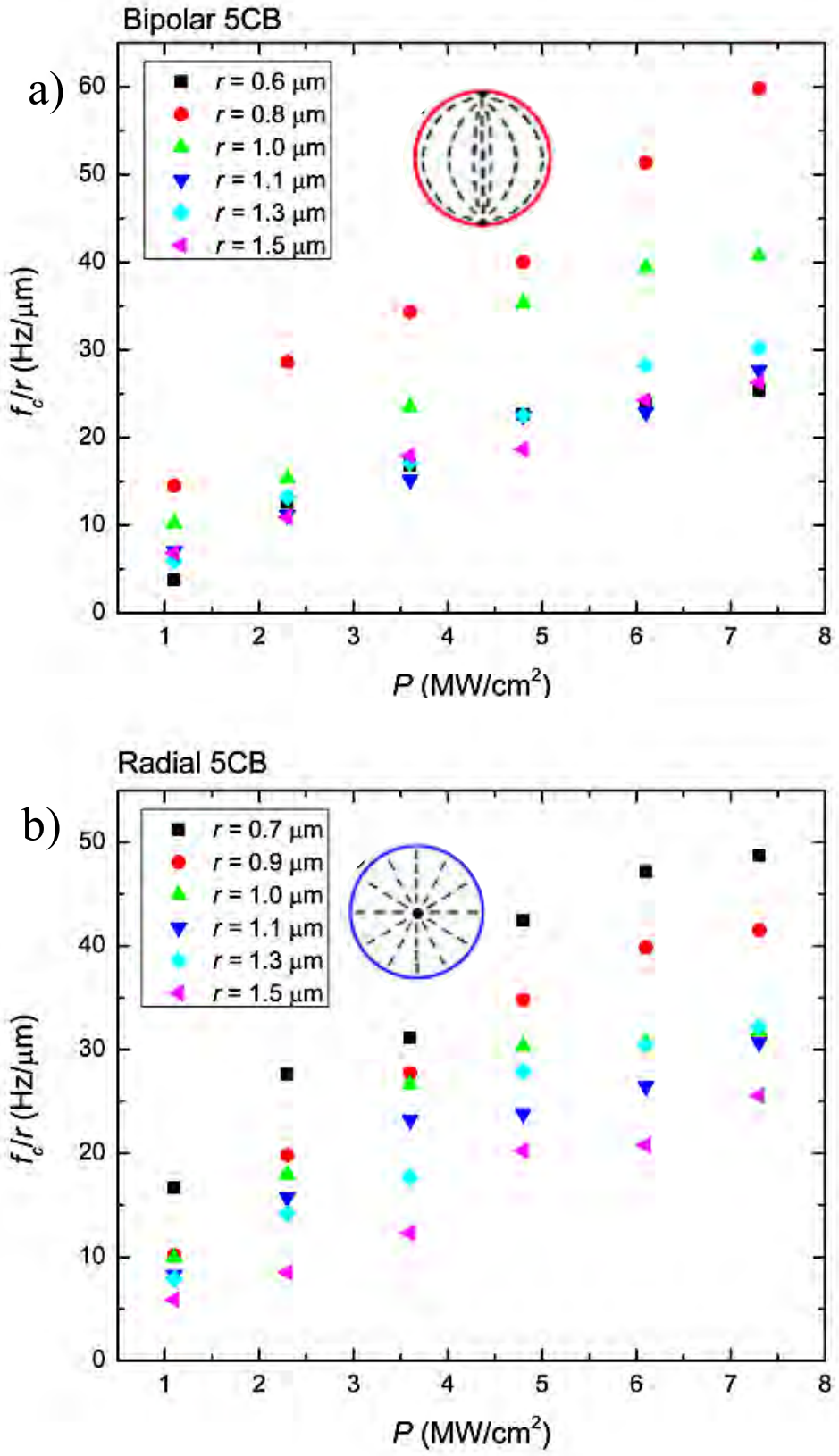


Figure 4.26. Graph of corner frequency per microdroplet radius ($\frac{f_c}{r}$) versus optical power density (P) for (a) bipolar and (b) radial.

05-4506832 pustaka.upsi.edu.my Perpustakaan Tuanku Bainun Kampus Sultan Abdul Jalil Shah PustakaTBainun ptbupsi

05-4506832 pustaka.upsi.edu.my Perpustakaan Tuanku Bainun Kampus Sultan Abdul Jalil Shah PustakaTBainun ptbupsi

For the bipolar 5CB microdroplets, $\frac{f_c}{r}$ was increased with the increasing of the P, as shown in Figure 4.26 (a) for all selected sizes. This showed that k_T was also increased with the increase of the laser power as in Equation 2.17. This means that the confinement of the bipolar 5CB microdroplet inside the optical trap increased when the used P increased (Yeng & Ayop, 2022; Yusuf & Ayop, 2020). Using higher P contributes to the stronger gradient force related in Equation 2.6. The 5CB microdroplet of 0.8 μm radius showed the highest $\frac{f_c}{r}$ indicate the strongest optical stiffness measured. At the same time, the bipolar 5CB microdroplet of 0.6 μm showed the lowest $\frac{f_c}{r}$ indicated the weakest optical stiffness measured.

In the context of 5CB with radial internal configuration, all the selected sizes of the trapped radial 5CB microdroplets showed $\frac{f_c}{r}$ increased with the increase of P used as shown in Figure 4.26 (b). The radial microdroplet of 0.7 μm has the highest $\frac{f_c}{r}$ indicated the stronger optical stiffness measured. Meanwhile, the radial microdroplet of 1.5 μm showed the lowest $\frac{f_c}{r}$ which directly means that the optical trap strength measured was the lowest.

From Figure 4.26, the trend of $\frac{f_c}{r}$ against P was increasing but not linear (Yeng, Ayop, & Mustapa, 2022). This was the novelty of optical stiffness characteristic when the optical trapping of soft matter such as liquid crystal microdroplets was performed. The possible reason for the non-linearity was the physical state of the soft microdroplet (Yusuf & Ayop, 2020). The optical trapping of a solid particle such as a polystyrene bead showed a precise linear trend of $\frac{f_c}{r}$ against P because solid particles (polystyrene

05-4506832 pustaka.upsi.edu.my Perpustakaan Tuanku Bainun Kampus Sultan Abdul Jalil Shah PustakaTBainun ptbupsi

05-4506832 pustaka.upsi.edu.my Perpustakaan Tuanku Bainun Kampus Sultan Abdul Jalil Shah PustakaTBainun ptbupsi

bead) have a rigid form and do not tend to deform during confinement in an optical trap (Horst et al., 2010; Malagnino et al., 2002).

Besides that, the dependency of f_c with r of 5CB microdroplet was also investigated. f_c is related to r by the Equation 2.17. Hence, the f_c should be inversely proportional to r. Figure 4.27 shows the relationship between $\frac{f_c}{r}$ and r of the trapped 5CB microdroplet. The graph of corner frequency per microdroplet radius ($\frac{f_c}{r}$) against microdroplet radius at varied optical power densities for (a) bipolar and (b) radial were shown in Figure 4.27.

05-4506832 pustaka.upsi.edu.my Perpustakaan Tuanku Bainun Kampus Sultan Abdul Jalil Shah PustakaTBainun ptbupsi
05-4506832 pustaka.upsi.edu.my Perpustakaan Tuanku Bainun Kampus Sultan Abdul Jalil Shah PustakaTBainun ptbupsi

05-4506832 pustaka.upsi.edu.my Perpustakaan Tuanku Bainun Kampus Sultan Abdul Jalil Shah PustakaTBainun ptbupsi

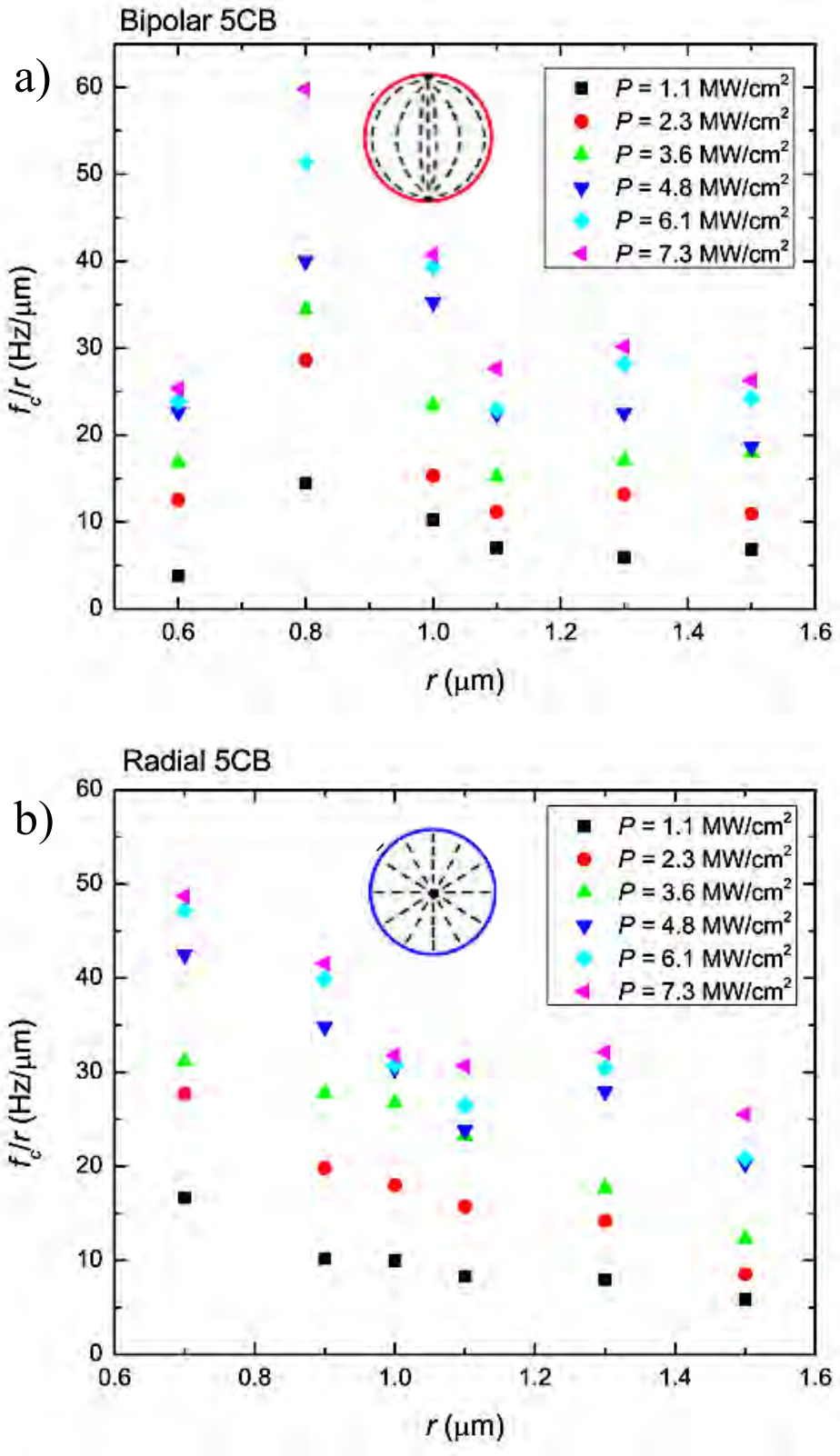


Figure 4.27. Graph of corner frequency per microdroplet radius ($\frac{f_c}{r}$) against microdroplet radius at varied optical power density.

05-45068 upsi
05-4506832 pustaka.upsi.edu.my Perpustakaan Tuanku Bainun Kampus Sultan Abdul Jalil Shah PustakaTBainun ptbupsi

05-4506832 pustaka.upsi.edu.my Perpustakaan Tuanku Bainun Kampus Sultan Abdul Jalil Shah PustakaTBainun ptbupsi

In the context of bipolar 5CB microdroplet, the trend of $\frac{f_c}{r}$ increased from $r = 0.6 \pm 0.1$ µm to 0.8 ± 0.1 µm as shown in Figure 4.27 (a). Then $\frac{f_c}{r}$ trend showed decrement from $r = 0.8 \pm 0.1$ to 1.5 ± 0.1 µm. The smallest $\frac{f_c}{r}$ trend was observed when *P* used was 1.1 MW/cm^2 and the highest $\frac{f_c}{r}$ when *P* used was 7.3 MW/cm^2. For radial 5CB microdroplet, $\frac{f_c}{r}$ showed the reduction trend from $r = 0.7 \pm 0.1$ to 1.5 ± 0.1 µm as shown in Figure 4.27 (b). The highest $\frac{f_c}{r}$ was highlighted when the *P* used was 7.3 MW/cm^2 and the lowest $\frac{f_c}{r}$ when *P* was 1.1 MW/cm^2.

The trend of $\frac{f_c}{r}$ for bipolar and radial 5CB microdroplets in Figures 4.27 (a) and (b) was explained by using ray optics (Mie Regime) to describe the interaction of the gradient force and scattering force on the microdroplet of specific size as shown in Figure 4.28 (Malagnino et al., 2002). This is because, the size of the trapped microdroplet ($r > 1.2 \pm 0.1$ µm) was larger than the trapping laser wavelength (λ =1.0 µm), ($r > \lambda$) (Tsuji et al., 2022).

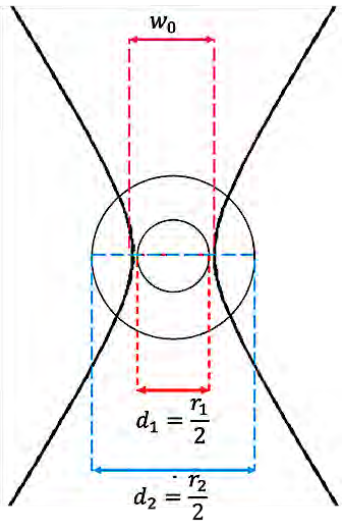


Figure 4.28. The ray optics diagram of laser focus of w_0 beam waist trapped two spheres of diameter d_1 and d_2 (Malagnino et al., 2002).

05-4506832 pustaka.upsi.edu.my Perpustakaan Tuanku Bainun Kampus Sultan Abdul Jalil Shah PustakaTBainun ptbupsi

05-4506832 pustaka.upsi.edu.my Perpustakaan Tuanku Bainun Kampus Sultan Abdul Jalil Shah PustakaTBainun ptbupsi

The laser beam waist (w_0) used in this study was 1.1 µm. Figure 4.28 shows a ray optics diagram of a trapping beam of a specific beam waist w_0, and two spheres of diameter d_1 and d_2 trapped at the center of the trapping beam. As long the gradient force is bigger than the scattering force, the optical trapping is stable (Polimeno et al., 2018). However, the strength of the optical force depends on r. In the case of ($d_1 < w_0$), the gradient force is increasing with r (Simmons et al., 1996). The smaller sphere size has a small surface area exposed to the laser beam. Thus, only a small fraction of light from w_0 refracted on the surface of d_1. The small fraction of refracted light resulted in a smaller gradient force. As a result, small $\frac{f_c}{r}$ was measured. The increasing of size increases the surface area and $\frac{f_c}{r}$ measured for case ($d_1 < w_0$). This explained the $\frac{f_c}{r}$ trend of 0.6 ± 0.1 µm to 0.8 ± 0.1 µm in Figure 4.27 (a).

05-4506832 pustaka.upsi.edu.my Perpustakaan Tuanku Bainun Kampus Sultan Abdul Jalil Shah PustakaTBainun ptbupsi

In the case of ($d \approx w_0$), the gradient force is maximum (Simmons et al., 1996). This is because the whole surface area of the sphere is exposed to the maximum of w_0. This resulted in optimum refraction at the sphere surface and generated optimum gradient force. As a result, the measure $\frac{f_c}{r}$ was maximum. This explained the $\frac{f_c}{r}$ of 0.7 ± 0.1 µm in Figure 4.27 (b). In the case of ($d_2 > w_0$), the gradient force is reduced with the increasing of sphere size (Simmons et al., 1996). The bigger sphere has a larger surface area exposed to the maximum w_0 laser beam. The bigger sphere caused the light to refract and trapped light to spread out over a larger distance, and weakening the gradient force generated (Simmons et al., 1996). At the same time, the increasing of sphere size also adds to the mass of the sphere, which also reduces the gradient force. These factors cause the gradient force to be weaker and the measure $\frac{f_c}{r}$ decreasing over

05-4506832 pustaka.upsi.edu.my Perpustakaan Tuanku Bainun Kampus Sultan Abdul Jalil Shah PustakaTBainun ptbupsi

05-4506832 pustaka.upsi.edu.my Perpustakaan Tuanku Bainun Kampus Sultan Abdul Jalil Shah PustakaTBainun ptbupsi

larger r. This can explain the $\frac{f_c}{r}$ trends for $r = 0.8 \pm 0.1$ μm to 1.5 ± 0.1 μm of bipolar 5CB microdroplet in Figure 4.27 (a), r 0.9 ± 0.1 μm to 1.5 ± 0.1 μm of radial 5CB in Figure 4.27 (b).

The $\frac{f_c}{r}$ of the trapped 5CB microdroplet was compared with chloroform, toluene, and 1,2-dichlorobenzene microdroplet trapping (Yusof et al., 2020) at P = 6.1 to 6.3 MW/cm^2 as listed in Table 4.2.

05-4506832 pustaka.upsi.edu.my Perpustakaan Tuanku Bainun Kampus Sultan Abdul Jalil Shah PustakaTBainun ptbupsi
05-4506832 pustaka.upsi.edu.my Perpustakaan Tuanku Bainun Kampus Sultan Abdul Jalil Shah PustakaTBainun ptbupsi

05-4506832 pustaka.upsi.edu.my Perpustakaan Tuanku Bainun Kampus Sultan Abdul Jalil Shah PustakaTBainun ptbupsi

Table 4.2

Comparison of $\frac{f_c}{r}$ at P = 6.1 to 6.3 MW/cm² for chloroform, toluene, 1,2-dicholorobenzene and 5CB microdroplets.

Chloroform (Yusof et al., 2020).		Toluene (Yusof et al., 2020).		1,2-dichlorobenzene (Yusof et al., 2020).		Bipolar 5CB		Radial 5CB	
r (μm)	$\frac{f_c}{r}$ (Hz/μm)	r (μm)	$\frac{f_c}{r}$ (Hz/μm)	r (μm)	$\frac{f_c}{r}$ (Hz/μm)	r (μm)	$\frac{f_c}{r}$ (Hz/μm)	r (μm)	$\frac{f_c}{r}$ (Hz/μm)
1.00	25.81	1.00	36.43	1.05	46.57	0.60	23.82	0.70	47.17
1.10	21.02	1.05	36.02	1.10	41.25	0.80	51.37	0.90	39.88
1.15	20.84	1.15	28.06	1.15	44.70	1.00	39.34	1.00	30.71
1.25	32.5	1.20	24.33	1.20	39.24	1.10	22.90	1.10	26.46
1.30	14.81	1.25	28.28	1.25	24.27	1.30	28.20	1.30	30.43
1.35	19.68	1.40	16.23	1.30	27.79	1.50	24.24	1.50	20.79
1.45	15.51	1.45	14.92	1.35	31.25				
1.50	10.25	1.50	14.32	1.40	26.72				

(*continue*)

05-4506832 pustaka.upsi.edu.my Perpustakaan Tuanku Bainun Kampus Sultan Abdul Jalil Shah PustakaTBainun ptbupsi

05-4506832 pustaka.upsi.edu.my Perpustakaan Tuanku Bainun Kampus Sultan Abdul Jalil Shah PustakaTBainun ptbupsi

Table 4.2 (*continue*)

Chloroform (Yusof et al., 2020).		Toluene (Yusof et al., 2020).		1,2-dichlorobenzene (Yusof et al., 2020).		Bipolar 5CB		Radial 5CB	
r (μm)	$\frac{f_c}{r}$ (Hz/μm)	r (μm)	$\frac{f_c}{r}$ (Hz/μm)	r (μm)	$\frac{f_c}{r}$ (Hz/μm)	r (μm)	$\frac{f_c}{r}$ (Hz/μm)	r (μm)	$\frac{f_c}{r}$ (Hz/μm)
				1.45	26.40				
				1.50	34.03				
*Average	20.05*		24.82*		35.23*		31.64*		32.58*

05-4506832 pustaka.upsi.edu.my Perpustakaan Tuanku Bainun Kampus Sultan Abdul Jalil Shah PustakaTBainun ptbupsi

05-4506832 pustaka.upsi.edu.my Perpustakaan Tuanku Bainun Kampus Sultan Abdul Jalil Shah PustakaTBainun ptbupsi

05-4506832 pustaka.upsi.edu.my Perpustakaan Tuanku Bainun Kampus Sultan Abdul Jalil Shah PustakaTBainun ptbupsi

Table 4.3.
Comparison of density, refractive index, and solubility of Chloroform, Toluene, 1,2-dichlorobenzene, and 5CB.

Sample	Density (g/cm^3)	Refractive Index	Solubility (g/L)
Chloroform	1.48	1.445	8.7
Toluene	1.31	1.496	0.52
1,2-dichlorobenzene	0.87	1.551	0.13
5CB	1.008	1.54-1.74	0.00007

Based on Table 4.2, the trapping of a single microdroplet at optical power density ~ 6.1 to 6.3 MW/cm^2 for different samples was presented. The signature trapping of a single liquid microdroplet at fixed optical power density showed the variation in $\frac{f_c}{r}$. At fixed optical power density, P, the increasing microdroplet radius showed the variation and scattered in $\frac{f_c}{r}$ trends. Despite that, it was challenging to find the direct relationship between f_c and diameter (D) of the trapped liquid microdroplet (Yusuf & Ayop, 2020). The f_c reported for chloroform, toluene, and 1,2-dichlorobenzene microdroplet optical trapping showed scattered plots and broad range values because the particle is liquid, the shape was not perfectly spherical and caused the variation in the measured f_c and k_T (Yusof et al., 2020). The existing theory assumes that the trapped particle must be solid and perfectly spherical (Simmons et al., 1996). In the context of homogenous liquid microdroplets between chloroform, toluene, and 1,2-dichlorobenzene, 1,2-dichlorobenzene microdroplet trapping shows the highest average $\frac{f_c}{r}$ due to the highest refractive index correlated to the strong gradient force

05-4506832 pustaka.upsi.edu.my Perpustakaan Tuanku Bainun Kampus Sultan Abdul Jalil Shah PustakaTBainun ptbupsi

05-4506832 pustaka.upsi.edu.my Perpustakaan Tuanku Bainun Kampus Sultan Abdul Jalil Shah PustakaTBainun ptbupsi

and strong microdroplet confinement as in Equation 2.6. In comparison with 1,2-dichlorobenzene and 5CB, the average $\frac{f_c}{r}$ was higher for 1,2-dichlorobenzene compared to 5CB despite the small difference in refractive index. However, the possible reason why $\frac{f_c}{r}$ of 1,2-dichlorobenzene highest compared to 5CB was the density of 1,2-dichlorobenzene was lower than 5CB. The lower density reflects the lower mass. The light 1,2-dichlorobenzene microdroplet was more easily confined to the laser spot than the heavy microdroplet.

Even though the trapping of the 1,2-dichlorobenzene shows higher $\frac{f_c}{r}$ than 5CB, 5CB microdroplet has birefringence properties and specific liquid crystal molecule configuration inside the microdroplet, which is not present in 1,2-dichlorobenzene microdroplets (Yeng, Ayop, & Mustapa, 2022). It also noted that bipolar and radial 5CB have different averages $\frac{f_c}{r}$ due to different liquid crystal configurations, which significantly affect $\frac{f_c}{r}$ even though both are the same material. The trapped 5CB microdroplet could be trapped and rotated because the liquid crystal molecules inside the 5CB microdroplet due to the effect of polarization control during the optical trapping process (Murazawa, Juodkazis, Matsuo, et al., 2005). In actuating and sensing applications, the trapping of 5CB microdroplets was superior to other homogenous liquid microdroplets.

4.8 Angular Speed (ω) Analysis

A linearly polarized laser trapping beam carries linear momentum to the trapped 5CB

05-4506832 pustaka.upsi.edu.my Perpustakaan Tuanku Bainun Kampus Sultan Abdul Jalil Shah PustakaTBainun ptbupsi

05-4506832 pustaka.upsi.edu.my Perpustakaan Tuanku Bainun Kampus Sultan Abdul Jalil Shah PustakaTBainun ptbupsi

microdroplet. Using a quarter wave plate changes the linearly polarized laser beam to the circularly polarized one. This circularly polarized laser beam carries angular momentum. The angular momentum of the circularly polarized laser beam can be transferred to the trap 5CB microdroplet during the optical trapping process. Due to the fact that the 5CB microdroplet is a birefringence material, the angular momentum of the circularly polarized laser beam was transferred to the 5CB microdroplet. The angular momentum transfer to the 5CB microdroplet resulted in an optical torque. This optical torque produce rotates the 5CB microdroplet, and the light that passes through the 5CB microdroplet converts back to the linearly polarized laser beam. The equation can relate the optical torque resulting from the trapped 5CB microdroplet-induced rotation

$$\Gamma = D\omega \tag{2.20}$$

05-4506832 pustaka.upsi.edu.my Perpustakaan Tuanku Bainun Kampus Sultan Abdul Jalil Shah PustakaTBainun ptbupsi

where Γ is optical torque, D is the rotational drag coefficient (Stoke's coefficient) $D = 8\pi\eta r^3$ where η is liquid viscosity, r is microdroplet radius, and ω is angular speed. The final expression becomes

$$\Gamma = 8\pi\eta r^3\omega \tag{2.21}$$

The optical torque increased with the increasing optical power density used. The angular speed of the rotating microdroplet is inversely proportional to the radius of the rotating trapped microdroplet.

Next, the angular speed (ω) of the trapped 5CB microdroplet under a circularly polarized laser beam was studied. A single 5CB microdroplet (bipolar or radial) of varied sizes was trapped and rotated clockwise and counterclockwise by the circularly

05-4506832 pustaka.upsi.edu.my Perpustakaan Tuanku Bainun Kampus Sultan Abdul Jalil Shah PustakaTBainun ptbupsi

05-4506832 pustaka.upsi.edu.my Perpustakaan Tuanku Bainun Kampus Sultan Abdul Jalil Shah PustakaTBainun ptbupsi

polarized laser beam at P = 1.1, 1.6, 2.0, 2.5, 2.9, and 3.4 MW/cm^2. The ω of the rotated 5CB microdroplet was measured by analyzing the QPD signal collected during the rotation. The relationship between optical power density used (P), microdroplet radius (r), and angular speed of rotated microdroplets (ω) was investigated.

The relationship between ω and P is shown in Figure 4.29. Figure 4.29 shows the graph of angular speed (ω) versus optical power density (P) of clockwise rotation (a) bipolar 5CB microdroplet and (b) radial 5CB microdroplet. In the context of bipolar 5CB, ω of the bipolar 5CB microdroplet showed an increasing trend with the increase of P, as illustrated in Figure 4.29 (a). The radial 5CB microdroplet showed the same trend in Figure 4.29 (b).

05-4506832 pustaka.upsi.edu.my Perpustakaan Tuanku Bainun Kampus Sultan Abdul Jalil Shah PustakaTBainun ptbupsi
05-4506832 pustaka.upsi.edu.my Perpustakaan Tuanku Bainun Kampus Sultan Abdul Jalil Shah PustakaTBainun ptbupsi

05-4506832 pustaka.upsi.edu.my Perpustakaan Tuanku Bainun Kampus Sultan Abdul Jalil Shah PustakaTBainun ptbupsi

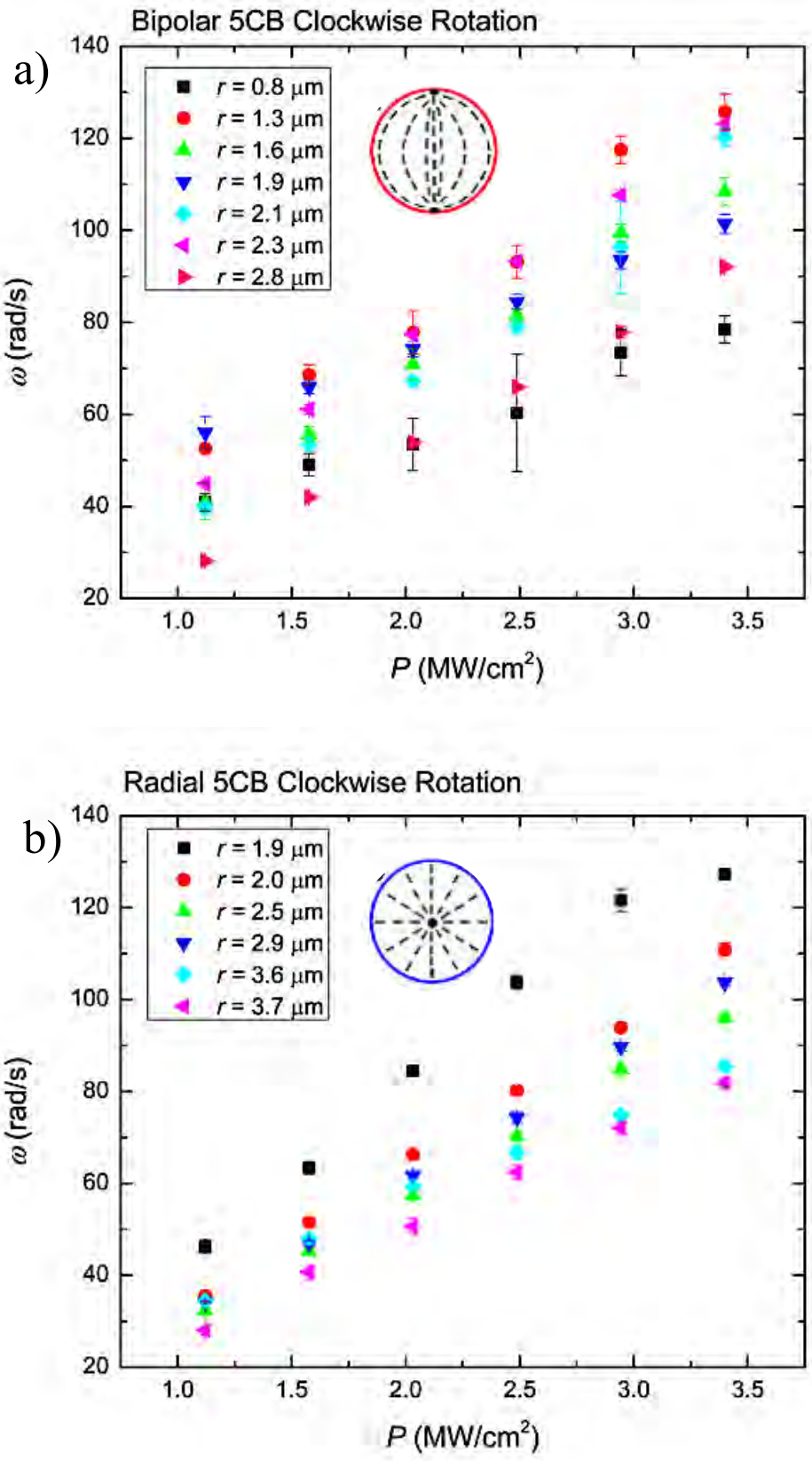


Figure 4.29. Graph of angular speed (ω) versus optical power density (P) of clockwise rotation for (a) bipolar 5CB and (b) radial 5CB microdroplets.

05-4506832 pustaka.upsi.edu.my Perpustakaan Tuanku Bainun Kampus Sultan Abdul Jalil Shah PustakaTBainun ptbupsi

05-4506832 pustaka.upsi.edu.my Perpustakaan Tuanku Bainun Kampus Sultan Abdul Jalil Shah PustakaTBainun ptbupsi

The ratio between angular speed per microdroplet radius ($\frac{\omega}{r}$) was calculated to compare at different P used. Then the graph of angular speed per microdroplet radius $\frac{\omega}{r}$ versus optical power density (P) of clockwise rotation for (a) bipolar 5CB and (b) radial 5CB was plotted based on Figure 4.30. In the context of a bipolar 5CB microdroplet trapped under a circularly polarized laser beam, the $\frac{\omega}{r}$ showed an increasing trend with the increasing P as shown in Figure 4.30 (a). The $\frac{\omega}{r}$ decreased with the increasing bipolar 5CB microdroplet size (r). The smallest bipolar 5CB microdroplet of 0.8 μm trapped and rotated under a circularly polarized laser beam showed the highest $\frac{\omega}{r}$. Meanwhile, the largest bipolar 5CB microdroplet of 2.8 μm radius showed the least $\frac{\omega}{r}$. It is noted that bipolar 5CB microdroplets can be trapped and rotated at a smaller radius of 0.8 μm. The bipolar 5CB microdroplet with a radius below 0.8 μm can be trapped. However, the rotating behavior is difficult to observe visually via a CCD camera. This is the limited resolution of the objective lens ~ 500 nm. The QPD signal also could not show the rotational signal of the trapped 5CB microdroplet. This is because the laser spot is bigger than the trapped microdroplet radius. The rotational of a small 5CB microdroplet inside the big focal spot does not change the laser intensity detected by the QPD. Hence, no rotational signal is observable.

On the other hand, the $\frac{\omega}{r}$ of the radial 5CB microdroplet increased with the increasing of P as shown in Figure 4.30 (b). It could be seen from Figure 4.30 (b), that the $\frac{\omega}{r}$ of radial 5CB microdroplets decreased with the increase of the microdroplet radius (r). The smallest radial 5CB microdroplet of 1.9 μm radius was trapped under a

05-4506832 pustaka.upsi.edu.my Perpustakaan Tuanku Bainun Kampus Sultan Abdul Jalil Shah PustakaTBainun ptbupsi

05-4506832 pustaka.upsi.edu.my Perpustakaan Tuanku Bainun Kampus Sultan Abdul Jalil Shah PustakaTBainun ptbupsi

circularly polarized laser beam and showed the highest $\frac{\omega}{r}$. In this study, the radial 5CB microdroplet of radius less than 1.9 μm did not rotate in our experiment with optical power density used. The possible reason why the radial 5CB microdroplet does not rotate at lower optical power density is because of small birefringence due to the radial structure; thus, the mechanism of angular momentum was different from the bipolar 5CB microdroplet (Murazawa, Juodkazis, Matsuo, et al., 2005). It is possible to rotate the small microdroplet, but it requires a very strong optical power density. It was reported that radial 5CB microdroplet rotated at higher laser power because the higher laser power causes the reconfiguration of the liquid crystal molecules because the light polarization electric field is strong enough to overcome viscoelastic and elastic forces of the liquid crystal molecules (Murazawa, Juodkazis, Matsuo, et al., 2005). Hence, the reconfiguration of liquid crystal molecules inside radial 5CB microdroplet induced birefringence and caused it to be rotated at higher laser power (Murazawa, Juodkazis, Matsuo, et al., 2005). However, strong optical power density is not recommended as the 5CB is a thermotropic liquid crystal sensitive to heat change when intense laser-induced heat. Meanwhile, the largest radial 5CB microdroplet of 3.7 μm radius showed the lowest $\frac{\omega}{r}$ trends. This is following the fact that the ω is inversely proportional to r as in Equation 2.21. The strong optical power density used drives the faster angular speed of the rotated 5CB microdroplet as in Equation 2.22.

05-4506832 pustaka.upsi.edu.my Perpustakaan Tuanku Bainun Kampus Sultan Abdul Jalil Shah PustakaTBainun ptbupsi

05-4506832 pustaka.upsi.edu.my Perpustakaan Tuanku Bainun Kampus Sultan Abdul Jalil Shah PustakaTBainun ptbupsi

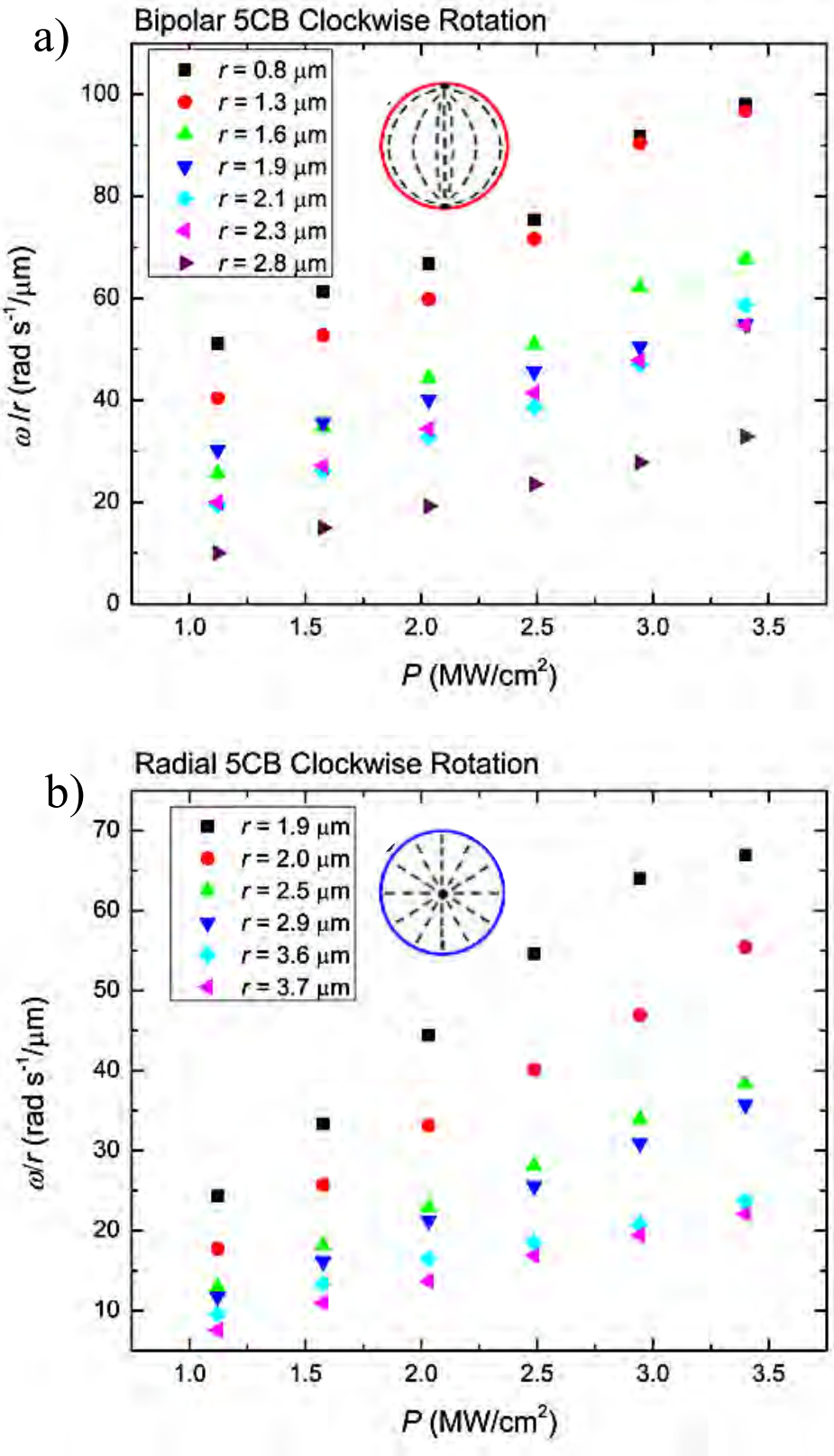


Figure 4.30. Graph of angular speed per microdroplet radius ($\frac{\omega}{r}$) versus optical power density (P) of clockwise rotation for (a) bipolar 5CB and (b) radial 5CB microdroplets.

05-4506832 pustaka.upsi.edu.my Perpustakaan Tuanku Bainun Kampus Sultan Abdul Jalil Shah PustakaTBainun ptbupsi

05-4506832 pustaka.upsi.edu.my Perpustakaan Tuanku Bainun Kampus Sultan Abdul Jalil Shah PustakaTBainun ptbupsi

Furthermore, the 5CB microdroplet could also be rotated counterclockwise by optical tweezers. The relationship between angular speed (ω) and the optical power density (P) is shown in Figure 4.31. Figure 4.31 shows the graph of angular speed (ω) versus optical power density (P) of counterclockwise rotation for (a) bipolar 5CB and (b) radial 5CB microdroplets. In the context of bipolar 5CB counterclockwise rotation, the angular speed of the bipolar 5CB microdroplet, ω, showed an increasing trend with the increasing optical power density (P), as shown in Figure 4.31 (a). This implies that the optical torque increased with the optical laser power used. As a result, the faster angular speed was obtained at a higher optical power density. Meanwhile, in the context of radial 5CB microdroplet, ω showed a similar trend of increasing when the optical power density (P) used was increased, as shown in Figure 4.31 (b).

05-4506832 pustaka.upsi.edu.my Perpustakaan Tuanku Bainun Kampus Sultan Abdul Jalil Shah PustakaTBainun ptbupsi
05-4506832 pustaka.upsi.edu.my Perpustakaan Tuanku Bainun Kampus Sultan Abdul Jalil Shah PustakaTBainun ptbupsi

05-4506832 pustaka.upsi.edu.my Perpustakaan Tuanku Bainun Kampus Sultan Abdul Jalil Shah PustakaTBainun ptbupsi

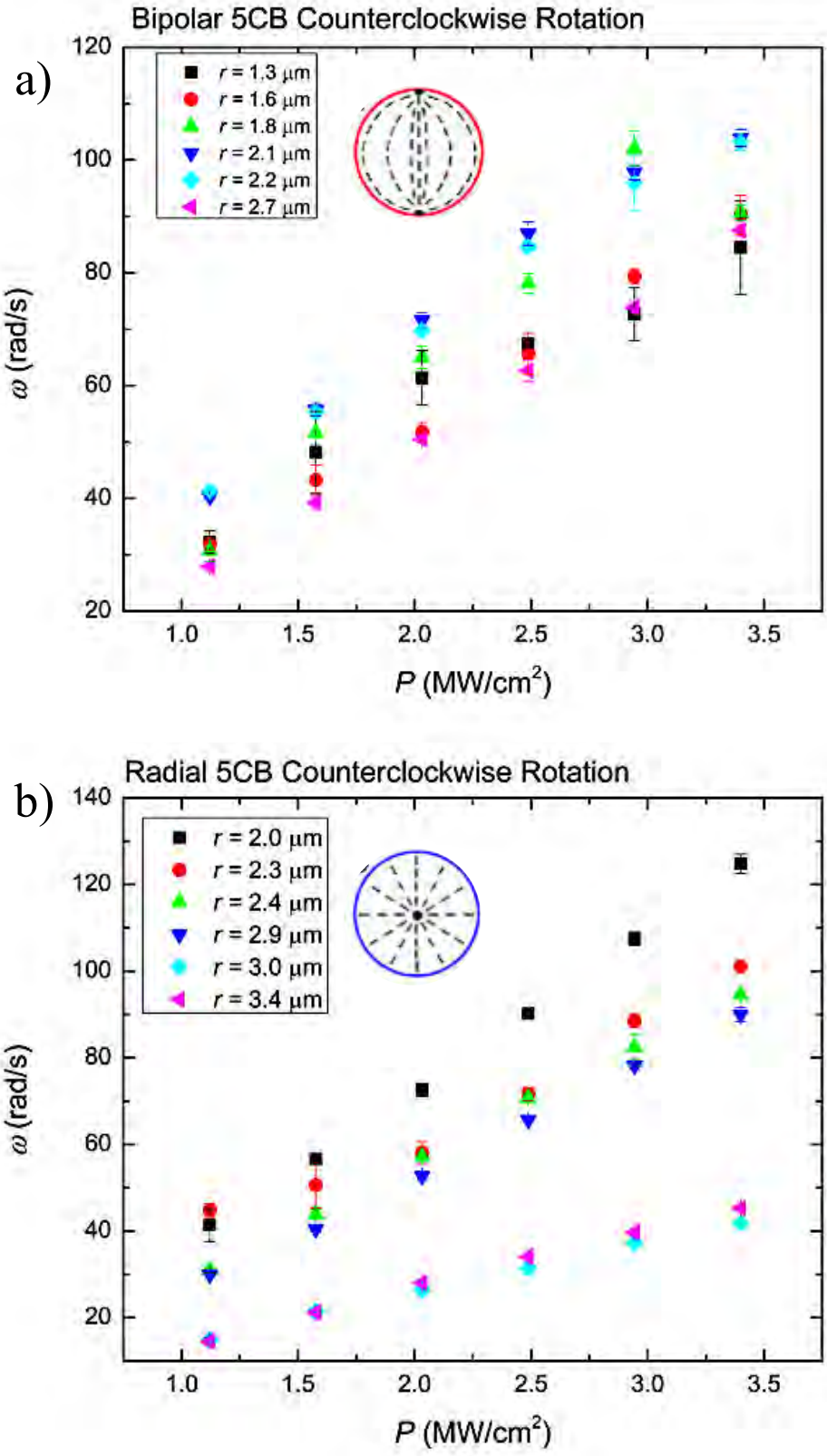


Figure 4.31. Graph of angular speed (ω) versus optical power density (P) of counterclockwise rotation for (a) bipolar 5CB and (b) radial 5CB microdroplets.

05-4506832 pustaka.upsi.edu.my Perpustakaan Tuanku Bainun Kampus Sultan Abdul Jalil Shah PustakaTBainun ptbupsi

05-4506832 pustaka.upsi.edu.my Perpustakaan Tuanku Bainun Kampus Sultan Abdul Jalil Shah PustakaTBainun ptbupsi

Next, the angular speed ratio per microdroplet radius was calculated to make a comparison between ω with microdroplets of different sizes. The graph in Figure 4.31 is replotted in the context of angular speed per microdroplet radius ($\frac{\omega}{r}$) against the optical power density used (P). Figure 4.32 shows the graph of angular speed per microdroplet radius ($\frac{\omega}{r}$) versus optical power density (P) of clockwise rotation for (a) bipolar 5CB and (b) radial 5CB microdroplets. In the context of bipolar 5CB counterclockwise rotation, the trend of $\frac{\omega}{r}$ showed that it increases with the increasing optical power density. It can be seen from Figure 4.32 (a) that the smallest bipolar 5CB microdroplet of 1.3 μm radius shows the highest $\frac{\omega}{r}$ of counterclockwise rotation. This implied that the optical torque on the 1.3 μm bipolar 5CB microdroplet was strongest when the strong optical power density was used. The strong optical produces faster rotation of the trapped bipolar 5CB microdroplet as represented by 1.3 μm bipolar 5CB microdroplet. Meanwhile, the largest bipolar 5CB microdroplet trapped was 2.7 μm showed the lowest $\frac{\omega}{r}$ trend. This implied that the optical torque induced on the 2.7 μm bipolar 5CB microdroplet was small. Small optical torque resulted in the slower rotation of the trapped bipolar 5CB microdroplet. In terms of bipolar 5CB microdroplet radius, it could be highlighted that $\frac{\omega}{r}$ significantly reduced with the increasing microdroplet radius. This means that the optical torque becomes smaller on the bigger microdroplet, thus reducing the capability to rotate the trapped 5CB microdroplet.

In the context of radial 5CB microdroplet, the $\frac{\omega}{r}$ trend was increased when the optical power density (P) used increased, as illustrated in Figure 4.32 (b). It could be seen from Figure 4.32 (b), that the $\frac{\omega}{r}$ trend was highest when the trapped radial 5CB

05-4506832 pustaka.upsi.edu.my Perpustakaan Tuanku Bainun Kampus Sultan Abdul Jalil Shah PustakaTBainun ptbupsi

05-4506832 pustaka.upsi.edu.my Perpustakaan Tuanku Bainun Kampus Sultan Abdul Jalil Shah PustakaTBainun ptbupsi

microdroplet used was 2.0 µm. This implied that the optical torque produced on the 2.0 µm radial 5CB microdroplet increased as the optical power density used to rotate increased. As a result, the larger optical torque produced a faster rotation of the trapped 2.0 µm radial 5CB microdroplet. Meanwhile, the largest radial 5CB microdroplet radius, 3.4 µm, showed the lowest $\frac{\omega}{r}$ trend, as illustrated in Figure 4.32 (b). This indicated that the optical torque imposed due to the circularly polarized laser beam was smaller. The smaller optical torque resulted in the slower rotation of the 3.4 µm radial 5CB microdroplet. It also noted that the $\frac{\omega}{r}$ significantly decreased with increasing the radial 5CB microdroplet radius. The significant increase of the radial 5CB microdroplet also directly increased the mass of the radial 5CB microdroplet. The optical torque can substantially affect the lighter radial 5CB microdroplet compared to the weighter microdroplet. Thus, the smaller radial microdroplet feels a strong optical torque and rotates faster than the larger one.

05-4506832 pustaka.upsi.edu.my Perpustakaan Tuanku Bainun Kampus Sultan Abdul Jalil Shah PustakaTBainun ptbupsi

05-4506832 pustaka.upsi.edu.my Perpustakaan Tuanku Bainun Kampus Sultan Abdul Jalil Shah PustakaTBainun ptbupsi

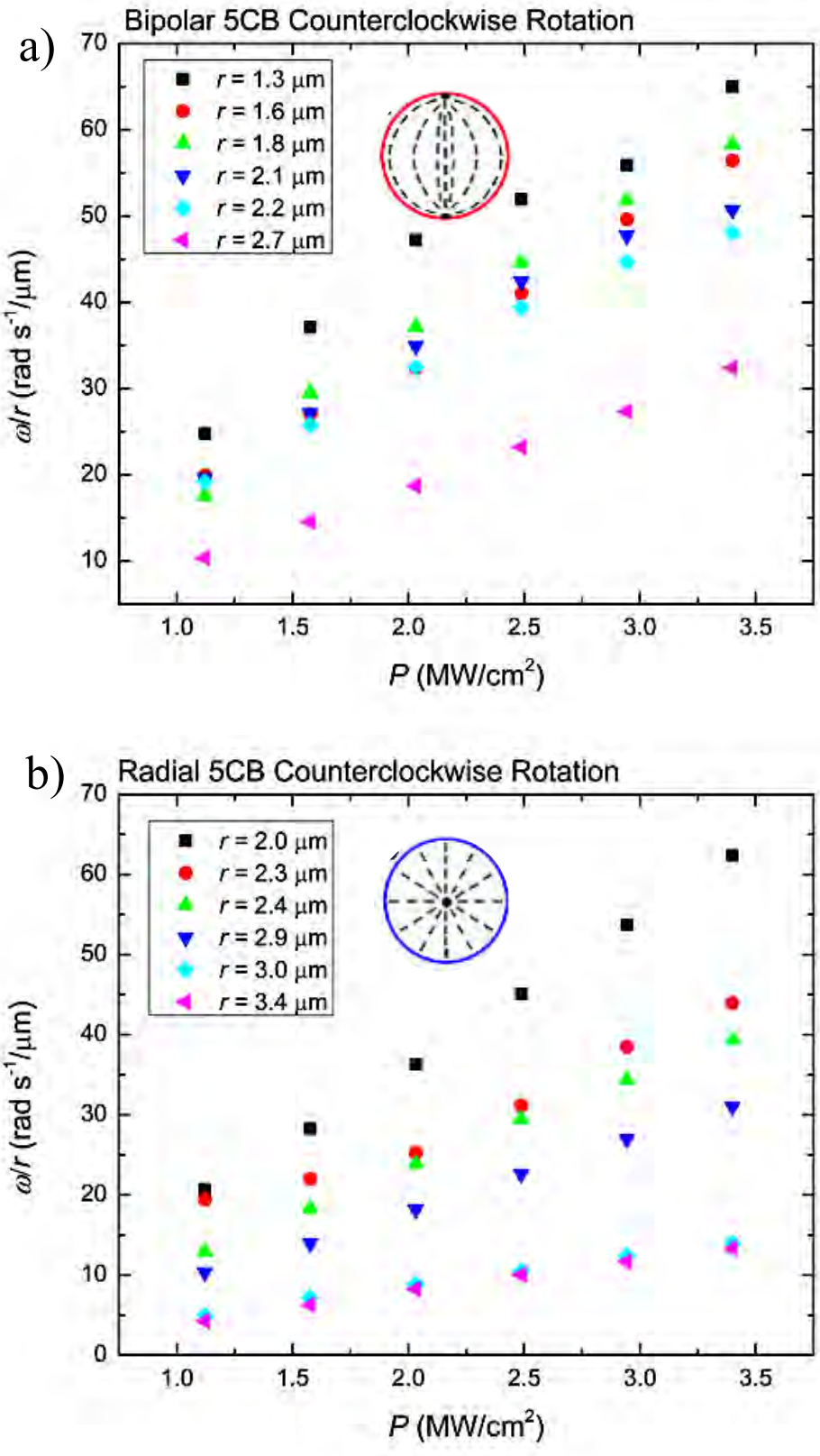


Figure 4.32. Graph of angular speed per microdroplet radius ($\frac{\omega}{r}$) versus optical power density (P) of clockwise rotation for (a) bipolar 5CB and (b) radial 5CB microdroplets.

05-4506832 pustaka.upsi.edu.my Perpustakaan Tuanku Bainun Kampus Sultan Abdul Jalil Shah PustakaTBainun ptbupsi

05-4506832 pustaka.upsi.edu.my Perpustakaan Tuanku Bainun Kampus Sultan Abdul Jalil Shah PustakaTBainun ptbupsi

The $\frac{\omega}{r}$ values obtained from this study are compared with the previous study from Murazawa and friends (Murazawa, Juodkazis, & Misawa, 2005). The $\frac{\omega}{r}$ values are compared in terms of laser power (P) and the size of the 5CB microdroplet trapped and rotated under a circularly polarized laser beam. Table 4.4 shows the comparison of laser power (P), microdroplet radius (r), and angular speed per microdroplet radius ($\frac{\omega}{r}$) for bipolar 5CB microdroplet. According to Table 4.4, it can be seen that the experimental value of $\frac{\omega}{r}$ obtained from the study show the same trend where $\frac{\omega}{r}$ increasing with the laser power used P as reported by (Murazawa, Juodkazis, & Misawa, 2005). This is because the increase in laser power used creates an increase in gradient force, as in Equation 2.6. The increase in gradient force significantly increased the optical torque because optical torque is related to the gradient force by expression $\Gamma = F_g \times r$. The increase in optical torque increases the angular speed of the rotated bipolar 5CB microdroplet, as in Equation 2.20. The bipolar 5CB microdroplet rotated at the small threshold laser power because of significant birefringence (Murazawa, Juodkazis, Matsuo, et al., 2005). It can also be highlighted that the experimental values of $\frac{\omega}{r}$ decrease with the increasing microdroplet radius (r) reported by Murazawa, as shown in Table 4.4. This study provided significant information that the lower laser power (P = 10.65 mW) can establish the rotation of the small bipolar 5CB microdroplet of 0.8 μm radius. Meanwhile, Murazawa reported the rotation of a small bipolar 5CB microdroplet of 0.95 μm radius at a laser power of 31.03 mW. This study showed that the laser power could be reduced by about 65.68 % to rotate the small 5CB microdroplet, resulting in higher $\frac{\omega}{r}$. The lowest laser power used is significant in the optical trapping of 5CB microdroplets to reduce the laser heating effect and sustain the nematic phase of the trapped bipolar 5CB microdroplet.

05-4506832 pustaka.upsi.edu.my Perpustakaan Tuanku Bainun Kampus Sultan Abdul Jalil Shah PustakaTBainun ptbupsi

05-4506832 pustaka.upsi.edu.my Perpustakaan Tuanku Bainun Kampus Sultan Abdul Jalil Shah PustakaTBainun ptbupsi

Table 4.4

Comparison of $\frac{\omega}{r}$ for bipolar 5CB reported by Murazawa and this study.

Bipolar 5CB Microdroplet (Murazawa, Juodkazis, & Misawa, 2005)						Bipolar 5CB Microdroplet (Study results)					
r = 0.95 µm		r = 1.25 µm		r = 1.60 µm		r = 0.80 µm		r = 1.30 µm		r = 1.60 µm	
P (mW)	$\frac{\omega}{r}$ (Hz/µm)	P (mW)	$\frac{\omega}{r}$ (Hz/µm)	P (mW)	$\frac{\omega}{r}$ (Hz/µm)	P (mW)	$\frac{\omega}{r}$ (Hz/µm)	P (mW)	$\frac{\omega}{r}$ (Hz/µm)	P (mW)	$\frac{\omega}{r}$ (Hz/µm)
31.03	39.16	29.12	22.69	31.08	11.99	10.65	51.14	10.65	40.46	10.65	25.68
62.07	75.64	62.40	50.52	63.19	23.39	14.98	61.33	14.98	52.76	14.98	34.76
124.14	170.08	185.08	138.29	123.28	47.17	19.31	66.78	19.31	59.82	19.31	44.31
187.24	226.93	247.46	184.74	186.50	75.92	23.64	75.40	23.64	71.65	23.64	50.96
249.31	310.63	309.83	225.06	248.63	94.34	27.96	91.84	27.96	90.41	27.96	62.15
309.31	378.20	348.25	237.63	308.71	113.54	32.29	98.07	32.29	96.74	32.29	67.74
346.55	440.24			347.03	126.34						

05-4506832 pustaka.upsi.edu.my Perpustakaan Tuanku Bainun Kampus Sultan Abdul Jalil Shah PustakaTBainun ptbupsi

05-4506832 pustaka.upsi.edu.my Perpustakaan Tuanku Bainun Kampus Sultan Abdul Jalil Shah PustakaTBainun ptbupsi

Table 4.5

Comparison of $\frac{\omega}{r}$ for radial 5CB reported by Murazawa and this study.

Radial 5CB Microdroplet (Murazawa, Juodkazis, & Misawa, 2005)						Radial 5CB Microdroplet (Study results)					
r = 2.40 µm		r = 2.70 µm		r = 3.35 µm		r = 1.90 µm		r = 2.00 µm		r = 2.50 µm	
P (mW)	$\frac{\omega}{r}$ (Hz/µm)	P (mW)	$\frac{\omega}{r}$ (Hz/µm)	P (mW)	$\frac{\omega}{r}$ (Hz/µm)	P (mW)	$\frac{\omega}{r}$ (Hz/µm)	P (mW)	$\frac{\omega}{r}$ (Hz/µm)	P (mW)	$\frac{\omega}{r}$ (Hz/µm)
341.10	44.23	309.28	29.00	248.84	16.35	10.65	23.34	10.65	17.76	10.65	12.91
372.66	45.21	341.36	30.38	279.16	17.25	14.98	33.34	14.98	25.75	14.98	18.16
402.94	46.34	370.38	31.51	310.74	17.24	19.31	44.46	19.31	33.13	19.31	22.95
433.26	46.20	401.97	30.89	342.32	17.34	23.64	54.61	23.64	40.13	23.64	28.07
464.84	46.34	433.52	32.02	372.63	17.63	27.96	64.01	27.96	46.95	27.96	33.91
		465.08	32.52	406.74	18.03	32.29	66.96	32.29	55.45	32.29	38.41
				435.79	18.22						
				467.37	19.22						

05-4506832 pustaka.upsi.edu.my Perpustakaan Tuanku Bainun Kampus Sultan Abdul Jalil Shah PustakaTBainun ptbupsi

05-4506832 pustaka.upsi.edu.my Perpustakaan Tuanku Bainun Kampus Sultan Abdul Jalil Shah PustakaTBainun ptbupsi

The radial 5CB microdroplet $\frac{\omega}{r}$ values were also compared with the $\frac{\omega}{r}$ reported by Murazawa and friends. The comparison between findings from this study was compared with Murazawas' findings in terms of laser power (P), microdroplet radius (r), and angular speed per microdroplet radius ($\frac{\omega}{r}$) as illustrated in Table 4.5. This research finding shows that the radial 5CB microdroplet $\frac{\omega}{r}$ increases with the laser power (P) as shown in Table 4.5. The similar trend of the radial 5CB microdroplet $\frac{\omega}{r}$ reported by Murazawa also shows similar trends as shown in Table 4.5. The increasing trends of $\frac{w}{r}$ contributed to the increase in of laser power. The optical torque is proportional to the laser power by Equation 2.22. The increase in optical torque significantly increased the angular speed because of proportionality related to Equation 2.20. It also can be seen that the research finding highlights that the $\frac{\omega}{r}$ decreased with the increasing of the radial 5CB microdroplet radius (r), as shown in Table 4.5. The trend of the $\frac{\omega}{r}$ was supported by the Murazawa finding where the $\frac{\omega}{r}$ reduces with the increasing of the microdroplet radius (r). It could be seen that the threshold laser power to rotate the 5CB radial microdroplet was relatively higher than the bipolar 5CB microdroplet. This study traps a single radial 5CB microdroplet of 1.90 μm radius at the lowest laser power of 10.65 mW. However, Murazawa reported that to rotate a single radial 5CB microdroplet of 2.40 μm radius, the laser power used was 341 mW. It can be seen that Murazawa used extreme laser power to rotate a 2.40 μm radial 5CB microdroplet. Our study used a relatively lower laser power, 10.65 mW, to successfully rotate a single radial 5CB microdroplet. We reported the highest ($\frac{\omega}{r}$) radial 5CB microdroplet at the lowest laser power and smaller radial 5CB microdroplet radius. We reduced the laser power used to rotate radial 5CB microdroplets to about 96.9%.

05-4506832 pustaka.upsi.edu.my Perpustakaan Tuanku Bainun Kampus Sultan Abdul Jalil Shah PustakaTBainun ptbupsi

05-4506832 pustaka.upsi.edu.my Perpustakaan Tuanku Bainun Kampus Sultan Abdul Jalil Shah PustakaTBainun ptbupsi

It can also be highlighted that the threshold laser power to initiate the rotation of bipolar and radial 5CB microdroplets showed a significant difference. This can be proved by trapping and rotating the same 5CB microdroplet while triggering the internal configurational change inside the microdroplet. In this study, the radial 5CB microdroplet of size less than 1.90 µm at 1.1 MW/cm^2 did not rotate in Figure 4.30 (b), but the bipolar 5CB microdroplet rotated at size less than 1.90 µm in Figure 4.30 (a). This highlights the significance difference in threshold laser power because of the birefringence difference between bipolar and radial 5CB (Murazawa, Juodkazis, Matsuo, et al., 2005). The bipolar 5CB microdroplet rotates at smaller laser power and the smaller bipolar 5CB microdroplet rotates faster at higher laser power. The radial 5CB microdroplet has different threshold laser power to initiate the rotation of the microdroplet. The radial 5CB microdroplet requires the highest laser power to initiate the rotation (Murazawa, Juodkazis, & Misawa, 2005). The smallest radial 5CB microdroplet requires the highest laser power to initiate the rotation of more than 310 mW (Murazawa, Juodkazis, & Misawa, 2005). This is why the smaller radial 5CB microdroplet of less than 1.90 µm radius does not rotate at the lower laser power range used in this study. One should note that the bipolar 5CB microdroplet rotated at lower laser power, and the radial 5CB microdroplet rotated at higher laser power. This unique characteristic can be used as the indicator for sensing as the configurational change affects the rotated microdroplet's angular speed.

05-4506832 pustaka.upsi.edu.my Perpustakaan Tuanku Bainun Kampus Sultan Abdul Jalil Shah PustakaTBainun ptbupsi

05-4506832 pustaka.upsi.edu.my Perpustakaan Tuanku Bainun Kampus Sultan Abdul Jalil Shah PustakaTBainun ptbupsi

4.9 Trapped 5CB Microdroplet Sensing Mechanism

The interaction between the 5CB microdroplet and CTAB molecules was studied. The dispersion of the liquid 5CB in water produces microdroplets in the water. Naturally, in the water, the 5CB microdroplet acquired a spherical shape due to the surface tension of the water. The liquid 5CB dispersed in deionized water usually produced a 5CB microdroplet with a bipolar internal configuration, known as the stable state of the nematic phase. In the bipolar state, the liquid crystal molecules inside the microdroplet aligned parallel to the surface of the microdroplet. Figure 4.33 shows the interaction and the effect of the addition of CTAB solution on the internal configuration inside the 5CB microdroplet.

05-4506832 pustaka.upsi.edu.my Perpustakaan Tuanku Bainun Kampus Sultan Abdul Jalil Shah PustakaTBainun ptbupsi

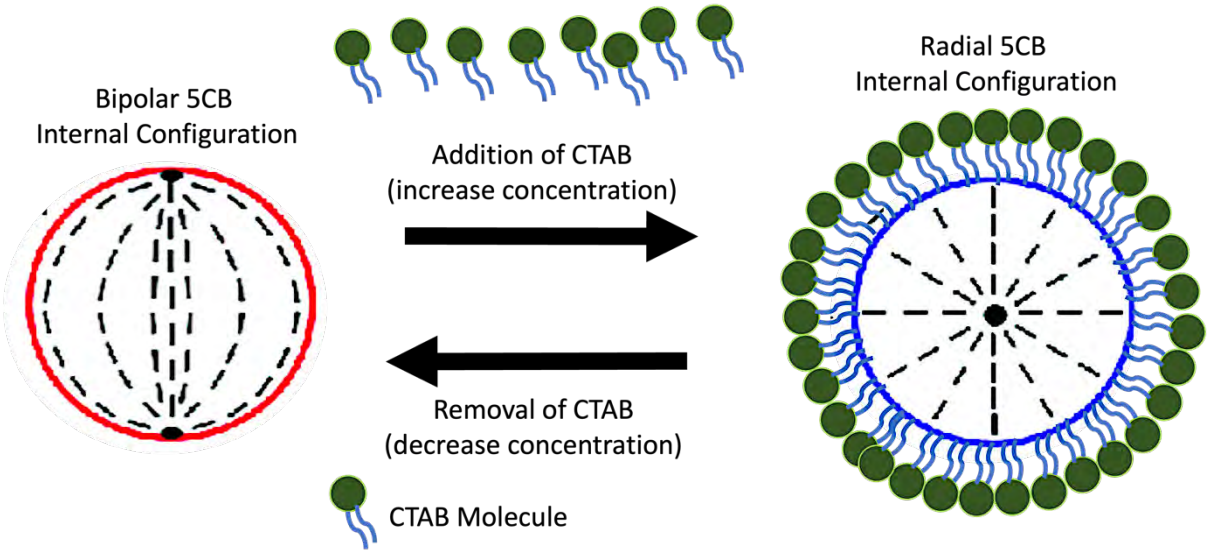


Figure 4.33. The schematic mechanism of the interaction between the 5CB microdroplet with the CTAB molecules and the effect on the internal configuration inside the microdroplet.

05-4506832 pustaka.upsi.edu.my Perpustakaan Tuanku Bainun Kampus Sultan Abdul Jalil Shah PustakaTBainun ptbupsi

05-4506832 pustaka.upsi.edu.my Perpustakaan Tuanku Bainun Kampus Sultan Abdul Jalil Shah PustakaTBainun ptbupsi

CTAB is a kind of surfactant that is usually used to alter the internal configuration of the liquid crystal microdroplet. CTAB molecules generally comprise a round hydrophilic polar head and a hydrophobic polar tail. The CTAB naturally exists as a white powder dissolved in water to form a CTAB solution. The concentration of the CTAB solution can be controlled by adjusting the mass of the CTAB powder dissolved in the water. The CTAB solution must achieve critical micelle concentration (CMC) to transition the internal configuration inside the 5CB microdroplet. It was reported that CTAB needs about 13 μM of CMC concentration to cause bipolar internal configuration change to the radial internal configuration in a microdroplet (Murazawa, Juodkazis, & Misawa, 2005). Introducing the CTAB solution to the 5CB microdroplet exposes the CTAB molecules in the environment medium, for example, water. CTAB solution slowly diffuses in the water environment, causing the CTAB molecules to disperse in the water medium.

The 5CB microdroplet suspended in water interacts with CTAB molecules when both components are in contact. The CTAB molecules tend to bind and adhere to the surface of the 5CB microdroplet due to the long hydrophobic tail leading to the formation of the CTAB-bind 5CB surface. At the same time, the interface of the 5CB microdroplet was sensitive to the chemical reaction on its surface when the CTAB molecules bind with 5CB. The binding of the CTAB molecules on the 5CB microdroplet surface causes the initial bipolar configuration to reconfigure and rearrange to form a radial internal configuration. This was when the CTAB molecule was introduced to the 5CB microdroplet suspended in the water. The bipolar internal configuration transition to the radial internal configuration can be reversible. The removal of the CTAB molecules bound on the surface of the 5CB microdroplet can

05-4506832 pustaka.upsi.edu.my Perpustakaan Tuanku Bainun Kampus Sultan Abdul Jalil Shah PustakaTBainun ptbupsi

05-4506832 pustaka.upsi.edu.my Perpustakaan Tuanku Bainun Kampus Sultan Abdul Jalil Shah PustakaTBainun ptbupsi

cause the radial internal configuration inside the microdroplet to change to a bipolar internal configuration. This process requires the existence of the CTAB solution to be reduced below the CMC values or removed the CTAB solution. The simplest way to remove the CTAB molecules was to flush a constant deionized water flow. Other than that, it is also possible to remove the CTAB molecules by introducing another molecule to the environment, for example, glucose, cholic acid, and others. These molecules compete with the CTAB molecules on the 5CB microdroplet surface and replace them. Even though optical microscopy cannot see the molecules of the CTAB and the exact arrangement of liquid crystal molecules, this limitation can be overcome by using a cross-polarization view and introducing the lasing technique. This study quantifies the internal configuration change inside the 5CB microdroplet by introducing optical trapping and interpreting the optical signal resulting from the trapping of the 5CB microdroplet. This study is significant in verifying that the optical trapping signal could be used to transduce the transitional change inside the 5CB microdroplet quantitatively and empirically.

4.9.1 5CB Microdroplet CTAB Sensing

Besides, the optical force change during the transition change of the internal configuration inside a single trapped 5CB microdroplet by a linearly polarized laser beam was studied. The schematic diagram of 5CB interaction with the CTAB is summarized in Figure 4.33. In this study, the sensing mechanism was based on the transition change of the internal configuration of the trapped 5CB microdroplet from bipolar to radial. This mechanism was observable under visual observation of a cross-

05-4506832 pustaka.upsi.edu.my Perpustakaan Tuanku Bainun Kampus Sultan Abdul Jalil Shah PustakaTBainun ptbupsi

05-4506832 pustaka.upsi.edu.my Perpustakaan Tuanku Bainun Kampus Sultan Abdul Jalil Shah PustakaTBainun ptbupsi

polarized view and the scattered optical trapping signal. In general, exposing the single trapping 5CB to CTAB solution triggers the 5CB molecules inside the to rearrange from the bipolar configuration, which is represented by the red sphere, to the radial configuration, which is represented by the blue sphere as shown in Figure 4.33. The attachment of the CTAB molecules on the surface of the trapped 5CB microdroplet was responsible for the configurational change observed.

A single 5CB microdroplet having a bipolar internal configuration was initially trapped and observed under optical microscopy and cross-polarization. The initial internal configuration image was snapped, and the QPD signal was recorded. At t =1 minute, two drops of CTAB solution (10^{-3}g/mL) were dropped at the edge of the cover glass (refer to Figure 3.76) containing the trap bipolar 5CB. The internal configuration change of the trapped 5CB microdroplet was monitored until it wholly changed from bipolar to radial configuration because the detection requires the transition to change to the stable state (bipolar to radial). Figure 4.34 shows the transition sequence change of the bipolar 5CB microdroplet to the radial internal configuration of 1.4 μm trapped at 0.2 MW/cm^2 linearly polarized laser beam.

05-4506832 pustaka.upsi.edu.my Perpustakaan Tuanku Bainun Kampus Sultan Abdul Jalil Shah PustakaTBainun ptbupsi

05-4506832 pustaka.upsi.edu.my Perpustakaan Tuanku Bainun Kampus Sultan Abdul Jalil Shah PustakaTBainun ptbupsi

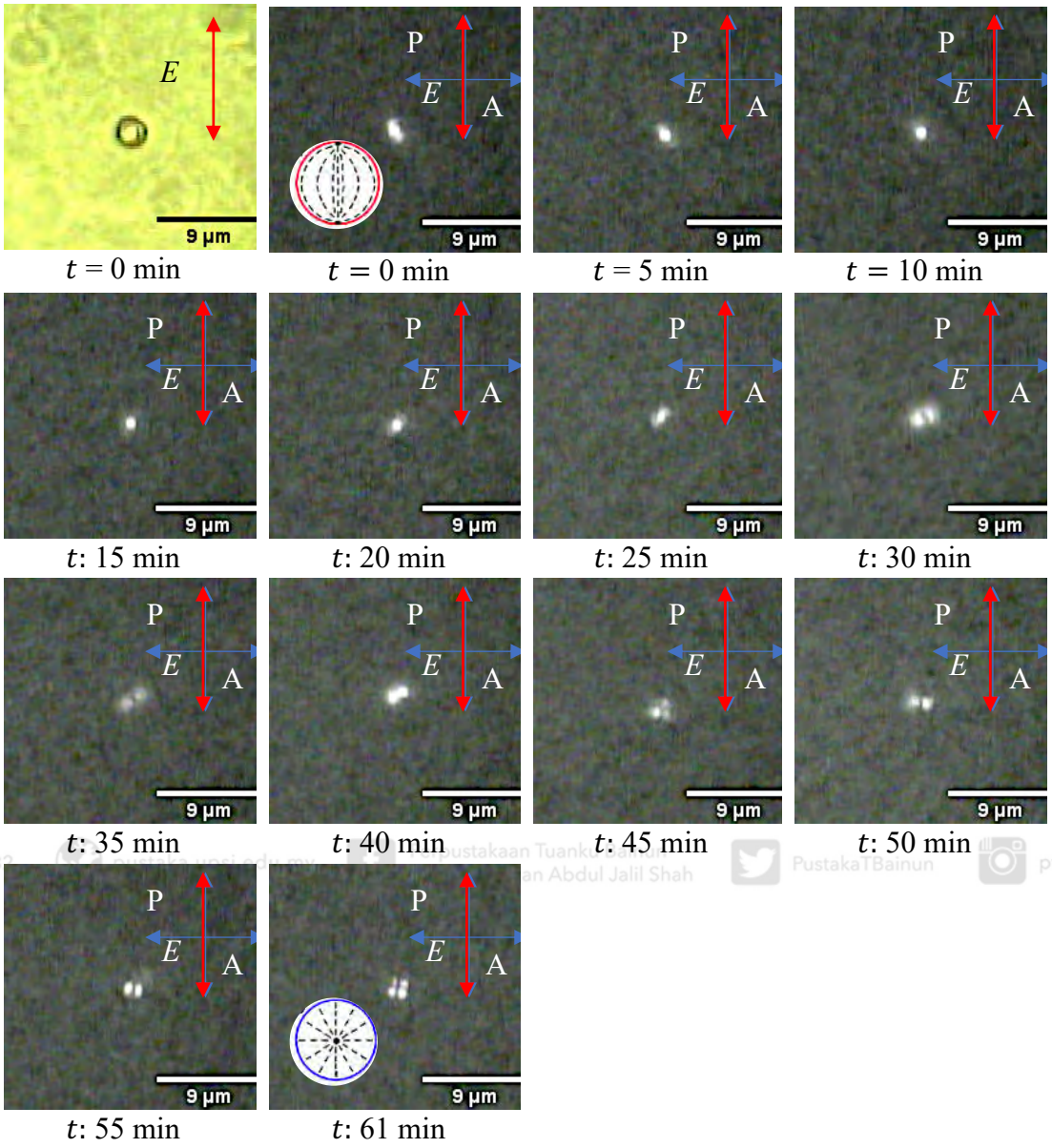


Figure 4.34. The transition sequence changed of the bipolar 5CB microdroplet to the radial internal configuration of 1.4 µm trapped at 0.2 MW/cm^2 linearly polarized laser beam.

Based on Figure 4.34, at t = 0 min, the initial internal configuration of the trapped 5CB microdroplet was in a bipolar state. The 10 µL of CTAB was directly introduced to the trapped bipolar 5CB microdroplet to allow interaction of CTAB molecule attach to the 5CB microdroplet surface at t = 1 minute. The cross-polarization view images of the trapped bipolar 5CB microdroplet were monitored, and the QPD

05-4506832 pustaka.upsi.edu.my Perpustakaan Tuanku Bainun Kampus Sultan Abdul Jalil Shah PustakaTBainun ptbupsi

05-4506832 pustaka.upsi.edu.my Perpustakaan Tuanku Bainun Kampus Sultan Abdul Jalil Shah PustakaTBainun ptbupsi

signal was recorded for more than 1-hour to ensure bipolar 5CB completely changed to radial. At t = 40 minutes, the trapped bipolar 5CB microdroplet started to change to the radial configuration, as shown in Figure 4.34. The Maltese cross structure was formed at $t = 61$ minutes, indicating that the trapped bipolar 5CB microdroplet has wholly changed to the radial configuration, as shown in Figure 4.34. The corresponding QPD signal based on Figure 4.34 is shown in Figure 4.35. The QPD signal recorded the trajectory of the trapped 5CB microdroplet until it completely changed to radial configuration. The trajectory data was used to calculate the displacement variance (σ^2) of the trapped 5CB microdroplet, representing the confinement of the trapped particle due to the optical force. The small σ^2 indicated the strong confinement of the optical force as related by Equation 2.11. When the CTAB molecules are attached to the surface of the bipolar 5CB microdroplet, it triggers the 5CB molecules inside the microdroplet to change to radial configuration—the change in the internal configuration change in the effective refractive index (ordinary refractive index, n_0: 1.54 and extraordinary refractive index, n_e:1.74) of the 5CB microdroplet (Niu et al., 2016). Since the refractive index affects the optical force, the change in bipolar to radial configuration directly can be transduced to an optical signal. Figure 4.35 shows the graph of displacement variance versus time of 1.4 μm bipolar 5CB microdroplet trapped by a linearly polarized laser beam at 0.2 MW/cm^2.

05-4506832 pustaka.upsi.edu.my Perpustakaan Tuanku Bainun Kampus Sultan Abdul Jalil Shah PustakaTBainun ptbupsi

05-4506832 pustaka.upsi.edu.my Perpustakaan Tuanku Bainun Kampus Sultan Abdul Jalil Shah PustakaTBainun ptbupsi

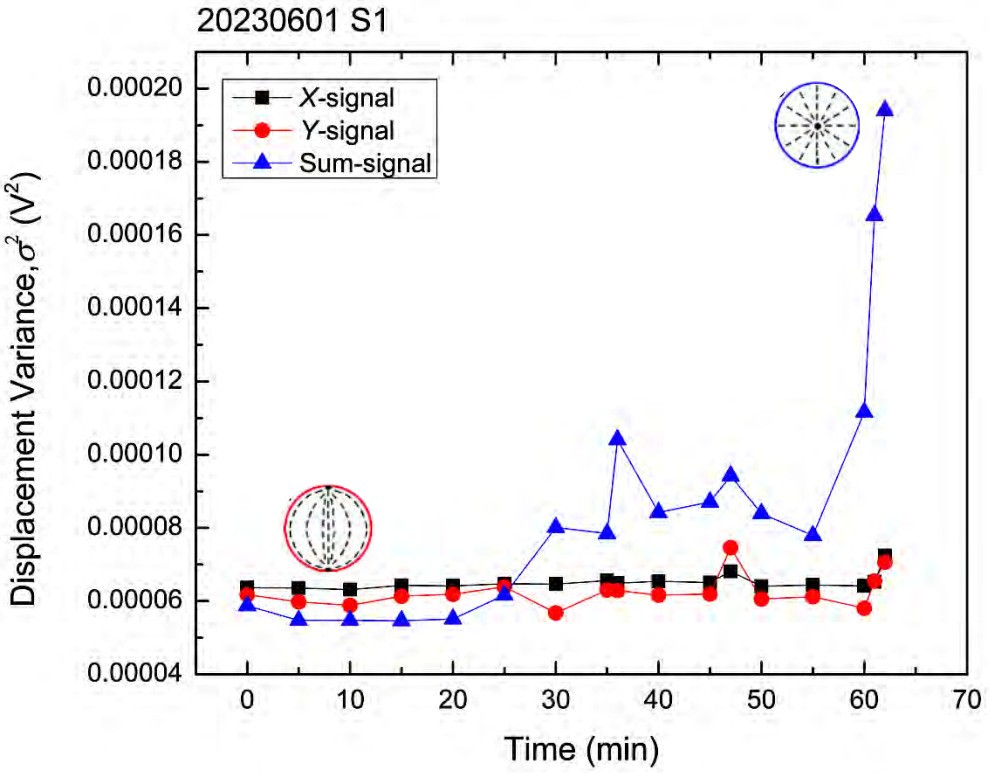


Figure 4.35. Graph of displacement variance (σ^2) versus time of 1.4 µm bipolar 5CB microdroplet trapped by a linearly polarized laser beam at 0.2 MW/cm^2.

Figure 4.35 shows the *x*-signal, *y*-signal, and *sum*-signal of the calculated σ^2 based on the trajectory of the trapped 5CB microdroplet. The signals were stable from t = 0 minutes until 25 minutes, as shown in Figure 4.35. The signal was stable due to the small amount of CTAB molecules attached to the bipolar 5CB microdroplet, which was not enough to change the internal configuration inside the microdroplet to become radial. At t = 30 minutes until 60 minutes, the fluctuation of the signals was observed in Figure 4.35 due to CTAB molecules attached to the 5CB microdroplet starting to change the internal configuration inside the trapped microdroplet corresponding to an internal configurational change from t = 30 minutes to t = 60 minutes in Figure 4.34. The CTAB molecule's hydrophobic part binds and adsorbs on the surface of the 5CB microdroplet, while the hydrophilic part is exposed to water as illustrate in Figure 4.33.

05-4506832 pustaka.upsi.edu.my Perpustakaan Tuanku Bainun Kampus Sultan Abdul Jalil Shah PustakaTBainun ptbupsi

05-4506832 pustaka.upsi.edu.my Perpustakaan Tuanku Bainun Kampus Sultan Abdul Jalil Shah PustakaTBainun ptbupsi

The binding of CTAB molecules disrupts the delicate balance of anchoring energy and bulk elastic energy of 5CB microdroplets that keep bipolar configuration and cause it to be triggered to radial configuration (Popov et al., 2017). Table 4.6 shows the displacement variance of *x*, *y*, and *sum* signals at a particular time. The signal was highest when t = 61 minutes, indicating that the trapped bipolar 5CB microdroplet has entirely changed to the radial configuration. The signals were highest when the trapped 5CB microdroplet was in a radial state compared to the bipolar state. This indicated that the σ^2 of the trapped 5CB microdroplet in the radial state is higher than the initial bipolar state, which is lower as shown in Table 4.6. This indirectly implied that the optical force was smaller in a radial state than in a bipolar state. It was reported that the experimental birefringence (Δn) of bipolar and radial 5CB microdroplets was 0.04 ± 0.01 and 0.022 ± 0.015, respectively (Murazawa, Juodkazis, & Misawa, 2005). Since the birefringence is related to the refractive index of the 5CB, and the refractive index is related to the gradient force of the laser beam by Equation 2.6. It was expected that bipolar 5CB microdroplets would experience a stronger gradient force compared to radial 5CB microdroplets. This hypothesis is in alignment with the reported results as shown in Table 4.6 where σ^2 of *x*, *y* and *sum*-signals were smaller for bipolar compared to radial 5CB microdroplets.

Table 4.6
Displacement variance (σ^2) at a particular time.

Time (min)	Displacement Variance (σ^2/V^2)		
	x-signal	*y*-signal	*sum*-signal
0	6.37×10^{-5}	6.17×10^{-5}	5.87×10^{-5}
61	6.53×10^{-5}	6.55×10^{-5}	1.65×10^{-4}

This showed that the optical signal of the trapped 5CB microdroplet could be

05-4506832 pustaka.upsi.edu.my Perpustakaan Tuanku Bainun Kampus Sultan Abdul Jalil Shah PustakaTBainun ptbupsi

05-4506832 pustaka.upsi.edu.my Perpustakaan Tuanku Bainun Kampus Sultan Abdul Jalil Shah PustakaTBainun ptbupsi

used to transduce the sensing mechanism of the 5CB microdroplet and CTAB molecules.

In conclusion, exposing the CTAB solution to the trapped 5CB microdroplet caused the internal configuration change from bipolar to radial for 1 hour of monitoring time. This change was observed under the cross-polarized view in Figure 4.35, starting from a bright spot into the Maltase-cross pattern. The change in Figure 4.35 was quantified by monitoring the σ^2 change in Figure 4.36 and σ^2 was smaller for bipolar and bigger for radial 5CB microdroplets. This highlights that σ^2 was a significant characteristic signal for liquid crystal-based sensors by applying optical trapping of 5CB microdroplet.

05-4506832 pustaka.upsi.edu.my Perpustakaan Tuanku Bainun Kampus Sultan Abdul Jalil Shah PustakaTBainun ptbupsi

4.10 Summary

In conclusion, the findings showed that the size distribution of the 5CB microdroplets decreased with sonication time; it also stables and sustains within 1-hour of monitoring time. The 5CB microdroplet could be trapped linearly and rotated using a circularly polarized laser beam, enabling linear translation and micro-control in combination with a piezostage system. It was found that the corner frequency (f_c) and angular frequency (ω) showed an increasing trend with the increase of power density (P). Exposing CTAB solution to trapped 5CB microdroplets changes the internal configuration from bipolar to radial. This study implies that single optical trapping of 5CB microdroplets in water can be used for prospective actuating and sensing

05-4506832 pustaka.upsi.edu.my Perpustakaan Tuanku Bainun Kampus Sultan Abdul Jalil Shah PustakaTBainun ptbupsi

05-4506832 pustaka.upsi.edu.my Perpustakaan Tuanku Bainun Kampus Sultan Abdul Jalil Shah PustakaTBainun ptbupsi

applications.

Optical manipulation of 5CB microdroplets has huge potential in actuating and sensing applications. The actuating application required the control probe to perform a mechanical work or movements. The optical manipulation of the optically trapped 5CB microdroplet in water offers various micro-control and movements controls for actuation applications. For example, the optically trapped 5CB microdroplet can be translated and moved to a specific direction in water. In addition, the internal configuration inside the 5CB microdroplet can also be controlled contactless using optical trapping. The exposure of circularly polarized light on the bipolar and radial 5CB microdroplets resulted in a rotational effect. All these results, micro-controlled by optically trapped 5CB microdroplets, create a mechanical work or movement that can be applied for actuating application. The corner frequency (f_c) and angular speed (ω) were dependent on the optical power density (P); hence, the strength of the confinement and rotation could be increased or decreased. This is the benefit of the optically trapped 5CB microdroplet in water to assist in for actuating application.

In the context of sensing applications, the 5CB microdroplet-based sensor is based on the transition change of internal configuration from bipolar to radial or from radial to bipolar. Optical trapping of 5CB microdroplet in water offers a technique to sense and detect quantitatively optical signals of the transition of internal configuration from bipolar to radial internal configuration in this study. f_c, ω and σ^2 can be used as the sensing characteristic for detection during the transition change. For example, the optical force confinement on the same bipolar and radial 5CB microdroplet optically trapped was different as indicated by σ^2 measured. In addition,

05-4506832 pustaka.upsi.edu.my Perpustakaan Tuanku Bainun Kampus Sultan Abdul Jalil Shah PustakaTBainun ptbupsi

05-4506832 pustaka.upsi.edu.my Perpustakaan Tuanku Bainun Kampus Sultan Abdul Jalil Shah PustakaTBainun ptbupsi

the rotation of 5CB microdroplets between bipolar and radial due to circularly polarized light showed a different trend in rotational behavior, and was dependent on the size. The bipolar 5CB rotated in the center of the laser spot, while the radial 5CB microdroplet rotated by orbiting around the laser spot. Hence, all these differences in σ^2, rotational behavior during optical trapping of a single 5CB microdroplet in water is beneficial to assist for sensing applications.

05-4506832 pustaka.upsi.edu.my Perpustakaan Tuanku Bainun Kampus Sultan Abdul Jalil Shah PustakaTBainun ptbupsi
05-4506832 pustaka.upsi.edu.my Perpustakaan Tuanku Bainun Kampus Sultan Abdul Jalil Shah PustakaTBainun ptbupsi

05-4506832 pustaka.upsi.edu.my Perpustakaan Tuanku Bainun Kampus Sultan Abdul Jalil Shah PustakaTBainun

CHAPTER 5

CONCLUSIONS AND RECOMMENDATION

05-4506832 pustaka.upsi.edu.my Perpustakaan Tuanku Bainun Kampus Sultan Abdul Jalil Shah PustakaTBainun ptbupsi

5.1 Introduction

This chapter concludes the findings of this study. First, the chapter concludes the formulation of the 5CB microdroplet suspension in water. Next, the optical trapping of a single 5CB microdroplet in water at a specific optical power density and microdroplet radius is concluded. In addition, the micro-control of a single 5CB microdroplet using optical tweezers is also concluded. Finally, this section concludes the conclusion on the corner frequency (f_c), angular speed (ω), and displacement variance (σ^2) of the optically trapped 5CB microdroplet is concluded in this section.

05-4506832 pustaka.upsi.edu.my Perpustakaan Tuanku Bainun Kampus Sultan Abdul Jalil Shah PustakaTBainun ptbupsi

05-4506832 pustaka.upsi.edu.my Perpustakaan Tuanku Bainun Kampus Sultan Abdul Jalil Shah PustakaTBainun ptbupsi

5.2 Conclusion

The conclusions are drawn based on the outlined objectives.

Objective 1: To formulate the production of 5CB microdroplets within a suitable range to be optically trapped.

There were two types of 5CB microdroplet suspension formulated in this study: bipolar and radial. The bipolar 5CB microdroplet suspensions was produced by adjusting the ratio of liquid 5CB and deionized water by (1:4000), the radial 5CB microdroplet suspensions was produced by adjusting the ratio of liquid 5CB, cetyltrimethylammonium bromide (CTAB) solution and deionized water by (1:40:4000) and sonication times ranging from 1, 2, 3, and 10 minutes. It was found that for both bipolar and radial 5CB microdroplets, suspension generated:

a) The distribution size of both 5CB microdroplets was reduced with the sonication time.
b) Both 5CB microdroplet suspensions were stable and sustained for 1 hour of monitoring time.

Objective 2: To optically trap a single 5CB microdroplet within a suitable size range using 976 nm laser.

It was found that the single 5CB microdroplet could be trapped using the linearly polarized laser beam. The range of suitable optical power density used to trap a single 5CB microdroplet in this study optically was 0.2 MW/cm^2 to 7.3 MW/cm^2.

05-4506832 pustaka.upsi.edu.my Perpustakaan Tuanku Bainun Kampus Sultan Abdul Jalil Shah PustakaTBainun ptbupsi

05-4506832 pustaka.upsi.edu.my Perpustakaan Tuanku Bainun Kampus Sultan Abdul Jalil Shah PustakaTBainun ptbupsi

Meanwhile, the range of 5CB microdroplets successfully trapped in this study was 0.6 μm to 3.7 μm radius.

Objective 3: To optically micro-control a single 5CB microdroplet using a circularly polarized laser.

It was found that:

a) The internal configuration of the optically trapped bipolar 5CB microdroplet corresponds to the polarization direction of the linearly polarized laser beam. Meanwhile, the optically trapped radial 5CB microdroplet does not respond to the linearly polarized laser beam directional change.
b) The single optical trapping of bipolar and radial 5CB microdroplets rotated under the circularly polarized laser beam.
c) The 5CB microdroplet could be linearly translated and rotated using a circularly polarized laser beam, enabling simultaneous linear translation and micro-control.

Objective 4: To quantitatively determine factors that affect the optical manipulation of the 5CB microdroplet for actuating and sensing applications.

It was found that the optical trapping of a single bipolar and radial:

a) The f_c increased with the increase of the optical power density, P.
b) The ω increased with the optical power density increase, P.

05-4506832 pustaka.upsi.edu.my Perpustakaan Tuanku Bainun Kampus Sultan Abdul Jalil Shah PustakaTBainun ptbupsi

05-4506832 pustaka.upsi.edu.my Perpustakaan Tuanku Bainun Kampus Sultan Abdul Jalil Shah PustakaTBainun ptbupsi

c) The σ^2 changed with the internal configurational change of the trapped radial 5CB microdroplet.

d) The corner frequency, f_c, angular speed, ω, and displacement variance, σ^2 could be used as the characteristic sensing parameter for liquid crystal-based sensors.

5.3 The Research Novelties

The optical trapping technique provides a novel control of 5CB microdroplets in water. Not all material in the form of liquid can be trapped and manipulated. The birefringence characteristic of the 5CB enables it to be optically trapped at the laser focus. The trapped 5CB microdroplet can be manipulated in 3-dimension *x*-, *y*-, and *z*. The 5CB microdroplet in bipolar configuration can be oriented by controlling the direction of trap laser polarization. The circularly polarized laser beam can rotate the trapped 5CB microdroplet. The power density of the trapping laser enables the speed control of the rotating 5CB microdroplet. In addition, the rotated 5CB microdroplet could be simultaneously translated. All the manipulation and controlled techniques prove the novel use of 5CB microdroplet trapping for actuating applications either in bipolar or radial internal configurations. This manipulation and control technique could be applied to control the flow of the liquid in a system or measure the viscosity of the liquid based on the rotation of the trapped rotating 5CB microdroplet-based actuator.

Next, this study's novelty was quantifying the optical signal of the single trapped 5CB microdroplet in water to internal configurational change inside the microdroplet.

05-4506832 pustaka.upsi.edu.my Perpustakaan Tuanku Bainun Kampus Sultan Abdul Jalil Shah PustakaTBainun ptbupsi

05-4506832 pustaka.upsi.edu.my Perpustakaan Tuanku Bainun Kampus Sultan Abdul Jalil Shah PustakaTBainun ptbupsi

Prior researchers focused on qualitatively observing the 5CB microdroplet optical trapping without studying the optical signal. The quantification of the optical signal based on the 5CB microdroplet configuration change shows a significant difference in the optical force strength which is represented by the corner frequency (f_c) parameter. Depending on their internal configuration, the same 5CB microdroplet could experience different optical forces. The determination of f_c for bipolar and radial 5CB microdroplets showed a slight difference in optical strength. This slight difference in optical force strength was proven by studying the simultaneous transition change of the trapped 5CB microdroplet from bipolar to radial state exposed to CTAB solution. The displacement variance (σ^2), which represents optical force strength, was higher for bipolar than radial 5CB microdroplets. This highlights that the novel change in internal configuration inside the 5CB microdroplet also affects its effective refractive index. Since optical force depends on the effective refractive index, this small change in refractive index due to internal configuration transition can be translated to an optical signal. Hence, f_c and σ^2 parameters can be potentially used for sensing applications.

In addition, the 5CB internal configuration also has a different mechanism for angular momentum transfer. Our finding highlights 5CB microdroplets of 1.3 μm radius rotated when exposed to 1.1 MW/cm^2 optical power density, but the exact size of radial 5CB microdroplets does not rotate. The radial 5CB has a smaller birefringence due to the radial structure than the bipolar 5CB. This highlights that the internal configuration of bipolar and radial 5CB microdroplets affects angular momentum transfer. The characteristic could be used as a novel sensing mechanism based on the rotational-configurational change of the 5CB.

05-4506832 pustaka.upsi.edu.my Perpustakaan Tuanku Bainun Kampus Sultan Abdul Jalil Shah PustakaTBainun ptbupsi

05-4506832 pustaka.upsi.edu.my Perpustakaan Tuanku Bainun Kampus Sultan Abdul Jalil Shah PustakaTBainun ptbupsi

5.4 Implications

This study demonstrated that the optical trapping of a single 5CB microdroplet in water is possible even though the optical trapping in a liquid microdroplet is challenging compared to the trapping of a solid particle. It has been shown that 5CB microdroplets could be optically trapped in the water with the appropriate optical power density and suitable microdroplet size. Besides, the optical trapping technique offers the manipulation and micro-control of the 5CB microdroplet in the water. The internal configuration inside the trapped 5CB microdroplet could be oriented by controlling the polarization direction of the linearly polarized light. Besides, the circularly polarized light on the trapped 5CB microdroplet produces an optical torque that rotates the trapped 5CB microdroplet. The rotation direction could also be controlled by adjusting the angle of the quarter-wave plate. This showed that polarization control could impose different dynamic behavior on the trapped 5CB microdroplet. It is also interesting that the simultaneous linear translating and micro-control on the trapped 5CB microdroplet could be performed without the 5CB microdroplet escaping from the trap spot. These features of 5CB micro-control during optical trapping highlight the possibilities of 5CB micro-actuator applications.

Besides, 5CB is unique because it has a stable bipolar and radial configuration in microdroplet form. This study quantified the optical signal of bipolar and radial 5CB microdroplets trapped by the optical tweezers. The optical signal is analyzed to measure the optical stiffness of the trapped bipolar and radial 5CB microdroplet. The parameter corner frequency justifies the strength of the optical stiffness for both single optically trapped bipolar and radial 5CB microdroplets. The corner frequency of the optically

05-4506832 pustaka.upsi.edu.my Perpustakaan Tuanku Bainun Kampus Sultan Abdul Jalil Shah PustakaTBainun ptbupsi

05-4506832 pustaka.upsi.edu.my Perpustakaan Tuanku Bainun Kampus Sultan Abdul Jalil Shah PustakaTBainun ptbupsi

trapped bipolar and radial 5CB microdroplet showed dependency on the laser power used. The trend of corner frequency for bipolar 5CB microdroplets shows a sharp gradient compared to radial 5CB microdroplets. This indicated the strong optical confinement of the bipolar 5CB microdroplet compared to the radial 5CB microdroplet. This highlights that corner frequency could be used as the characteristic sensing parameter, especially in sensor applications.

In addition, the angular speed of the optically trapped bipolar and radial 5CB microdroplet also depends on the laser power. The signature of the angular speed comparison between bipolar and radial 5CB microdroplets is that the small bipolar 5CB microdroplet rotates at the small laser power. In contrast, the small radial 5CB microdroplet shows no rotation at lower laser power. The bipolar 5CB microdroplet rotates can easily rotate when trapped by circularly polarized light at lower threshold laser power. Meanwhile, the radial 5CB rotation starts at a higher threshold laser power, especially when the microdroplet size is smaller. In simple words, at the same laser power used and the same size, the bipolar 5CB rotates while the radial 5CB does not rotate. This unique behavior can be the sensing parameter by observing the rotational dynamic of the trapped 5CB bipolar and radial. Lastly, the instantaneous configurational change from bipolar to the radial configuration of the single 5CB trapping exposed to the CTAB solution was studied to prove that the configurational change affects the optical stiffness change. The parameter called displacement variance is introduced to study the trajectory based on the optical signal when the trapped 5CB microdroplet changes from bipolar to radial configuration. Displacement variance is inversely proportional to optical stiffness. It is unique to find that the displacement variance for bipolar 5CB is higher than radial. This indicated that the stiffness reduced

05-4506832 pustaka.upsi.edu.my Perpustakaan Tuanku Bainun Kampus Sultan Abdul Jalil Shah PustakaTBainun ptbupsi

05-4506832 pustaka.upsi.edu.my Perpustakaan Tuanku Bainun Kampus Sultan Abdul Jalil Shah PustakaTBainun ptbupsi

when the bipolar 5CB transitioned to radial. The study showed that parameter corner frequency, angular speed, and displacement variance could be the sensing parameter, especially for 5CB-based sensor applications.

5.5 Recommendations

The optical trapping of the 5CB microdroplet in the water can be used in microactuator and sensing applications. However, this application requires the minimization of the 5CB microdroplet size. Smaller microdroplet sizes are beneficial since the surface-to-aspect ratio can be increased for higher-sensitivity sensors. The size of the 5CB microdroplet can be further decreased by increasing the sonication time. Other techniques, such as microfluidic, can also produce a homogenous size of the 5CB microdroplet, but the size of the 5CB microdroplet was relatively larger. It also recommended combining homogenizer and sonication to produce the smaller 5CB microdroplets. Smaller microdroplet sizes come with the cost of a sensing mechanism, which requires a method different from that used by optical tweezers and QPD.

The distribution size of the 5CB microdroplet size measurement using ImageJ software is sufficient. However, to increase the accuracy of the measurement made, the distribution size of the 5CB microdroplet can be done using a static light scattering (SLS) instrument based on Mie and Fraunhofer scattering theories (CILAS particle size analyzer, Model 1090). This instrument determines the particle size from the intensity-time fluctuation of the two laser beams scattered from a sample at an angle of 173º and

05-4506832 pustaka.upsi.edu.my Perpustakaan Tuanku Bainun Kampus Sultan Abdul Jalil Shah PustakaTBainun ptbupsi

05-4506832 pustaka.upsi.edu.my Perpustakaan Tuanku Bainun Kampus Sultan Abdul Jalil Shah PustakaTBainun ptbupsi

90º. This technique provides a more sensitive and accurate particle size measurement than ImageJ software.

The current study uses an oil-immersion type objective lens to create a strong optical tarp in the sample. However, using an oil-immersion type objective lens has limited working distance. The focal spot has limited control in the *z*-axis control, which becomes problematic when the cell chamber is thicker. The focal spot should be placed far from the glass wall of the cell chamber to reduce the glass interfacial effect on the optical signal. It is recommended to use an air-type objective lens with a long-range working distance for *z*-control and flexibility of 5CB microdroplet control to prevent the deformation of fragile liquid droplets.

Deionized water is the medium of the optical trapping of the 5CB microdroplet used in this study. The water medium can be changed to another medium, such as Phosphate Buffer Saline (PBS) solution, to mimic the actual environment to study internal configurational change, especially for sensing applications. The selected medium refractive index must be lower than the refractive index of the 5CB to ensure the 5CB is trapped at the laser focal spot.

In addition, this study could not trap 5CB microdroplets of size 0.5 μm and less. This is because the size of the 5CB microdroplet is too tiny and does not appear clear on the CCD camera. This is probably due to the limited resolution of the CCD camera (~ 500 nm). Using the CCD camera with a higher resolution would be recommended to observe the small 5CB microdroplet. Another alternative to increase the visibility of the small 5CB microdroplet is doping with dye particles. However, using the dye particle

05-4506832 pustaka.upsi.edu.my Perpustakaan Tuanku Bainun Kampus Sultan Abdul Jalil Shah PustakaTBainun ptbupsi

05-4506832 pustaka.upsi.edu.my Perpustakaan Tuanku Bainun Kampus Sultan Abdul Jalil Shah PustakaTBainun ptbupsi

requires a particular component, fluorescent microscopy, to observe the small microdroplet less than 0.5 μm.

Lastly, extending this study by examining the multiple optical trapping of 5CB microdroplets at definite laser power is also recommended. The multiple trapping of 5CB microdroplets at the focal spot might contribute to the formation of microdroplet cluster assembly, which has a definite structure. It would be expected that the size of the microdroplet cluster depends on the laser power used. There is also the possibility that this microdroplet cluster assembly might combine and form a single larger 5CB microdroplet during the optical trapping process. In addition, it is also interesting to study the different dynamics of the microdroplet cluster assembly when it is exposed to circularly polarized laser beams for both bipolar and radial.

05-4506832 pustaka.upsi.edu.my Perpustakaan Tuanku Bainun Kampus Sultan Abdul Jalil Shah PustakaTBainun ptbupsi

5.6 Summary

This chapter discussed the conclusion and the recommendation of the study. The formulation of the 5CB microdroplet suspension in water was successfully studied in the context of distribution size and stability. The single optical trapping of 5CB microdroplets in water is possible using a linearly polarized laser within appropriate laser power and microdroplet radius. The laser beam's linear translating and polarization control could control the optically trapped 5CB microdroplet. The corner frequency and angular speed dependency on the optical power density of a single 5CB trapping was investigated. It was verified that the displacement variance of the single trapping 5CB changed with the internal configurational change.

05-4506832 pustaka.upsi.edu.my Perpustakaan Tuanku Bainun Kampus Sultan Abdul Jalil Shah PustakaTBainun ptbupsi

05-4506832 pustaka.upsi.edu.my Perpustakaan Tuanku Bainun Kampus Sultan Abdul Jalil Shah PustakaTBainun ptbupsi

Recommendations and suggestions to improve this study in the future were made. Some of the improvements suggested, such as the technique to produce smaller 5CB microdroplets, technique to measure distribution size, objective lens used, type of medium, increase of CCD camera resolution, and dye doping technique, are suggested. Multiple 5CB trapping was also suggested to study the trapping assembly to open a new field of trapping assembly. This improvement will encourage this study to be more comprehensive and more meaningful.

05-4506832 pustaka.upsi.edu.my Perpustakaan Tuanku Bainun Kampus Sultan Abdul Jalil Shah PustakaTBainun ptbupsi

05-4506832 pustaka.upsi.edu.my Perpustakaan Tuanku Bainun Kampus Sultan Abdul Jalil Shah PustakaTBainun ptbupsi

05-4506832 pustaka.upsi.edu.my Perpustakaan Tuanku Bainun Kampus Sultan Abdul Jalil Shah PustakaTBainun ptbupsi

REFERENCES

Aas, M., Jonáš, A., & Kiraz, A. (2013). Lasing in optically manipulated, dye-doped emulsion microdroplets. *Optics Communications*, *290*, 183–187. https://doi.org/10.1016/j.optcom.2012.10.036

Adamow, A., Sznitko, L., & Mysliwiec, J. (2017). The influence of homogenization process on lasing performance in polymer-nematic liquid crystal emulsions. *Optical Materials*, *69*, 81–86. https://doi.org/10.1016/j.optmat.2017.04.011

Aery, S., Parry, A., Araiza-Calahorra, A., Evans, S. D., Gleeson, H. F., Dan, A., & Sarkar, A. (2023). Ultra-stable liquid crystal droplets coated by sustainable plant-based materials for optical sensing of chemical and biological analytes. *Journal of Materials Chemistry C*, *11*(17), 5831–5845. https://doi.org/10.1039/d3tc00598d

Asadinezhad, S., Khodaiyan, F., Salami, M., Hosseini, H., & Ghanbarzadeh, B. (2019). Effect of different parameters on orange oil nanoemulsion particle size: combination of low energy and high energy methods. *Journal of Food Measurement and Characterization*, *13*(4), 2501–2509. https://doi.org/10.1007/s11694-019-00170-z

Ashkin, A. (1997). Optical trapping and manipulation of neutral particles. *Proceeding of the National Academy of Sciences of United States of America*, *94*(May), 4853–4860.

Aziz, W. N. S., Ayop, S. K., Hamid, M. Y., & Munajat, Y. (2016). Simple Determination of the Stiffness of an Optical Trap Using Video Microscopy and Particle Tracking. *Buletin Optik 2016*, *1*(2), 1–6.

Aziz, W. N. S., Ayop, S. K., & Riyanto, S. (2015). The potential of optical tweezer (OT) for viscoelastivity measurement of nanocellulose solution. *Jurnal Teknologi*, *74*(8), 45–48. https://doi.org/10.11113/jt.v74.4722

Baek, J.-H., Hwang, S., & Lee, Y.-G. (2007). Trap stiffness in optical tweezers. *Asian Symposium for Precision Engineering and Nanotechnology*, *685*, 1100.

Bartoš, D., Wang, L., Anker, A. S., Rewers, M., Aalling-Frederiksen, O., Jensen, K. M. Ø., & Sørensen, T. J. (2022). Synthesis of fluorescent polystyrene nanoparticles: a reproducible and scalable method. *PeerJ Materials Science*, *4*, e22. https://doi.org/10.7717/peerj-matsci.22

Berg-Sørensen, K., & Flyvbjerg, H. (2004). Power spectrum analysis for optical tweezers. *Review of Scientific Instruments*, *75*(3), 594–612. https://doi.org/10.1063/1.1645654

Brasselet, E. (2008). Statics and dynamics of radial nematic liquid-crystal droplets manipulated by laser tweezers. *Physical Review E*, *77*(041704), 1–7. https://doi.org/10.1103/PhysRevE.77.041704

05-4506832 pustaka.upsi.edu.my Perpustakaan Tuanku Bainun Kampus Sultan Abdul Jalil Shah PustakaTBainun ptbupsi

05-4506832 pustaka.upsi.edu.my Perpustakaan Tuanku Bainun Kampus Sultan Abdul Jalil Shah PustakaTBainun ptbupsi

Brasselet, E., Doyon, B., Galstian, T. V, & Dube, L. J. (2003). Optically induced dynamics in nematic liquid crystals: The role of twist deformation and asymmetry. *Optic Comunications*, *186*, 291–302. https://doi.org/10.1103/PhysRevE.67.031706

Brasselet, E., & Juodkazis, S. (2009a). Optical angular manipulation of liquid crystal droplets in laser tweezers. *Nonlinear Optic Physics*, *18*(2), 167–194.

Brasselet, E., & Juodkazis, S. (2009b). Optical angular manipulation of liquid crystal droplets in laser tweezers. *Journal of Nonlinear Optical Physics and Materials*, *18*(2), 167–194. https://doi.org/10.1142/S0218863509004580

Buosciolo, A., Pesce, G., & Sasso, A. (2004). New calibration method for position detector for simultaneous measurements of force constants and local viscosity in optical tweezers. *Optics Communications*, *230*(4–6), 357–368. https://doi.org/10.1016/j.optcom.2003.11.062

Català, F., Marsà, F., Montes-Usategui, M., Farré, A., & Martín-Badosa, E. (2017). Influence of experimental parameters on the laser heating of an optical trap. *Scientific Reports*, *7*(1), 1–9. https://doi.org/10.1038/s41598-017-15904-6

Chen, Z., Cai, Z., Liu, W., & Yan, Z. (2022). Optical trapping and manipulation for single-particle spectroscopy and microscopy. *Journal of Chemical Physics*, *157*(5). https://doi.org/10.1063/5.0086328

Choi, Y., Lee, K., Gupta, K. C., Park, S. Y., & Kang, I. K. (2015). The role of ligand-receptor interactions in visual detection of HepG2 cells using a liquid crystal microdroplet-based biosensor. *Journal of Materials Chemistry B*, *3*(44), 8659–8669. https://doi.org/10.1039/c5tb01213a

Concellón, A. (2023). Liquid Crystal Emulsions: A Versatile Platform for Photonics, Sensing, and Active Matter. *Angewandte Chemie - International Edition*, *202308857*. https://doi.org/10.1002/anie.202308857

David, C. B. W., Ayop, S. K., & Kremer, F. (2013). Resolvability Between Bare and DNA-Grafted Microsphere by Flow Resistance Measurement using Optical Tweezers. *J. Sci. Math. Lett. UPSI*, *1*, 28–34. https://ejournal.upsi.edu.my/issuedetails/268

Deng, J., Han, D., & Yang, J. (2021). Applications of microfluidics in liquid crystal-based biosensors. *Biosensors*, *11*(10). https://doi.org/10.3390/bios11100385

Dienerowitz, M., Mazilu, M., & Dholakia, K. (2010). Optical manipulation of nanoparticles: A review. *SPIE Reviews*, *1*(1), 1–32. https://doi.org/10.1117/1.2992045

05-4506832 pustaka.upsi.edu.my Perpustakaan Tuanku Bainun Kampus Sultan Abdul Jalil Shah PustakaTBainun ptbupsi

05-4506832 pustaka.upsi.edu.my Perpustakaan Tuanku Bainun Kampus Sultan Abdul Jalil Shah PustakaTBainun ptbupsi

Dierking, I., & Al-zangana, S. (2017). Lyotropic Liquid Crystal Phases from Anisotropic Nanomaterials. *Nanomaterials*, *7*(305). https://doi.org/10.3390/nano7100305

Donato, M. G., Mazzulla, A., Pagliusi, P., Magazzù, A., Hernandez, R. J., Provenzano, C., Gucciardi, P. G., Maragò, O. M., & Cipparrone, G. (2016). Light-induced rotations of chiral birefringent microparticles in optical tweezers. *Scientific Reports*, *6*(September). https://doi.org/10.1038/srep31977

Duan, R., Hao, X., Li, Y., & Li, H. (2020). Detection of acetylcholinesterase and its inhibitors by liquid crystal biosensor based on whispering gallery mode. *Sensors and Actuators B : Chemical*, *308*(November 2019), 127672. https://doi.org/10.1016/j.snb.2020.127672

Duan, R., Li, Y., Shi, B., Li, H., & Yang, J. (2020). Real-time, quantitative and sensitive detection of urea by whispering gallery mode lasing in liquid crystal microdroplet. *Talanta*, *209*(October). https://doi.org/10.1016/j.talanta.2019.120513

Duan, R., Yanzeng, L., Hanyang, L., & Jun, Y. (2019). Detection of heavy metal ions using whispering gallery mode lasing in functionalized liquid crystal microdroplets. *Biomedical Optics Express*, *10*(12), 6073–6083.

Eom, N., Sedev, R., Wedding, B., & Connor, J. (2014). Probing Fluid Flow Using the Force Measurement Capability of Optical Trapping. *Advanced Power Technology*, *25*(4), 1249–1253.

Esteves, C., Ramou, E., Porteira, A. R. P., Moura Barbosa, A. J., & Roque, A. C. A. (2020). Seeing the Unseen: The Role of Liquid Crystals in Gas-Sensing Technologies. *Advanced Optical Materials*, *8*(11). https://doi.org/10.1002/adom.201902117

Fernández-Canto, N., Romero-Rodríguez, M. Á., Ramos-Cabrer, A. M., Pereira-Lorenzo, S., & Lombardero-Fernández, M. (2023). Polarized light microscopy guarantees the use of autochthonous wheat in the production of flour for the Protected Geographical Indication 'Galician Bread.' *Food Control*, *147*(November 2022). https://doi.org/10.1016/j.foodcont.2022.109597

Ferreira, T., & Rasband, W. (2012). User Guide ImageJ. *Image J User Guide*, *1.46r*. https://doi.org/10.1038/nmeth.2019

Garratt, R. C., & Bachega, F. R. (2013). Optical Tweezers. In *Biophysics* (pp. 1800–1807). https://doi.org/10.1007/978-3-642-16712-6

Gleeson, H. F., Wood, T. A., & Dickinson, M. (2006). Laser manipulation in liquid crystals: An approach to microfluidics and micromachines. *Philosophical Transactions of the Royal Society A: Mathematical, Physical and Engineering Sciences*, *364*(1847), 2789–2805. https://doi.org/10.1098/rsta.2006.1855

05-4506832 pustaka.upsi.edu.my Perpustakaan Tuanku Bainun Kampus Sultan Abdul Jalil Shah PustakaTBainun ptbupsi

05-4506832 pustaka.upsi.edu.my Perpustakaan Tuanku Bainun Kampus Sultan Abdul Jalil Shah PustakaTBainun ptbupsi

Goswami, D. (2018). Nobel Prize in Physics – 2018. *Resonance*, *23*(12), 1333–1341. https://doi.org/10.1007/s12045-018-0744-6

Hamid, M. Y., Ayop, S. K., Aziz, W. N. S., & Munajat, Y. (2016). Spatial Distribution of an Optically Trapped Bead in Water. *Buletin Optik 2016*, *33*(2), 2–5. https://doi.org/10.15011/jasma.33.330211

Hanemann, T., Haase, W., Svoboda, I., & Fuess, H. (1995). Crystal structure of 4'-pentyl-4-cyanobiphenyl (5CB). *Liquid Crystals*, *19*(5), 699–702. https://doi.org/10.1080/02678299508031086

Hegner, M., Gerber, C., Arntz, Y., Zhang, J., & Bertoncini, P. (2003). Biological Single Molecule Applications and Advanced Biosensing. *Journal of Chromatography Library*, *13*, 241–263.

Horst, A. Van Der, Forde, N. R., van der Horst, A., & Forde, N. R. (2010). Power spectral analysis for optical trap stiffness calibration from high-speed camera position detection with limited bandwidth. *Optics Express*, *18*(8), 7670. https://doi.org/10.1364/oe.18.007670

Humar, M., & Muševič, I. (2011). Surfactant sensing based on whispering-gallery-mode lasing in liquid-crystal microdroplets. *Optics Express*, *19*(21), 19836. https://doi.org/10.1364/oe.19.019836

Ito, K., Frusawa, H., & Kimura, M. (2012). Precise switching control of liquid crystalline microgears driven by circularly polarized light. *Optics Express*, *20*(4), 1991–1996.

Iwabata, K., Sugai, U., Seki, Y., Furue, H., & Sakaguchi, K. (2013). Applications of Biomaterials to Liquid Crystals. *Molecules*, 4703–4717. https://doi.org/10.3390/molecules18044703

Josue H., R. (2012). *Optical trapping and manipulation exploiting liquid crystalline systems*.

Juodkazis, S., Shikata, M., Takahashi, T., Matsuo, S., & Misawa, H. (1999). Fast optical switching by a laser-manipulated microdroplet of liquid crystal. *Applied Physics Letters*, *74*(24), 3627–3629. https://doi.org/10.1063/1.123203

Khoo, I. C. (2009). Nonlinear optics of liquid crystalline materials. In *Physics Reports* (Vol. 471, Issues 5–6, pp. 221–267). Elsevier B.V. https://doi.org/10.1016/j.physrep.2009.01.001

Kiang-Ia, J., Taeudomkul, R., Prajongtat, P., Tin, P., Pattanaporkratana, A., & Chattham, N. (2021). Anomalous lehmann rotation of achiral nematic liquid crystal droplets trapped under linearly polarized optical tweezers. *Molecules*, *26*(14). https://doi.org/10.3390/molecules26144108

05-4506832 pustaka.upsi.edu.my Perpustakaan Tuanku Bainun Kampus Sultan Abdul Jalil Shah PustakaTBainun ptbupsi

05-4506832 pustaka.upsi.edu.my Perpustakaan Tuanku Bainun Kampus Sultan Abdul Jalil Shah PustakaTBainun ptbupsi

Konyshev, I., & Byvalov, A. (2021). Model systems for optical trapping: the physical basis and biological applications The theory of optical trapping at macro-, meso-, and microscopic levels of detail. *Biophysical Reviews*, *13*, 515–529. https://doi.org/10.1007/s12551-021-00823-8

Kudo, T., Wang, S., Yuyama, K., & Masuhara, H. (2016). *Optical Trapping-Formed Colloidal Assembly with Horns Extended to the Outside of a Focus through Light Propagation*. https://doi.org/10.1021/acs.nanolett.6b00123

Kulkarni, S., Kumar, S., & Thareja, P. (2021). Colloidal and fumed particles in nematic liquid crystals: Self-assembly, confinement and implications on rheology. In *Journal of Molecular Liquids* (Vol. 336, p. 116241). Elsevier B.V. https://doi.org/10.1016/j.molliq.2021.116241

Lee, G., Araoka, F., Ishikawa, K., Momoi, Y., & Haba, O. (2013). Photoinduced Ordering Transition in Microdroplets of Liquid Crystals with Azo-Dendrimer. *Particle & Particle System Characterization*, *30*, 847–852. https://doi.org/10.1002/ppsc.201300110

Lee, K., Gupta, C., Park, S., & Kang, I. (2015a). Anti-IgG-anchored liquid crystal microdroplets for label free detection of IgG. *Journal of Materials Chemistry B*. https://doi.org/10.1039/C5TB02131F

Li, X., Sha, X. M., Yang, H. S., Ren, Z. Y., & Tu, Z. C. (2023). Ultrasonic treatment regulates the properties of gelatin emulsion to obtain high-quality gelatin film. *Food Chemistry: X*, *18*(April), 100673. https://doi.org/10.1016/j.fochx.2023.100673

Liu, Q., Asavei, T., Lee, T., Rubinsztein-dunlop, H., He, S., & Smalyukh, I. I. (2011). Measurement of viscosity of lyotropic liquid crystals by means of rotating laser-trapped microparticles. *Optical Society of America*, *19*(25), 25134–25143.

Loussert, C., Delabre, U., & Brasselet, E. (2013). Manipulating the Orbital Angular Momentum of Light at the Micron Scale with Nematic Disclinations in a Liquid Crystal Film. *Physical Review Letters*, *037802*(July), 1–4. https://doi.org/10.1103/PhysRevLett.111.037802

Malagnino, N., Pesce, G., Sasso, A., & Arimondo, E. (2002). Measurements of trapping efficiency and stiffness in optical tweeser. *Optics Communications*, *214*, 15–24.

Malmqvist, L., & Hertz, H. M. (1992). Trapped particle optical microscopy. *Optics Communications*, *94*(1–3), 19–24. https://doi.org/10.1016/0030-4018(92)90398-B

Manzo, C., Paparo, D., Marrucci, L., & Jánossy, I. (2006). Light-induced rotation of dye-doped liquid crystal droplets. *Physical Review E - Statistical, Nonlinear, and Soft Matter Physics*, *73*(5). https://doi.org/10.1103/PhysRevE.73.051707

05-4506832 pustaka.upsi.edu.my Perpustakaan Tuanku Bainun Kampus Sultan Abdul Jalil Shah PustakaTBainun ptbupsi

05-4506832 pustaka.upsi.edu.my Perpustakaan Tuanku Bainun Kampus Sultan Abdul Jalil Shah PustakaTBainun ptbupsi

Mas, J., Farré, A., Cuadros, J., Juvells, I., & Carnicer, A. (2011). Understanding optical trapping phenomena: A simulation for undergraduates. *IEEE Transactions on Education*, *54*(1), 133–140. https://doi.org/10.1109/TE.2010.2047107

Merola, F., Grilli, S., Coppola, S., Vespini, V., De Nicola, S., Maddalena, P., Carfagna, C., & Ferraro, P. (2013). Pyroelectric manipulation of liquid crystal droplets. *Proceeding of SPIE*, *8792*, 87920V. https://doi.org/10.1117/12.2020555

Mertelj, A., & Lisjak, D. (2017). Ferromagnetic nematic liquid crystals. *Liquid Crystals Reviews*, *5*(1), 1–33. https://doi.org/10.1080/21680396.2017.1304835

Mirantsev, L. V., de Oliveira, E. J. L., de Oliveira, I. N., & Lyra, M. L. (2016). Defect structures in nematic liquid crystal shells of different shapes. *Liquid Crystals Reviews*, *4*(1), 35–58. https://doi.org/10.1080/21680396.2016.1183151

Miura, A., Nakajima, R., Abe, S., & Kitamura, N. (2020). Optical Trapping-Microspectroscopy of Single Aerosol Microdroplets in Air: Supercooling of Dimethylsulfoxide Microdroplets. *Journal of Physical Chemistry A*, *124*(43), 9035–9043. https://doi.org/10.1021/acs.jpca.0c06179

Mohammad, S., Winson, W. T., & Bahman, A. (2014). Comparative study of methods to calibrate the stiffness of a single-beam gradient-force optical tweezers over various laser trapping powers. *Journal of Biomedical Optics*, *11*, 115001. https://doi.org/10.1109/iembs.1999.802433

Müllenbroich, M. C., McAlinden, N., & Wright, A. J. (2013). Adaptive optics in an optical trapping system for enhanced lateral trap stiffness at depth. *Journal of Optics (United Kingdom)*, *15*(7). https://doi.org/10.1088/2040-8978/15/7/075305

Murazawa, N., Juodkazis, S., Matsuo, S., & Misawa, H. (2005). Control of the Molecular Alignment Inside Liquid- Crystal Droplets by Use of Laser Tweezers. *Small*, *6*, 656–661. https://doi.org/10.1002/smll.200500038

Murazawa, N., Juodkazis, S., & Misawa, H. (2005). Characterization of bipolar and radial nematic liquid crystal droplets using laser-tweezers. *Journal of Physics D: Applied Physics*, *38*(16), 2923–2927. https://doi.org/10.1088/0022-3727/38/16/027

Murazawa, N., Juodkazis, S., & Misawa, H. (2006a). Laser manipulation and characterization of liquid crystal droplets. *Proceeding of SPIE*, *6326*, 1–9. https://doi.org/10.1117/12.685058

Murazawa, N., Juodkazis, S., & Misawa, H. (2006b). Laser manipulation of a smectic liquid-crystal droplet. *The European Physical Journal E*, *439*, 435–439. https://doi.org/10.1140/epje/i2006-10033-1

Neuman, K. C., & Block, S. M. (2004). Optical trapping. *Review of Scientific Instruments*, *75*(9), 2787–2809. https://doi.org/10.1063/1.1785844

05-4506832 pustaka.upsi.edu.my Perpustakaan Tuanku Bainun Kampus Sultan Abdul Jalil Shah PustakaTBainun ptbupsi

05-4506832 pustaka.upsi.edu.my Perpustakaan Tuanku Bainun Kampus Sultan Abdul Jalil Shah PustakaTBainun ptbupsi

Neves, A. A. R., Jones, P. H., Luo, L., & Maragò, O. M. (2015). Optical cooling and trapping: introduction. *Journal of the Optical Society of America B*, *32*(5), OCT1. https://doi.org/10.1364/josab.32.00oct1

Nieminen, T. A., Du Preez-Wilkinson, N., Stilgoe, A. B., Loke, V. L. Y., Bui, A. A. M., & Rubinsztein-Dunlop, H. (2014). Optical tweezers: Theory and modelling. *Journal of Quantitative Spectroscopy and Radiative Transfer*, *146*, 59–80. https://doi.org/10.1016/j.jqsrt.2014.04.003

Nishii, H. (2021). Effect of Measurement Parameters on UV-VIS Absorption Spectra. *UV Talk Letter*, *21*, 1–14.

Niu, X., Luo, D., Chen, R., Wang, F., Sun, X., & Dai, H. (2016). Optical biosensor based on liquid crystal droplets for detection of cholic acid. *Optics Communications*, *381*, 286–291. https://doi.org/10.1016/j.optcom.2016.07.016

Oster, L. M., Shechter, J., Strain, B., Shivrayan, M., Thayumanavan, S. T., & Ross, J. L. (2022). Controlling Liquid Crystal Configuration and Phase Using Multiple Molecular Triggers. *Molecules*, *27*(3), 1–17. https://doi.org/10.3390/molecules27030878

Pai, P., Zandrini, T., Mart, R., & Bragheri, F. (2018). Particle Manipulation by Optical Forces in Microfluidic Devices. *Micromachines*, *9*(200), 1–21. https://doi.org/10.3390/mi9050200

05-4506832 pustaka.upsi.edu.my Perpustakaan Tuanku Bainun Kampus Sultan Abdul Jalil Shah PustakaTBainun ptbupsi

Palffy-muhoray, P. (2007). The diverse world of liquid crystals. *Physics Today*, *54*(2007), 54–60. https://doi.org/10.1063/1.2784685

Parmentier, E. A., Arroyo, P. C., Bibawi, S., Esat, K., & Signorell, R. (2021). Photochemistry of single optically trapped oleic acid droplets. *Journal of Aerosol Science*, *151*(August 2020), 0–10. https://doi.org/https://doi.org/10.1016/j.jaerosci.2020.105660

Patel, N., Rawat, S., Joglekar, M., Chhaniwal, V., Dubey, S. K., O'Connor, T., Javidi, B., & Anand, A. (2021). Compact and low-cost instrument for digital holographic microscopy of immobilized micro-particles. *Optics and Lasers in Engineering*, *137*(May 2020). https://doi.org/10.1016/j.optlaseng.2020.106397

Paul, D., Chand, R., & Kumar, G. V. P. (2022). Optothermal Evolution of Active Colloidal Matter in a Defocused Laser Trap. *ACS Photonics*, *9*(10), 3440–3449. https://doi.org/10.1021/acsphotonics.2c01083

Peddireddy, K., Kumar, P., Thutupalli, S., Herminghaus, S., & Bahr, C. (2012). Solubilization of thermotropic liquid crystal compounds in aqueous surfactant solutions. *Langmuir*, *28*(34), 12426–12431. https://doi.org/10.1021/la3015817

Peterman, E. J. G., Gittes, F., & Schmidt, C. F. (2003). Laser-induced heating in optical traps. *Biophysical Journal*, *84*(2 I), 1308–1316. https://doi.org/10.1016/S0006-3495(03)74946-7

05-4506832 pustaka.upsi.edu.my Perpustakaan Tuanku Bainun Kampus Sultan Abdul Jalil Shah PustakaTBainun ptbupsi

05-4506832 pustaka.upsi.edu.my Perpustakaan Tuanku Bainun Kampus Sultan Abdul Jalil Shah PustakaTBainun ptbupsi

Phanphak, S., Pattanaporkratana, A., Limtrakul, J., & Chattham, N. (2014). Precession mechanism of nematic liquid crystal droplets under low power optical tweezers. *Ferroelectrics*, *468*(1), 114–122. https://doi.org/10.1080/00150193.2014.933663

Polimeno, P., Magazzù, A., Iatì, M. A., Patti, F., Saija, R., Esposti Boschi, C. D., Donato, M. G., Gucciardi, P. G., Jones, P. H., Volpe, G., & Maragò, O. M. (2018). Optical tweezers and their applications. *Journal of Quantitative Spectroscopy and Radiative Transfer*, *218*, 131–150. https://doi.org/10.1016/j.jqsrt.2018.07.013

Popov, N., Honaker, L. W., Popova, M., Usol'tseva, N., Mann, E. K., Jákli, A., & Popov, P. (2017). Thermotropic liquid crystal-assisted chemical and biological sensors. In *Materials* (Vol. 11, Issue 1, pp. 14–17). https://doi.org/10.3390/ma11010020

Popov, Piotr, K. Mann, Elizabeth, Jakli, Antal. (2017). Thermotropic Liquid Crystal Films for Biosensor and Beyond. *Journal of Materials Chemistry B*. https://doi.org/10.1039/C7TB00809K

Prakash, J., Parveen, A., Kumar, Y., & Kaushik, A. (2020). Nanotechnology-assisted liquid crystals-based biosensors : Towards fundamental to advanced applications. *Biosensors and Bioelectronics*, *168*(June), 112562. https://doi.org/10.1016/j.bios.2020.112562

Qin, L., Liu, X., & Yu, Y. (2021). Soft Actuators of Liquid Crystal Polymers Fueled by Light from Ultraviolet to Near Infrared. *Advanced Optical Materials*, *9*(7), 1–27. https://doi.org/10.1002/adom.202001743

Ribeiro, R. S. R., Dahal, P., Guerreiro, A., & Jorge, P. A. S. (2017). Fabrication of Fresnel plates on optical fibres by FIB milling for optical trapping , manipulation and detection of single cells. *Nature Scientific Report*, *May*, 1–14. https://doi.org/10.1038/s41598-017-04490-2

Rui, G., Li, Y., Gu, B., Cui, Y., & Zhan, Q. (2021). Optical manipulation of nanoparticles with structured light. In *Thin Film Nanophotonics: Conclusions from the Third International Workshop on Thin Films for Electronics, Electro-Optics, Energy and Sensors (TFE3S)*. LTD. https://doi.org/10.1016/B978-0-12-822085-6.00008-X

Saito, K., & Kimura, Y. (2022). Optically driven liquid crystal droplet rotator. *Scientific Reports*, *12*(1), 1–8. https://doi.org/10.1038/s41598-022-21146-y

Sanders, J. L., Yang, Y., Dickinson, M. R., & Gleeson, H. F. (2013b). Pushing, pulling and twisting liquid crystal systems: Exploring new directions with laser manipulation. *Philosophical Transactions of the Royal Society A: Mathematical, Physical and Engineering Sciences*, *371*(1988), 20120265. https://doi.org/10.1098/rsta.2012.0265

05-4506832 pustaka.upsi.edu.my Perpustakaan Tuanku Bainun Kampus Sultan Abdul Jalil Shah PustakaTBainun ptbupsi

05-4506832 pustaka.upsi.edu.my Perpustakaan Tuanku Bainun Kampus Sultan Abdul Jalil Shah PustakaTBainun ptbupsi

Sarshar, M., Wong, W. T., & Anvari, B. (2014). Comparative study of methods to calibrate the stiffness of a single-beam gradient-force optical tweezers over various laser trapping powers. *Journal of Biomedical Optics*, *19*(11), 115001. https://doi.org/10.1117/1.jbo.19.11.115001

Scharf, T. (2006). Polarized Light in Liquid Crystals and Polymers. In *Polarized Light in Liquid Crystals and Polymers*. John Wiley & Sons. https://doi.org/10.1002/9780470074374

Sen, A., Kupcho, K. A., Grinwald, B. A., Vantreeck, H. J., & Acharya, B. R. (2013). Liquid crystal-based sensors for selective and quantitative detection of nitrogen dioxide. *Sensors and Actuators, B: Chemical*, *178*, 222–227. https://doi.org/10.1016/j.snb.2012.12.036

Sengupta, A., Herminghaus, S., & Bahr, C. (2014). Liquid crystal microfluidics: surface, elastic and viscous interactions at microscales. *Liquid Crystals Reviews*, *2*(2), 73–110. https://doi.org/10.1080/21680396.2014.963716

Shafiei, M., Kazemzadeh, Y., Martyushev, D. A., Dai, Z., & Riazi, M. (2023). Effect of chemicals on the phase and viscosity behavior of water in oil emulsions. *Scientific Reports*, *13*(1), 1–14. https://doi.org/10.1038/s41598-023-31379-0

Shechter, J., Atzin, N., Mozaffari, A., Zhang, R., Zhou, Y., Strain, B., Oster, L. M., De Pablo, J. J., & Ross, J. L. (2020). Direct Observation of Liquid Crystal Droplet Configurational Transitions using Optical Tweezers. *Langmuir*, *36*(25), 7074–7082. https://doi.org/10.1021/acs.langmuir.9b03629

Shen, Y., & Dierking, I. (2019). Perspectives in Liquid-Crystal-Aided Nanotechnology and Nanoscience. *Appl. Sci.*, *9*, 2512.

Shih, T. W., Hsu, C. L., Chen, L. Y., Huang, Y. C., Chen, C. J., Inoue, Y., & Sugiyama, T. (2021). Optical Trapping-Induced New Polymorphism of β-Cyclodextrin in Unsaturated Solution. *Crystal Growth and Design*, *21*(12), 6913–6923. https://doi.org/10.1021/acs.cgd.1c00822

Simmons, R. M., Finer, J. T., Chu, S., & Spudich, J. A. (1996). Quantitative measurements of force and displacement using an optical trap. *Biophysical Journal*, *70*(4), 1813–1822. https://doi.org/10.1016/S0006-3495(96)79746-1

Škarabot, M., Osterman, N., Lokar, Ž., & Muševič, I. (2014). Manipulation of particles by laser tweezers-induced gradient of order in the nematic liquid crystal. *Optical Trapping and Optical Micromanipulation XI*, *9164*, 91642B. https://doi.org/10.1117/12.2061308

Smalyukh, I. I., Kachynski, A. V, Kuzmin, A. N., & Prasad, P. N. (2006). Laser trapping in anisotropic fluids and polarization-controlled particle dynamics. *Proceeding of the National Academy of Sciences of United States of America*, *103*(48).

05-4506832 pustaka.upsi.edu.my Perpustakaan Tuanku Bainun Kampus Sultan Abdul Jalil Shah PustakaTBainun ptbupsi

05-4506832 pustaka.upsi.edu.my Perpustakaan Tuanku Bainun Kampus Sultan Abdul Jalil Shah PustakaTBainun ptbupsi

Smalyukh, I. I., Kaputa, D. S., Kachynski, A. V., Kuzmin, A. N., & Prasad, P. N. (2007). Optical trapping of director structures and defects in liquid crystals using laser tweezers. *Optics Express*, *15*(7), 4359. https://doi.org/10.1364/oe.15.004359

Sofi, J. A., & Dhara, S. (2019). Stability of liquid crystal micro-droplets based optical microresonators. *Liquid Crystals*, *46*(4), 629–639. https://doi.org/10.1080/02678292.2018.1515373

Sotolongo-Costa, O., Moreno-Vega, Y., Lloveras-González, J. J., & Antoranz, J. C. (1996). Criticality in Droplet Fragmentation. *Physical Review Letters*, *76*(1), 42–45. https://doi.org/10.1103/PhysRevLett.76.42

Srivastava, G., Jaiswal, M., Singh, P., Iqbal, A., Dabrowski, R., & Dhar, R. (2023). Enhanced stability of the nematic phase of 4-pentyl-4′-cyanobiphenyl due to the dispersion of copper nanoparticles. *Liquid Crystals*, *00*(00), 1–14. https://doi.org/10.1080/02678292.2023.2219990

Suga, M., Suda, S., Ichikawa, M., & Kimura, Y. (2018). Self-propelled motion switching in nematic liquid crystal droplets in aqueous surfactant solutions. *Physical Review E - Statistical, Nonlinear, and Soft Matter Physics*, *062703*, 1–8. https://doi.org/10.1103/PhysRevE.97.062703

Sugiyama, T., Yuyama, K., & Masuhara, H. (2012). Laser trapping chemistry: From polymer assembly to amino acid crystallization. *Accounts of Chemical Research*, *45*(11), 1946–1954. https://doi.org/10.1021/ar300161g

Supian, F. L., Richardson, T. H., Deasy, M., Kelleher, F., Ward, J. P., & McKee, V. (2010). Interaction between Langmuir and Langmuir-Blodgett films of two calix[4]arenes with aqueous copper and lithium ions. *Langmuir*, *26*(13), 10906–10912. https://doi.org/10.1021/la100808r

Tadros, T. F. (2013). *Emulsion Formation and Stability*.

Taylor, P., Kleman, M., & Lavrentovich, O. D. (2006). Topological point defects in nematic liquid crystals. *Philosophical Magazine*, *86*(September 2012), 37–41. https://doi.org/10.1080/14786430600593016

Taylor, P., Ward, A. D., Longhurst, M., & Quirke, N. (2005). The optical trapping of airborne hydrocarbon droplets from an oil mist. *Journal of Experimental Nanoscience*, *1*(1), 75–82. https://doi.org/10.1080/17458080500328003

Tsuji, T., Doi, K., & Kawano, S. (2022). Optical trapping in micro- and nanoconfinement systems: Role of thermo-fluid dynamics and applications. *Journal of Photochemistry and Photobiology C: Photochemistry Reviews*, *52*(October 2021), 100533. https://doi.org/10.1016/j.jphotochemrev.2022.100533

T-thienprasert, J., Limtrakul, J., Zentgraf, T., Chattham, N., Meyer, F., Schlickriede, C., Chaisakul, P., & Zentgraf, T. (2019). Miniaturized Metalens Based Optical Tweezers on Optical Motors. *Crystals*, *9*(515).

05-4506832 pustaka.upsi.edu.my Perpustakaan Tuanku Bainun Kampus Sultan Abdul Jalil Shah PustakaTBainun ptbupsi

05-4506832 pustaka.upsi.edu.my Perpustakaan Tuanku Bainun Kampus Sultan Abdul Jalil Shah PustakaTBainun ptbupsi

Upadhyay, P., Rastogi, M. K., & Kumar, D. (2015). Polarizability study of nematic liquid crystal 4-cyano-4 0 -pentylbiphenyl (5CB) and its nitrogen derivatives. *Chemical Physics*, *456*, 41–46. https://doi.org/10.1016/j.chemphys.2015.03.011

Urbanski, M., Reyes, C. G., Noh, J., Sharma, A., Geng, Y., Subba Rao Jampani, V., & Lagerwall, J. P. F. (2017). Liquid crystals in micron-scale droplets , shells and fibers. *Journal of Physics: Condensed Matter*, *29*(13), 53. https://doi.org/10.1088/1361-648X/aa5706

Usman, A., Chiang, W., Uwada, T., & Masuhara, H. (2012). Laser Trapping-Induced Reconfiguration of Individual Smectic Liquid Crystal Micro-Droplet Showing Size-Dependent Dynamics. *SPIE*, *8274*, 1–8. https://doi.org/10.1117/12.906305

Usman, A., Chiang, W., Uwada, T., & Masuhara, H. (2013). Polarization and Droplet Size Effects in the Laser-Trapping-Induced Reconfiguration in Individual Nematic Liquid Crystal Microdroplets. *The Journal of Physical Chemistry B*, *117*, 4536–4540.

Usman, A., Uwada, T., & Masuhara, H. (2011). Optical Reorientation and Trapping of Nematic Liquid Crystals Leading to the Formation of Micrometer-Sized Domain. *The Journal of Physical Chemistry*, 11906–11913.

Wang, H., Qin, Q. H., Ji, H., & Sun, Y. (2011). Comparison among different modeling techniques of 3D micromechanical modeling of damage in unidirectional composites. *Advanced Science Letters*, *4*(2), 400–407. https://doi.org/10.1166/asl.2011.1261

Wang, X., Bukusoglu, E., & Abbott, N. L. (2017). A practical guide to the preparation of liquid crystal-templated microparticles. *Chemistry of Materials*, *29*(1), 53–61. https://doi.org/10.1021/acs.chemmater.6b02668

Wang, Y., Li, H., Zhao, L., Liu, Y., Liu, S., & Yang, J. (2016). Tunable whispering gallery modes lasing in dye-doped cholesteric liquid crystal microdroplets. *Applied Physics Letters*, *109*(23). https://doi.org/10.1063/1.4971973

Wang, Z., Zhang, Y., Gong, X., Yuan, Z., Feng, S., Xu, T., Liu, T., & Chen, Y. (2020). Bio-electrostatic sensitive droplet lasers for molecular detection. *Nanoscale Advanced*, 1–7. https://doi.org/10.1039/d0na00107d

Wei, Y. Y., Sun, Z. Q., Ren, H. H., & Li, L. (2019). Advances in Microdroplet Generation Methods. *Chinese Journal of Analytical Chemistry*, *47*(6), 795–804. https://doi.org/10.1016/S1872-2040(19)61162-X

Wo, T., Wurzbach, I., Kirres, J., Kostidou, A., Kapernaum, N., Litterscheidt, J., Haenle, J. C., Sta, P., Baro, A., Giesselmann, F., & Laschat, S. (2015). Discotic Liquid Crystals. *Chemical Reviews*. https://doi.org/10.1021/acs.chemrev.5b00190

05-4506832 pustaka.upsi.edu.my Perpustakaan Tuanku Bainun Kampus Sultan Abdul Jalil Shah PustakaTBainun ptbupsi

05-4506832 pustaka.upsi.edu.my Perpustakaan Tuanku Bainun Kampus Sultan Abdul Jalil Shah PustakaTBainun ptbupsi

Wood, T. A., Gleeson, H. F., Dickinson, M. R., & Wright, A. J. (2004). Mechanisms of optical angular momentum transfer to nematic liquid crystalline droplets. *Applied Physics Letters*, *84*(21), 4292–4294. https://doi.org/10.1063/1.1753067

Wright, W. H., Sonek, G. J., & Berns, M. W. (1994). Parametric study of the forces on microspheres held by optical tweezers. *Applied Optics*, *33*(9), 1735–1748.

Wu, C. S., Hsieh, P. Y., Yuyama, K. I., Masuhara, H., & Sugiyama, T. (2018). Pseudopolymorph Control of l -Phenylalanine Achieved by Laser Trapping. *Crystal Growth and Design*, *18*(9), 5417–5425. https://doi.org/10.1021/acs.cgd.8b00796

Wulff, D., Chan, A., Liu, Q., Gu, F. X., & Aucoin, M. G. (2020). Characterizing internal cavity modulation of corn starch microcapsules. *Heliyon*, *6*(10), e05294. https://doi.org/10.1016/j.heliyon.2020.e05294

Xie, M. (2021). Principle of optical tweezers trapping. *Autonomous Robot-Aided Optical Manipulation for Biological Cells*, 3–13. https://doi.org/10.1016/b978-0-12-823449-5.00003-4

Yan, Wang., Hanyang, Li., Liyuan, Zhao., Yongjun, Liu., Shuangqiang, Liu., & Jun, Yang. (2017). Tapered optical fiber waveguide coupling to whispering gallery modes of liquid crystal microdroplet for thermal sensing application. *Optics Express*, *25*(2), 3240–3247.
05-4506832 pustaka.upsi.edu.my Perpustakaan Tuanku Bainun Kampus Sultan Abdul Jalil Shah PustakaTBainun ptbupsi
Yang, Y., Brimicombe, P. D., Roberts, N. W., Dickinson, M. R., Osipov, M., & Gleeson, H. F. (2008). Continuously rotating chiral liquid crystal droplets in a linearly polarized laser trap. *Optics Express*, *16*(10), 6877–6882.

Yeng, M. S. M., & Ayop, S. K. (2022). The trapping of a single 4-cyano-4-pentylbiphenyl (5CB) microdroplet in water using optical tweezers. *Proceeding of SPIE*, *12479*(December), 191. https://doi.org/10.1117/12.2658779

Yeng, M. S. M., Ayop, S. K., & Hamid, M. Y. (2017). The Determination of Laser Spot Size of an Optical Tweezers by Stuck Bead Method. *Journal of Science and Technology*, *9*(3), 70–74.

Yeng, M. S. M., Ayop, S. K., Mustapa, I. R., & Sasaki, K. (2022). Optical Stiffness of an Optically Trapped 4-Cyano-4'-Pentylbiphenyl (5CB) in the form of a Microdroplet in Water. *Central Asia and the Caucasus*, *23*(1), 3008–3016.

Yeng, M. S. M., Ayop, S. K., & Sasaki, K. (2022). Optical Manipulation of a Liquid Crystal (LC) Microdroplet by Optical Force. *Crystal Research and Technology*, *n/a*(n/a), 2200080. https://doi.org/https://doi.org/10.1002/crat.202200080

Yeng, M. S. M., Ayop, S. K., & Sasaki, K. (2023). Optical Trapping of a Single Chloroform Microdroplet. *Jurnal Teknologi*, *85*(3), 117–123. https://doi.org/https://doi.org/10.11113/jurnalteknologi.v85.19303

05-4506832 pustaka.upsi.edu.my Perpustakaan Tuanku Bainun Kampus Sultan Abdul Jalil Shah PustakaTBainun ptbupsi

05-4506832 pustaka.upsi.edu.my Perpustakaan Tuanku Bainun Kampus Sultan Abdul Jalil Shah PustakaTBainun ptbupsi

Yusof, M. F. M., Ayop, S. K., Supian, F. L., & Juahir, Y. (2020). Optical trapping of organic solvents in the form of microdroplets in water. *Chemical Physics Letters*, *749*(January), 137407. https://doi.org/10.1016/j.cplett.2020.137407

Yusuf, M. F. M., & Ayop, S. K. (2020). The trapping of a single chloroform microdroplet in water using optical tweezers. *SPIE*, *11522*(June), 18. https://doi.org/10.1117/12.2573528

Zeng, H. (2017). *Light Driven Microscopic Robot* (Issue October). https://doi.org/10.13140/RG.2.2.28029.46564

Zhang, J., Liu, W., Zhu, Z., Yuan, X., & Qin, S. (2016). Towards nano-optical tweezers with graphene plasmons : Numerical investigation of trapping 10-nm particles with mid-infrared light. *Nature Publishing Group*, *November*, 1–7. https://doi.org/10.1038/srep38086

Zhong, M. C., Wang, Z. Q., & Li, Y. M. (2017). Oscillations of absorbing particles at the water-air interface induced by laser tweezers. *Optics Express*, *25*(3), 2481–2488. https://doi.org/10.1364/OE.25.002481

Zhu, C., Lu, Y., Jiang, L., & Yu, Y. (2021). Liquid Crystal Soft Actuators and Robots toward Mixed Reality. *Advanced Functional Materials*, *2009835*, 1–21. https://doi.org/10.1002/adfm.202009835

05-4506832 pustaka.upsi.edu.my Perpustakaan Tuanku Bainun Kampus Sultan Abdul Jalil Shah PustakaTBainun ptbupsi
05-4506832 pustaka.upsi.edu.my Perpustakaan Tuanku Bainun Kampus Sultan Abdul Jalil Shah PustakaTBainun ptbupsi

05-4506832 pustaka.upsi.edu.my Perpustakaan Tuanku Bainun Kampus Sultan Abdul Jalil Shah PustakaTBainun ptbupsi

APPENDICES

APPENDIX A: KNOWLEDGE DISSEMINATION

A) PUBLICATIONS

1. **M. S. M. Yeng** and S.K. Ayop, "The Production of the 4-Cyano-4-Pentylbiphenyl (5CB) Microdroplets in the Water for Optical Trapping Applications," in *JSAP Spring Meeting*, 2022, p. 2022.

2. **M. S. M. Yeng** and S. K. Ayop, "The trapping of a single 4-cyano-4-pentylbiphenyl (5CB) microdroplet in water using optical tweezers," *Proceeding of SPIE*, vol. 12479, no. December, p. 191, 2022,

3. **M. S. M. Yeng,** S. K. Ayop, and K. Sasaki, "Optical Manipulation of a Liquid Crystal (LC) Microdroplet by Optical Force," *Crystal Research and Technology*, vol. n/a, no. n/a, p. 2200080, 2022.

4. **M. S. M. Yeng**, S. K. Ayop, I. R. Mustapa, and K. Sasaki, "Optical Stiffness of an Optically Trapped 4-Cyano-4'-Pentylbiphenyl (5CB) in the form of a Microdroplet in Water," *Central Asian and The Caucasus*, vol. 23, no. 1, pp. 3008–3016, 2022.

5. N. I. Mahadi, F. L. Supian, S. K. Ayop, and **M. S. M. Yeng**, "Power Density Limit for Stable Optical Trapping of a Single Microcluster of Calix [4] arene in Water," *Central Asian and The Caucasus*, vol. 23, no. 1, pp. 3000–3007, 2022.

6. **M. S. M. Yeng**, S. K. Ayop, and K. Sasaki, "Optical Trapping of a Single Chloroform Microdroplet," *J Teknol*, vol. 85, no. 3, pp. 117–123, 2023, d

7. **M. S. M. Yeng**, S. K. Ayop, and I. R. Mustapa, "The Effect of Sonication and Suspension Stability of 4-Cyano-4'-pentylbiphenyl (5CB) Microdroplets in Water for Prospective Microdroplet Applications," Jurnal Fizik Malaysia. (Under Reviewed).

05-4506832 pustaka.upsi.edu.my Perpustakaan Tuanku Bainun Kampus Sultan Abdul Jalil Shah PustakaTBainun ptbupsi

05-4506832 pustaka.upsi.edu.my Perpustakaan Tuanku Bainun Kampus Sultan Abdul Jalil Shah PustakaTBainun ptbupsi

B) CONFERENCES

1. **M. S. M. Yeng** and S.K. Ayop, "The Production of the 4-Cyano-4-Pentylbiphenyl (5CB) Microdroplets in the Water for Optical Trapping Applications," in *JSAP Spring Meeting*, 2022, p. 2022. Presented at The 69th JSAP Spring Meeting 2022, 22-26 March 2022, Sagamihara Campus, Aoyama Gakuin University & Online.

2. **M. S. M. Yeng** and S. K. Ayop, "The trapping of a single 4-cyano-4-pentylbiphenyl (5CB) microdroplet in water using optical tweezers," *Proceeding of SPIE*, vol. 12479, no. December, p. 191, 2022. Presented at Optical Manipulation and Structured Materials (OMC), Optics & Photonics International Congress OPIC 2022, 19-22 April 2022, Yokohama, Japan and online.

3. **M. S. M. Yeng**, S. K. Ayop, I. R. Mustapa, and K. Sasaki, "Optical Stiffness of an Optically Trapped 4-Cyano-4'-Pentylbiphenyl (5CB) in the form of a Microdroplet in Water," *Central Asian and The Caucasus*, vol. 23, no. 1, pp. 3008–3016, 2022. Presented at International Conference on Science, Technology, Engineering, and Mathematics, in conjunction with International Postgraduate Conference on Science and Mathematics, ICSTEM 2021 & IPCSM 2021, UPSI, Malaysia, Virtual Conference.

4. **M. S. M. Yeng**, S. K. Ayop, and I. R. Mustapa, "The Production and Suspension Stability of 4-Cyano-4'-pentylbiphenyl (5CB) Microdroplets in Water for Prospective Microdroplet Applications," Jurnal Fizik Malaysia. Presented at the National Physics Conference 2022, 6 December 2022 - 8 December 2022, Malaysia Institute of Physics, Virtual Conference.

05-4506832 pustaka.upsi.edu.my Perpustakaan Tuanku Bainun Kampus Sultan Abdul Jalil Shah PustakaTBainun ptbupsi

05-4506832 pustaka.upsi.edu.my Perpustakaan Tuanku Bainun Kampus Sultan Abdul Jalil Shah PustakaTBainun ptbupsi

APPENDIX B: SYSTEM SPECIFICATION

A. OT Specification

Item	OTKB/M
Trap Force	~10 pN
Spot Size	1.1 µm
Depth of Focus	1.0 µm
Laser Wavelength	976 nm
Max Power at The Fiber Output	340 mW

B. Piezostage Specification

05-4506832 pustaka.upsi.edu.my Perpustakaan Tuanku Bainun Kampus Sultan Abdul Jalil Shah PustakaTBainun ptbupsi

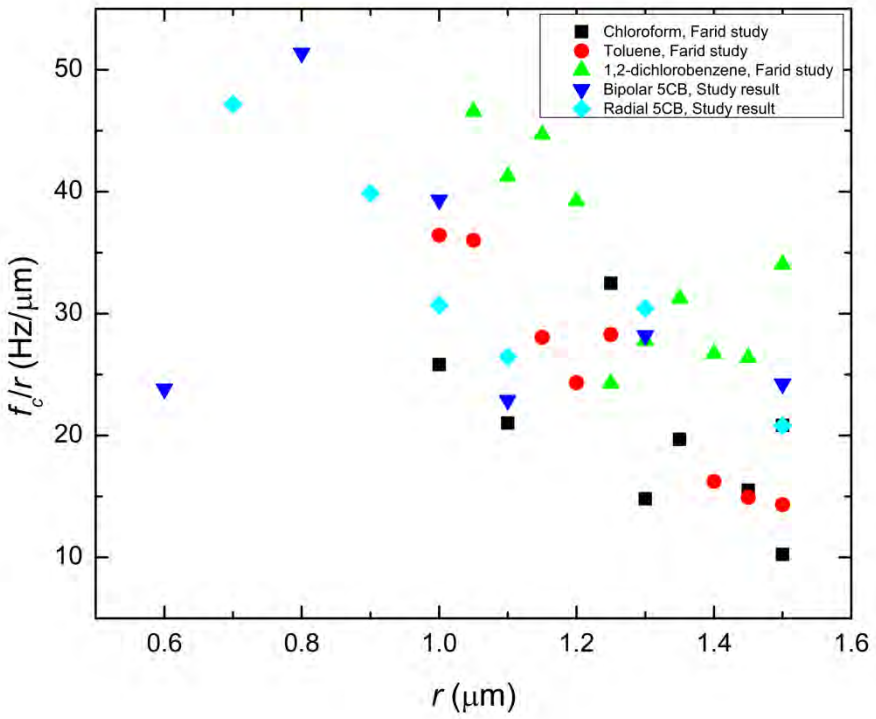
Item #	MAX311D(/M)
Manual Drive Specifications	
Item #	DRV3
Travel Range	4 mm (0.16") 300 µm Fine
Coarse Adjustment	500 µm/rev
Fine Adjustment (with Vernier Scale)	50 µm/rev
Piezo Specifications	
Control	Closed Loop
Voltage Range	0 - 75 V
Travel Range	20 µm
Theoretical Resolution	5 nm
Bidirectional Repeatability	50 nm
Absolute On-Axis Accuracy	1.0 µm

05-4506832 pustaka.upsi.edu.my Perpustakaan Tuanku Bainun Kampus Sultan Abdul Jalil Shah PustakaTBainun ptbupsi

05-4506832 pustaka.upsi.edu.my Perpustakaan Tuanku Bainun Kampus Sultan Abdul Jalil Shah PustakaTBainun ptbupsi

APPENDIX C: COMPARISON OF CORNER FREQUENCY PER MICRODROPLET RADIUS COMPARISON

A. Comparison of Corner Frequency per Microdroplet Radius ($\frac{f_c}{r}$) against microdroplet radius (r) for chloroform, toluene, 1,2-dichlorobenzene, bipolar 5CB, and radial 5CB microdroplets.

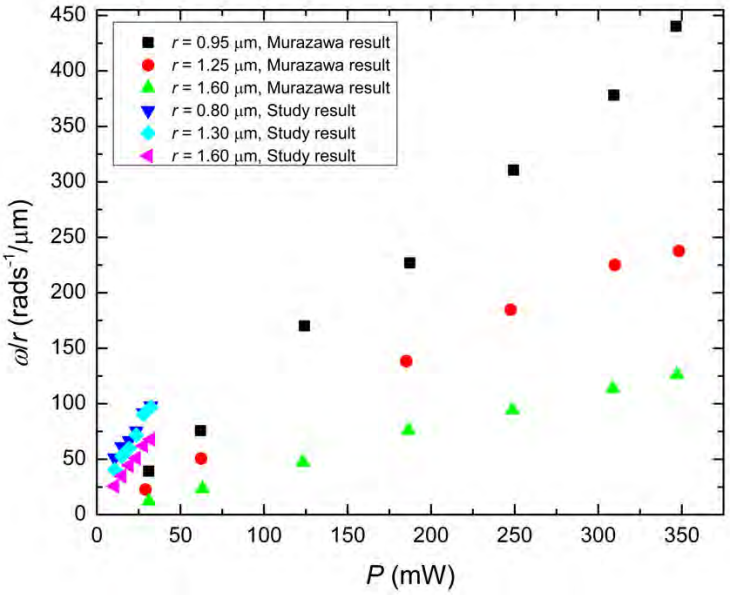


05-4506832 pustaka.upsi.edu.my Perpustakaan Tuanku Bainun Kampus Sultan Abdul Jalil Shah PustakaTBainun ptbupsi

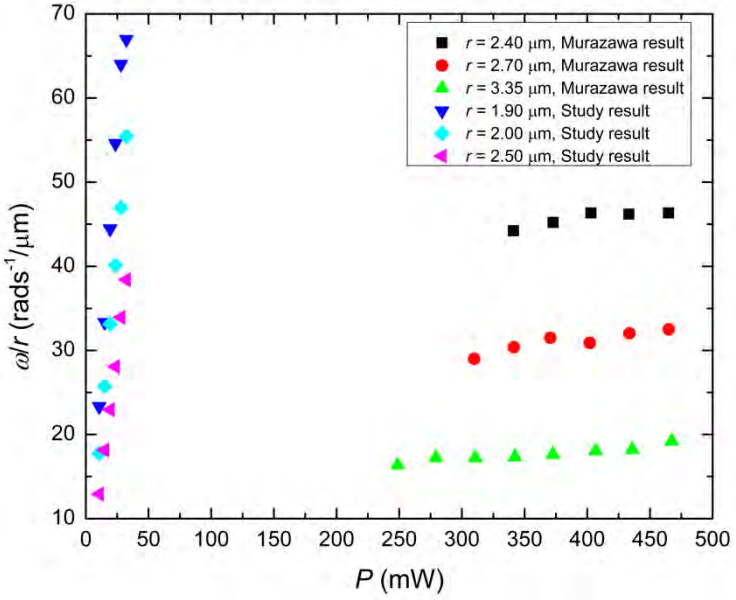
05-4506832 pustaka.upsi.edu.my Perpustakaan Tuanku Bainun Kampus Sultan Abdul Jalil Shah PustakaTBainun ptbupsi

APPENDIX D: ANGULAR SPEED PER MICRODROPLET RADIUS COMPARISON

A. Bipolar 5CB Microdroplet



B. Radial 5CB Microdroplet



05-4506832 pustaka.upsi.edu.my Perpustakaan Tuanku Bainun Kampus Sultan Abdul Jalil Shah PustakaTBainun ptbupsi